

MODERN DEVELOPMENT OF MAGNETIC RESONANCE

abstracts

2022

KAZAN * RUSSIA





Conference is supported by:



Ministry of Science
and Higher Education
of the Russian Federation



Ministry of Education and Science
of the Republic of Tatarstan



Federal Research Center
"Kazan Scientific Center of
the Russian Academy of Sciences"



Zavoisky Physical-Technical
Institute FRC KazanSC RAS



Kazan Federal University



Academy of Sciences
of the Republic of Tatarstan



Government
of the Republic of Tatarstan



MODERN DEVELOPMENT OF MAGNETIC RESONANCE

ABSTRACTS OF THE
INTERNATIONAL CONFERENCE
AND WORKSHOP
"SENSING AND QUANTUM INFORMATION
IN FLUORISCENT NANOMATERIALS"

Editor:
KEV M. SALIKHOV

KAZAN, OCTOBER 3–7, 2022

This work is subject to copyright.

All rights are reserved, whether the whole or part of the material is concerned, specifically those of translation, reprinting, re-use of illustrations, broadcasting, reproduction by photocopying machines or similar means, and storage in data banks.

© 2022 Zavoisky Physical-Technical Institute, FRC Kazan Scientific Center of RAS, Kazan

© 2022 Igor A. Aksenov, graphic design

Printed in Russian Federation

Published by Zavoisky Physical-Technical Institute, FRC Kazan Scientific Center of RAS, Kazan

www.kfti.knc.ru

CHAIRMEN

Sergey M. Khantimerov
Kev M. Salikhov

PROGRAM COMMITTEE

Kev Salikhov, chairman (Russia)
Vadim Atsarkin (Russia)
Elena Bagryanskaya (Russia)
Pavel Baranov (Russia)
Marina Bennati (Germany)
Robert Bittl (Germany)
Bernhard Blümich (Germany)
Michael Bowman (USA)
Gerd Buntkowsky (Germany)
Sergei Demishev (Russia)
Sabine Van Doorslaer (Belgium)
Rushana Eremina (Russia)
Jack Freed (USA)
Marat Gafurov (Russia)
Alexey Kalachev (Russia)
Vladislav Kataev (Germany)
Walter Kockenberger (Great Britain)
Wolfgang Lubitz (Germany)
Anders Lund (Sweden)
Sergei Nikitin (Russia)
Klaus Möbius (Germany)
Hitoshi Ohta (Japan)
Igor Ovchinnikov (Russia)
Vladimir Skirda (Russia)
Alexander Smirnov (Russia)
Graham Smith (Great Britain)
Mark Smith (Great Britain)
Murat Tagirov (Russia)
Takeji Takui (Japan)
Valery Tarasov (Russia)
Violeta Voronkova (Russia)

LOCAL ORGANIZING COMMITTEE

Khantimerov S.M., chairman
Mamin R.F., vice-chairman
Latypov V.A., vice-chairman
Voronkova V.K., scientific secretary
Gavrilova T.P., scientific secretary
Akhmetgalieva A.M.
Akhmin S.M.
Falin M.L.
Garipov R.R.
Gubaidulina A.Z.
Guseva R.R.
Kamashev A.A.
Khabibullina V.I.
Khakimova L.N.
Konovalov D.A.
Kupriyanova O.O.
Kurkina N.G.
Likerov R.F.
Mosina L.V.
Morozova A.S.
Oladoshkin Yu.V.
Salikhov K.M.
Yanduganova O.B.

SCIENTIFIC SECRETARIAT

Violeta K. Voronkova
Laila V. Mosina
Vladislav A. Latypov

CONTENTS

ZAVOISKY AWARD LECTURE

- The development of in vivo FT-EPR imaging at 300 MHz:
Applications in cancer research
S. Subramanian 2

PLENARY LECTURES

- Spin phenomena in wide-gap semiconductors and their nanostructures
P.G. Baranov 4
- How nature fertilizes the earth: Nitrogenase mechanism, and the roles
of FeMo-cofactor CFe₆ core and “capping” Mo and Fe ions
B.M. Hoffman 5
- Research into dinitrosyl iron complexes in living organisms through
EPR as an example of applying this method in biology
A.F. Vanin 6
- Current state of the spin chemistry theory
K.M. Salikhov 7
- Strange forms of magnetic dipole interactions for anisotropic spins
M.K. Bowman, A.G. Maryasov 8
- Modified Landau-Lifshitz equation of motion for description
of the spin dynamics in strongly correlated materials
S.V. Demishev 9
- New developments in multi-extreme THz ESR
H. Ohta, S. Okubo, E. Ohmichi, T. Sakurai, H. Takahashi, S. Hara 11
- Combining operando CW EPR and pulsed EPR spectroscopy
for understanding heterogeneous catalysis
*G. Jeschke, S.P. Schmid, M. Agrachev, J. Fischer, A. Ashuiev,
D. Klose* 12
- Insights into cation-anion hydrogen bonding in mesogenic ionic
liquids from solid-state NMR
D. Majhi, J. Dai, S.V. Dvinskikh 13

SECTION 1
THEORY OF MAGNETIC RESONANCE

- Bridging the gap between fictitious spin-1/2 and true spin Hamiltonian approaches for spin quartet states with sizable ZFS tensors
T. Yamane, K. Sugisaki, K. Sato, K. Toyota, D. Shiomi, T. Takui 15
- Bloch-Siegert effect in anisotropic paramagnetic centers with effective spin of 1/2
A.G. Maryasov, M.K. Bowman 16
- A possible manifestation of superabsorption in EPR spectroscopy
I.I. Geru 17
- Multiple-quantum NMR spectral intensity profiles under decoherence effects
V.E. Zobov, A.A. Lundin 19

SECTION 2
FULLERENES AND FULLERENE-BASED MATERIALS

- Self-organization of fullerene derivatives in solutions and biological cells studied by pulsed field gradient NMR
V. Volkov, I. Avilova, A. Chernyak, P. Troshin 21
- Spin dynamics of endohedral fullerene $\text{Sc}_2@C_{80}(\text{CH}_2\text{Ph})$
Yu.E. Kandrashkin, R.B. Zaripov 23
- Application of endofullerene $\text{Sc}_2@C_{80}(\text{CH}_2\text{Ph})$ as a spectroscopic ruler
R.B. Zaripov, Yu.E. Kandrashkin 24
- Study of spin coherence processes of endohedral fullerene $\text{Sc}_2@C_{80}(\text{CH}_2\text{Ph})$
I.T. Khairutdinov, R.B. Zaripov, Yu.E. Kandrashkin 25

SECTION 3
CHEMICAL AND BIOLOGICAL SYSTEMS

- New applications of MOFs aided by EPR
M.V. Fedin, A.S. Poryvaev, D.M. Polyukhov, O.A. Krumkacheva 27
- Observation of triplet charge separation state (3CS) with time-resolved electron paramagnetic resonance spectra in compact electron donor-acceptor dyads
J. Zhao, X. Zhao, A.A. Sukhanov, V.K. Voronkova 28
- Probing small-angle molecular motions with EPR spectroscopy: Dynamical transition and molecular packing in disordered solids
S.A. Dzuba, E.A. Golysheva 31

Application of EPR spectroscopy to determine the content of nitric oxide in the brain and heart of rats <i>Kh.L. Gainutdinov, V.V. Andrianov, A.A. Sukhanov, R.B. Zaripov, L.V. Bazan, N.G. Shayakhmetov, M.M. Bakirov, G.G. Yafarova</i>	32
Dynamics of spin centers in TiO ₂ nanotubes/Cu _x O composites <i>E.A. Konstantinova, E.V. Kytina, T.P. Savchuk</i>	34
Supramolecular materials: design, application, and perspectives <i>E. Skorb, A. Timralieva, P. Nesterov, A. Kokorin</i>	36
Structure and catalytic properties of Cu(II) complexes with fluorinated ligands <i>A.I. Kokorin, N.A. Chumakova, Yu.N. Kozlov, A.A. Shubin</i>	37
Photoinduced reactions of spin centers in Nb and N doped titania nanocrystals <i>E.V. Kytina, E.A. Konstantinova, A.V. Marikutsa</i>	40
Structure-dependent functional self-assemblies based on a thiobarbiturate-barbiturate-melamine three-component system <i>I. Moskalenko, V. Shilovskikh, A. Timralieva, P. Nesterov, E. Skorb, A. Kokorin</i>	42
Investigation of structural rearrangements of ionic liquids during glass transition by EPR and MD methods <i>D. Alimov, M. Ivanov, S. Pylaeva</i>	43
Study of crown-containing styryl dyes and peculiarities of their photoreactions <i>A. Kondratenko, N. Alexandrova, N. Lobova</i>	44
“Smart” supramolecular materials for reactive oxygen species trap and storage <i>A. Timralieva, P. Nesterov, I. Moskalenko, A. Kokorin</i>	45
 SECTION 4 SPIN-BASED INFORMATION PROCESSING	
Magneto-optical imaging of coherent spin dynamics <i>Yu.M. Bunkov, in collaboration with V.I. Belotelov, P.O. Kapralov, G.A. Knyazev, A.N. Kuzmichev, P.E. Petrov, P.M. Vetoshko</i>	47
Engineering of exchange spin-waves spectra in ferromagnetic alloys with spatially variable composition <i>A. Gumarov, I. Yanilkin, I. Golovchanskiy, B. Gabbasov, A. Kiiamov, R. Yusupov, L. Tagirov</i>	50
Clustering into three groups on a quantum processor of five spins S = 1, controlled by pulses of resonant RF fields <i>I.S. Pichkovskiy, V.E. Zobov</i>	51

SECTION 5
NEW TRENDS IN SPIN CHEMISTRY

- Probing coherent spin dynamics in low field regime by transient absorption detected pulsed magnetic field effect
K. Maeda 53
- New polyfluorinated systems producing X-ray generated exciplexes with magnetosensitive emission due to spin control of recombination
D.V. Stass, E.M. Glebov, R.G. Fedunov, L.V. Kuibida, P.V. Nikul'shin 54
- Readout of spin quantum beats in a charge-separated radical pair by pump-push spectroscopy
D. Mims, J. Herpich, N.N. Lukzen, U.E. Steiner, Ch. Lambert 56

SECTION 6
STRONGLY CORRELATED ELECTRON SYSTEMS

- Peculiar physics of heavy fermion metals:
Theory versus experimental facts
V.R. Shaginyan 58
- Zeeman coupling in the $\text{Bi}_{1.08}\text{Sn}_{0.02}\text{Sb}_{0.9}\text{Te}_2\text{S}$ topological insulator as revealed from the quantum oscillations
V. Sakhin, L. Morgun, V. Pudalov, G. Teitel'baum 59
- Magnetic irreversibilities and nonreciprocity of the microwave absorption of FeCr_2O_4 spinel
R.V. Yusupov, M.A. Cherosov, B.F. Gabbasov, K.V. Vasin, R.G. Batulin, A.G. Kiiamov, A.L. Zinnatullin, M.V. Eremin 60

SECTION 7
LOW-DIMENSIONAL SYSTEMS AND NANO-SYSTEMS

- Electron spin resonance of spinon liquid with interaction
A.I. Smirnov, K.Yu. Povarov, T.A. Soldatov, Ren-Bo Wang, A. Zheludev, O.A. Starykh 63
- Observation of skyrmions by magnetic resonance method in $\text{Sr}_2\text{MnTiO}_6$
R.M. Eremina, I.V. Yatsyk, T.I. Chupakhina 65
- Spin probe technique for investigation of inner structure of graphene oxide membranes – possibilities and prospects
N.A. Chumakova 66
- Electron paramagnetic resonance of nanocrystalline titanium dioxide containing manganese and its changes under the influence of ultraviolet irradiation
D.A. Saritsky, A.M. Ziatdinov, D.P. Opra, V.V. Zheleznov 67

Short range proximity effect in tunnel-coupled magnetic and nonmagnetic quantum wells <i>E. Kirstein, N.V. Kozyrev, M.M. Afanasiev, V.K. Kalevich, M. Salewski, Yu.G. Kusrayev, E.A. Zhukov, D.R. Yakovlev, M. Bayer</i>	69
EPR investigation of acetonitrile intercalated into the inter-plane space of graphite oxide <i>D.A. Astvatsaturov, N.A. Chumakova</i>	72
Magnetic resonance in metal-insulator nanogranular composites with paramagnetic ions in insulating matrix <i>A.B. Drovosekov, N.M. Kreines, A.V. Sitnikov, S.N. Nikolaev, V.V. Rylkov</i>	73
Spin and pseudo-spin ferromagnetic phase transitions in the regime of quantum Hall effect <i>R. Khisameeva, S.A. Lopatina, G.A. Nikolaev, A.V. Shchepetilnikov, I.V. Kukushkin</i>	75
Coherent control of optically polarized V_B^- spin sublevels in hBN <i>I. Gracheva, M. Sadovnikova, G. Mamin, R. Yusupov, F. Murzakhanov</i>	77
Peculiarities of the ion transport of water molecules and alkali metal cations in sulfonic cation-exchange membranes studied by NMR <i>N. Slesarenko, A. Chernyak, V. Volkov</i>	79

SECTION 8

PERSPECTIVES OF MAGNETIC RESONANCE IN SCIENCE AND SPIN TECHNOLOGY

Electron-nuclear interactions and coherent properties of axial and basal NV centers in $^4\text{H-SiC}$ crystal <i>I. Gracheva, M. Sadovnikova, G. Mamin, F. Murzakhanov</i>	82
Non-Kramers iron $S = 2$ ions in $\beta\text{-Ga}_2\text{O}_3$ crystals: high-frequency low temperature EPR study <i>R.A. Babunts, A.S. Gurin, E.V. Edinach, H.-J. Drouhin, V.I. Safarov, P.G. Baranov</i>	84

SECTION 9

MAGNETIC RESONANCE INSTRUMENTATION

Construction and application of dry 6 K ultra-low temperature continuous wave and pulsed EPR <i>F. Yingying, T. Yulan, Q. Zirui, L. Wenyu, L. Yong, S. Zhifu, Y. Haijun</i>	87
Use of adiabatic pulses for spin-echo experiments in magnetic materials <i>I. Mershiey, G. Kupriyanova, S. Wurmehl</i>	89

Pulse X-band EPR-spectrometer with microwave digital synthesizer, 300 W solid-state power amplifier, and AWG unit <i>K. Lomanovich, E. Bagryanskaya, S. Veber, N. Isaev, A. Melnikov, M. Dugin, M. Bowman, M. Ivanov, D. Polovyanenko</i>	91
A new player in the EPR spectroscopy market: high-tech solutions for X- and W-band from ZHONGTAI <i>M.L. Kuklinov, A.S. Petrov, A.I. Chazov</i>	92
 SECTION 10 ELECTRON SPIN BASED METHODS FOR ELECTRONIC AND SPATIAL STRUCTURE DETERMINATION IN PHYSICS, CHEMISTRY AND BIOLOGY	
Spin-dependent afterglow of irradiated crystals: an ODMR study <i>N.G. Romanov</i>	95
EPR spectroscopy of Ytterbium dimer associates in synthetic forsterite Mg_2SiO_4 <i>V. Tarasov, A. Sukhanov, K. Salikhov, E. Zharikov, K. Subbotin, V. Dudnikova</i>	96
Graphene oxide membranes: the connection between inner structure and sorption properties <i>A. Rebrikova, A. Kaplin, M. Matveev, N. Chumakova, M. Korobov</i>	97
Room temperature coherent control of negatively charged NV defect in silicon carbide <i>K. Sannikov, I. Gracheva, G. Mamin, F. Murzakhanov, V. Soltamov</i>	98
Manganese impurity dynamic polar centres in $SrTiO_3$ <i>B. Gabbasov, R. Yusupov, D. Zverev, A. Rodionov, L. Jastrabik, V. Trepakov</i>	99
 SECTION 11 OTHER APPLICATIONS OF MAGNETIC RESONANCE	
Experimental manifestation of spin polariton in dilute solutions of nitroxyl radicals <i>K.M. Salikhov, M.M. Bakirov, R.B. Zaripov, I.T. Khairutdinov</i>	102
Gyroscope based on NV color center in diamond <i>V.V. Soshenko, S.V. Bolshedvorskii, O.R. Rubinas, I.S. Cojocar, V.N. Sorokin, A.N. Smolyaninov, A.V. Akimov</i>	103
NQR detection system of nitrogen compounds in large inspection volumes <i>G.V. Mozzhukhin, E. Doğan, A.F. Cakal, B. Colak, P. Kupriyanov, R. Khusnutdinov, B. Rameev</i>	104

Molecular structure and parameters of magnetic interactions in Ni-F _{int} paramagnetic centers synthesized in BaF ₂ crystal: EPR data <i>R.B. Zaripov, V.A. Ulanov, I.V. Yatsyk, G.S. Shakurov</i>	106
Voice diseases diagnostics using 3T dynamic MRI and original vocal tests <i>M. Fattakhova, R. Khabipov, V. Krasnozhon, V. Fedorova, E. Bekmacheva, A. Akhatov</i>	107
Spin and valence states of ions in nanosized bimetallic coordination compounds and their changes upon immobilization in polymer matrix <i>V.R. Polishchuk, A.M. Ziatdinov</i>	108
 SECTION 12 MODERN METHODS OF MAGNETIC RESONANCE	
Development of sensors for the study of agricultural objects in an MRI system with a field of 0.4 T <i>A. Bayazitov, A. Fakhrutdinov, Ya. Fattakhov, V. Odivanov, V. Shagalov</i>	112
Formation of nutation line in powerful non-uniform field in nuclear magnetic measurers with flowing liquid <i>I. Kochetkov, V. Davydov, R. Davydov</i>	113
Features of longitudinal relaxation time T ₁ measuring in condensed media by nuclear magnetic resonance method with using a modulation technique in weak magnetic fields <i>M. Davydov, V. Davydov, A. Goldberg, R. Davydov</i>	116
Experimental investigation of free induction decay in zigzag spin chains of hambergite in multiple quantum NMR <i>S.G. Vasil'ev, G.A. Bochkin, E.B. Fel'dman, D.P. Kiryukhin, P.P. Kushch</i>	118
 WORKSHOP SENSING AND QUANTUM INFORMATION IN FLUORISCENT NANOMATERIALS	
Opportunities for biosensing with fluorescent diamond and phosphor nanoparticles <i>P. Hemmer</i>	121
Optical magnetometry with home-synthesized fluorescent nanodiamonds <i>A.V. Leontyev, D.K. Zharkov, A.G. Shmelev, V.G. Nikiforov, V.S. Lobkov, E.O. Mityushkin, M.H. Alkahtani</i>	122
YVO ₄ :Yb, Er UCNP – insight to the nano thermosensor <i>A.G. Shmelev, D.K. Zharkov, A.V. Leontyev, V.G. Nikiforov, D.N. Petrov, M.F. Krylov, J.E. Clavijo, E.O. Mityushkin, V.S. Lobkov</i>	123

Highly efficient broadband superconducting quantum memory <i>A.R. Matanin, K.I. Gerasimov, E.S. Moiseev, N.S. Smirnov, A.I. Ivanov, E.I. Malevannaya, V.I. Polozov, E.V. Zikiy, A.A. Samoilov, I.A. Rodionov, S.A. Moiseev</i>	124
Atomic frequency comb memory for polarization state of light in a $^{153}\text{Eu}:\text{Y}_2\text{SiO}_5$ crystal <i>R.A. Akhmedzhanov, L.A. Gushchin, N.A. Nizov, V.A. Nizov, D.A. Sobgayda, I.V. Zelensky</i>	126
Photonic crystal cavities for GeV&SnV diamond <i>A.V. Akimov</i>	128
Quantum memory in nanodiamonds with color centers <i>A.D. Berezhnoi, A.A. Kalachev</i>	129
 POSTERS	
W-band EPR and quantum-chemical calculation of radicals in calcium gluconate <i>M.M. Akhmetov, G.G. Gumarov, R.B. Zaripov, G.N. Konygin, D.S. Rybin</i>	131
EPR study of the content of nitric oxide and copper in the hippocampus of rats after brain injury and hemorrhagic stroke <i>V.V. Andrianov, G.G. Yafarova, A.S. Zamaro, Y.P. Tokalchik, L.V. Bazan, T.Kh. Bogodvid, V.S. Iyudin, V.A. Kulchitchky, Kh.L. Gainutdinov</i>	133
Experimental observation of spin polariton in dilute solutions of nitroxide radicals <i>M.M. Bakirov, K.M. Salikhov, R.B. Zaripov, I.T. Khairutdinov</i>	135
Electron spin dynamics of photoexcited bodipy dimers <i>H. Cao, A.A. Sukhanov, M.M. Bakirov, Yu.E. Kandrashkin, J. Zhao, V.K. Voronkova</i>	136
Development of sensors for the study of small animals in an MRI system with a field of 0.4 T <i>A. Bayazitov, A. Fakhrutdinov, Ya. Fattakhov, V. Odivanov, V. Shagalov</i>	138
Determination of the zero field splitting parameters of the cobalt(II) ion in diamagnetically diluted samples using circularly polarized radiation <i>A.V. Borodulina, A.R. Melnikov, S.L. Veber</i>	139
Photoresistivity of the film heterostructure $\text{Ba}_{0.8}\text{Sr}_{0.2}\text{TiO}_3/\text{Ba}_{0.8}\text{Sr}_{0.2}\text{TiO}_3$ on MgO substrate <i>A.O. Chibirev, A.V. Leontyev, N.N. Garif'yanov, R.F. Mamin</i>	140

Anisotropic rotation of nitroxide radical in the pore system of metal-organic framework induced by guest solvents <i>A.A. Efremov, A.S. Poryvaev, D.M. Polyukhov, M.V. Fedin</i>	141
ESR of Dy ³⁺ ion at cubic sites in Cs ₂ KYF ₆ crystals <i>M.L. Falin, V.A. Latypov, N.M. Khaidukov</i>	142
An estimate of the activation energy of the solid-phase recrystallization of ion implanted Si (111) by an optical diffraction method <i>B.F. Farrakhov, Ya.V. Fattakhov</i>	143
Effect of the anion nature on the spin properties of new Fe (III) complexes with tridentate ligands <i>E. Frolova, A. Sharipova, L. Bazan, O. Turanova, I. Ovchinnikov</i>	145
W-band EPR investigation of mechanoactivated and γ -irradiated calcium gluconate <i>A.R. Gafarova, G.G. Gumarov, R.B. Zaripov, D.S. Rybin, G.N. Konygin</i>	146
Reversible intercalation of lithium ions into the structure of Li ₃ V ₂ (PO ₄) ₃ cathode material for lithium-ion batteries: ESR measurements <i>T.P. Gavrilova, I.V. Yatsyk, J.A. Deeva, T.I. Chupakhina, N.M. Suleimanov, S.M. Khantimerov</i>	147
Features of the temperature behavior of the ESR spectra of Cr ³⁺ ions in the 3D Dirac semimetal Cd ₃ As ₂ <i>Yu. Goryunov, A. Nateprov</i>	148
Synthesis and investigation of magnetic properties of thin film systems Fe ₃ Al and Fe ₃ Al/Pt <i>A.Hh. Kadikova</i>	150
Study of the features direction of the magnetization vector in two-layer system Fe/LiNbO ₃ <i>A.A. Kamashev, A.V. Leontyev, R.F. Mamin, I.A. Garifullin</i>	152
Phase transformation in the system “Brodie graphite oxide-acetonitrile” according to EPR and XRD data <i>A.V. Kaplin, N.A. Chumakova, D.S. Popov, A.T. Rebrikova, M.V. Korobov, O.N. Khrykina</i>	153
Phase cycling sequences designing in CPMG method to eliminate unwanted echoes <i>I.T. Khairutdinov, R.B. Zaripov, M.M. Bakirov, M.Yu. Volkov</i>	155
Spin-orbit interaction in GaN/AlGaN heterojunctions probed by ESR <i>R. Khisameeva, A.V. Shchepetilnikov, V.V. Solovyev, T. Mikolajick, A. Großer, S. Schmult, I.V. Kukushkin</i>	157
Creation of new methods of mid-field magnetic resonance imaging <i>A. Kolesova, T. Islamov, I. Sidorov, V. Skirda, A. Alexandrov, D. Melnikova, Ya. Fattakhov, V. Odivanov</i>	158

Lipid peroxidation processes involving thiosemicarbozones <i>V. Koshman, E. Shelepova, O. Selyutina, N. Polyakov</i>	159
Polarizing insensitive nuclei at ultralow magnetic fields using parahydrogen: a facile route to optimize adiabatic magnetic field sweeps <i>V.P. Kozinenko, A.S. Kiryutin, A.V. Yurkovskaya</i>	160
Effect of transition metal ions to hydrodynamic behavior of human serum albumin <i>A.M. Kusova, K.R. Mirsalimova, A.N. Turanov, Yu.F. Zuev</i>	161
Electron spin resonance of ^{51}V ions in scandium orthosilicate monocrystal <i>R.F. Likеров, I.V. Yatsyk, R.B. Zaripov, K.B. Konov, V.A. Shustov, R.M. Eremina</i>	162
Strategy of simulation of the EPR spectra angular dependence for nitroxide spin probes in graphene oxide membranes <i>M. Matveev</i>	164
Dual-compensated composite pulses for nuclear quadrupole resonance spectroscopy <i>I. Mershiey, G. Kupriyanova</i>	166
Determining patient compliance with low-dose aspirin therapy using $^1\text{H-NMR}$ <i>I. Mershiey, G. Kupriyanova, V. Rafalskiy, E. Moiseeva</i>	167
ESR of heterometallic Mg-Mn warwickites <i>A.R. Muftakhutdinov, R.M. Eremina, E.M. Moshkina</i>	169
Base-pair opening and closing kinetics in DNA duplex containing oxoG:A mismatch <i>D. Nasonov, S. Ovcherenko, A. Shernyukov, A. Endutkin, D. Zharkov, E. Bagryanskaya</i>	170
EPR study of nitrogen P1 centers in nature and synthetic diamonds <i>Yu. Bogachev, V. Zubkov, A. Nikitina, M. Shishkina, S. Sukharzhevsky</i>	172
Increasing the accuracy of diffusion parameters measurements by NMR <i>V. Odivanov, Ya. Fattakhov</i>	173
Improving the accuracy of NMR fluid flow measurements <i>V. Odivanov, Ya. Fattakhov</i>	175
Spatial structure of the fibril-forming PAP(85-120) peptide in a complex with dodecylphosphocholine micelles by high-resolution NMR spectroscopy <i>D. Osetrina, V. Klochkov, D. Blokhin</i>	176
Investigation of the features of translational mobility of liquid molecules in porous media by PFG NMR <i>D.A. Parfenova, D.L. Melnikova, A.S. Gordeev, V.D. Skirda</i>	178

ESR spectroscopy of Ziegler catalytic systems <i>D.V. Pavlov, Yu.Yu. Titova</i>	179
EPR and DFT study of the radiation-induced defects in Si(OH) ₄ <i>A.A. Petrova, A.A. Rodionov, M.R. Gafurov</i>	180
EPR study of iron oxide magnetic nanoparticles in water suspensions <i>Yu. Bogachev, A. Gorbunov, A. Nikitina, E. Pobedimova, M. Shishkina</i>	181
Magnetization, specific heat and ESR measurements of ludwigite Mn _{1.17} Co _{1.83} BO ₅ <i>D.V. Popov, T.P. Gavrilova, I.V. Yatsyk, M.A. Cherosov, E.M. Moshkina, V.A. Shustov, R.M. Eremina</i>	182
EPR study of hydrocarbons sorption in metal-organic frameworks <i>A. Poryvaev, A. Yazikova, A. Efremov, D. Polyukhov, M. Fedin</i>	184
EPR study of LaF ₃ nanoparticles doped with Er ³⁺ ions <i>M.S. Pudovkin, R.M. Rakhmatullin, A.A. Rodionov</i>	185
Two-pulse NMR responses in solids with internal molecular mobility <i>D.S. Ryabushkin</i>	186
Investigation of tricalcium phosphate ceramics doped with gadolinium ions by electron paramagnetic resonance <i>M.A. Sadovnikova, G.V. Mamin, A.A. Forysenkova, I.V. Fadeeva, F.F. Murzakhonov, M.R. Gafurov</i>	188
Paramagnetic derivatives of molecules, clusters and crystals of phenanthroline induced by ultraviolet irradiation <i>N.S. Saenko, A.M. Ziatdinov, A.S. Shishov, A.G. Mirochnik</i>	190
Spin exchange interactions in nitronyl nitroxide biradical studied by X-band EPR spectroscopy <i>A.A. Samsonenko, M.V. Fedin, S.L. Veber</i>	192
EPR of CaMoO ₄ :Er ³⁺ crystal <i>G.S. Shakurov, R.B. Zaripov, V.A. Isaev, A.V. Lebedev, S.A. Avanesov</i>	193
Definition of β-Enaminone isomerism by 2D NMR and X-Ray <i>A. Sharipova, M. Volkov, A. Gubaidullin, O. Turanova, A. Turanov</i>	194
Photoisomerization studies by NMR, UV-visible spectroscopy and DFT of stilbene-like compounds <i>A. Shaidullina, A. Sharipova, M. Volkov, L. Savostina, L. Gafiyatullin, O. Turanova, A. Turanov</i>	195
Influence of environment parameters on the internal mobility of pillar[5]arene according to NMR spectroscopy data <i>L.V. Sharipova, A.N. Turanov, B.I. Khayrutdinov, Yu.F. Zuev</i>	196
Peculiarities of the Q-band EPR spectra of the PbTe crystal with Mn and Cu impurities <i>A.V. Shestakov, I.I. Fazlizhanov, V.A. Ulanov</i>	197

Advantages of using focusing short-drawn tapered fibers in vibration sensors <i>O.P. Shindyev, A.V. Shkalikov</i>	199
EPR study of calcium phosphate powders <i>D. Shurtakova, G. Mamin, M. Gafurov</i>	201
Electron spin resonance of spinon liquid with interaction <i>A.I. Smirnov, K.Yu. Povarov, T.A. Soldatov, Ren-Bo Wang, A. Zheludev, O.A. Starykh</i>	203
Application of high-resolution NMR to study the influence of platinum nanoparticles on tryptophan amino-acid <i>M. Smirnov, G. Kupriyanova</i>	205
Extremely low concentrations of the antimicrobial peptide chalciporin influence membrane lipid organization <i>A.S. Smorygina, V.N. Syryamina, B. Biondi, C. Peggion, F. Forrmaggio, S.A. Dzuba</i>	208
Study of pulse time-resolved EPR of naphthalimide-phenothiazine compact donor-acceptor dyad <i>A.A. Sukhanov, V.K. Voronkova, K. Ye, J. Zhao</i>	210
Change in the distance between P_{700}^+ and A_1^- radicals in the reaction centers of photosystem I upon removal of iron-sulfur clusters <i>A.A. Sukhanov, M.D. Mamedov, G.E. Milanovsky, A.Y. Semenov, K.M. Salikhov</i>	211
Creation and investigation of thin-film heterostructures based on Fe/Nb <i>A.A. Validov, M.I. Nasyrova, R.R. Khabibullin, I.A. Garifullin</i>	212
The self-diffusion of 128-arm star-shaped polydimethylsiloxanes with a dendritic branching center <i>S.G. Vasil'ev, K.V. Panicheva, P.A. Tikhonov, A.M. Muzafarov</i>	213
Study of a spin-variable Fe(III) complex by ^1H NMR spectroscopy <i>M. Volkov, E. Batueva, O. Turanova, A. Turanov</i>	215
NMR structure of antimicrobial peptide megin-1 <i>P. Skvortsova, M. Volkov, Yu. Zuev, E. Ermakova</i>	217
Unusually slow intramolecular triplet-triplet energy transfer in naphthalenediimide-anthracene compact donor-acceptor dyads. TR EPR study <i>A.A. Sukhanov, V.K. Voronkova, Xi Chen, M. Taddei, J. Zhao, M.Di Donato</i>	219
EPR study of ATP-sensitive potassium channels and nitric oxide role in preconditioning effect to brain stroke <i>Kh. Gainutdinov, G. Yafarova, S. Gavrilova, O. Deryagin, V. Andrianov, V. Iyudin, S. Buravkov, M. Akhmetshina, A. Erdiakov, V. Koshelev</i>	220

pH-Sensitive spin probes for determination of water acidity in the inter-plane space of graphite oxide <i>T.S. Yankova, N.A. Chumakova</i>	222
Investigation of gallium iron oxide by the ESR method <i>I.V. Yatsyk, R.M. Eremina, E.M. Moshkina</i>	223
Impact of the lithium deficiency to the electrochemical performance of $\text{Li}_3\text{V}_2(\text{PO}_4)_3/\text{Li}_3\text{PO}_4$ composites <i>T.P. Gavrilova, I.V. Yatsyk, J.A. Deeva, T.I. Chupakhina, N.M. Suleimanov, S.M. Khantimerov</i>	225
Study of nitrogen monoxide sorption into robust radical-containing materials by EPR spectroscopy <i>A. Yazikova, A. Poryvaev, D. Polyukhov, A. Efremov, M. Fedin</i>	227
Nuclear gamma resonance studies of natural iron-rich borates vonsenite and hulsite <i>A.L. Zinnatullin, Y.P. Biryukov, F.G. Vagizov</i>	228
SPONSOR	229
AUTHOR INDEX	231

ZAVOISKY AWARD LECTURE

The development of in vivo FT-EPR imaging at 300 MHz: Applications in cancer research

S. Subramanian

Department of Chemistry, Indian Institute of Technology Madras,
Chennai 600036, India subukannan@gmail.com

Nuclear Magnetic Resonance imaging (MRI) is by now a globally recognized and important radiological technique providing invaluable diagnostic and functional physiological details to the physician. An absolutely identical technique, Electron Paramagnetic Resonance, EPR (ESR) discovered in 1944 by Yevgeny Zavoisky of Kazan (Tatstan, Russia) is an equally powerful spectroscopic

technique. Parallel development of EPR spectroscopy and imaging in biology had to wait since intrinsic paramagnetic probes with unpaired electrons to image bio systems are generally unstable and short-lived. With the availability of stable non-toxic radicals based on triarylmethyl with very narrow EPR resonances it has been possible to develop instrumentation for small animal in vivo EPR imaging. Since EPR line width (T_2 and T_2^*) and spin lattice relaxation T_1 of most systems are dependent on the partial pressure of oxygen, pO_2 , relaxation weighted in vivo images can generate quantitative oxygen dependent contrast to map oxygen distribution in vivo. Since hypoxia monitoring can help understanding the radiation treatment of cancer and also quantitative EPR imaging based oximetry can help in the development of tumor drugs and cancer treatment monitoring. The challenges involved in developing instruments for dealing with electron relaxation times of micro to nanoseconds and innovative pure phase-encoding imaging approach to generate ultra high resolution oximetric imaging and representative results will be presented and discussed.

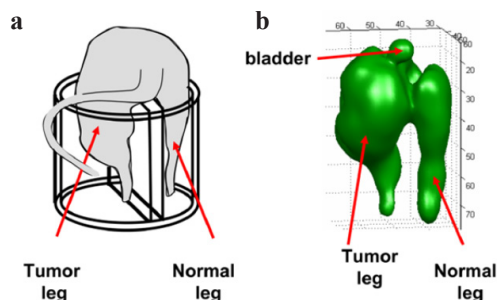


Fig. 1. **a** Tumor-bearing and normal leg infused with triaryl methyl. **b** Surface-rendered EPR image.

1. Subramanian S., Krishna M.C.: Dancing with the electrons: Time-domain and CW in vivo EPR Imaging, *Magn. Reson. Insights* Sep 24; 2, 43–74 (2008) doi: 10.4137/mri.s1131.
2. Krishna M.C., Subramanian S.: The development of time-domain in vivo EPR imaging at NCI, *Applied Magnetic Resonance* **52**, 1291–1309 (2021)

PLENARY LECTURES

Spin phenomena in wide-gap semiconductors and their nanostructures

P.G. Baranov

Ioffe Institute, St. Petersburg 194021, Russia, pavel.baranov@mail.ioffe.ru

A specific feature of wide-gap semiconductors is the possibility of forming a wide variety of levels of intrinsic and impurity spin centers within the band gap. In this case, it becomes possible to form a wide range of charge states of the centers, as well as to optically excite and detect luminescence with photon energies less than the band gap, which freely pass into the semiconductor. Also in these semiconductors, a unique isotopic composition of the matrix with a variety of nuclear magnetic moments is realized. Semiconductors A_4B_4 (diamond, SiC) and A_2B_6 (ZnO, CdS, etc.) contain isotopes with both zero and nonzero nuclear magnetic moments, which makes it possible to use isotope engineering to modify the isotopic composition in research and applied purposes (quantum sensors, qubits, gyroscopic devices based on optical NMR registration methods). In semiconductors A_3B_5 (AlN, GaN, BN), all isotopes have nuclear magnetic moments and nuclear spins larger than $1/2$, which makes it possible, along with hyperfine interactions, to register nuclear quadrupole interactions, that is, to probe the distribution of electric fields in semiconductors.

The report will analyze recent EPR, ODMR, ESE, and ENDOR research of transition and rare earth elements, as well as various types of radiation defects in SiC, ZnO, AlN, GaN and other crystals. A special place is given to recent studies on the use of unique features of high-temperature optically induced alignment of electron and nuclear spins of vacancy centers in silicon carbide with a modified isotopic composition as a material basis for quantum calculations and small rotation measurements.

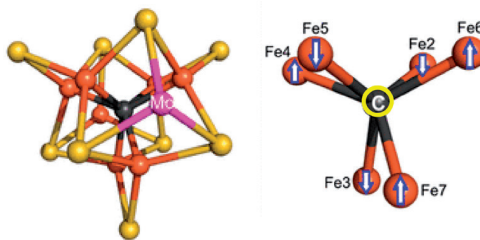
This work was supported by the Russian Science Foundation (Project No. 20-12-00216).

How nature fertilizes the earth: Nitrogenase mechanism, and the roles of FeMo-cofactor CFe₆ core and “capping” Mo and Fe ions

B.M. Hoffman

Departments of Chemistry and Molecular Biosciences, Northwestern University, Evanston, IL,
USA 60201

We will begin by presenting the central features of the mechanism by which the nitrogenase FeMo-cofactor is activated to bind and reduce N₂, as revealed by recent work by ‘the team’ comprising Seefeldt, Dean, Raugei, and coworkers, and Lukoyanov in the NU laboratory. We will then discuss the roles of the components of the catalytic active-site, [Fe₇MoCS₉] FeMo-cofactor – the CFe₆ Core, with its mysterious and unparalleled central carbon, and the ‘capping’ metal ions, Mo and Fe.



Research into dinitrosyl iron complexes in living organisms through EPR as an example of applying this method in biology

A.F. Vanin

N.N. Semenov Federal Research Center for Chemical Physics Russian Academy of Sciences

Successful application of the EPR method to researching into dinitrosyl iron complexes (DNICs) with thiol-containing ligands, which are currently considered as a “working form” of a universal metabolic process regulator in almost all living organisms – nitrogen monoxide (NO) will be demonstrated. This method made it possible not only to discover these complexes in living organisms, but also to identify centers responsible for the $g_{av.} = 2.03$ signal, which is characteristic of the mononuclear form of DNICs, as DNICs with thiol-containing ligands (using only this method). Finally, using the EPR method (together with other experimental approaches), a mechanism for synthesizing these complexes was suggested. This mechanism shows that DNICs with thiol-containing ligands can be donors of both nitrogen monoxide molecules and nitrosonium cations (NO^+) in living organisms. Various biological activities of these complexes will be considered.

Current state of the spin chemistry theory

K.M. Salikhov

Zavoisky Physical-Technical Institute, FRC Kazan Scientific Center of RAS, Kazan 420029,
Russia

The main theoretical provisions of modern spin chemistry will be presented. Special attention will be paid to the discussion of the kinetic equation for the density matrix of radical pairs, taking into account their spin-dependent recombination.

For the first time, well-founded kinetic equations for the density matrix of an ensemble of non-interacting radical pairs (RPs) are derived taking into account their spin-dependent recombination. The basic equation is obtained for the situation when all RPs of the ensemble start in the same pure quantum state. The obtained kinetic equations are generalized to the case when the initial state of the system is mixed.

The spin density matrix $\rho(t)$ can be represented as the product of the RP density matrix (hypothetical pair) $\rho_0(t)$, in which the recombination of radicals is not included, and the probability $f(t)$ that the RP in the time interval $(0, t)$ survived, i.e. did not recombine: $\rho(t) = f(t)\rho_0(t)$. In this work, kinetic equations for $f(t)$ and $\rho(t)$ are obtained.

For example, in the case when only RPs in the singlet state can recombine, the contribution of recombination to the kinetic equation is

$$(\partial\rho(t)/\partial t)_{\text{rec}} = -K_s\rho_{\text{oss}}(t)\rho(t) . \quad (1)$$

It should be emphasized that Eq. (1) was obtained under the assumption that the initial state of the RP is a pure quantum state.

We note that Eq. (1) can be interpreted as the usual kinetic equation for unimolecular (quasi-unimolecular) reactions, if we consider $K_s\rho_{\text{oss}}(t)$ as the instantaneous value of the “constant” of the reaction rate. It turns out that the singlet-triplet evolution of pair spins modulates the effective “constant” of quasi-unimolecular recombination of RPs.

1. Salikhov K.M., Molin Yu.N., Sagdeev R.Z., Buchachenko A.L.: Spin Polarization and Magnetic Effects in Radical Reactions. Academic Kiado Budapest, Elsevier Amsterdam (1984)
2. Johnson R.C., Merrifield R.E., Avakian P., Flippen R.B.: Phys. Rev. Letters **19**, 285 (1967)
3. Haberkorn R.: Mol. Phys. **32**, 1491–1493 (1976)
4. Jones J.A., Maeda K., Hore P.J.: Chem. Phys. Lett. **507**, 269–273 (2011)

Strange forms of magnetic dipole interactions for anisotropic spins

M.K. Bowman^{1,2}, A.G. Maryasov¹

¹Novosibirsk Institute of Organic Chemistry of the Siberian Branch of the Russian Academy of Sciences, Novosibirsk 630090, Russia, maryasov@nioch.nsc.ru

²Department of Chemistry & Biochemistry, The University of Alabama, Tuscaloosa, AL 35487, USA, mkbowman@ua.edu

The dipole-dipole interaction between magnetic dipoles of paramagnetic centers (PC) is the foundation for pulse dipolar spectroscopy used to measure distances and to determine structures in a wide range of biomaterials and nanostructures. They play an important role in relaxation, coherence lifetimes, and spin dynamics in dynamic nuclear polarization, magnetic materials, and quantum computing. The spin Hamiltonian for the dipole-dipole interaction between two PCs with isotropic g -factors is quite simple in strong magnetic fields. The dipole moment of each PC has a constant magnitude, quantized along the magnetic field. The result is the well-known dipolar spin Hamiltonian sorted by Abragam into an alphabet of six letters [1]. The dipolar interaction is traceless and axially symmetric for isotropic PCs.

The spin Hamiltonian for anisotropic PCs is quite different although the basic interaction between magnetic dipoles remains the same. The differences arise because each magnetic moment is generally NOT aligned along the magnetic field; and because each magnetic moment becomes stronger or weaker as the direction of the magnetic field changes. The dipolar alphabet is altered, and three new letters must be added [2]. Or the spin Hamiltonian can be sorted into a set of terms with different symmetries. A major term is a traceless dipolar interaction with some rhombicity; but a $J S_1 S_2$ term appears with the symmetry of an exchange interaction but a coefficient proportional to the dipolar interaction times the g -matrix anisotropy. More surprising is a term having the form of the antisymmetric Dzyloshinskii-Moriya exchange interaction as a natural result of a classic dipolar interaction between anisotropic PCs.

The work was supported by the Ministry of Science and Higher Education of the Russian Federation (grant 14.W03.31.0034).

1. Abragam A.: The Principles of Nuclear Magnetism (Clarendon Press, Oxford, 1961)
2. Bedilo A.F., Maryasov A.G.: J. Magn. Reson. A **116**, 87–96 (1995)

Modified Landau-Lifshitz equation of motion for description of the spin dynamics in strongly correlated materials

S.V. Demishev

Prokhorov General Physics Institute of the Russian Academy of Sciences, Moscow 119991, Russia,
demis@lt.gpi.ru;

National Research University Higher School of Economics, Moscow 101000, Russia

The description of electron paramagnetic resonance (EPR) in strongly correlated electronic systems is a complex scientific problem. On the one hand, only a few examples are known in which the dynamic magnetic susceptibility was calculated [1, 2], and in some cases the theoretical dependences obtained are presented in a form that makes it difficult to use them to analyze the shape of the absorption line and find the spectroscopic parameters [1]. Therefore, at present, to analyze spin dynamics data in strongly correlated systems, the semiclassical approximation in the form of the Landau-Lifshitz (LL) equation is most often used [3]. In the standard paradigm, the LL equation is reduced to describing the precession of the magnetization vector \mathbf{M} around an external magnetic field \mathbf{H} and, therefore, at first glance, all “strongly correlated physics” is contained in static magnetization. From this point of view, the situation looks like that EPR does not provide fundamentally new physical information about systems with strong electronic correlations. At the same time, the analysis of experimental data shows that in the EPR of strongly correlated electron systems, a number of effects are observed that are difficult to interpret in the framework of the conventional approach [3, 4].

In this report, we consider examples of the modification of the LL equation and give examples of the application of modified equations to describe the EPR in those cases that have not yet been satisfactorily explained.

At first, the effect of quantum fluctuations of the magnetic moment is considered [5]. The LL spin dynamics for averaged magnetization acquires the form

$$\begin{aligned} \frac{dm_x}{dt} &= \gamma H_0 m_y - \gamma M_0 (1+a) h_y - \mathbf{v} \cdot \mathbf{m}_x (1+a) \\ \frac{dm_y}{dt} &= -\gamma H_0 m_x + \gamma M_0 (1+a) h_x - \mathbf{v} \cdot \mathbf{m}_y (1+a) \quad . \end{aligned} \quad (1)$$

We assume that \mathbf{H} is located along the z axis and oscillations of the magnetization occur in the x - y plane and may be described by small vector $\mathbf{m} = (m_x, m_y, 0)$. In Eq. (1), H_0 is the magnitude of external field, γ and \mathbf{v} stand for gyromagnetic ratio and relaxation frequency respectively. The quantum corrections depend on a single dimensionless parameter $a = 2\Delta M_z^2 / \mu_B M_0$, where ΔM_z^2 and M_0 are the amplitude of fluctuations and the average value of the magnetic moment per magnetic ion. On the basis of Eq. (1) a number of new effects in EPR in strongly correlated electronic systems are predicted, including: an

increase in the integral intensity and the appearance of universal relations connecting the contribution to the linewidth, the shift of the resonance field, and integrated intensity [5]. This model provides an explanation of EPR paradox in CeB_6 , where oscillating magnetization may exceed static magnetization [3, 5].

Secondly, a generalization of the LL equation of motion with anisotropic gyromagnetic ratio and spin relaxation is proposed and applied to the case of EPR. In the Faraday geometry, the model predicts polarization effect consisting in strong dependence of the EPR line shape and magnitude on orientation of vector \mathbf{h} of oscillating magnetization with respect to the crystal structure, so that EPR may be suppressed for some directions of \mathbf{h} . The EPR with anisotropic parameters possesses specific magnetic oscillations, which are different from standard circular rotation of the magnetization vector around the direction of external magnetic field. In general case the trajectory of the magnetization vector end is either elongated quasi-ellipse, the position of the main axis of which depends on the magnitude of the external magnetic field, or magnetic oscillations may acquire almost linear character. The model is successfully applied for the quantitative accounting of the polarization effect for EPR mode observed in CuGeO_3 doped with 2% of Co impurity, which remained unexplained for more than 15 years [4].

1. Abrahams E., Wölfle P.: Phys. Rev. B **78**, 104423 (2008)
2. Oshikawa M., Affleck I.: Phys. Rev. B **65**, 134410 (2002)
3. Demishev S.V.: Applied Magnetic Resonance, **51**, 473 (2020)
4. Demishev S.V., Semeno A.V., Ohta H.: Applied Magnetic Resonance **52**, 379 (2021)
5. Demishev S.V.: Doklady Physics **66**, 187 (2021)

New developments in multi-extreme THz ESR

**H. Ohta^{1,2}, S. Okubo^{1,2}, E. Ohmichi², T. Sakurai³, H. Takahashi^{1,2},
S. Hara³**

¹Molecular Photoscience Research Center, Kobe University, Japan, hohta@kobe-u.ac.jp

²Graduate School of Science, Kobe University, Japan

³Research Facility Center for Science and Technology, Kobe University, Japan

Our multi-extreme THz ESR covers the frequency region between 0.03 and 7 THz [1], the temperature region between 1.8 and 300 K [1], the magnetic field region up to 55 T [1], and the pressure region is extended from 1.5 GPa [2] to 2.5 GPa using the hybrid-type pressure cell [2]. Moreover, it also includes our recent developments of the torque magnetometry [4] and mechanically detected ESR [5] measurements using a commercially available membrane-type surface stress sensor, which is the extension from our micro-cantilever ESR [6], and it was applied to the microliter solution sample (myoglobin) [7]. Especially, our high-pressure THz ESR is extended up to 25 T [8] and applied to Cs₂CuCl₄ [9] and CsCuCl₃ [10] triangular antiferromagnets. Our multi-extreme THz ESR and other related topics on THz ESR are summarized in the special issue “Terahertz Spectroscopy” of Appl. Mag. Res. [11].

1. Ohta H. et al.: *J. Low Temp. Phys.* **170**, 511 (2013)
2. Sakurai T. et al.: *Rev. Sci. Instr.* **78**, 065107 (2007)
3. Fujimoto K. et al.: *Appl. Mag. Res.* **44**, 893 (2013); H. Ohta et al.: *J. Phys. Chem. B* **119**, 13755 (2015); Sakurai T. et al.: *J. Mag. Res.* **259**, 108 (2015); T. Sakurai et al.: *J. Phys. Soc. Jpn.* **87**, 033701 (2018)
4. Takahashi H. et al.: *J. Phys. Soc. Jpn.* **86**, 063002 (2017) (Editor’s Choice)
5. Takahashi H. et al.: *Rev. Sci. Instrum.* **89**, 036108 (2018)
6. Ohta H. et al.: *AIP Conf. Proceedings* **850**, 1643 (2006); E. Ohmichi et al.: *Rev. Sci. Instrum.* **79**, 103903 (2008); Takahashi H., Ohmichi E., Ohta H.: *Appl. Phys. Lett.*, **107**, 182405 (2015)
7. Okamoto T. et al.: *Appl. Phys. Lett.* **113**, 223702 (2018) (Editors Picks)
8. Sakurai T. et al.: *J. Mag. Res.* **296**, 1–4 (2018)
9. Zvyagin S.A. et al.: *Nature Communications* **10**, 1064 (2019)
10. Yamamoto et al.: *Nature Communications* **12**, 4263 (2021).
11. Ohta H., Sakai T. eds.: *Appl. Mag. Res.* **52**(4), 263–564 (2021), Special Issue “Terahertz Spectroscopy”.

Combining operando CW EPR and pulsed EPR spectroscopy for understanding heterogeneous catalysis

G. Jeschke¹, S.P. Schmid¹, M. Agrachev¹, J. Fischer¹, A. Ashuiev^{1,2}, D. Klose¹

¹Department for Chemistry and Applied Biosciences, ETH Zurich, Zurich, CH-8093, Switzerland, gjeschke@ethz.ch

²current address: Department of Chemistry, MIT, Boston (MA), 02139, USA

Most redox catalysts assume at least one paramagnetic state during a reaction cycle and active species of quite a few other transition metal catalysts are paramagnetic, too. Electron paramagnetic resonance (EPR) spectroscopy is certainly the most informative technique regarding electronic structure of such catalysts and may be the most informative technique regarding spatial structure. However, most heterogeneous catalysts feature spectator species in addition to the active surface species of interest. Sometimes, active species can be identified by changing catalyst composition and analyzing correlation of the EPR spectrum with activity. We will exemplify such a case on the Ziegler-Natta catalyst active in ethylene polymerization [1]. In other cases, operando EPR spectroscopy is required for assigning active species or proving that a species observed by EPR spectroscopy is involved in the reaction. Here, we discuss the main features of our current operando CW EPR setup and show examples for the information that can be obtained. Once an active catalyst species or other paramagnetic species involved in the reaction cycle has been identified, it can be characterized in more detail by applying advanced pulsed EPR techniques, thus shedding light on the mechanism of catalysis. We exemplify this for a radical driven path in zeolite-catalyzed conversion of methanol and methyl chloride to hydrocarbons and for Ziegler-Natta catalysis [2]. In the latter case, understanding of the EPR spectra profited tremendously from comparison with a well-defined species prepared by surface organometallic chemistry.

1. Ashuiev A., Humbert M., Norsic S., Blahut J., Gajan D., Searles K., Klose D., Lesage A., Pintacuda G., Raynaud J., Monteil V., Coperet C., Jeschke G.: *J. Am. Chem. Soc.* **150**, 143, 9791–9797 (2021)
2. Cesarini A., Mitchell S., Zichittella G., Agrachev M., Schmid S.P., Jeschke G., Pan Z.Y., Bodi A., Hemberger P., Perez-Ramirez J.: *Nature Catalysis* (2022), DOI : 10.1038/s41929-022-00808-0.

Insights into cation-anion hydrogen bonding in mesogenic ionic liquids from solid-state NMR

D. Majhi^{1,2}, J. Dai¹, S.V. Dvinskikh¹

¹Royal Institute of Technology, Stockholm, Sweden, sergeid@kth.se

²Stockholm University, Stockholm, Sweden

Ionic liquid crystals have the typical characteristics of ionic liquids and, at the same time, a nano-scale-organized structure of liquid crystals [1]. This leads to the unique combination of ionic conductivity of ionic liquids and the anisotropic physical and chemical properties of liquid crystalline materials. Although intermolecular forces in these ionic materials are dominated by long-range non-directional electrostatic interaction, weaker and more local hydrogen-bonding interactions have a profound effect on mesophase stabilization and are fundamental for the properties of mesogenic ionic liquids [2–4].

In this work, hydrogen-bonding interaction is studied in imidazolium-based mesogenic ionic liquids in their isotropic, smectic, and solid phases and in a nanoconfined state by proton solid-state NMR. The strong cation-anion hydrogen bonding observed in smectic phases provides direct support for the presence of ionic sub-layers which form in ionic liquid crystals regardless of location and alignment of the charged group in cation, particularly irrespective of whether charged group occupies a terminal or central position in cation structure. A comparison of the experimental results obtained in different phases shows that in the bulk materials the dynamic state of ions ranging from high reorientational and translational freedom to partial orientation and positional order to full immobilization, respectively, has no strong impact on the cation-anion hydrogen bond strength. On the other hand, nanoconfinement of ionic liquid crystals led to hydrogen bond disruption due to competing interactions of anions with the solid interface.

1. Goossens K., Lava K., Bielawski C.W., Binnemans K.: *Chem. Rev.* **116**, 4643 (2016)
2. Majhi D., Dai J., Komolkin A.V., Dvinskikh S.V.: *Phys. Chem. Chem. Phys.* **22**, 13408 (2020)
3. Dai J., Majhi D., Kharkov B.B., Dvinskikh S.V.: *Crystals* **9**, 495 (2019)
4. Dvinskikh S.V.: *Liq. Cryst.* **47**, 1975 (2020)

SECTION 1

THEORY OF MAGNETIC RESONANCE

Bridging the gap between fictitious spin-1/2 and true spin Hamiltonian approaches for spin quartet states with sizable ZFS tensors

T. Yamane¹, K. Sugisaki^{1,2}, K. Sato¹, K. Toyota¹,
D. Shiomi¹, T. Takui¹

¹Department of Chemistry and Molecular Materials Science, Graduate School of Science, Osaka Metropolitan University/Osaka City University, 3-3-138 Sugimoto, Sumiyoshi-ku, Osaka 558-8585, Japan, takui@omu.ac.jp, takui@sci.osaka-cu.ac.jp
²JST PRESTO, 4-1-8 Honcho, Kawaguchi, Saitama, Japan

High-spin (electron spin quantum number $S \geq 1$) metallocomplexes with sizable zero-field splitting (ZFS) tensors have kept attracting attention in various fields such as biological science, materials science including synthetic inorganic chemistry and spin qubit applications. In recently emerging fields, from the viewpoint of molecular designing, tuning of spin-orbit couplings is the focus of subjects relevant to molecular functionalities. We note that in view of theoretical calculations of magnetic tensors for the high-spin complexes sophisticated quantum chemical calculations have been developed and relevant DFT calculations frequently invoked to attempt to disclose their important electronic structures in spite of the fact that the DFT approach lacks reliability in some cases.

From the experimental side, the magnetic properties of high-spin metallocomplexes have frequently been determined by conventional X-band ESR spectroscopy with the help of fictitious spin-1/2 Hamiltonian approaches, noting that frequency domain Fourier transform ZFS spectroscopy has emerged, affording methodological advance in the experimental determination of sizable ZFS tensors of the high-spin complexes. The determined g_{eff} -values, however, never agree, in a straightforward manner, with those (g_{true} -values) of the true \mathbf{g} -tensors, which are obtained from reliable quantum chemical calculations. The discrepancy occurs also for their hyperfine tensors. In this work, we have attempted to revisit so far documented X-band ESR spectra of important penta-coordinated cobalt(II) complexes in their spin quartet states, in which their absolute D -values amount to $\sim 10 \text{ cm}^{-1}$ ($D < 0$) for the complexes. In order to fully analyze their X-band ESR fine-structure spectra, we have derived the general analytical expressions for magnetic-tensor relationships between the fictitious spin-1/2 and true magnetic tensors including hyperfine ones. Double perturbation treatments accommodating the Zeeman and hyperfine interaction perturbations have been developed to derive the relationships, bridging the gap between the two approaches and giving physical insights into the complex but exact or extremely accurate relationships. In this work, the rank-2 ZFS Hamiltonian is non-perturbed. Accuracy relevant to the derived expressions for the relationships have been discussed.

Bloch-Siegert effect in anisotropic paramagnetic centers with effective spin of 1/2

A.G. Maryasov¹, M.K. Bowman^{1,2}

¹Novosibirsk Institute of Organic Chemistry of the Siberian Branch of the Russian Academy of Sciences, Novosibirsk 630090, Russia, maryasov@nioch.nsc.ru

²Department of Chemistry & Biochemistry, The University of Alabama, Tuscaloosa, AL 35487, USA, mkbowman@ua.edu

The ground states of Kramers systems may be described as paramagnetic centers (PCs) having effective spin of 1/2 and anisotropic g -tensor, or, more accurately, g -matrix \overleftrightarrow{g} . External magnetic field $\mathbf{B} = \mathbf{B}_0 + \mathbf{B}_1$ (constant component, index 0, is parallel to z axis of the laboratory frame, LF; mw component, index 1, is parallel to x axis of LF) interacts with the magnetic moment of a PC, $\hat{\boldsymbol{\mu}}$, thus splitting energy levels of a Kramers doublet. Spin Hamiltonian of Zeeman interaction is $\hat{H}_Z = -\mathbf{B}^T \hat{\boldsymbol{\mu}}$. Upper index T means transposition of vector or matrix. The spin, $\hat{\mathbf{S}}$, and magnetic moment are closely related, $\hat{\boldsymbol{\mu}} = -\beta \overleftrightarrow{g} \hat{\mathbf{S}}$. The spin dynamics of anisotropic PCs has several features which are different as those of PCs with small anisotropy, e.g. organic free radicals PCs [1, 2]. The Zeeman Hamiltonian may be presented as interaction of spin with effective magnetic field \mathbf{B}_{eff} , $\hat{H}_Z = \beta \mathbf{B}_{\text{eff}}^T \hat{\mathbf{S}}$. The effective field is $\mathbf{B}_{\text{eff}} = \overleftrightarrow{g}^T \mathbf{B}$, it consists of two parts, the constant one, $\overleftrightarrow{g}^T \mathbf{B}_0$, and the alternating mw one, $\overleftrightarrow{g}^T \mathbf{B}_1$. It is important that these two parts are not perpendicular to each other whereas \mathbf{B}_0 and \mathbf{B}_1 are.

The Bloch-Siegert effect (BSE) describes influence of off-resonance component of mw field on magnetic resonance effect. In the case of isotropic PC this effect shifts resonance frequency by $\sim (B_1)^2/B_0$. Anisotropy in such situation leads to two off-resonance fields in the tilted rotating frame [2], the first along the quantization axis and the second perpendicular to it. The BSE is calculated up to the second order in small parameter B_1/B_0 . The resonance frequency shift and Rabi frequency correction are derived as function of g -matrix anisotropy. It is shown that BSE takes place even for circularly polarized mw field for anisotropic PCs.

The work was supported by the Ministry of Science and Higher Education of the Russian Federation (grant 14.W03.31.0034).

1. Maryasov A.G., Bowman M.K.: Applied Magn. Reson. **51**, 1201 (2020)
2. Maryasov A.G., Bowman M.K.: J. Magn. Reson. **221**, 69 (2012)

A possible manifestation of superabsorption in EPR spectroscopy

I.I. Geru

Academy of Sciences of Moldova, Department of Exact and Engineering Sciences,
Bd. Stefan cel Mare 1, MD 2001 Chisinau, Republic of Moldova, iongeru11@gmail.com

It is shown that if the concentration of paramagnetic centers is less than the maximum allowable for an EPR spectrometer, then it can be determined by registering paramagnetic superabsorption instead of paramagnetic absorption. Superabsorption is recorded as a time-reversed process of superradiance [1] with phase control of superradiance in the microwave resonator in presence of a dc magnetic field of resonance value. In this case, to implement superabsorption it is necessary to reverse in time not only the coherent state of the spin system, but also the collective state of microwave photons. For optical transitions in atoms, the transformation of superradiance into superabsorption under time-reversal was realized experimentally [2-4].

For a system of N spin-1/2 particles, the superradiant state is a spin-coherent state $|\psi\rangle_S$, which is localized within the equator on the N -particle Bloch sphere ($\mathbf{S} = N/2$, $M_S = 0$) and is defined in terms of the collective spin operator, \mathbf{S} ,

$$\hat{S}_\mu = \frac{\hbar}{2} \sum_{k=1}^N \hat{\sigma}_{k\mu}, \quad (1)$$

where \hbar is Planck's constant and $\hat{\sigma}_{k\mu}$ ($\mu = x, y, z$) represent the Pauli matrices for the k -th particle. In the absence of an input field, but in the presence of a dc resonance magnetic field, the emission process of superradiant spin state $|\psi\rangle_S$ in a microwave cavity can be described by a relation analogous to [2]:

$$\hat{U}(t)|\psi\rangle_S|0\rangle \approx |\psi'\rangle_S|\alpha\rangle, \quad (2)$$

where $\hat{U}(t) = \exp(-\frac{i}{\hbar}\hat{H}t)$ denotes the time-evolution operator of the Hamiltonian

$$\hat{H} = \hbar g \sum_{k=1}^N (\hat{a}^+ \hat{\sigma}_{k-} + \hat{a} \hat{\sigma}_{k+}). \quad (3)$$

In the Eq. (3) $\hat{\sigma}_\pm = \hat{\sigma}_{kx} \pm i\hat{\sigma}_{ky}$, g is the spin-cavity coupling constant (not to be confused with the g -factor) and \hat{a} (\hat{a}^+) is the annihilation (creation) operator. In the Eq. (2) the ket vector $|0\rangle$ denotes a photonic vacuum state, $|\alpha\rangle$ represents a photonic coherent state, and $|\psi'\rangle_S$ is the resulting spin state in the time evolution. This equation describes a process of superradiance (by analogy with the case of superradiance in the atomic systems[2]), where the average photon number of $|\alpha\rangle$ is proportional to N^2 . The approximation used in the equation (2) is valid at $g\tau \ll 1$, where τ is the spin-alternative magnetic field interaction time for paramagnetic centers in the cavity in presence of a resonance dc magnetic field. The final spin

state $|\psi'\rangle_S$ is a state rotated downwards by an angle in the order of $(g\tau)^2$ from the initial spin state $|\psi\rangle_S$ in the N -particle Bloch sphere, likewise with the case of atomic systems [2]. In this scheme, in the absence of an input field (but in the presence a resonance dc magnetic field), the superradiant state of correlated spins would generate a coherent-state superradiant field with its phase determined by that of the spin superradiant state. By controlling the phase of the prospective superradiant field opposite to that of an input microwave field in a cavity, we can make the superradiant state undergo an upwards transition in the Dicke ladder, resulting in a time reversal of the superradiance into superabsorption [2]. By introducing a field-phase-flipping operator $\hat{R}_\pi = \exp(-i\pi \hat{a}^\dagger \hat{a})$, that corresponds to π -rotation in the field phase space, and using the rotation $\hat{R}_\pi \hat{U}(t) \hat{R}_\pi^\dagger = \hat{U}(-t)$, one can obtain the relation:

$$\hat{U}(t)|\psi'\rangle_S|-\alpha\rangle \simeq |\psi\rangle_S|0\rangle. \quad (4)$$

Thus, by preparing the cavity with an initial photonic coherent state $|-\alpha\rangle$, we can achieve the time reversal of the superradiance process of the equation (2). The spin state returns to the initial state and the cavity microwave field is completely absorbed to become the vacuum state with the adsorbed number of microwave photons proportional to N^2 , as occurs in the case of superabsorption of optical photons in atomic systems [2].

1. Dicke R.H.: Coherence in spontaneous radiation processes. *Rhys. Rev.* **93**, 99–110 (1954)
2. Yang D., Oh S.-H., Han J. et al.: Realization of superabsorption by time reversal of superradiation, *Nature Photonics* **15**, 272–276 (2021)
3. Zens M. and Rotter S.: Superabsorption by time-reversal superradiance, *Nature Photonics* **15**, 251–252 (2021)
4. Higgins K.D.R., Benjamin S.C., Stace T.M., et al.: Superabsorption of light via quantum engineering, *Nat. Commun.* **5**, 4705 (2014)

Multiple-quantum NMR spectral intensity profiles under decoherence effects

V.E. Zobov¹, A.A. Lundin²

¹Kirensky Institute of Physics, Federal Research Center KSC SB RAS, Krasnoyarsk 660036, Russia, zobov.ve@gmail.com

²Semenov Institute of Chemical Physics, Russian Academy of Sciences, Moscow 117977, Russia, ya-andylun2012@yandex.ru

Multiple quantum (MQ) NMR spectroscopy of solids makes it possible not only to observe the growth and degradation of clusters of dynamically correlated spins, but also to control these processes using a controlled perturbation [1, 2]. The observed MQ spectrum is the sum of the MQ spectra from clusters with different numbers of spins K [3, 4] formed in a preparatory period of duration T . The contribution to above sum from different clusters of K spins we represented by a Gaussian MQ spectrum with a dispersion of $K/2$ multiplied by the weight function [3, 4] and by the function $\exp(-KB^2\tau^2/2)\exp(-A^2M^2\tau^2)$ what describes the cluster degradation [4]. The parameter B^2 characterizes the uncorrelated contribution to the local dipole field at the every spin of a cluster, and it does not depend on the local field at others spins, while parameter A^2 characterizes the field averaged over the cluster, and it acts in a correlated manner on all spins of the cluster. M is the coherence order. According the scheme of the experiment [1], $\tau = t_1$ is the duration of the evolution interval located between the preparatory interval and the mixing one, while with the scheme [2], $\tau = pt_T$, where t_T is the average time of occurrence of coherence on the interval $[0, T]$ [4], p is a small parameter. We have calculated the observed MQ spectrum numerically, and also obtained a simple formula for it by the saddle-point method:

$$G_M(T, \tau) \sim \exp\left\{-2\sqrt{2M^2(1 + \bar{K}_0 B^2 \tau^2 / 4)} / \bar{K}_0 - A^2 M^2 \tau^2\right\},$$

where $\bar{K}_0 = 1 + 2sh^2(T/\sqrt{2})$.

The formula obtained qualitatively correctly describes the results of calculations of the MQ spectra and experimental facts: the transformation of the Gaussian profile into an exponential one, the dependence of the relaxation rate of the MQ spectrum on M [1], and also the narrowing and stabilization of the MQ spectrum under the action of a perturbation [2].

1. Krojanski H.G., Suter D.: Phys. Rev. Lett. **93**, 090501 (2004)
2. Alvarez G.A., Suter D.: Phys. Rev. A **84**, 012320 (2011)
3. Lundin A.A., Zobov V.E.: J. Exp. Theor. Phys. **120**, 762 (2015)
4. Zobov V.E., Lundin A.A.: Appl. Magn. Res. **52**, 879 (2021)

SECTION 2

FULLERENES AND FULLERENE-BASED MATERIALS

Self-organization of fullerene derivatives in solutions and biological cells studied by pulsed field gradient NMR

V. Volkov^{1,2}, I. Avilova¹, A. Chernyak^{1,2}, P. Troshin¹

¹Institute of Problems of Chemical Physics RAS, Chernogolovka, Russia, vitwolf@mail.ru

²Science Center in Chernogolovka RAS, Chernogolovka, Russia

Self-organization of differently functionalized fullerene derivatives in solvents with various polarities was revealed by pulsed field gradient nuclear magnetic resonance (PFG NMR) of ¹H, ¹⁹F and ³¹P nuclei. Fullerene derivatives comprising no polar groups do not undergo any noticeable aggregation in carbon disulfide, deuterated chloroform and toluene-d₈. The particle diameters calculated from Stokes-Einstein equation vary from 1.2 to 1.4 nm for these solutions which is very close to the van der Waals diameter of the fullerene derivative molecules. The fullerene derivatives comprising polar –COOH, –COOK and –P(O)(OH)₂ groups appended to the carbon cage undergo self-assembling in solutions. The diameters of the formed clusters varied from 2.2 to 9.6 nm depending on the solvent and the temperature. The strongest tendency to self-assembling was revealed for water soluble fullerene derivatives in aqueous solutions where, presumably, water molecules are also incorporated in the structure of the clusters [1].

The self-organization of a water-soluble sulfur-containing fullerene adduct with captopril in deuterated water was studied by PFG NMR. Two types of fullerene particles characterized by the self-diffusion coefficients D_{s1} and D_{s2} of $(4.0 \pm 0.5) \cdot 10^{-10}$ and $(6.5 \pm 0.3) \cdot 10^{-11}$ m²/s, respectively, were revealed. The lifetime of fullerene aggregates was estimated [2].

Self-diffusion of water-soluble fullerene derivative (WSFD) C₆₀[S(CH₂)₃SO₃Na] 5H in mouse red blood cells (RBC) was characterized by ¹H PFG NMR. It was found that a fraction of fullerene molecules (~13% of the fullerene derivative added in aqueous RBC suspension) shows a self-diffusion coefficient of $(5.5 \pm 0.8) \cdot 10^{-12}$ m²/s, which is matching the coefficient of the lateral diffusion of lipids in the erythrocyte membrane ($D_L = (5.4 \pm 0.8) \cdot 10^{-12}$ m²/s). This experimental finding evidences the absorption of the fullerene derivative by RBC. Fullerene derivative molecules are also absorbed by RBC ghosts and phosphatidylcholine liposomes as manifested in self-diffusion coefficients of $(7.9 \pm 1.2) \cdot 10^{-12}$ m²/s and $(7.7 \pm 1.2) \cdot 10^{-12}$ m²/s, which are also close to the lateral diffusion coefficients of $(6.5 \pm 1.0) \cdot 10^{-12}$ m²/s and $(8.5 \pm 1.3) \cdot 10^{-12}$ m²/s, respectively. The obtained results suggest that fullerene derivative molecules are, probably, fixed on the RBC surface. The average residence time of the fullerene derivative molecule on RBC was estimated as 440 ± 70 ms. Thus, the pulsed field gradient NMR was shown to be a versatile technique for investigation of the interactions of the fullerene derivatives with blood cells providing essential information, which can be projected on their behavior *in-vivo* after intravenous administration while screening as potential drug candidates [3, 4].

NMR measurements were performed using equipment of the Multi-User Analytical Center of the Institute of Problems of Chemical Physics RAS and Science Center in Chernogolovka RAS with the support of State Assignment of the Institute of Problems of Chemical Physics RAS (state registration no. 0089-2019-0010/AAAA-A19-119071190044-3).

1. Chernyak A.V., Avilova I.A., Khakina E.A., Mumyatov A.V., Zabrodin V.A., Troshin P.A., Volkov V.I.: *Appl. Magn. Reson.* **47**, 859 (2016)
2. Avilova I.A., Chernyak A.V., Zhilenkov A.V., Troshin P.A., Volkov V.I. *Mendeleev Commun.* **26**, 146 (2016)
3. Avilova I., Khakina E., Kraevaya O., Kotelnikov A., Kotelnikova R., Troshin P., Volkov V. *Biochim. Biophys. Acta - Biomembr.* **1860**, 1537 (2018)
4. Avilova I.A., Soldatova Yu.V., Kraevaya O.A., Zhilenkov A.V., Dolgikh E.A., Kotel'nikova R.A., Troshin P.A., Volkov V.I. *Russ. J. Phys. Chem. A* **95**, 213 (2021)

Spin dynamics of endohedral fullerene $\text{Sc}_2@C_{80}(\text{CH}_2\text{Ph})$

Yu.E. Kandrashkin, R.B. Zaripov

Zavoisky Physical-Technical Institute, FRC Kazan Scientific Center of RAS, Kazan 420029, Russia, yuk@kfti.knc.ru

The endofullerene $\text{Sc}_2@C_{80}(\text{CH}_2\text{Ph})$ features one electron spin $1/2$ localized at the Sc_2 dimer interacting strongly (510 MHz) with two equivalent ^{45}Sc nuclear spins $7/2$, which yields 64 well resolved EPR transitions determined by the total nuclear spin j and its magnetic number m [1,2]. The isolation of the electron-nuclear spin system from the environment inside the fullerene cage and strong hyperfine interaction (HFI) provide many unique properties of these endofullerenes. The resonance conditions depend significantly on non-secular part of the HFI. Even a small variation of the external field changes the mutual distance between these lines.

The properties of the resonance lines in a liquid phase can be treated within the model of the rotational diffusion. Both, analytical expressions and numerical examination provide an excellent agreement between the experimental and simulated spectra. The studied endofullerene allows to examine with high accuracy the Wilson-Kivelson series over the j - and m -values. The distribution of the widths of all 64 homogeneously broadened lines can be described with only four adjustable parameters, including the anisotropic parts of the Zeeman and HFI, the correlation time, and the residual linewidth.

The analysis of the experimental data confirms the independence of the fullerene cage and the Sc_2 core motions. Three regimes of molecular motion were detected with the decreasing of the temperature: the free rotation of both the fullerene cage and its bi-metal core, the motion of the core in the frozen fullerene cage, and, finally, a state with a fixed structure of both parts of the metallofullerene molecules.

The authors thank RSF (Project Nr. 22-43-04424) for supporting of this research activity and the CSF-SAC FRC KSC RAS for providing necessary facilities to carry out this work.

1. Zaripov R.B., Kandrashkin Yu.E., Salikhov K.M., Büchner B., Liu F., Rosenkranz M., Popov A.A., Kataev V.: *Nanoscale* **12**, 20513 (2020)
2. Kandrashkin Yu.E., Zaripov R.B., Liu F., Büchner B., Kataev V., Popov A.A.: *Physical Chemistry Chemical Physics* **23**, 18206 (2021)

Application of endofullerene $\text{Sc}_2@C_{80}(\text{CH}_2\text{Ph})$ as a spectroscopic ruler

R.B. Zaripov, Yu.E. Kandrashkin

Zavoisky Physical-Technical Institute, FRC Kazan Scientific Center of RAS, Kazan 420029, Russia, zaripovruslan@gmail.com

Often, electron paramagnetic resonance (EPR) experiments require a precise calibration of the applied magnetic field. Typically, the stable radicals DPPH, BDPA and metal ions of chromium and manganese are used as a calibration standard. Here, we report results the calibration procedure based on the resonance properties of the dimetallofullerene $\text{Sc}_2@C_{80}(\text{CH}_2\text{Ph})$. In this molecule, a single unpaired electron is delocalized between two

scandium atoms encapsulated in a fullerene cage [1, 2]. The unusually strong hyperfine interaction, $a = 18.2$ mT (~ 510 MHz) with two equivalent nuclei provides a fully resolved EPR spectrum that consists of 64 resolved lines. At room temperature, the reference EPR transitions with the maximal $m = j$ and minimal $m = -j$ projection of the total nuclear spin are found to be evenly spaced over a large interval (ca. 0.25 T). The equidistance distribution of the reference points allows the examination of linear and non-linear properties of the magnetic field produced by the ion-core electromagnets. As an example, the application of the calibration procedure is demonstrated for Elexsys E580 spectrometer (Bruker, Germany), which is equipped with an ER 073 magnet.

The authors thank RSF (Project Nr. 22-43-04424) for supporting of this research activity and the CSF-SAC FRC KSC RAS for providing necessary facilities to carry out this work.

1. Zaripov R.B., Kandrashkin Yu.E., Salikhov K.M., Büchner B., Liu F., Rosenkranz M., Popov A.A., Kataev V.: *Nanoscale* **12**, 20513 (2020)
2. Kandrashkin Yu.E., Zaripov R.B., F. Liu F., B. Büchner B., Kataev V., Popov A.A.: *Physical Chemistry Chemical Physics* **23**, 18206 (2021)

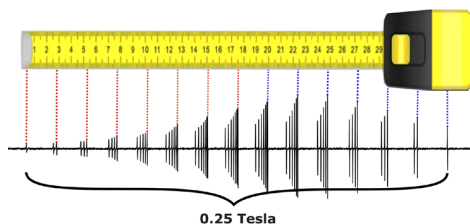


Fig. 1. EPR spectra of $\text{Sc}_2@C_{80}(\text{CH}_2\text{Ph})$ at liquid toluene recorded at Q-band (34.2 GHz) at room temperature. The dotted lines show the reference lines that are used in the calibration procedure.

Study of spin coherence processes of endohedral fullerene $\text{Sc}_2@C_{80}(\text{CH}_2\text{Ph})$

I.T. Khairutdinov, R.B. Zaripov, Yu.E. Kandrashkin

Zavoisky Physical-Technical Institute, FRC Kazan Scientific Center of RAS, Kazan 420029, Russia, semak-olic@mail.ru

Endohedral fullerenes represent an interesting class of the molecules with the encapsulated kernel isolated from the environment. Thus, the endofullerenes with the unpaired electrons are promising materials for quantum information and quantum processing research. Endofullerene $\text{Sc}_2@C_{80}(\text{CH}_2\text{Ph})$ has one unpaired electron ($S = 1/2$) delocalized over the two scandium atoms and is characterized by a strong hyperfine interactions (HFI) with two equivalent nuclear spins ^{45}Sc ($I = 7/2$). Due to the significant contribution of the non-secular part of the HFI, all 64 EPR transitions are well-resolved [1, 2] (see Fig. 1). Each transition corresponds to a certain value of the total nuclear spin j and its projection m . The steady state EPR linewidths can be derived within the expanded Kivelson model [3]. A good correlation between the linewidths and the quantum numbers m and j were obtained [2].

Here we present the results of the investigation of the transverse magnetization dephasing by the Hahn echo method. The measurements were carried out on several resonant transitions at different temperatures. The dependence of the phase relaxation time on the quantum numbers m and j is obtained. The analysis of the experimental data within the Kivelson expansion terms is discussed.

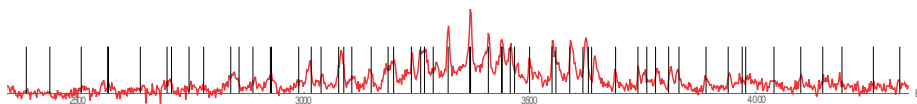


Fig. 1. X-Band EPR spectra of $\text{Sc}_2@C_{80}(\text{CH}_2\text{Ph})$ at 80 K. Vertical lines indicate the positions of resonant transitions for the molecules with different quantum numbers j and m .

The authors thank RSF (Project Nr. 22-43-04424) for supporting of this research activity and the CSF-SAC FRC KSC RAS for providing necessary facilities to carry out this work.

1. Kandrashkin Yu.E., Zaripov R.B., Fupin Liu, Buchner Bernd, Kataev V.E., Popov A.A.: Phys. Chem. Chem. Phys. **23**, 18206–18220 (2021)
2. Kandrashkin Yu.E., Zaripov R.B., Salikhov K.M., Rosenkranz Marco, Fupin Liu, Büchner Bernd, Kataev V.E., Popov A.A.: Nanoscale **12**, 20513 (2020)
3. Wilson R., Kivelson D., ESR Linewidths in Solution. I. Experiments on Anisotropic and Spin-Rotational Effects, J. Chem. Phys. **44**, 154–168 (1966)

SECTION 3

CHEMICAL AND BIOLOGICAL SYSTEMS

New applications of MOFs aided by EPR

M.V. Fedin, A.S. Poryvaev, D.M. Polyukhov, O.A. Krumkacheva

International Tomography Center SB RAS, Novosibirsk 630090, Russia, mfedin@tomo.nsc.ru

Metal-organic frameworks (MOFs) draw high attention over past decades, being broadly studied for their basic structural/functional properties and potential practical applications. MOFs are mesoporous solids, which can be used for gas separation/storage, molecular sieving, catalysis, drug delivery etc. Most pristine MOFs are either diamagnetic or magnetically-concentrated, thus limiting information provided by EPR spectroscopy in MOF research. At the same time, large enough pores and channels of MOFs allow incorporating various guest molecules, including paramagnetic spin probes, which makes EPR detection straightforward.

In recent series of works we have developed methodology of encapsulated spin probes to study internal surface and functionality of MOFs using EPR [1–6]. In this approach, stable nitroxide radicals are embedded into the MOF cavities during synthesis and remain permanently entrapped. It has been shown that they report valuable information on the solvent molecules present/absent in the MOF cavities, on the pore filling kinetics and on the pore structure [1, 2]. Using this method, one can successfully adjust conditions for separation of liquid mixtures, e.g. separation of xylene isomers [1, 2], separation of benzene/cyclohexane mixtures [3]. It is also convenient to assess micro- vs. macrodiffusion in shaped MOF particles prepared for particular applications [4]. Amorphization of MOFs under pressure can be mitigated upon spin-probe EPR control [5]. Finally, drug delivery applications of MOFs can also be benchmarked using this methodology [6]. In this report we review recent progress in spin-probe EPR study of MOF's functionality and sketch future directions and opportunities.

This work was supported by Russian Science Foundation (drug delivery in MOFs: 20-73-10239; guest molecules diffusion in MOFs: 22-73-10239).

1. Polyukhov D.M. et al.: *Nano Lett.* **19**, 6506 (2019)
2. Polyukhov D.M. et al.: *ACS Appl. Mater. Interf.* **13**, 40830 (2021)
3. Poryvaev A.S. et al.: *Micropor. Mesopor. Mat.* **330**, 111564 (2022)
4. Efremov A.A. et al.: *Micropor. Mesopor. Mat.* **330**, 111713 (2022)
5. Poryvaev A.S. et al.: *ACS Appl. Mater. Interf.* **12**, 16655 (2020)
6. Poryvaev A.S. et al.: *J. Phys. Chem. C* **125**, 15606 (2021)

Observation of triplet charge separation state (3CS) with time-resolved electron paramagnetic resonance spectra in compact electron donor-acceptor dyads

J. Zhao¹, X. Zhao¹, A.A. Sukhanov², V.K. Voronkova²

¹State Key Laboratory of Fine Chemicals, School of Chemical Engineering, Dalian University of Technology, Dalian, 116024, P. R. China, zhaojzh@dlut.edu.cn

²Zavoisky Physical-Technical Institute, FRC Kazan Scientific Center of RAS, Kazan 420029, Russia, vio@kfti.knc.ru

Long-lived charge separated (CS) states are important for fundamental photochemistry study, as well as for application in photocatalysis, photovoltaics and artificial photosynthesis, etc.[1] Conventionally, long CS state was observed in electron donor-acceptor dyads containing long, saturated linker, with the purpose to reduce the electronic coupling between the electron donor and acceptors. Another method is to construct polyads containing multiple electron acceptors with gradient electron accepting ability, so that the final CS state is with very weak coupling between the donor and the acceptor. However, this is with the expense of difficult synthesis, and low CS state energy. Thus, it is highly desired to develop a simple molecular structure profile to attain long-lived CS state.

One new strategy to attain the long-lived CS state is using the electron spin control method, i.e. to form the triplet CS state (3CS), instead of the 1CS state or the spin correlated radical pair (SCR) [1]. The charge recombination (CR) is electron spin selective, thus the CR of the 3CS@S0 is forbidden, whereas

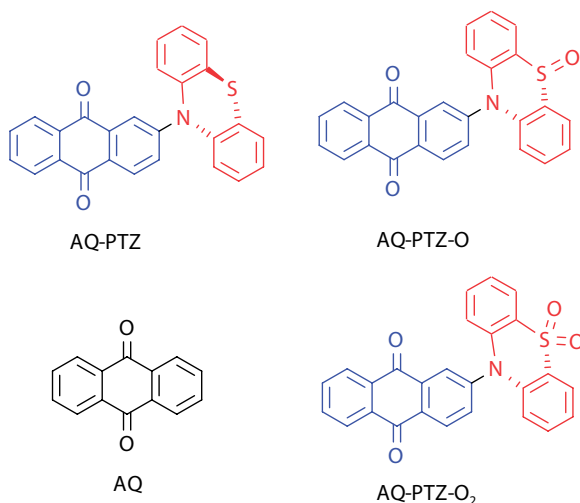


Fig. 1. The electron donor-acceptor dyads AQ-PTZ, AQ-PTZ-O, AQ-PTZ-O₂ and the reference compound AQ.

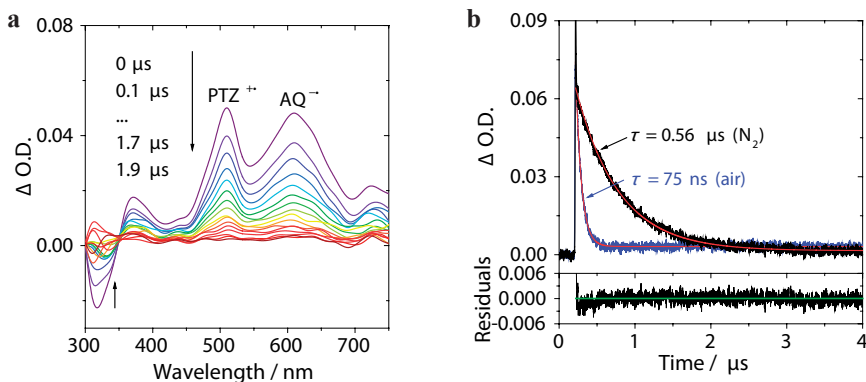


Fig. 2. **a** Nanosecond transient absorption spectra of AQ-PTZ, $c = 1.0 \cdot 10^{-4}$ M, $\lambda_{\text{ex}} = 355$ nm. In deaerated CHX. **b** Decay traces at 510 nm in deaerated and aerated CHX, 25°C.

1CS@S0 is electron spin allowed. Some electron donor-acceptor dyads showing the long-lived 3CS state based on the electron spin control method have been developed, but more examples are needed to study the molecular structure-property relationship. Herein we studied a few anthraquinone (AQ)-phenothiazine (PTZ) dyads (Fig. 1) [2]. A long-lived triplet charge separated state (3CS, Lifetime: 0.56 ms) was observed in AQ-PTZ, a compact electron donor-acceptor dyad with electron donor phenothiazine (PTZ) and acceptor anthraquinone (AQ) directly connected by a single C-N bond (AQ-PTZ, Fig. 2). The 1CS state energy (2.0 eV in cyclohexane) is lower than the 3AQ (2.7 eV) or the 3PTZ state (2.6 eV). By oxidation of the PTZ unit, thus increasing of the 1CS state energy (2.7 eV. In cyclohexane), thermally activated delayed fluorescence (TADF) was observed [$t = 17.7$ ns (99.9%)/1.5 ms (0.1%)] for AQ-PTZ-O and AQ-PTZ-O₂. Time-resolved electron paramagnetic resonance (TREPR) spectra confirm the electron

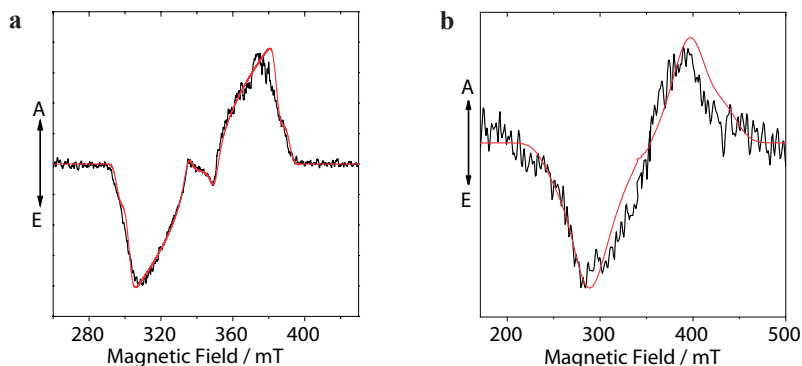


Fig. 3. Experimental TREPR spectra (black lines) and simulations (red line) at 80 K. **(a)** AQ-PTZ in frozen DCM/MeTHF (1:3, v/v), $c = 1.0 \cdot 10^{-4}$ M, $\lambda_{\text{ex}} = 420$ nm, **(b)** AQ in frozen 2-propanol, $c = 3.0 \cdot 10^{-4}$ M, $\lambda_{\text{ex}} = 355$ nm.

spin multiplicity of the ^3CS state, and the zero-field-splitting (ZFS) parameters $|D|$ and $|E|$ are 48.2 mT and 11.2 mT, respectively (Fig. 3.). The references compounds show much large ZFS D parameters (Fig. 3), thus confirm that the transient species we observed for AQ-PTZ is ^3CS state. These results are useful for design of compact electron donor-acceptor dyads to access the long-lived ^3CS state and study of the TADF mechanism.

1. Verhoeven J.W.: *J. Photochem. Photobiol., C Photochem. Rev.* **7**, 40-60 (2006)
2. Zhao X., Sukhanov A., A. Jiang X., Zhao J., Voronkova V.K.: *J. Phys. Chem. Lett.* **13**, 2533–2539 (2022)

Probing small-angle molecular motions with EPR spectroscopy: Dynamical transition and molecular packing in disordered solids

S.A. Dzuba, E.A. Golysheva

Voevodsky Institute of Chemical Kinetics and Combustion, Russian Academy of Sciences,
Novosibirsk 630090, Russia, dzuba@kinetics.nsc.ru

Disordered molecular solids present a rather broad class of substances of different origin – amorphous polymers, materials for photonics and optoelectronics, amorphous pharmaceuticals, simple molecular glass formers, other glassy materials. Frozen biological media also in many respects may be referred to this class. These media are interesting from both practical and fundamental points of view. Their theoretical description however still does not exist, and only phenomenological models of the dynamics and structure can be developed explaining results of the experimental approaches used. Among other approaches, electron paramagnetic resonance (EPR) applied to spin probes and labels can deliver useful information. EPR is employed in its conventional continuous wave (CW) and pulsed – electron spin echo (ESE) – versions. It allows probing small-angle orientational molecular motions, intrinsically inherent to all molecular solids. CW EPR spectra are sensitive to dynamical librations of molecules while ESE probes stochastic molecular librations. In this lecture, different manifestations of small-angle motions in EPR of spin probes and labels are discussed. It is shown that data on EPR-detected dynamical librations provide information comparable to the results of studying of mean-squared atomic displacement in neutron scattering, and that ESE-detected stochastic librations allow concluding about features of nanoscale molecular packing. The possible applications are analyzed for gel-phase lipid bilayers and biological membranes interacting with proteins, peptides and cryoprotectants, for globular proteins and intrinsically disordered proteins (IDPs), and for other molecular solids.

Application of EPR spectroscopy to determine the content of nitric oxide in the brain and heart of rats

**Kh.L. Gainutdinov^{1,2}, V.V. Andrianov^{1,2}, A.A. Sukhanov¹, R.B. Zaripov¹,
L.V. Bazan¹, N.G. Shayakhmetov³, M.M. Bakirov¹, G.G. Yafarova²**

¹Zavoisky Physical-Technical Institute, FRC Kazan Scientific Center of RAS, Kazan 420029, Russia, kh_gainutdinov@mail.ru

²Institute of Fundamental Medicine and Biology of Kazan Federal University, Kazan 420008, Russia

³Interregional Clinical Diagnostic Center, Kazan 420101, Russia

Nitric oxide (NO) is known as one of the most important signaling molecules regulating the physiological functions of the organism and the metabolism of cells [1]. NO participates in the regulation of intracellular concentration of Ca^{2+} ions through activation of hem-containing soluble guanylylcyclase and ADP-ribosyltransferase, and is involved in the regulation of pH during cerebral ischemia [2]. According to the current understanding the development of cerebral ischemia and the subsequent stroke is associated with impaired cerebral blood flow, as well as violations of its regulation by the NO system [3]. Due to a significant decrease in physical activity, especially in children and people who are not engaged in physical labor, the problem of changes in physiological functions and mechanisms of their development, including the role of NO, in conditions of limited motor activity has become more urgent [4].

There are many methods of measuring NO production in biological systems. Precise measurement of both the steady concentration of NO and the speed of NO generation in biological systems is a difficult task due to the low activity of NO synthases and its short half-life. In last years electronic paramagnetic resonance (EPR) proved to be one of the most efficient methods for the detection and quantification of nitric oxide in biological tissues [2, 5]. We used EPR spectroscopy to study the dynamics of NO in the brain and heart of rats after modeling a number of pathological processes. The intensity of NO production by EPR spectroscopy was measured using the spin trap technique [2, 6], which is based on the reaction of a radical (in this case NO) with the spin trap. The complex of Fe^{2+} with diethyldithiocarbamate (DETC) was used to capture NO and to form a stable ternary complex $(\text{DETC})_2\text{-Fe}^{2+}\text{-NO}$ in the animal tissues. Those complexes are characterized by an easily recognizable EPR spectrum with g -factor $g = 2.035\text{--}2.040$ and a triplet hyperfine structure [5, 6]. The spectra of the complex $(\text{DETC})_2\text{-Fe}^{2+}\text{-NO}$ were measured on Bruker X spectrometers (9.50 GHz) EMX/plus with a temperature module ER 4112HV and ER 200 SRC with a magnetic field modulation of 100 kHz and a modulation amplitude of 2 G, with a microwave power of 30 mW, a time constant of 200 ms and a temperature of 77 K in a finger Dewar of the Bruker company.

By the methods of EPR spectroscopy our team has evaluated effect of ischemic stroke on the intensity of NO production in the tissues of the brain, heart and liver of rats *in vivo*. Brain ischemia was simulated by ligation at the level

of bifurcation of the common carotid arteries. The measurements of NO and copper were carried out by EPR spectroscopy. It was found a significant reduction of NO content in the olfactory bulb of the brain of rats on the 1st and 2nd days after modeling of ischemia caused by ligation of the carotid arteries. The level of NO production was also reduced on the 1st and 2nd days after ischemia in rats after modeling of the ischemia with immediate intranasal administration of mesenchymal stem cells as compared to with the group of intact animals. It was not found the significant difference of the NO content in rats after modeling of the ischemia with immediate intranasal administration of mesenchymal stem cells relative to ischemic rats.

It was found an increase in the intensity of production of NO in the rats hearts after 90-days hypokinezia. Of nonselective blockade of NO-synthase activity by L-NAME to hypokinezed rats resulted in a decrease of content of NO in atrias and ventricles of the heart by 67–70%. Selective blockade of inducible NO-synthase caused a decrease of the content of NO in the tissues of the atrias and ventricles by 60–65%. The obtained results suggest that increasing of NO production under hypokinezia occurs through the activation of NO-synthase activity.

EPR measurements were performed with the financial support from the government assignment for FRC Kazan Scientific Center of RAS. The processing of the results was carried out at Kazan Federal University in the framework of fulfilling the state assignment no. 0671-2020-0059.

1. Vanin A.F.: Nitric Oxide **54**, 15–29 (2016)
2. Vanin A.F., Huisman A. et al.: Methods in Enzymology **359**, 27–42 (2003)
3. Pacher P., Beckman J.S., Liaudet L.: Physiol. Rev. **87**, 315–427 (2007)
4. Andrianov V.V., Sitdikov F.G. et al.: Ontogenez **39**, no. 6, 437–442 (2008)
5. Hawkins C.L., Davies M.J.: Biochimica et Biophysica Acta **1840** 708–721 (2014)
6. Mikoyan V.D., Kubrina L.N. et al.: Biochim. Biophys. Acta **1336**, No 2, 225–234 (1997)

Dynamics of spin centers in TiO₂ nanotubes/Cu_xO composites

E.A. Konstantinova¹, E.V. Kytina¹, T.P. Savchuk^{1,2}

¹Physics Department, M.V. Lomonosov Moscow State University, Russia, liza35@mail.ru

²National Research University of Electronic Technology – MIET, Zelenograd, Moscow, Russia

Nanostructured titanium dioxide (TiO₂) is currently being actively studied by the world scientific community, since it has a number of properties that are important from a practical point of view [1]. Very important property is the presence of a large specific surface area accessible to environmental molecules, which makes this material promising for use as photocatalysts or sensors [2]. The actual task of today is the development of efficient photocatalysts based on TiO₂ nanotubes for converting carbon dioxide into more energy-intensive hydrocarbon compounds and the study of their electronic properties, in particular, the nature and main characteristics of defects. Therefore, the aim of this study was to identify the spin centers (defects) in the TiO₂ nanotubes (TiO₂ NTs) with different morphology and to study their properties. Since the most of defects in the TiO₂ is paramagnetic, we used EPR spectroscopy.

The synthesis of multi-walled and single-walled TiO₂ nanotubes (MW-TiO₂ NTs and SW-TiO₂ NTs) is described in [3]. Note that the multi-wall NTs means that ones have an outer layer of pure titania and an inner layer of carbon doped titania; single-wall NTs have only an outer layer. Copper oxide Cu_xO was deposited onto the surface of the MW-TiO₂ NTs arrays using the Successive Ionic Layer Adsorption and Reaction (SILAR) method. The source of copper ions was an aqueous solution of CuCl₂ · 2H₂O, the pH of which was adjusted to 10 with a solution of 25% ammonia (NH₄OH). A solution of ethyl alcohol heated to 70 °C with deionized water in a ratio of 1:3 was used as an anion source. The SILAR method consists of three stages. At the first stage, the sample is immersed in an aqueous solution of copper chloride for 30 seconds, which contains [Cu(NH₃)₄]⁺² ions. In the second step, the sample is immersed in a solution of ethyl alcohol with deionized water for 7 seconds. At the third stage, the sample is washed in deionized water for 30 seconds. The amount of copper oxide Cu_xO deposited on MW-TiO₂ NTs was varied by varying the number of ion deposition cycles: 10, 30, and 60 monolayers (samples MW-TiO₂NTs/Cu_xO-10, MW-TiO₂NTs/Cu_xO-30, MW-TiO₂NTs/Cu_xO-60 and SW-TiO₂NTs/Cu_xO-10, SW-TiO₂NTs/Cu_xO-30, SW-TiO₂NTs/Cu_xO-60, respectively). After ion layering, the resulting structures were subjected to heat treatment in an air atmosphere at a temperature of 300 °C for 60 minutes at a heating rate of 30 °C/min.

The EPR spectrum of the initial MW-TiO₂NTs samples is dominated by the signal from dangling carbon bonds (C[·]), the Landé *g* factor *g* = 2.0027, while the EPR spectrum of SW-TiO₂NTs is due to the Ti³⁺/oxygen vacancies centers, *g*₁ = 1.9961, *g*₂ = .9697 [4]. The presence of carbon in the samples is probably due to the presence of ethylene glycol in the electrolyte and is also confirmed by elemental analysis data. The EPR spectra of the TiO₂NTs/Cu_xO nanocom-

posites are a superposition of several EPR signals. First, a strong EPR signal from copper ions Cu^{2+} ($g = 2.1612$) [4] is recorded, which indicates the presence of the CuO phase. We also observed a superposition of lines from defects of the C^{\bullet} type (detected in the initial structures), and from O_2^- radicals ($g_1 = 2.029$, $g_2 = 2.009$, $g_3 = 2.003$). The appearance of O_2^- radicals can be explained by the adsorption of oxygen molecules on oxygen vacancies on the surface of TiO_2 and, probably, on the surface of copper oxide nanoparticles, followed by the capture of electrons from the conduction band. This can lead to a limitation of the electron transport and, accordingly, to a decrease in the conductivity in the $\text{TiO}_2\text{NTs}/\text{Cu}_x\text{O}$ nanocomposites compared to the initial TiO_2 NTs, what we observe in the experiment. With an increase in the number of copper oxide deposition cycles, the intensity of the line from Cu^{2+} ions increases. In addition, the intensity of the EPR signal from O_2^- radicals also increases.

The results obtained open up new possibilities for the development of photocatalysts based on $\text{TiO}_2\text{NTs}/\text{Cu}_x\text{O}$ composites. The study was supported by a grant from Russian Science Foundation № 21-19-00494.

1. Chiesa M., Livraghi S., Paganini M. C., Salvadori E., Giamello E.: Nitrogen-Doped Semiconducting Oxides. Implications on Photochemical, Photocatalytic and Electronic Properties Derived from EPR Spectroscopy. *Chem. Sci.* **11** (26), 6623 (2020)
2. Low J., Yu J.; Jaroniec M., Wageh S., Al-Ghamdi A.A.: Heterojunction Photocatalysts. *Adv. Mater.* **29** (20), 1601694 (2017)
3. Gavrilin I., Dronov A., Volkov R., Savchuk T., Dronova D., Borgardt N., Pavlikov A., Gavrilov S., Gromov D.: *Appl. Surf. Sci.* **516**, 146120 (2020)
4. Kokorin A.I.: "Electron spin resonance of nanostructured oxide semiconductors", in: "Chemical physics of nanostructured semiconductors", edited by Kokorin A.I., Bahnemann D.W., VSP-Brill Academic Publishers, Boston (2003)

Supramolecular materials: design, application, and perspectives

E. Skorb¹, A. Timralieva¹, P. Nesterov¹, A. Kokorin^{2,3}

¹Infochemistry Scientific Center, ITMO University, St Petersburg 197101, Russia, skorb@itmo.ru

²N.N. Semenov Federal Research Center for Chemical Physics Russian Academy of Sciences, Moscow 119991, Russia

³Plekhanov Russian University of Economics, Moscow 115093, Russia

Supramolecular chemistry is a perspective area of chemical science nowadays. These assemblies are held together *via* non-covalent interactions that greatly depend on input stimuli. This feature opens the way to achieve programmable ‘smart’ materials with switching properties.

Supramolecular assemblies show a great potential as encapsulation systems for different organic and active molecules such as dyes [1]. Guest molecules become the center of nucleation of supramolecular melamine barbiturate with the decrease of crystal twinning and release during crystals’ destruction under pH change. Supramolecular crystals with encapsulated dyes can be used for time-prolonged bacteria staining [2]. Supramolecular material such as melamine cyanurate tend to form *via* two different ways because of the initial components’ ratio [3]. It is a simple approach to vary properties of supramolecular materials and simplify the encapsulation process using different design schemes.

The most interesting, melamine barbiturate supramolecular assembly shows a great potential in radical trapping [4]. It contains two different radical centers, the first one is associated with O-radicals. The number of spins increases during the light irradiation in more than two times and does not decrease to the initial level even after seven days [5]. Furthermore, the number of spins and the sensitivity of the light irradiation greatly depends on pH value. Thus, supramolecular materials such as melamine barbiturate and melamine barbiturate can be used as encapsulation systems for different bioactive molecules and radicals with pH or light activation.

The work was carried out with the support of the Ministry of Science and Higher Education of the Russian Federation (agreement № 075-15-2021-1349).

1. Nesterov P., Shilovskikh V., Sokolov A., Gurzhiy V., Novikov A., Timralieva A., Belogub E., Kondratyuk N., Orekhov N., Skorb E.: *Symmetry* **13**, 1119 (2021)
2. Imoro N., Shilovskikh V., Nesterov P., Timralieva A., Gets D., Nebalueva A., Lavrentev F., Novikov A., Kondratyuk N., Orekhov N., Skorb E.: *ACS Omega* **6**, 17267–17275 (2021)
3. Orekhov N., Kondratyuk N., Logunov M., Timralieva A., Shilovskikh V., Skorb E.: *Crystal Growth & Design* **21**, 1984–1992 (2021)
4. Shilovskikh V., Timralieva A., Belogub E., Konstantinova E., Kokorin A., Skorb E.: *Applied Magnetic Resonance* **51**, 1–11 (2020)
5. Shilovskikh V., Timralieva A., Nesterov P., Novikov A., Sitnikov P., Konstantinova E., Kokorin A., Skorb E.: *Chem. Eur. J.* **26**, 16603 (2020)

Structure and catalytic properties of Cu(II) complexes with fluorinated ligands

A.I. Kokorin^{1,2}, N.A. Chumakova^{1,3}, Yu.N. Kozlov^{1,2}, A.A. Shubin⁴

¹Department of Dynamics of Chem-Bio Processes, N.N. Semenov Federal Research Center for Chemical Physics RAS, Moscow 119991, Russia, alex-kokorin@yandex.ru

²Dept. of Chemistry, Plekhanov Russian University of Economics, Moscow 115093, Russia

³M.V. Lomonosov Moscow State University, Chemistry Department, Moscow 119991, Russia, harmonic2011@yandex.ru

⁴Institute of Solid State Chemistry and Mechanochemistry SB RAS, Novosibirsk 630128, Russia, aashubin@ngs.ru

Copper(II) complex with fluorinated ligands $\text{Cu}[\text{CF}_3\text{-C}(\text{NH})\text{-CF}=\text{C}(\text{NH})\text{-CF}_3]_2$ (Fig. 1) has been synthesized and studied by the X-ray analysis in [1]. It was found that this complex can exist in three thermochromic phases (α , β , γ) and six polymorphic modifications in a crystalline state which were structurally characterized. Such Cu(II) complexes can be in principle rather active oxidative homogeneous catalysts [2].

Therefore, we have studied this complex by the X-band EPR spectroscopy, DFT calculations and kinetically in the test reaction of hydrogen peroxide catalytic decomposition in CH_3CN and in H_2O : $\text{CH}_3\text{CN} = 1:5$ mixed solutions at 313 K. EPR spectra were recorded on Bruker EMX500 Plus spectrometer.

Figures 2 and 3 represent experimental and DFT calculated EPR spectra of Cu(II) complex dissolved in CH_3CN solution (Fig. 2) at 298 and in toluene at 90 K (Fig. 3). Evidently, the spectra simulation reproduces well both hyperfine structure (hfs) and super-hfs due to partial delocalization of the unpaired electron spin density to the nitrogen ^{14}N atoms of both bidentate ligands. All measured and calculated spin Hamiltonian parameters will be given in the report as well as details and the results of DFT calculations showed the difference between

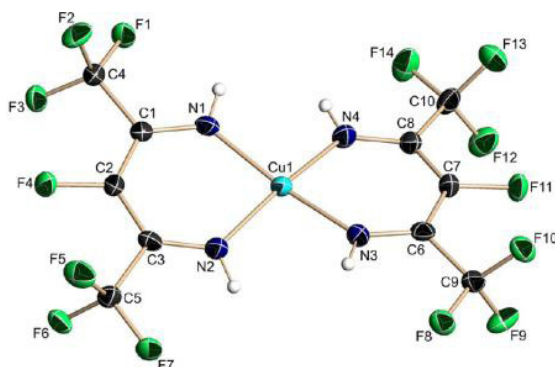


Fig. 1. Molecular structure of Cu(II) complex from X-ray diffraction [1].

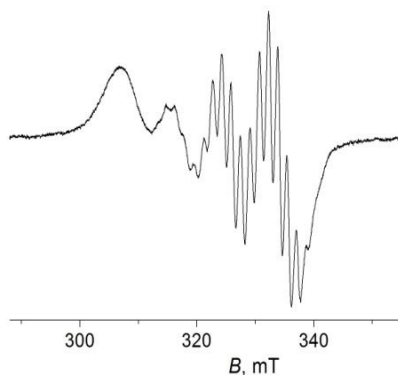


Fig. 2. Experimental EPR spectrum of Cu(II) complex dissolved in CH₃CN and recorded at 298 K.

square-planar and slightly distorted spatial configurations of the equatorial plane. We have also observed by EPR a phase transition between two phases, presumably α and β .

Catalytic properties of the Cu(II) complex were studied kinetically in the test reaction of H₂O₂ catalytic decomposition using UV-Vis and EPR spectroscopy.

Figure 4 illustrates two main results obtained: (1) H₂O₂ undergoes rather effective decomposition, and (2) Cu(II) complex initiating the reaction is also changes becoming diamagnetic, hence, this complex is not a real catalyst. At the end of the reaction, solution becomes transparent and colorless but a dark-yellowish precipitate is formed. After addition slightly acidic H₂SO₄, precipitate dissolves and solution becomes slightly blue. Most likely this precipitate is Cu(II) hydroxide.

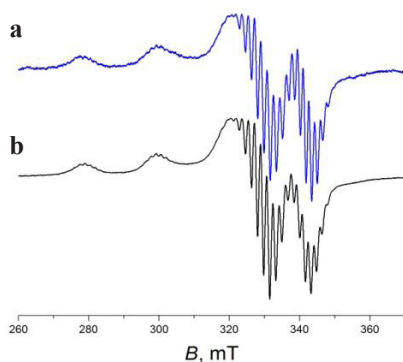


Fig. 3. **a** The optimized spectrum of Cu(II) complex in toluene at 90 K. **b** The DFT calculated EPR spectrum.

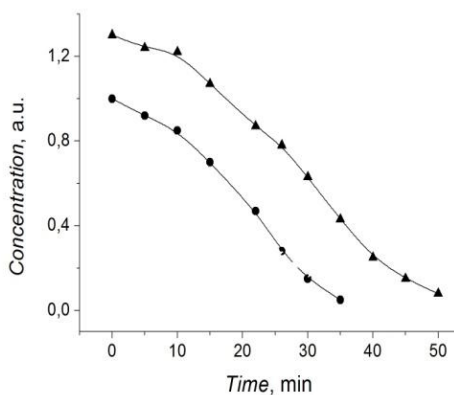


Fig. 4. Kinetic curves of H_2O_2 (▲) and Cu(II) complex (●) obtained by optical absorption at 313 K.

Acknowledgements. This work was funded by Russian Foundation for Basic Research (Project no. 21-53-54001) and within the framework of the Program of Fundamental Research of the Russian Federation (Reg. no. 122040500068-0). A.A.S. thanks the Ministry of Science and High Education of Russian Federation for financial support (grant No. 121032500059-4).

1. Khrustalev V.N., Kostenko S.O. et al.: *Inorg. Chem.* **51**, 10590–10602 (2012)
2. Temkin O.N.: *Homogeneous Catalysis with Metal Complexes: Kinetic Aspects and Mechanisms*. John Wiley & Sons, Ltd, New York (2012)

Photoinduced reactions of spin centers in Nb and N doped titania nanocrystals

E.V. Kytina, E.A. Konstantinova, A.V. Marikutsa

M.V. Lomonosov Moscow State University, Moscow, Russia, kata13012002@mail.ru

Nanocrystalline titania (TiO_2) is very promising material for modern sensor applications, having unique properties such as large specific surface area. The interest in TiO_2 is due to its high photoactivity, which manifests itself in the high rate of electron-hole pair generation and similar rate of radical generation due to the capture of photoexcited charge carriers by water and oxygen molecules adsorbed on the titania surface [1]. In this work, aiming to create a nanocrystalline material by a very simple technology, we provide a detailed analysis of the spin centers and their photoinduced reactions in Nb and N codoped TiO_2 nanocrystals.

Nanostructured TiO_2 samples doped with different concentration Nb and N were synthesized by ammonia-assisted coprecipitation of metal hydroxides aqueous chemical deposition. Analytical pure-grade TiCl_4 and $\text{H}_3\text{NbO}(\text{C}_2\text{O}_4)_3 \cdot 7.5 \text{H}_2\text{O}$ (Sigma-Aldrich) were dissolved in a mixture of conc. HCl and H_2O_2 solutions. Aqueous 1 M ammonia was poured into the stirred solution of precursors to precipitate and Ti(IV) and Nb(V) hydroxides at $\text{pH} = 7$. Ammonia also served as a source of nitrogen dopant. The precipitates were annealed at 773 K for 24 h in air. The obtained nanocrystalline $\text{TiO}_2(\text{Nb})$ samples were modified by Au (1 wt.%) by colloidal adsorption. Nb-doped titania was suspended in a solution of HAuCl_4 which was neutralized by 2 M NaOH at $\text{pH} = 7$. The solid residue

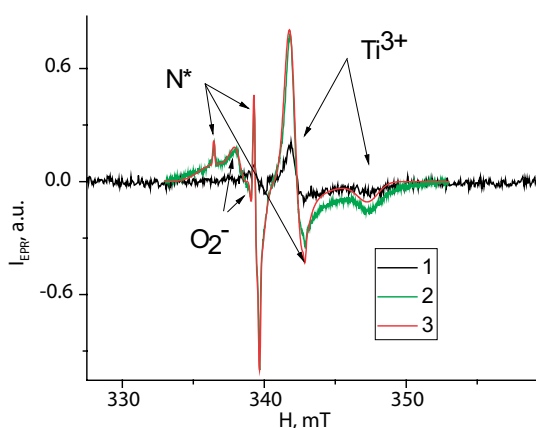


Fig. 1. Experimental (1-dark, 2-light) and calculated (3) EPR spectra of the Nb-N- TiO_2 sample recorded at 130 K.

was dried and annealed at 573 K to decompose the deposited $\text{Au}(\text{OH})_3$ colloid. The EPR spectra were recorded with a Bruker spectrometer ELEXSYS-E500. The samples were illuminated directly in the spectrometer cavity by visible or UV light sources.

Experimental and calculated EPR spectra of the Nb(3%)-N-TiO₂ sample (as example) are shown in Fig. 1. They show the existence of superposition of several EPR signals, which may be related to different spin centers. The simulation of EPR spectra allowed us to determine spin-Hamiltonian parameters (\hat{g} and hyperfine splitting, \hat{A} tensor values). These data are necessary for the correct interpretation of the chemical nature of spin centers contributing to the EPR spectra. According to the simulation results, only a low-intensity rhombic-type EPR signal corresponding to Ti^{3+} centers [2] with $g_1 = g_2 = 1.9897$, $g_3 = 1.9592$ can be clearly distinguished in the Nb(3%)-N-TiO₂ EPR spectrum recorded in the dark. Also, the spectrum shows a weak line in the region of ~ 338 mT, the nature of which is not quite clear if we do not consider the spectra of illuminated samples. Under illumination we observed not only a sharp increase in the amplitude of the Ti^{3+} center signal, but also we see the appearance of a new signal with peaks corresponding to the superfine splitting in nitrogen radicals ($g_1 = 2.0055$, $g_2 = 2.0053$, $g_3 = 2.0035$, $A_1 = 0.2$ mT, $A_2 = 0.34$ mT, $A_3 = 3.2$ mT) [2]. The relatively low concentration of these spin centers corresponds to the selected low level of nitrogen doping. Now we can say that the weak signal in the dark spectrum also corresponds to nitrogen centers. We have detected the appearance of an additional signal near $H = 340$ mT corresponding to O_2^- radicals according to our simulation and literature data ($g_1 = 2.025$, $g_2 = 2.011$, $g_3 = 2.0043$) [2]. We assume the following reactions of O_2^- radical formation: (a) $\hbar\omega \rightarrow h + e^-$ (interband light absorption), and $\text{O}_2 + e^- \rightarrow \text{O}_2^-$ (b). Nb(6%)-N-TiO₂ samples have similar EPR signals but O_2^- signal has lower intensity. Nb(3%)-TiO₂ samples are characterized only by Ti^{3+} centers, no O_2^- radicals! Therefore, the presence of nitrogen in the samples promotes the formation of O_2^- radicals.

The results obtained open up new possibilities for the development of gas sensors with improved selectivity based on nanocrystalline Nb-N-doped titania.

The study was supported by a grant from Russian Science Foundation № 22-73-10038. We thank Dr. A. Minnekhanov for help in simulation of EPR spectra. The experiments were performed using the facilities of the Collective Use Center at the Moscow State University (including the Bruker ER 4112 HV temperature control system of the Moscow State University Development Program).

1. Zaleska-Medynska A.: Metal Oxide-Based Photocatalysis: Elsevier (2018)
2. Kokorin A.I., Bahnemann D.W.: Chemical physics of nanostructured semiconductors. Boston: VSP-Brill Academic Publishers (2003)

Structure-dependent functional self-assemblies based on a thiobarbiturate-barbiturate-melamine three-component system

**I. Moskalenko¹, V. Shilovskikh², A. Timralieva¹, P. Nesterov¹, E. Skorb¹,
A. Kokorin³**

¹ITMO University, St. Petersburg 197101, Russia, i.v.m.rostov.yar@gmail.com

²Immanuel Kant Baltic Federal University, Kaliningrad, Russia

³N.N. Semenov Research Center of Chemical Physics, Moscow, Russia

Previously, new self-assemblies of melamine and barbituric acid [1] capable of capturing reactive oxygen species from aqueous solutions were discovered at our center. In this work, we studied and characterized the technique of X-ray phase analysis, fluorescence microscopy, and scanning electron microscopy of new self-assemblies based on the ternary melamine-barbituric acid-thiobarbituric acid system. With the help of quantum chemical calculations (DFT B3LYP) and the method of molecular dynamics, the most profitable options for the formation of self-assemblies were found. The EPR method (X-band) was used to study the radical activity of these crystals.

1. Shilovskikh V.V., Timralieva A.A., Nesterov P.V., Novikov A.S., Sitnikov P.A., Konstantinova E.A., Kokorin A.I., Skorb E.V.: *Chem. Eur. J.* **119991**, 16603 (2020)

Investigation of structural rearrangements of ionic liquids during glass transition by EPR and MD methods

D. Alimov^{1,2}, M. Ivanov², S. Pylaeva³

¹Physics department, Novosibirsk State University, Novosibirsk 630090, Russia, d.alimov@g.nsu.ru

²International Tomography Center SB RAS, Novosibirsk 630090, Russia, m.ivanov@tomo.nsc.ru

³University of Paderborn, Paderborn 33098, Germany, svetlana.pylaeva@upb.de

Understanding the heterogeneous nanostructures of various organic glasses is important for many applications. Structural rearrangements of various organic glasses near their glass transition temperatures have been studied by EPR spectroscopy. An anomalous dependence of microviscosity on temperature was found [1].

The purpose of this work is to study the dibutyl phthalate/TEMPO and [Bmim]BF₄ model systems using the molecular dynamics method in order to understand the mechanism of this phenomenon.

The simulation was carried out in the GROMACS package using the OPLS-AA force field. A system of 500 dibutyl phthalate molecules / [Bmim]BF₄ ionic pairs and 1 TEMPO nitroxyl radical was formed. Series of NVT trajectories are obtained for temperatures in the vicinity of the glass transition temperature: 160 K, 180 K, 190 K.

Radial distributions of atomic groups, rotational correlation functions, and solvent clustering have been studied. The coexistence of two types of solvation of the radical by alkyl chains of the solvent was found. The first type allows only low-amplitude rotational vibrations of the radical and corresponds to clamping by the carboxyl groups of the solvent. The second type of solvation allows rotation with a larger amplitude, coupled with the dynamics of butyl solvent chains. Qualitative agreement with experiment was obtained. A detailed dynamic analysis of the trajectories made it possible to establish the role of alkyl chains in the formation of the anomaly. Solvent clustering and correlation with radical motion were also studied. Based on the two systems under study, structural patterns were established that affect the effect observed in the EPR [2].

1. Ivanov M.Y., Krumkacheva O.A., Fedin M.V.: *Physical Chemistry Chemical Physics* **19**, 38, 26158–26163 (2017)
2. Ivanov M.Y., Bakulina O.D., Alimov D.V.: *Nanoscale Advances* **3**, 17, 4973–4978 (2021)

Study of crown-containing styryl dyes and peculiarities of their photoreactions

A. Kondratenko^{1,2}, N. Alexandrova², N. Lobova^{1,2}

¹The School of Electronics, Photonics and Molecular Physics, MIPT, Dolgoprudny 141701, Russia, kondratenko.ad@phystech.edu

²Sensorics laboratory, Photochemistry center of RAS, Moscow 119421, Russia

Photochemical reactions contribute significantly to carbon-carbon bond formation reactions. They can be used to produce exceptional molecular structures that cannot be formed in the usual way. The [2+2]-photocycloaddition reaction is one of the most important reactions in photochemistry: it can produce cyclobutane derivatives that are virtually impossible or very difficult to obtain by other means [1]. Styryl dyes are a class of organic photosensitive compounds with various applications in science, engineering and medicine. Styryl dyes containing the crown ether fragment are promising ligands for creating new functional materials, sensory devices, fluorescent markers, etc. [2]. These systems are also promising for incorporation into polymers [3].

The ionophoric analogues of styryl dyes are considered in this work and their ability to form homo- and hetero-containing dimeric structures as well as to participate in the [2+2]-photocycloaddition reaction in various media is studied. The ability of styryl dyes containing a crown ether fragment to form stable complexes with cucurbit[8]uril and γ -cyclodextrin in water, to undergo *E/Z*-photoisomerization and stereoselective [2+2]-photocycloaddition reactions is studied.

Depending on the solution and the pre-organization of molecules in the dimer, the process of the photo-cycloaddition reaction can be controlled. In polycrystalline films, the PCA reaction proceeds in successfully pre-organized pseudo-dimers regardless of their heterostructure and counterion. For compounds with donor nitrogen as part of the chromophore, the PCA reaction becomes pH-controlled (Fig. 1). In aqueous solutions, the type of cavitand affects the type of dimer formed and the final photoproduct.

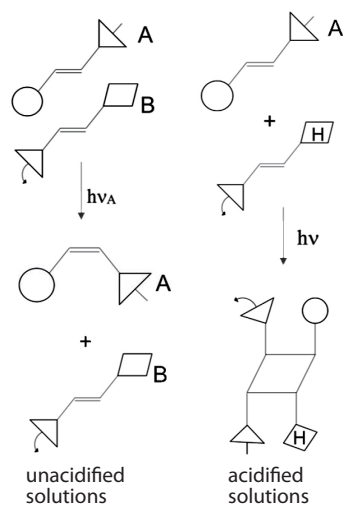


Fig. 1. pH-controlled process of PCA reaction.

1. Kuzmina L.G. et al.: Crystallographic approach to topochemical reactions of [2+2]-photocycloaddition of unsaturated compounds with single crystal preservation, *Crystallography* **4**, no. 5, 677–700 (2019)
2. Preto P.: A contribution to the theory of biological staining based on the principles for structural organization of biological macromolecules, *Biotech Histochem.* **76**, 137–161 (2001)
3. Zongjian Liua, Lin Yeb et al.: Cyclodextrin polymers: Structure, synthesis, and use as drug carriers, *Progress in Polymer Science*, **118**, 101408 (2021)

“Smart” supramolecular materials for reactive oxygen species trap and storage

A. Timralieva¹, P. Nesterov¹, I. Moskalenko¹, A. Kokorin^{2,3}

¹Infochemistry Scientific Center, ITMO University, St, Petersburg 197101, Russia, timralieva@itmo.ru

²N.N. Semenov Federal Research Center for Chemical Physics Russian Academy of Sciences, Moscow 119991, Russia

³Plekhanov Russian University of Economics, Moscow 115093, Russia

Recent years supramolecular materials expand its application area. The first advantage is the reversibility of non-covalent interactions that bind initial compounds together in the assembly. The pH control is the simplest way to switch on/off material's property.

In previous two years we demonstrated that melamine barbiturate supramolecular materials can be used as O-radicals trap with the light-induced expanding of spins [1]. The radical activity of melamine barbiturate depends on pH value due to the protonation/deprotonation of melamine and barbituric acid molecules in the assembly [2].

Further study confirmed that melamine barbiturate has two radical centers of different nature. The first one is associated with O-atom and seems to be hydroperoxyl radicals. It produces during the oxidation of initial compound in the assembly with the simultaneous formation of CH radical. Thus, melamine barbiturate can be considered as supramolecular radical trap system.

Both radicals seem to be extremely stable and do not initialize the further radical chain. Melamine barbiturate also can neutralize reactive oxygen species and act like a scavenger, which functions depend on pH value.

All the aspect of melamine barbiturate study firstly are based on the electron paramagnetic resonance measurements which are strengthened with the DFT calculations and morphological/structural characterization. The aim of the research is to demonstrate the applicability of novel controllable materials for radical trap and storage.

The work was carried out with the support of the Ministry of Science and Higher Education of the Russian Federation (agreement № 075-15-2021-1349).

1. Shilovskikh V., Timralieva A., Belogub E., Konstantinova E., Kokorin A., Skorb E.: Applied Magnetic Resonance **51**, 1–11 (2020)
2. Shilovskikh V., Timralieva A., Nesterov P., Novikov A., Sitnikov P., Konstantinova E., Kokorin A., Skorb E.: Chem. Eur. J. **26**, 16603 (2020)



SECTION 4

SPIN-BASED INFORMATION PROCESSING

Magneto-optical imaging of coherent spin dynamics

Yu.M. Bunkov,

**in collaboration with V.I. Belotelov, P.O. Kapralov, G.A. Knyazev,
A.N. Kuzmichev, P.E. Petrov, P.M. Vetoshko**

M-Granat, laboratory of quantum magnonics, Russian Quantum Center, 30, B. Bulvar,
Skolkovo, 121205, Moscow, Russia

The explosive development of quantum magnonics is associated with the possibility of its use as macroscopic quantum systems. They can find an application for quantum computing processors and other devices. The phenomenon of magnon Bose-Einstein condensation and coherent precession of magnetization can be used for these purposes. In this presentation we describe a method for the optical observation of the coherently precessing magnetization in conditions when the concentration of magnons reaches the value necessary for their quantum condensation. The investigations were conducted in the out-of-plane magnetized yttrium iron garnet films. The required magnon density was achieved by magnetic resonance technique. The magneto-optical imaging method provides such important parameters of the coherent spin dynamics as the amplitude and phase distributed all over the sample. It should become an indispensable read-out tool for the upcoming quantum technologies based on the magnon Bose-Einstein condensation.

We have developed a method of the mBEC investigation, based on the registration of optical radiation modulated by reflection from a magnetic film. Let us discuss the geometry of the experiment. The deflected magnetization precesses around the direction of magnetic field as shown in Fig. 1a. This type of motion corresponds to both the mBEC regime and linear ferromagnetic resonance. However, in the case of mBEC the precession phase is synchronized over the entire film even in the case of inhomogeneous magnetic field. We have chosen a configuration shown in Fig. 1a in which the variable component of the magnetization \mathbf{m}_{rot} rotates in the plane of the film. In this configuration it is most easy to observe the effect of spin superfluidity which makes this geometry promising for the development of magnon qubits. However, this geometry is less convenient

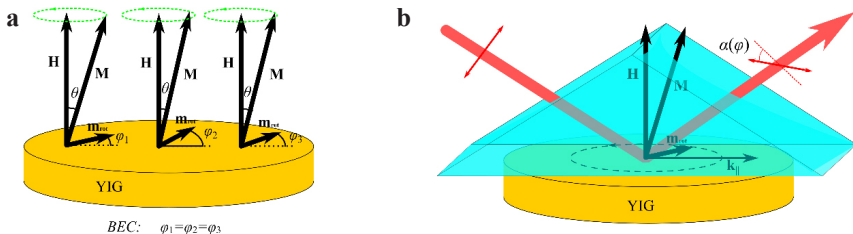


Fig. 1. Geometry of the experiment.

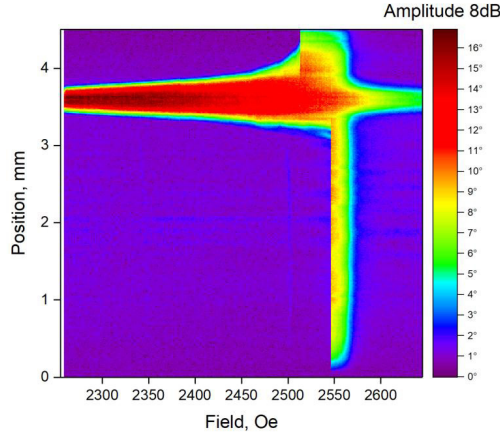


Fig. 2. Spatial distribution of magnetization precession at a field sweeps down.

for the optical measurements since the measurement of the in-plane component of the magnetization \mathbf{m}_{rot} requires oblique propagation of light relative to the film. In this case, the angle of incidence of light is limited by a high reflection coefficient of light from the film and substrate for oblique incidence. Therefore, we used a prism to illuminate the sample as shown in Fig. 1b.

The sample was glued to the prism by the substrate side through an immersion liquid. As a result, light from the prism entered the substrate first and then the film. After reflection from the air-YIG interface the light once again passed through the YIG film and the substrate. After passing through the output face of the prism it was directed to the receiving optical system of the setup. Due to the presence of a light wavevector component which is parallel to the YIG film the Faraday effect takes place and the reflected light acquires a rotation of polarization α proportional to the projection \mathbf{m}_{rot} onto the light wavevector into the prism. The phase of oscillations of the Faraday angle α is proportional to the angle φ at the frequency of magnetization precession. At the same time, the amplitude of α is proportional to the angle θ (see Fig. 1). Since \mathbf{m}_{rot} rotates in the film plane, the light polarization is modulated at the magnetization precession frequency.

We have succeeded to measure the spatial distribution of precessing magnetization in the various experimental conditions [1]. In particularly we have investigated the amplitude and phase distribution in the region far away from the region of magnon excitation. The experimental results strongly confirm the magnon Bose condensation and spin superfluidity in normally magnetized YIG film. In Fig. 2 is shown the example of experimental result. The spatial magnon distribution is measured as function of position along the 5 mm sample. Magnons was pumped by a strip line situated between 3.4 and 3.7 mm. At a sweep the external field down magnons starts to excite at a field higher then 2650 Oe. The field of linear resonance is about 2570 Oe. At a lower field the magnetization deflected, and the spin system remains at the resonance due to

demagnetization field decreases. It is clearly seen that the magnons field up at the sample at a field from 2570 Oe to a 2540 Oe (from 0 to 3.4 mm) and to 2520 Oe (from 3.7 to 5 mm). The phase of precession at these regions remains coherent. Our experiments shows directly the magnon Bose condensation and spin superfluidity in YIG film.

1. Petrov P.E., Kapralov P.O., Knyazev G.A., Kuzmichev A.N., Vetoshko P.M., Bunkov Yu.M., Belotelov V.I.: “Magneto-optical imaging of coherent spin dynamics in ferrites”, *Optics Express* **30**, 1737 (2022)

Engineering of exchange spin-waves spectra in ferromagnetic alloys with spatially variable composition

**A. Gumarov^{1,2}, I. Yanilkin², I. Golovchanskiy³, B. Gabbasov^{1,2},
A. Kiiamov², R. Yusupov², L. Tagirov¹**

¹Zavoisky Physical-Technical Institute, FRC Kazan Scientific Center of RAS, Kazan 420029, Russia, amir@gumarov.ru

²Institute of Physics, Kazan Federal University, Kazan, Russia.

³Moscow Institute for Steel and Alloys, Moscow, Russia

Exchange spin waves (SWs) in magnetic thin films and heterostructures are actively studied due to their charge-current free propagation in magnetic materials, thus being important for magnonics applications. The excitation of standing spin waves (SSWs) in thin magnetic films is commonly associated with surface anisotropy. However, it was elaborated theoretically that SSWs can also be excited in magnetically inhomogeneous films (see, for example, ref. [1]). It was shown that the dispersion law for spin waves depends on the character of the magnetic properties distribution in a film.

In this work, we present a technique how the programmed profiles can be created in the Pd-Fe alloy by controllable co-evaporation of Pd and Fe metals from effusion cells in the MBE machine. The temperature of palladium effusion cell during the deposition stayed constant, while the temperature variation of the Fe cell was programmed providing the required iron concentration profile. Using this approach, we have synthesized films with linear, sine, cosine, and other variants of iron distribution in the palladium matrix in the concentration range of 2–50 at.% and the thickness up to 200 nm.

SSWs were studied using a commercial X-band Bruker ESP300 ESR spectrometer in different geometries and measurement temperatures (10–300 K). The investigation has shown that the SW resonances can be engineered to get predetermined resonance fields and intensities. These circumstances make the Pd-Fe alloy an ideal material for components of magnon spintronics.

This work was supported by the Russian Science Foundation (Project no. 22-22-00629).

1. Ignatchenko V.A., D.S. Tsikalov: *J. Appl. Phys.* **127**, 123903 (2020)
2. Golovchanskiy I.A. et al.: *Phys. Rev. Materials* **6**, 064406 (2022)

Clustering into three groups on a quantum processor of five spins $S = 1$, controlled by pulses of resonant RF fields

I.S. Pichkovskiy, V.E. Zobov

Kirensky Institute of Physics, Federal Research Center KSC SB RAS, Krasnoyarsk, Russia,
rsa@iph.krasn.ru

Currently, quantum artificial neural networks are attracting more and more interest, due to their advantages over classical ones. In our previous works, we proposed to replace qubits to qutrits represented by spins $S = 1$, showed the advantages of such a replacement, and obtained a time-dependent effective Hamiltonian for clustering by means of quantum annealing [1, 2]. In this paper, we consider the control of a system of five spins using selective rectangular radio frequency (RF) pulses to solve the problem of clustering six points into three groups. The Hamiltonian of the pulse action in a coordinate system rotating with the pulse frequency W_{rf} takes the form:

$$H = \sum_{i=1}^{n=5} (W_i - W_{\text{rf}}) S_i^z + \sum_{i=1}^{n=5} Q_i (3(S_i^z)^2 - 2I) + H_y + H_{\text{dd}} ,$$

where W_i is the Larmor frequency of spin i , Q_i is quadrupole interaction (or zero-field splitting), S_i^α is spin projection operator on the corresponding axis $\alpha \in (x, y, z)$, I is identity matrix, $H_y = h_y \sum_{i=1}^5 S_i^y$ is Hamiltonian of the interaction with the transverse magnetic field of the RF pulse, h_y is the amplitude of the RF pulse, which must be small to reduce crosstalk, H_{dd} is dipole-dipole interaction Hamiltonian (DDI). The selectivity of the RF pulse is tuned using its frequency: $W_{\text{rf}} = -3Q_i + W_i$ for the transition between levels 1 and 2 of the qutrit i , and $W_{\text{rf}} = 3Q_i + W_i$ for the transition between levels 2 and 3. For selective rotation by an angle θ , we take the pulse duration $t_i = \theta/\sqrt{2}h_y$, and pulse amplitude $h_y = (W_i\theta)/(2\sqrt{2}\pi n)$ (n is an integer) such that the phase shifts of the energy levels are a multiple of 2π . We have found the parameters of RF pulses of all selective rotation required for the implementation of the above algorithm in the processor on five qutrits.

This work was supported by the Foundation for the Development of Theoretical Physics and Mathematics ‘‘Basis’’ under grant #20-1-5-41-1.

1. Zobov V.E., Pichkovskiy I.S.: Quantum Inf. Process **21**, 144 (2022)
2. Zobov V.E., Pichkovskiy I.S.: Proc. SPIE **12157**, 121571Z (2022)

SECTION 5

NEW TRENDS IN SPIN CHEMISTRY

Probing coherent spin dynamics in low field regime by transient absorption detected pulsed magnetic field effect

K. Maeda

Department of Chemistry, Graduate School of Science and Engineering,
Saitama University, kiminorimaeda@mail.saitama-u.ac.jp

The spin dynamics of radical pairs is an interesting subject in relation to magnetic field effects in molecular systems. For this purpose, transient absorption methods that allow time-resolved measurements of photochemical reactions are extremely useful. However, the usual transient absorption measurements often hardly distinguish the radical pair from the large background signal of the free radical and the other states. The Switched External Magnetic Field (SEMF) method has enabled us to measure the decay kinetics of RPs avoiding the interference of the background transient absorptions of the other species (Fig. 1). We have previously used nanosecond field switching methodologies to determine radical pair life-times in the low field region [2].

In addition, we recently found a novel methodology for finding spin coherence that is one of the origins of the low field effect (LFE). In theory, the origin of the low field effect is thought to be a mixture of coherent spin motion and spin mixing via avoided level crossing. A detailed analysis of transient absorption changes associated with small field jumping and delay time dependence on it in the low field regime is investigated precisely in various types of RPs. The variety of results may indicate different aspects of the spin dynamics of the radical pairs, and it is expected that a link to the mechanism of LFEs and decoherence time of the RPs can be discussed with theoretical model calculations.

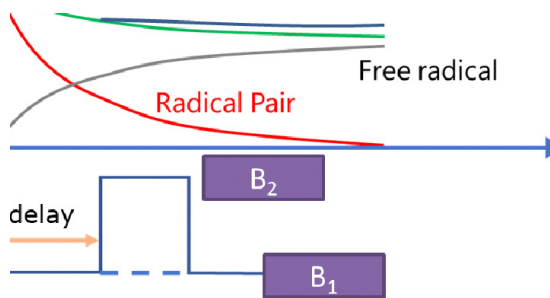


Fig. 1. Transient absorption signal of RP often overlaps with large free radicals and other chemical species produced by the photochemical processes. The SEMF technique interacts with Radical pairs and present the MFEs on RPs and Free radicals produced from RPs. The delay time dependence provides information on the kinetics of the RPs.

Acknowledgements. This work was supported by MEXT Q-LEAP Grant Number JPMXS0120330644.

New polyfluorinated systems producing X-ray generated exciplexes with magnetosensitive emission due to spin control of recombination

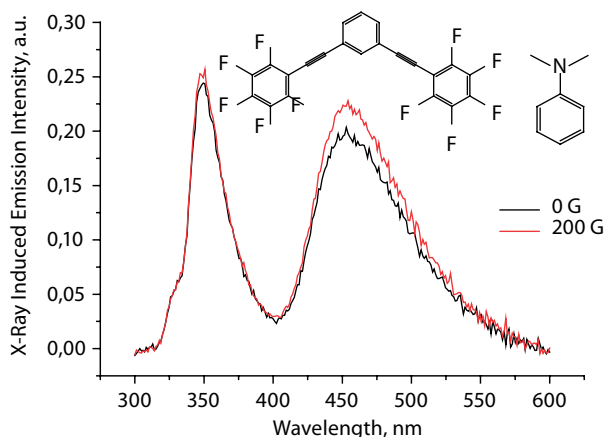
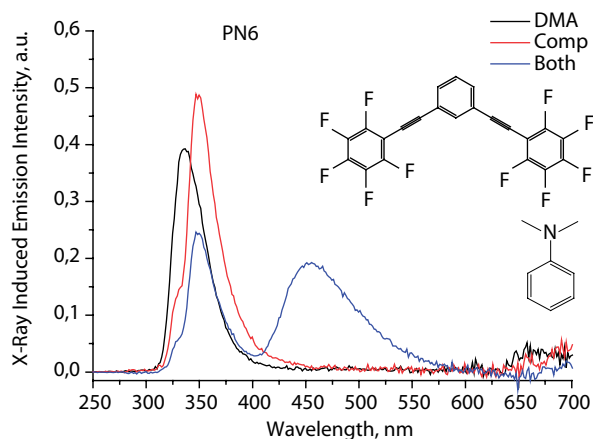
**D.V. Stass^{1,2}, E.M. Glebov¹, R.G. Fedunov¹, L.V. Kuibida¹,
P.V. Nikul'shin³**

¹Voevodsky Institute of Chemical Kinetics and Combustion, stass@ns.kinetics.nsc.ru

²International Tomography Center

³N.N. Vorozhtsov Novosibirsk Institute of Organic Chemistry, Novosibirsk 630090, Russia

Recombination of radical ion pairs featuring an aromatic luminophore in X-irradiated alkane solutions produces magnetosensitive luminescence due to spin-correlated nature of the pairs. Recently a new general trend of producing a recombination exciplex, rather than a locally excited molecular state, was



established [1], with suitable systems being pairs of dimethylaniline as the radical cation and a polyfluorinated radical anion. As the Figure shows, the shift of recombination-related emission to a separate longer-wavelength exciplex band boosts magnetic sensitivity of recombination luminescence, making it possible to observe MFE even in direct, rather than lock-in, detection [2]. In this contribution we shall discuss a series of newly synthesized and characterized systems of this type and their potential applications [3].

The authors are grateful to RSF, project No. 20-63-46034, for financial support.

1. Melnikov A.R., Kalneus E.V., Korolev V.V., Dranov I.G., Kruppa A.I., Stass D.V.: *Photochem. Photobiol. Sci.* **13**, 1169 (2014)
2. Melnikov A.R., Verkhovlyuk V.N., Kalneus E.V., Korolev V.V., Borovkov V.I., Sherin P.S., Davydova M.P., Vasilevsky S.F., Stass D.V.: *Z. Phys. Chem.* **231**, 239 (2017)
3. Melnikov A.R., Davydova M.P., Sherin P.S., Korolev V.V., Stepanov A.A., Kalneus E.V., Benassi E., Vasilevsky S.F., Stass D.V.: *J. Phys. Chem. A* **122**, 1235 (2018)

Readout of spin quantum beats in a charge-separated radical pair by pump-push spectroscopy

D. Mims¹, J. Herpich¹, N.N. Lukzen², U.E. Steiner³, Ch. Lambert^{1,4}

¹Institute of Organic Chemistry, University of Würzburg; Am Hubland 1, Würzburg, Germany

²International Tomography Center, Russia and Novosibirsk State University; Institutskaya 3a, Novosibirsk, Novosibirsk 630090, Russia, luk@tomo.nsc.ru

³Department of Chemistry, University of Konstanz, Universitätsstraße 10; 78464 Konstanz, Germany

⁴Center for Nanosystems Chemistry, University of Würzburg; Theodor-Boveri-Weg, 97074 Würzburg

Spin quantum beats prove the quantum nature of reactions involving radical pairs, the key species of spin chemistry. However, such quantum beats remain hidden to transient-absorption-based optical observation because the spin hardly affects the radical pairs' absorption properties. We succeeded in demonstrating such quantum beats in the photo-induced charge separated state (CSS) of an electron-donor-acceptor dyad by using two laser pulses, one for pumping the sample, and another one, with variable delay, for further exciting the CSS to a higher electronic state, wherein ultrafast recombination to distinct, optically detectable products of singlet or triplet multiplicity occurs. This represents a spin quantum measurement of the spin state of the CSS at the time instant of the second (push) pulse.

One of the authors, NNL is grateful for the financial support of Russian Foundation of Basic Research, grant No. 20-03-00234.

SECTION 6

STRONGLY CORRELATED ELECTRON SYSTEMS

Peculiar physics of heavy fermion metals: Theory versus experimental facts

V.R. Shaginyan

Petersburg Nuclear Physics Institute of NRC "Kurchatov Institute", Gatchina 188300, Russia

Our report considers the topological fermion condensation quantum phase transition (FCQPT) that leads to flat bands and allows one to elucidate the special behavior of heavy fermion (HF) metals that is not exhibited by common metals described within the framework of the Landau

Fermi liquid theory [1, 2]. We coordinate theoretical consideration within the framework of the fermion condensation theory based on FCQPT with experimental facts collected on HF metals. We show that very different HF metals demonstrate a universal behavior induced by FCQPT. We demonstrate that Fermi systems near FCQPT are controlled by Fermi quasiparticles with the effective mass M^* strongly depending on temperature T , magnetic field B , pressure P , etc. Our analysis permits to describe experimental results regarding the thermodynamic, transport and relaxation properties of HF metals. Based on the theory, we explain experimental facts, and show that the considered HF metals exhibit a number of peculiar properties like:

- 1) The universal T/B scaling behavior;
- 2) The linear dependence of the resistivity on T , $\rho(T) \sim T$, and the negative magnetoresistivity;
- 3) Asymmetrical dependence of the tunneling differential conductivity (resistivity) on the bias voltage;
- 4) In the case of flat band the superconducting critical temperature $T_c \sim g$ with g being the coupling constant, while the M^* becomes finite, so that $T_c \sim 1/M^*$ in contrast to common wisdom of BCS-like theories;
- 5) We show that the so called Planckian limit exhibited by the $\rho(T) \sim T$ is defined by the presence of flat band.

Our study of the experimental results suggests that the topological FCQPT is the intrinsic feature of many strongly correlated Fermi systems and can be viewed as the universal cause of both the non Fermi liquid behavior and the corresponding new state of matter [2].

1. Shaginyan V.R., Amusia M.Ya., Msezane A.Z., Popov K.G.: Phys. Rep. **492**, 31 (2010)
2. Amusya M.Ya., Shaginyan V.R., Strongly Correlated Fermi Systems: A New State of Matter, Springer Tracts in Modern Physics, Vol. 283. Springer Nature Switzerland AG, Cham (2020)

Zeeman coupling in the $\text{Bi}_{1.08}\text{Sn}_{0.02}\text{Sb}_{0.9}\text{Te}_2\text{S}$ topological insulator as revealed from the quantum oscillations

V. Sakhin¹, L. Morgun², V. Pudalov², G. Teitel'baum¹

¹Zavoisky Physical-Technical Institute, FRC Kazan Scientific Center of RAS, Kazan 420029, Russia, vsakhin@yahoo.com

²P.N. Lebedev Physical Institute, Moscow 119991, Russia

Topological insulators (TI) despite being gapped bulk insulators are known for their remarkable surface conduction state. Charge carriers on TI surface are Dirac fermions, which possess non-zero Berry phase. 2D Dirac quasiparticles can be distinguished by Shubnikov-de Haas (SdH) oscillations which was observed in various bismuth chalcogenides [1]. In the ideal case such system should exhibit Berry phase equal to π , but in many cases results diverge from this scenario. Variance of Berry phase can be attributed to Zeeman coupling and it was shown [2] that adding Zeeman term to $E(k)$ dispersion relation can shift Berry phase value.

Aim of our study was to observe Zeeman splitting in the $\text{Bi}_{1.08}\text{Sn}_{0.02}\text{Sb}_{0.9}\text{Te}_2\text{S}$ (BSSTS) TI, which has one of the largest contributions of surface transport to total conductivity among 3D TI. In previous work [3] using ESR method we obtained g -factor of conducting droplets formed inside the bulk. They exhibit $g_{\parallel} \approx 45$ and $g_{\perp} \approx 27$ due to strong renormalization by spin-orbit coupling. Unfortunately, ESR signal of surface carriers was unobservable, may be due to very large g -factor and low concentration of surface charge carriers. Therefore, we approached this problem with more convenient transport measurements.

We obtained SdH oscillations and used it to plot Landau level fan diagram, which is well-known numerical characteristic of quantum oscillations. As expected, the linear model, which is characteristic for spineless Dirac fermions, didn't provide good fit for our data, therefore we included Zeeman term in consideration. In result, we obtained reasonable fit that exhibits $g \approx 96$ and verification of Dirac fermions deviating from ideal behavior in BSSTS compound.

The work was supported by Russian Foundation for Basic Research (grant 20-02-00910 A) and Russian Science Foundation (project 21-72-20153).

1. Ren Z., Taskin A., Sasaki S., Segawa K., Ando Y.: Phys. Rev. B 241306 (2010)
2. Taskin A.A. and Ando Y.: Phys. Rev. B **84**, 035301(2011)
3. Sakhin V., Teitel'baum G., Morgun L., Pudalov V. et al.: JETP Letters **115**, 239 (2022)

Magnetic irreversibilities and nonreciprocity of the microwave absorption of FeCr_2O_4 spinel

R.V. Yusupov, M.A. Cherosov, B.F. Gabbasov, K.V. Vasin, R.G. Batulin, A.G. Kiiamov, A.L. Zinnatullin, M.V. Eremin

Institute of Physics, Kazan Federal University, Kazan 420008, Russia,
Roman.Yusupov@kpfu.ru

In the talk, we will report on the synthesis of the single crystal samples of the FeCr_2O_4 compound with the cubic spinel structure at room temperature, and its calorimetry and dc magnetometry studies, as well as with the magnetic resonance spectroscopy.

We have proposed and realized the new route for the synthesis of the FeCr_2O_4 compound and its single crystal growth by the optical floating zone method that ensures its single phase and near-ideal composition. The advantage of the proposed synthesis method is the creation of the reducing atmosphere in the oven needed for preserving the Fe^{2+} oxidation state via decomposition of the iron (II) oxalate FeC_2O_4 used as one of the initial components. The occurrence of the Fe^{3+} ions in the obtained polycrystalline samples as well as grown single crystals was carefully monitored by means of Mössbauer spectroscopy [1].

The temperature dependence of the specific heat indicates three phase transitions, corresponding to an establishment of the long-range orbital order in the Fe^{2+} -ion sublattice at 138 K, an onset of the collinear ferrimagnetic structure at ~ 65 K, and a development of the spiral magnetic structure at 38.5 K. The last two are revealed also in the temperature dependence of the magnetic susceptibility (Fig. 1). The shape of the $M(T)$ curve varies qualitatively with the magnitude of an applied magnetic field, with the other two anomalies observed at ~ 44 K

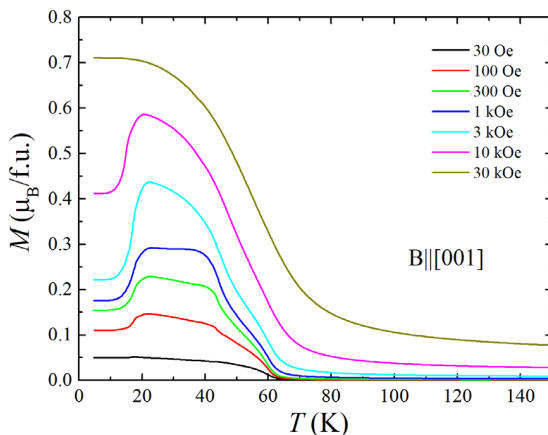


Fig. 1. Magnetic field variation of the FeCr_2O_4 $M(T)$ curve.

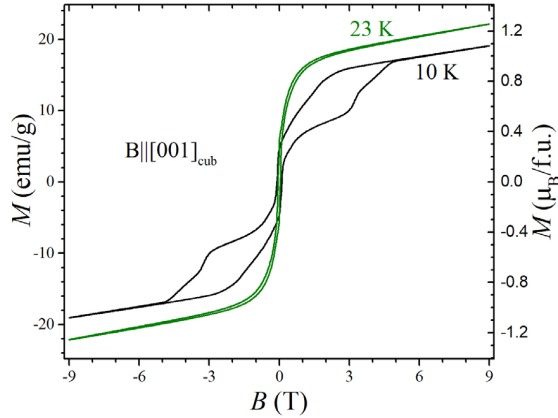


Fig. 2. Magnetic hysteresis curves of the FeCr_2O_4 single crystal at 23 K and 10 K.

and ~ 21 K that we associate with the magnetic-field induced rearrangement of the magnetic structure or modification of the magnetocrystalline anisotropy. A qualitatively similar observation in the FeCr_2S_4 isostructural sulfide compound was recently reported in [2].

The magnetic moment per unit cell at any temperature and a magnetic field less than 9 T doesn't exceed a value $1.25\mu_B$, which is less than $2\mu_B$ expected for a collinear ferrimagnetic arrangement between the Fe^{2+} and Cr^{3+} sublattices. This clearly shows that the magnetic structure of FeCr_2O_4 is more complicated. The shape of the hysteresis curves changes from narrow classic-one above 21 K to a butterfly-like below this temperature, with a pronounced irreversibility in the magnetic field range of $|B| < 5$ T.

Magnetic resonance study in the X-band has revealed a complex spectrum consisting of a minimum of 2 wide bands that varies with temperature and is observed only in the temperature range of 21–65 K. Interestingly, the orientation dependence investigation showed that the spectrum of a rectangular parallelepiped shaped sample with the faces perpendicular to the cubic $\langle 100 \rangle$ directions is not reproduced on the sample rotation by 180 degrees but rather demonstrates only a 360-degree periodicity. As either the crystalline structure or a shape symmetry is not lower than orthorhombic, we associate the described observation with the microwave non-reciprocity. The last is discussed in terms of the interference of the electric-dipole and magnetic-dipole transitions characteristic to multiferroic materials.

The support from Russian Science Foundation, project No. 19-12-00244, is gratefully acknowledged.

1. Batulin R., Cherosov M., Kiiamov A., Zinnatullin A., Vagizov F., Tayurskii D., Yusupov R.: *Magnetochemistry* **8**, 86 (2022)
2. Prodan L., Yasin S., Jesche A., Deisenhofer J., Krug von Nidda H.-A., Mayr F., Zherlitsyn S., Wosnitza J., Loidl A., Tsurkan V.: *Phys. Rev. B* **104**, L020410 (2021)
3. Yusupov R.V., Cherosov M.A., Gabbasov B.F., Vasin K.V., Batulin R.G., Kiiamov A.G., Eremin M.V.: *JETP Lett.* **115**, 167 (2022)

SECTION 7

LOW-DIMENSIONAL SYSTEMS AND NANO-SYSTEMS

Electron spin resonance of spinon liquid with interaction

**A.I. Smirnov¹, K.Yu. Povarov², T.A. Soldatov¹, Ren-Bo Wang³,
A. Zheludev², O.A. Starykh³**

¹P.L. Kapitza Institute for Physical Problems RAS, Moscow 119334, Russia,
smirnov@kapitza.ras.ru

²Laboratory for Solid State Physics, ETH Zürich, 8093 Zürich, Switzerland

³Department of Physics and Astronomy, University of Utah, Utah 84112, USA

The $S = 1/2$ Heisenberg antiferromagnetic spin chain has a critical ground state with the absence of the ordered spin components but with a strong spin-spin correlation. The ground state and excitations above it may be described in terms of quantized fractionalized dynamic spin structures referred to as spinons, see, e.g., [1]. These spinons are neutral $S = 1/2$ fermions. The theory of free fermions-spinons is supported by neutron scattering experiments with observation of a continuum of $S = 1$ excitations (so called two-spinon continuum) or by field-dependent soft modes within the continuum [1]. A specific fine structure of the two-spinon continuum was predicted for spin $S = 1/2$ chains with a uniform Dzyaloshinsky-Moriya (DM) interaction. This interaction causes a tiny shift of the continuum, results in an energy gap $\Delta = \pi D/2$ (D is the DM parameter) and a doublet of electron spin resonance (ESR) frequencies

$$\nu_{\pm} = (g\mu_B H \pm \Delta)/2\pi\hbar, \quad (1)$$

The ESR doublet ν_{\pm} was indeed experimentally observed in, e.g., [2]. This doublet enables one to measure extremely precise the width of the continuum by ESR method.

Now we report measurements of ESR spinon doublet for a quasi 1D $S = 1/2$ Heisenberg antiferromagnet $\text{K}_2\text{CuSO}_4\text{Br}_2$ in a strong magnetic field, where we observe a significant deviation of ESR modes ν_{\pm} from the relation (1). According

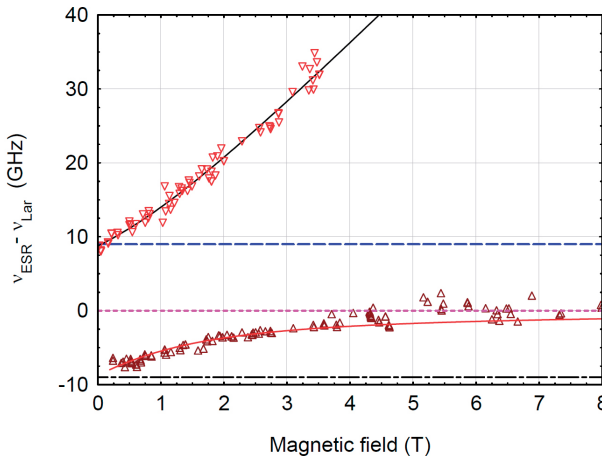


Fig. 1. $\nu_{\text{ESR}} - \nu_{\text{Lar}}$ vs magnetic field at $T = 0.5$ K. Solid lines— theory, dashed – see text.

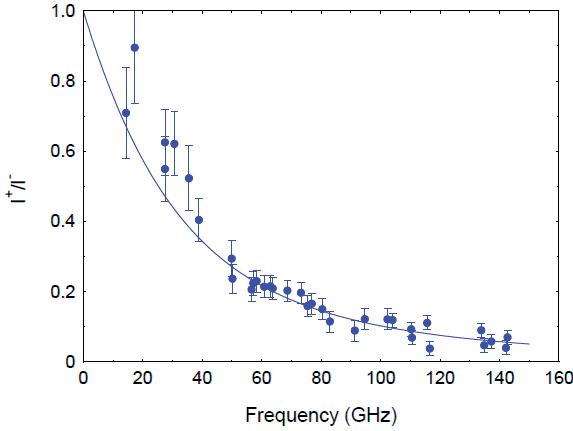


Fig. 2. Ratio of intensities within spinon doublet vs. frequency. $T = 0.5$ K.

to a recent theory [3], the additional shift of spinon energy should occur due to the interaction of a backscattering type between the spinons living near the right/left Fermi points of the one-dimensional Fermi surface. The interaction-induced energy gap is represented by $\Delta_{\text{int}} = uM/\mu_B$, here u is the parameter of interaction and M is the magnetic moment per unit length. Using these relations we explain (see [4]) the deviation of the experimentally observed frequencies of the spinon doublet from the above interaction-neglecting relation (1). Fig. 1 demonstrates the difference between the observed ESR frequencies and Larmor frequency $\nu_{\text{Lar}} = g\mu_B H/(2\pi\hbar)$ in different magnetic fields. This difference should be constant when the interaction between spinons is neglected (this behavior is illustrated by horizontal dashed lines at ± 8.7 GHz). The fit according to the predictions of [3] with the parameter $u = 3.5 \cdot 10^5$ cm/s (solid lines) demonstrates a good quantitative correspondence of the experiment and theory with a reasonable value of the parameter u which is about 50% larger than spinon velocity. Fig. 2 shows the frequency dependence of the intensity ratio I^+/I^- of the components of the ESR doublet along with the theoretical prediction [4] for this ratio. At $u = 0$, i.e. without spinon interaction, this ratio should be 1. A good correspondence of the data and theory on this graph explains the dramatic vanishing of the upper component of the doublet, which was a puzzling result of the experiment [2].

Thus, our experiment confirms a fundamental concept of interacting fermions-spinons as a basic feature of the ground state of $S = 1/2$ Heisenberg antiferromagnetic chain. The value of the spinon backscattering parameter is found experimentally. This reveals a Fermi-liquid (not a Fermi-gas) behavior of quasiparticles in a 1D antiferromagnet. Collective excitations of an antiferromagnetic chain demonstrate amazing analogy with electrons in a metal and Silin spin waves [5] in a normal metal.

Support of RSCF Grant 22-02-00259 is acknowledged.

1. D.C. Dender et al.: Phys. Rev. Lett. **79**, 1750 (1997)
2. A.I. Smirnov et al.: Phys. Rev. B **92**, 134417 (2015)
3. A. Keselman, L. Balents, O.A. Starykh: Phys. Rev. Lett. **125** (2020)
4. K.Yu. Povarov et al.: Phys. Phys. Rev. Lett. **128**, 187202 (2022)
5. V.P. Silin: Sov. Phys. JETP **6**, 945 (1958); V.P. Silin: Sov. Phys. JETP **8**, 870 (1959)

Observation of skyrmions by magnetic resonance method in $\text{Sr}_2\text{MnTiO}_6$

R.M. Eremina¹, I.V. Yatsyk¹, T.I. Chupakhina²

¹Zavoisky Physical-Technical Institute, FRC Kazan Scientific Center of RAS, Kazan 420029, Russia, REremina@yandex.ru

²Institute of Solid State Chemistry of the Russian Academy of Sciences (UB), Ekaterinburg 620990, Russia

In double perovskites, such phenomena as colossal magnetoresistance, ferroelectricity, multiferroicity, high temperature of the superconducting transition, and the behavior of a semimetal were observed. Double perovskites $\text{A}_2\text{B}_2\text{O}_6$ are very easy to modify the composition; the use of various cation ions in the B-position allows you to change their electrical, magnetic and thermal properties.

The aim of this work is to synthesize and study the magnetic properties of new double perovskites $\text{S}_2\text{B}'\text{B}''\text{O}_6$, where Ti acts as the B' cation, and the B'' position is occupied by Mn ions by magnetic resonance methods.

The exchange narrowed line with $g \sim 2$ is observed in a wide temperature range from 700 to 20 K. An additional line is observed in the magnetic resonance spectrum with $g \sim 13$ in a narrow temperature range from 43 to 39 K, where a phase transition is registered in the AC magnetization (see Fig. 1). We assume that this signal is associated with the formation of skyrmions in this sample, in which manganese ions are present as Mn^{3+} and Mn^{4+} .

The work was supported by a grant RSFN $\text{\textcircled{R}}$ 22-42-02014.

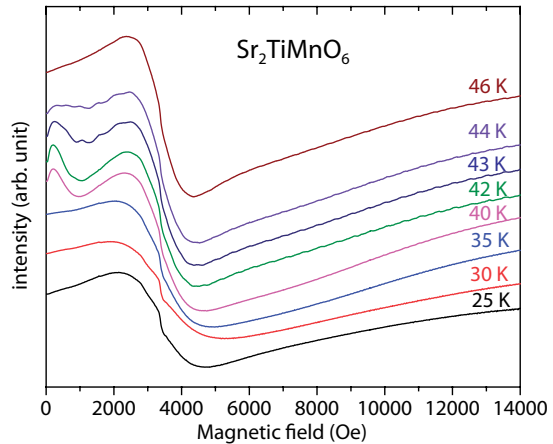


Fig. 1. Temperature dependencies of magnetic resonance spectra in $\text{Sr}_2\text{MnTiO}_6$.

Spin probe technique for investigation of inner structure of graphene oxide membranes – possibilities and prospects

N.A. Chumakova^{1,2}

¹N.N. Semenov Federal Research Center for Chemical Physics, Russian Academy of Science, Kosygin St. 4, Moscow 119991, Russia

²M.V. Lomonosov Moscow State University, Chemistry Department, Leninskiye Gory 1/3, Moscow 119991, Russia, harmonic2011@yandex.ru

Graphite oxide (GO) is a layered material formed by oxidized graphene planes. At present, GO is applied widely as a precursor for preparation of various graphene based materials. Of particular interest are graphene oxide membranes which were found to possess unique selective permeability for liquids and dissolved ions, so they can be considered as perspective materials for substances separation and water treatment. In spite of great practical prospects, the fundamentals of the amazing properties of GO membranes are still not clear. For this reason, the manufacture of the materials with desired properties is made mainly by trial and error. Investigation of molecular structure of GO membranes and properties of liquids intercalated in between oxidized graphene planes was hindered for a long time by lack of suitable experimental methods. In the report it will be shown that the spin probe technique is a useful tool for detailed study of the inner structure of GO membranes and for estimation of relationship between molecular organization and macroscopic properties of these materials. Quantitative characterization of the orientational ordering of GO membranes and determination of the phase state of liquids in the inter-plane space will be presented. The application of novel nitroxide radicals containing aromatic moieties for study of inner structure of GO membranes, as well as possibility of using of supercritical carbon dioxide for inserting of nitroxide radicals into the membranes will be discussed.

This work was performed partially within the framework of the Program of Fundamental Research of the Russian Federation (Reg. № 122040500068-0).

Electron paramagnetic resonance of nanocrystalline titanium dioxide containing manganese and its changes under the influence of ultraviolet irradiation

D.A. Saritsky, A.M. Ziatdinov, D.P. Opra, V.V. Zheleznov

Institute of Chemistry, Far Eastern Branch of the RAS, Vladivostok 690022, Russia,
denissaricki@mail.ru

Nanostructured materials based on titanium dioxide (TiO_2) are of great interest due to unique physical properties [1], which distinguish them favorably from macroscopic unstructured and microsized analogues. Many studies have shown (see, for example, [2, 3]) that the physicochemical properties of titanium dioxide can be changed over a wide range by doping with impurity ions.

This paper reports data on EPR studies of some spin characteristics for nanosized TiO_2 particles in the anatase modification (hereinafter, $\text{TiO}_2(\text{A})$) and the same particles doped with manganese ions (hereinafter, $\text{TiO}_2(\text{A})\text{:Mn}$). Doped samples were obtained by a one-stage synthesis method under hydrothermal conditions [4]. The EPR spectra of the samples were recorded on a JEOL-X330 spectrometer (JEOL, Japan) in the X-band at $T = -133^\circ\text{C}$.

Fig. 1 shows the EPR spectra of $\text{TiO}_2(\text{A})$ nanopowder before and after ultraviolet (UV) irradiation. The spectrum before irradiation contains several resonances that can be attributed to the F centers, Ti^{3+} ions in the bulk and/or at the surface of nanoparticles, and also O^- and O_2^- radicals [5, 6]. Under UV irradiation the intensity of resonance with $g = 2.0033$ decreases somewhat, at the same time, new resonances with g factors of 2.01 and 2.02 appear and grow in intensity.

The EPR spectrum of $\text{TiO}_2(\text{A})\text{:Mn}$ powder recorded under the same experimental conditions is shown in Fig. 2. It can be seen from figure that this spectrum is dominated by an intense broad resonance with a value of $g \sim 2.00$.

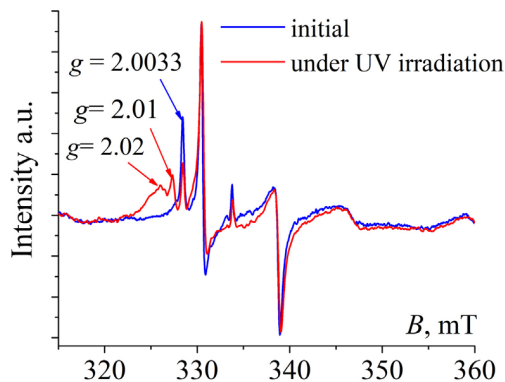


Fig. 1. The EPR spectra of $\text{TiO}_2(\text{A})$ before and after UV irradiation.

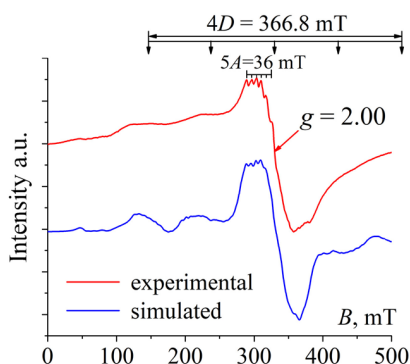


Fig. 2. The EPR spectrum of $\text{TiO}_2(\text{A})\text{:Mn}$ and its approximation.

A low-intensity sextet structure emerges on its weak-field wing. The average value of the interpeak intervals of sextet is 7.2 mT. The center of this sextet is shifted relative to the center of main component of the spectrum towards lower values of the magnetic field by $\Delta B = 22.1$ mT.

Considering the characteristic features of the experimental EPR spectrum of $\text{TiO}_2(\text{A})\text{:Mn}$, its simulation (Fig. 2) was carried out under the assumption that it belongs to Mn^{4+} ions located in an axial crystal field with a weak rhombic component and participates in exchange interactions with their nearest paramagnetic neighbors. It was also assumed that the angular dependence of the EPR spectrum of the Mn^{4+} ion in powder nanoparticles is described by the standard spin Hamiltonian:

$$\hat{H} = g\beta(\vec{B}, \vec{S}) + D \left(\hat{S}_z^2 - \frac{S(S+1)}{3} \right) + E \left(\hat{S}_x^2 - \hat{S}_y^2 \right) + A(\vec{I}, \vec{S}),$$

where all parameters have a well-known meaning. A contribution of the exchange interaction between Mn^{4+} ions to the formation of considered spectrum was taken into account using the expression for a shape of exchange averaged EPR lines given in [7].

It follows from the abovementioned that in $\text{TiO}_2(\text{A})\text{:Mn}$ sample manganese ions substituting the Ti^{4+} in crystal lattice and have an oxidation state of 4+. Upon this substitution, the oxygen octahedron acquires a significant axial distortion. We also discuss the nature of paramagnetic centers that appear upon UV irradiation of the original sample as well as the reasons for their absence in the irradiated doped samples.

1. Parrino F., Palmisano L.: Titanium Dioxide (TiO_2) and Its Applications: Elsevier 2020.
2. Nguyen K.C., Nguyen N.M., Duong V.Q. et al.: J. Electron. Mater. **50**, 1942 (2021)
3. He Z., Hong T., Chen J., Song S.: Sep. Purif. Technol. **96**, 50 (2012)
4. Zhelezov V.V., Opra D.P., Tkachenko I.A. et al.: Russ. J. Inorg. Chem. 2022. In print.
5. Misra S.K., Andronenko S.I., Tipikin D. et al.: J. Magn. Magn. Mater. **401**, 495 (2016)
6. Mohajernia S., Andryskova P., Zoppellaro G. et al.: J. Mater. Chem. A **8**, 1432 (2020)
7. Barney L., Willett D.: J. Chem. Phys. **80**, 2997 (1984)

Short range proximity effect in tunnel-coupled magnetic and nonmagnetic quantum wells

E. Kirstein², N.V. Kozyrev¹, M.M. Afanasiev¹, V.K. Kalevich¹,
M. Salewski², Yu.G. Kusrayev¹, E.A. Zhukov^{1,2}, D.R. Yakovlev^{1,2},
M. Bayer^{1,2}

¹Ioffe Institute, St. Petersburg 194021, Russia, kusrayev@orient.ioffe.ru

²Experimentelle Physik 2, Technische Universität Dortmund, 44221 Dortmund, Germany

The proximity effect is widely used in modern condensed matter physics to search for new hybrid structures and new interface properties. The hybrid structure obtained by the contact of different materials not only combines the properties of the ingredients, but also acquires qualitatively new properties, generated by the interactions between these systems. There are various types of such structures demonstrating proximity effect. For example, semiconductor / ferromagnetic; a ferromagnetic and a semiconductor quantum well (QW), separated by a nanometer-thick barrier. Hybrid structures could allow one not only to combine the functionalities of the individual constituents but also to perform mutual control of their properties [1].

Here we focus on a system of tunnel-coupled QWs, which are non-magnetic (NM) CdTe and magnetic (Cd,Mn)Te, 20 and 8 nm wide, separated from each other by a thin barrier (spacer) (Cd,Mg)Te of thickness varying from 5 to 11 monolayers for different samples [2]. The idea is as follows. Because of the strong exchange interaction with magnetic ions in a diluted magnetic semiconductor (DMS), the effective g -factor of the electron reaches large values ($g_e \sim 100$). In a double QW structure, where QWs are separated by a thin barrier,

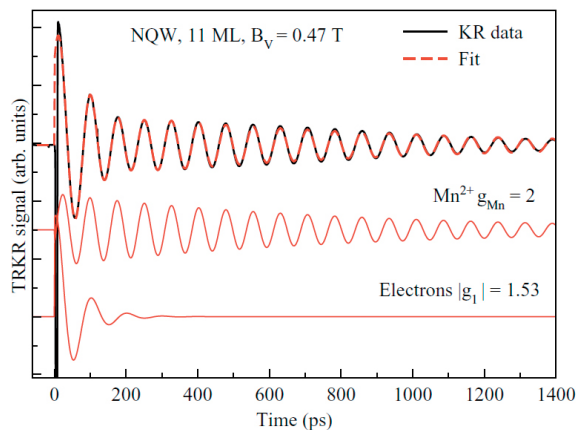


Fig. 1. Time resolved KR signal from 11-ML sample at $B_v = 0.47$ T (red lines – fitting). $E_{ex} = 1.657$ eV, $T = 5$ K.

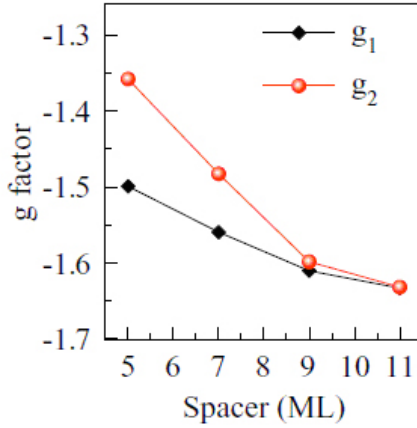


Fig. 2. Spacer thickness dependence of the g factors g_1 and g_2 . $T = 4.7$ K, $B = 0.4$ T. Symbols – experiment, lines – guides to the eye.

electrons can tunnel into neighboring wells. This process leads to the g -factor renormalization. Studies of spin dynamics in a transverse magnetic field allow one to accurately determine the value of the effective g -factor and, hence, the probability of an electron being in a particular well. To investigate the spin dynamics, we used the time resolved Kerr rotation (KR) pump-probe technique. Fig. 1 shows KR signal from the tunnel-coupled NM-CdTe and DMS-(Cd,Mn)Te QWs excited in the exciton region of DMS-(Cd,Mn)Te QW. In addition to the signal oscillating with a g -factor equal to 2 and reflecting the Larmor precession of optically induced manganese magnetic moment, a component with a g -factor equal to 1.53 is unexpectedly observed. This signal cannot display the Larmor precession of an electron from the magnetic QW, since its g -factor is close to 30. The g -factor equal to 1.53 rather reflects the Larmor precession of an electron in NM QW. The signal has significantly different KR components when excited with an energy corresponding to the CdTe QW exciton, where only two electron components are detected. These two frequencies (g -factors) originate from electrons in the NM QW being either part of excitons (g_1) or being resident ones (g_2). The g -factors of both components were found to depend on the thickness of the spacer as well as on the temperature. Fig. 2 demonstrates the dependence of these g -factors on the thickness of the barrier. It can be seen that the absolute values of the g -factors increase as the thickness of the spacer increases. As the temperature increases, the absolute value of the g -factor also increases and approaches the value of the g -factor for isolated QW. All these findings show that the spin dynamics of electrons in the wide (NM) QW strongly depends on the electron wave function penetration into the narrow QW and, consequently, by the strength of exchange interaction between the electrons and manganese ions. This interaction creates the proximity effect. As the thickness of the barrier between the QWs increases, the overlap of the

electron wave functions decreases and the g -factor tends to its value for the isolated well. This model also naturally explains the temperature dependence of the g -factor: as the temperature increases, the exchange field of magnetic ions (and, accordingly, their contribution to the spin splitting of electrons) decreases according to the Curie law ($\sim 1/T$).

This work was supported by the Russian Science Foundation (project № 22-12-00125).

1. Korenev V.L., Kalitukha I.V., Akimov I.A., V.F. Sapega, Zhukov E.A., E. Kirstein, Ken O.S., Kudlacik D., Karczewski G., Wiater M., Wojtowicz T., Ilyinskaya N.D., Lebedeva N.M., Komissarova T.A., Kusrayev Yu.G., Bayer M.: *Nat. Commun.* **10**, 2899 (2019)
2. Kirstein E., Kozyrev N.V., Afanasiev M.M., Mantsevich V.N., Krivenko I.S., Kalevich V.K., Salewski M., Chusnutdinov S., Wojtowicz T., Karczewski G., Kusrayev Yu.G., Zhukov E.A., Yakovlev D.R., Bayer M.: *Phys. Rev. B* **101**, 035301 (2020)

EPR investigation of acetonitrile intercalated into the inter-plane space of graphite oxide

D.A. Astvatsurov^{1,2}, N.A. Chumakova^{1,2}

¹N.N. Semenov Federal Research Center for Chemical Physics, Russian Academy of Science, Kosygin St. 4, Moscow 119991, Russia, ASTVaaaa@yandex.ru

²M.V. Lomonosov Moscow State University, Chemistry Department, Leninskiye Gory, 1/3, Moscow 119991, Russia

Graphite oxide (GO) is a non-stoichiometric derivative of graphite prepared by oxidation of pure graphite in acidic conditions. GO is a layered material consisting of monoatomic layers – graphene oxide planes – mainly formed by sp³-carbon atoms bonding to oxygen-containing groups – carboxyl, carbonyl, hydroxyl, epoxy, etc. Graphite oxide easily swells in polar liquids; swelling is accompanied by an increase in inter-plane distance from 5–7 Å in the dry material to 30–50 Å in the swollen state. Using differential scanning calorimetry it was found that liquids intercalated in between GO planes do not demonstrate phase transition “liquid-solid”; this means that properties of intercalated liquids differ from the properties of bulk liquids. The goal of this contribution is to study the molecular mobility of acetonitrile in between oxidized graphene planes using spin probe technique, which has never been used before for this aim.

We found out that two types of intercalated acetonitrile – liquid-like and solid-like – present simultaneously in between graphene planes; the substance with intermediate mobility was not observed. The ratio of the amount of liquid-like and solid-like intercalated acetonitrile depends on temperature. Micro-viscosity of liquid-like phase was found to be higher than one of bulk acetonitrile; this property depends on the amount of the intercalated liquid. It could be assumed that liquid-like acetonitrile is localized in unoxidized regions of graphite oxide, whereas solid-like one is localized in oxidized regions.

The financial support of the Program of Fundamental Research of the Russian Federation (Reg. № 122040500068-0) is gratefully acknowledged.

Magnetic resonance in metal-insulator nanogranular composites with paramagnetic ions in insulating matrix

**A.B. Drovosekov¹, N.M. Kreines¹, A.V. Sitnikov^{2,3}, S.N. Nikolaev³,
V.V. Rylkov³**

¹PL. Kapitza Institute for Physical Problems RAS, Moscow 119334, Russia,
drovosekov@kapitza.ras.ru

²Voronezh State Technical University, Voronezh 394026, Russia

³National Research Center “Kurchatov Institute”, Moscow 123182, Russia

Films of metal-insulator nanogranular composites $(\text{CoFeB})_x(\text{Al}_2\text{O}_3)_{100-x}$ and $(\text{CoFeB})_x(\text{LiNbO}_3)_{100-x}$ with various contents of ferromagnetic (FM) metal phase $x = 30 - 57$ at.% are studied by magnetic resonance in a wide range of frequencies ($f = 7 - 37$ GHz) and temperatures ($T = 4.2 - 360$ K) in magnetic fields applied at different angles with respect to the film plane. The films under study have a thickness of ~ 1 μm and are synthesized on glass-ceramic substrates by ion beam sputtering from composite targets of FM alloy $\text{Co}_{40}\text{Fe}_{40}\text{B}_{20}$ (CoFeB for brevity) and Al_2O_3 or LiNbO_3 oxides. The obtained nanocomposites consist of metallic FM nanogranules CoFeB randomly distributed inside the amorphous oxide matrix. At the same time a large number of Co and Fe ions prove to be dispersed in the matrix in the form of isolated paramagnetic (PM) centers [1].

Magnetic resonance spectra of the films demonstrate the presence of intensive absorption peak related to ferromagnetic resonance (FMR) from the ensemble of FM granules. Besides the FMR line, a much weaker additional peak is observed in lower fields (Fig. 1). The frequency-field dependence $f(H)$ for this peak is linear at high frequencies and characterized by effective g -factor $g \approx 4.3$ which is typical of electron paramagnetic resonance (EPR) of Fe^{3+} ions in amorphous solids. However, unlike common EPR, this peak demonstrates a number of unusual properties: (1) its intensity proves to be about the same in transverse ($\mathbf{h} \perp \mathbf{H}$) and longitudinal ($\mathbf{h} \parallel \mathbf{H}$) geometry of resonance excitation; (2) the position of the peak is dependent on the orientation of the magnetic field with respect to the film plane; (3) the dependence $f(H)$ shows a finite zero-field frequency (spectral gap) f_0 which increases with the content of the FM phase; (4) as temperature decreases, the peak shifts to lower fields and becomes weaker, disappearing below $T \approx 60$ K. As we have shown, many of these unusual properties can be explained within a relatively simple model taking into account magnetic interactions between PM ions and FM granules [2].

In particular the angular dependence of the EPR peak position is due to demagnetizing field acting on PM ions from the ensemble of FM granules. The spectral gap f_0 arises from FM exchange coupling between ions and granules. The growth of this coupling with FM phase content and with temperature decrease initiates the shift of the peak to weaker fields.

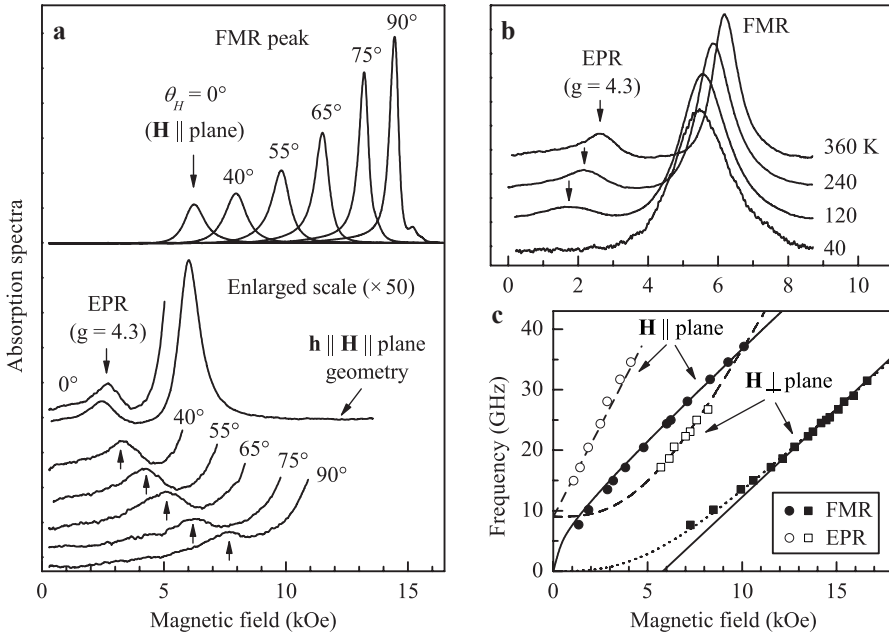


Fig. 1. **a** Room-temperature absorption spectra of $(\text{CoFeB})_{47}/(\text{Al}_2\text{O}_3)_{53}$ nanocomposite film at frequency $f \approx 25$ GHz obtained in magnetic field H applied at different angles θ_H with respect to the film plane. **b** Absorption spectra at different temperatures for the same sample and frequency in magnetic field oriented in the film plane and longitudinal excitation geometry ($h \parallel H \parallel \text{plane}$). **c** Frequency-field dependencies $f(H)$ for FMR and EPR peaks at room temperature. Points are experimental data; lines are their theoretical approximation [2].

The work is supported by the Russian Scientific Foundation (project 22-29-00392) in part of studying magnetic and electrophysical properties of the samples and by the Russian Foundation for Basic Research in part of synthesis of the films (project 19-29-03022).

1. Rylkov V.V., Sitnikov A.V., Nikolaev S.N. et al.: JMMM **459**, 197 (2018)
2. Drovosekov A.B., Kreines N.M., Kovalev O.A. et al.: JETP **134**, 725 (2022)

Spin and pseudo-spin ferromagnetic phase transitions in the regime of quantum Hall effect

**R. Khisameeva¹, S.A. Lopatina², G.A. Nikolaev³, A.V. Shchepetilnikov¹,
I.V. Kukushkin¹**

¹Institute of Solid State Physics RAS, Chernogolovka 142432, Moscow district, Russia,
akhisameeva@issp.ac.ru

²Higher School of Economics, 21/4 St. Basmannaya St., Bld. 5, Moscow 101000, Russia

³MIPT (National Research University), Dolgoprudny 141701, Russia

The strong electron-electron interaction leads to a whole bouquet of various beautiful physical phenomena, such as the fractional quantum Hall effect [1], Wigner crystallization [2], and Stoner instability [3]. Thus, repulsion between charged electrons at a sufficiently low electron density can lead to macroscopically large spin polarization, and the system goes into a state called a Stoner ferromagnet. An external magnetic field further increases the spin splitting and leads to the manifestation of ferromagnetism under weaker electron density conditions. Thus, changing the direction and magnitude of the magnetic field triggers chains of ferromagnetic phase transitions in the mode of the quantum Hall effect near even ν of the electronic system, which are nominally nonmagnetic in the one-particle approximation.

In present work, the evolution of the spin properties of high-quality two-dimensional electronic systems encapsulated in ZnO/MgZnO heterojunctions was studied by means of the electron spin resonance technique. Analysis of the resonance amplitude made it possible to establish that at a certain angle in the vicinity of the filling factor 2 a phase transition appeared in the two-dimensional electronic system accompanied by a large-scale change in spin polarization. Near the transition region the spin resonance was significantly broadened and split into several independent peaks. Such resonance behavior is apparently caused by splitting of the system into domains with different spin polarizations.

In quantized magnetic fields phase transitions may also be observed, with the appearance and disappearance of macroscopically large pseudo-spin polarization. Pseudo-spin degrees of freedom arise in multi-valley two-dimensional systems enclosed in broad AIs quantum wells. The magnitude of the pseudo-spin splitting can be controlled by the application of an external mechanical stress. In this work, the electron spin resonance technique was applied to study the pseudospin properties of a system of two-dimensional electrons confined in a wide AIs quantum well. Due to the peculiarities of the Lande factor tensor in AIs, the spin resonances of electrons filling different valleys are observed independently in close, but fundamentally different magnetic fields at a certain magnetic field orientation. Analysis of the relative amplitude of the resonances

allows us to directly assess the filling of each of the valleys and thus provides a unique opportunity to study the pseudospin properties of the system.

The study was supported by a grant from the Russian Science Foundation (Project No. 20-72-10097).

1. Tsui D.C. et al.: Phys. Rev. Lett. **48**, 1559 (1982)
2. Falson J. et al.: P*Nat. Mater.* **21**, 311–316 (2022)
3. Van'kov B. et al.: Phys. Rev. B **96**, 235401 (2017)

Coherent control of optically polarized V_B^- spin sublevels in hBN

**I. Gracheva, M. Sadovnikova, G. Mamin, R. Yusupov,
F. Murzakhanov**

Institute of Physics, Kazan Federal University, Kazan 420008, Russia,
murzakhanov.fadis@yandex.ru

Optically polarized spin states of defects in wide band gap semiconductors are one of the major building blocks of contemporary solid-state quantum technologies. The main idea of their use is that the high spin state ($S \geq 1$) of the defect, which is split in a zero magnetic field, can be initialized, manipulated, and subsequently read out by means of optical and radio frequencies, providing the possibility to control the spin [1]. Intensive exploration of this idea began after the discovery of the unique spin-optical properties of the negatively charged nitrogen vacancy defect (NV^- defect) in diamond and gave birth to several new scientific areas, such as room temperature spintronics, quantum sensing, and quantum information processing with defects [2].

We show that negatively charged boron vacancies (V_B^-) in hexagonal boron nitride (hBN) meet initial prerequisites for quantum applications. We demonstrate Hahn-echo coherence of the V_B^- spin with a characteristic decay

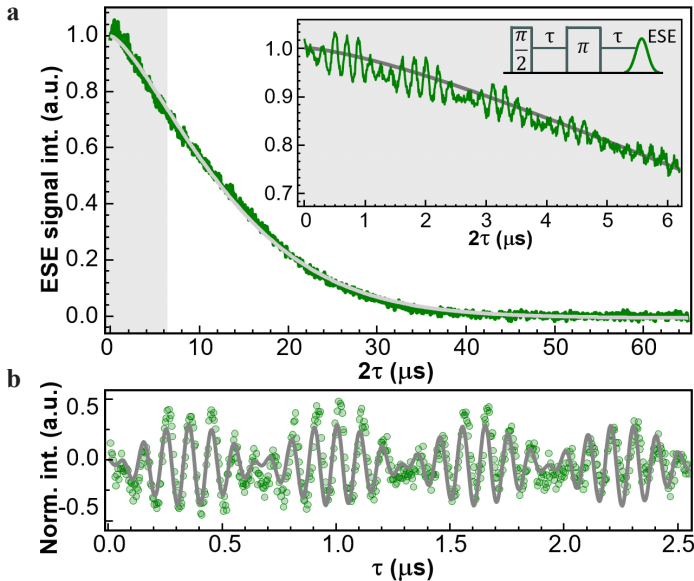


Fig. 1. **a** Decay of the transverse magnetization; **b** ESEEM modulation.

time $T_{\text{coh}} = 15 \mu\text{s}$, close to the theoretically predicted limit of $18 \mu\text{s}$ for defects in hBN (Fig. 1). The coherent control of V_{B}^- spin states was achieved by Rabi oscillations at various microwave powers. Modulation of the Hahn-echo decay is shown to be induced by coherent coupling of the V_{B}^- spin with the three nearest ^{14}N nuclei via a nuclear quadrupole interaction of 2.11 MHz. DFT calculation confirms that the electron-nuclear coupling is confined to the defective layer and stays almost unchanged with a transition from the bulk to the single layer.

The financial support of the Russian Science Foundation (Project No. 20-72-10068) is gratefully acknowledged.

1. Wolfowicz G.; Heremans F.J.: *Nat. Rev. Mater.* **6**, 10 (2021)
2. Murzakhanov F.F., Yavkin B.V., Mamin G.V.: *Phys. Rev. B* **103**, 245203 (2021)

Peculiarities of the ion transport of water molecules and alkali metal cations in sulfonic cation-exchange membranes studied by NMR

N. Slesarenko¹, A. Chernyak^{1,2}, V. Volkov^{1,2}

¹Institute of Problems of Chemical Physics RAS, Chernogolovka 142432, Russia,
wownik007@mail.ru

²Scientific Center in Chernogolovka RAS, Chernogolovka 142432, Russia

The features of hydration, ionic mobility and self-diffusion of cations of a number of alkali metals Li^+ , Na^+ , Cs^+ by the NMR method are considered using the example of sulfocation-exchange perfluorinated membranes Nafion. The hydration numbers h of the Li^+ , Na^+ , Cs^+ cations, calculated from the temperature dependences of the chemical shifts of the ^1H nuclei of water molecules, in Nafion membranes are 3.3 ± 0.4 , 3.3 ± 0.4 , 0.5 ± 0.2 at RH = 75%, respectively [1]. The self-diffusion coefficients of water molecules and, for the first time, the self-diffusion coefficients of Li^+ , Na^+ , and Cs^+ counterions were measured by NMR with a pulsed field gradient on ^1H , ^7Li , ^{23}Na , and ^{133}Cs nuclei [2].

Self-diffusion coefficients of water molecules and cations Li^+ , Na^+ , Cs^+ have been measured. The temperature dependences of the self-diffusion coefficient are approximated by the Arrhenius equation.

According to NMR data of the relaxation of nuclei ^7Li , ^{23}Na , ^{133}Cs it was found that the diffusion of cations is controlled by elementary jumps of ions between sulfo groups (Fig. 1).

The movement of Li^+ , Na^+ cations with high hydration energy occurs as a result of the rearrangement of hydrogen bonds between the water molecules of the first hydration shell and the water molecules of the next hydration spheres, the mean-square diffusion length jump is 0.15 nm. The Cs^+ cation performs direct translational motions between neighboring sulfo groups over a distance of about 0.7 nm.

The relationship between the structure of the polymer matrix of membranes, hydration of cations, and transport of cations and water molecules at different spatial scales can be explained on the basis of the structural model of nanochan-

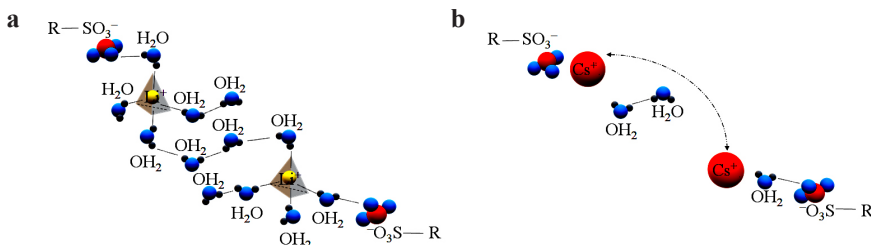


Fig. 1. Schematic representation of cation transport (a) Li^+ and (b) Cs^+ in the Nafion membrane.

nels in membranes [2, 3]. It follows from this model that it is the translational movements of cations between sulfo groups that control macroscopic transfer, which makes it possible to explain the observed features of ion transport.

NMR measurements were performed using equipment of the Multi-User Analytical Center of the Institute of Problems of Chemical Physics RAS and Science Center in Chernogolovka RAS with the support of State Assignment of the Institute of Problems of Chemical Physics RAS (state registration No 0089-2019-0010/AAAA-A19-119071190044-3).

1. Slesarenko N., Chernyak A., Avilova I., Zabrodin V., Volkov V.: *Mend. Comm.* **32**, 534 (2022)
2. Volkov V., Chernyak A., Avilova I., Slesarenko N., Melnikova D., Skirda V.: *Membranes* **11**, 385 (2021)
3. Volkov V., Chernyak A., Slesarenko N., Avilova I.: *Int. J. Mol. Sci.* **23**, 5011 (2022)

SECTION 8

PERSPECTIVES OF MAGNETIC RESONANCE IN SCIENCE AND SPIN TECHNOLOGY

Electron-nuclear interactions and coherent properties of axial and basal NV centers in $^4\text{H-SiC}$ crystal

I. Gracheva, M. Sadovnikova, G. Mamin, F. Murzakhanov

Institute of Physics, Kazan Federal University, Kazan 420008, Russia,
murzakhanov.fadis@gmail.com

One of the promising materials for extensive applications in semiconductor electronics is silicon carbide. Last decades SiC has developed into an perfect solid-state materials with color centers are desirable for variety quantum technologies. Spin-carrying defects or color centers with unique characteristics such as excellent photo-stability, spin addressing, and ease of device integration are among the promising building block candidates for contemporary quantum technologies. Quantum states of the color centers are extremely sensitive to the outer circumstances like temperature and magnetic field. Besides, those sizes are as small as atoms, which leads to atomic-level spatial resolution. Mentioned factors make color centers preferable for quantum applications [1, 2].

In this work axial NV_{hh} and basal NV_{kh} , NV_{hk} centers in silicon carbide crystal irradiated by protons were investigated at W-band frequency range. The main parameters of the spin Hamiltonian (the values of zero-field splitting D and E , the g -factor tensor) were precisely determined by the angular dependence of the sample. The results of measuring the electron-nuclear double resonance (Fig. 1)

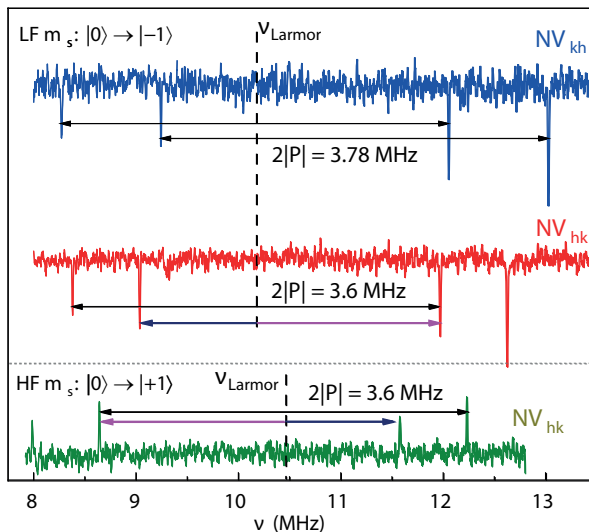


Fig. 1. ENDOR spectra of NV centers.

allowed us to determine the values of the anisotropic hyperfine and quadrupole interaction C_q , which gave information about the macroscopic model of the NV defect. Additionally, relaxation times and Rabi oscillation curves were measured for each type of center.

The work is carried out in accordance with the Strategic Academic Leadership Program “Priority 2030” of the Kazan Federal University of the Government of the Russian Federation.

1. Castelletto S., Boretti A. *Journal of Physics: Photonics* **2**, 022001 (2020)
2. Murzakhanov F.F., Yavkin B.V., Mamin G.V.: *Phys. Rev. B* **103**, 245203 (2021)

Non-Kramers iron $S = 2$ ions in β - Ga_2O_3 crystals: high-frequency low temperature EPR study

R.A. Babunts¹, A.S. Gurin¹, E.V. Edinach¹, H.-J. Drouhin²,
V.I. Safarov², P.G. Baranov¹

¹Ioffe Institute, St. Petersburg 194021, Russia

²Laboratoire des Solides Irradiés, Ecole Polytechnique, CEA/DRF/IRAMIS, CNRS,
Institut Polytechnique de Paris, 91128 Palaiseau, France

Gallium oxide in the β phase is an ultra wide-bandgap semiconductor with a band gap of 4.7 eV. It is attracting increasing attention because of its promises for high-power electronics, solar-blind photodetectors and other critical.

Transition metals tend to form deep levels in wide-gap semiconductors, limiting their electrical conductivity, and these impurities (in particular iron) are currently used to obtain semi-insulating materials. β - Ga_2O_3 has a monoclinic crystal structure with space group $C2/m$, which is described by the lattice vectors a , b , c and the angle between a and c . Two chemically-distinguishable cation sites are coordinated with oxygen ions in either tetrahedral or octahedral configuration.

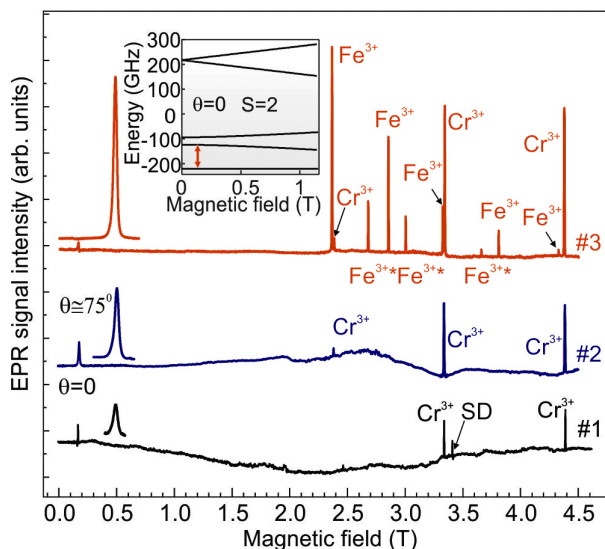


Fig. 1. EPR spectra of β - Ga_2O_3 Samples #1, #2, and #3 measured in cw EPR at 94 GHz for the magnetic field oriented along $[010]$ crystal axis ($\theta = 0^\circ$). Low-field signals are also shown for $\theta = 75^\circ$ crystal orientations (rotation around $[102]$ axis). Fe^{3+} signals of iron in the tetrahedral positions are marked with an asterisk, Fe^{3+*} . The inset shows a conventional energy-level diagram for the center with spin $S = 2$, which we attribute to Fe^{2+} . The arrow in the diagram indicates the observed EPR transition at 94 GHz for the orientation of the magnetic field along the z axis ($\theta = 0$).

The EPR spectra were studied in three β -Ga₂O₃ samples: #1 – pristine, i.e., non-irradiated; #2 – irradiated the samples with high-energy electrons at the dose of 180 mC/cm²; #3 – irradiated at the dose 500 mC/cm².

Using high-frequency EPR we have observed non-Kramers ions with a giant zero-field splitting of the order of 100 GHz in *n*-type β -Ga₂O₃ crystals. These EPR spectra were assigned to Fe²⁺ ions ⁵D (3d⁶) with *S* = 2. This interpretation was supported by experiments on Fermi level displacement induced by high-energy electron irradiation and photoexcitation of irradiated samples with 405-nm laser light. The sign of the parameter *D* was also determined to be positive.

The values and signs of the basic parameters of the spin Hamiltonian for ions, namely Cr³⁺ (*S* = 3/2) and Fe³⁺ (*S* = 5/2), were identified and the order of their spin levels was established.

The spectra were obtained thanks to the use the thigh-frequency 94 GHz EPR/ODMR spectrometer developed at the Ioffe Institute in cooperation with the DOK company [1].

This work was supported by the Russian Science Foundation under Grant № 20-12-00216. We thank the SIRIUS team for the beam time devoted to our investigation and personally A. Alessi, O. Cavani and A. Courpron for technical support. We are grateful to A. Woloś (Warsaw University) for preliminary EPR measurements and valuable suggestions and to M. Konczykowski and R. Grasset (LSI Ecole Polytechnique) for sample irradiations and fruitful discussions. We thank T. Huong Dang and Henri Jaffrès for their contribution to many discussions.

1. Babunts R.A., Badalyan A.G., Gurin A.S., Romanov N.G., Baranov P.G., Nalivkin A.V., Bogdanov L.Yu., Korneev D.O.: Applied Magnetic Resonance **51**, 1125–1143 (2020)



SECTION 9

MAGNETIC RESONANCE INSTRUMENTATION

Construction and application of dry 6 K ultra-low temperature continuous wave and pulsed EPR

F. Yingying^{1,2}, T. Yulan¹, Q. Zirui¹, L. Wenyu¹, L. Yong¹,
S. Zhifu², Y. Haijun¹

¹Department of Chemistry, Tsinghua University, Beijing 10084, China, cyhj@tsinghua.edu.cn

²Chinainstru & Quantumtech (Hefei) Co., Ltd., Hefei 230088, China

There were four main advantages of cryogenic technology in electron paramagnetic resonance spectroscopy (EPR) research: (1) Improve the sensitivity of the spectrometer; (2) Increase the sample stability; (3) Weaken the effect of polar solvents on solution samples; and (4) Extend T_1 and T_2 relaxation to better detection of spin echoes. Currently, the ultra-low temperature EPR was usually realized by the liquid helium cooling system. Due to issues such as insufficient global helium supply and rising gas prices, cryogenic systems were expensive (typically requiring 2L of liquid helium per hour) and difficult to run continuously for a long time, leading to many cryogenic studies being impractical. In collaboration with China's CIQTEK Company, a dry temperature-variable unit was developed independently and constructed successfully with helium as the circulating gas and a GM chiller as the cold source to achieve closed-cycle refrigeration. The dry temperature-variable unit was combined with CIQTEK's X-band EPR spectrometer (EPR100), which could achieve continuous wave and pulsed EPR in the temperature range of 6 K to 300 K to maintain stable work for more than 200 hours while costing less than ten percent of the cost of liquid helium cooling system. This cryogenic system was used to test continuous wave EPR of the coal sample at various temperature (Fig. 1), and the data indicated

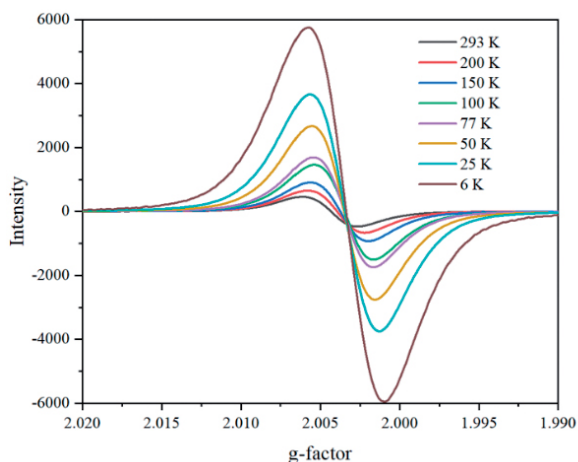


Fig. 1. EPR spectra of the coal sample at various temperature.

that the double integration area of the EPR signal at 6 K was nearly 42 times larger than that at 293 K. In addition, the following two experiments have been used dry 6 K ultra-low temperature EPR technology. (1) The forbidden half-field transition signal ($\Delta m_2 = \pm 2$, $g \approx 4.0$) of triplet diradical which is difficult to observe at room temperature was successfully recorded. The average spin–spin distance R (in angstroms) was calculated by the relative intensity between the signal of the allowed transition $|\Delta m_2 = 1|$ and that of the forbidden transition $|\Delta m_2 = 2|$ ($|\Delta m_2 = 2| / |\Delta m_2 = 1| = (F/r^6) (9.1/\nu)^2$, where ν is the resonance frequency in gigahertz and $F = 19.5$ for organic radicals). (2) The structure of Cu^{2+} complexes in solution were studied using electron spin echo envelope modulation (ESEEM) pulse experiments, and the presence of N and H nuclei around Cu^{2+} was resolved from the obtained frequency domain spectra. ESEEM may provide structural information such as atomic species directly and requires less fitting than the extended X-ray absorption fine structure (EXAFS) method. This novel form of dry temperature-variable unit basically did not consume helium due to closed circulation, which greatly saved helium and the costs of spectrometer's operating. It would considerably boost research in related fields.

1. Manabu A.: Chem. Rev. **7011**, 113 (2013)

Use of adiabatic pulses for spin-echo experiments in magnetic materials

I. Mershie¹, G. Kupriyanova¹, S. Wurmehl²

¹Institute of Physics and Technology, Immanuel Kant Baltic Federal University, Kaliningrad 236041, Russia

²Leibniz Institute for Solid State and Materials Research, Dresden, Germany, IMershie¹@kantiana.ru

In NMR, adiabatic pulses are generally magnitude and frequency or phase-modulated pulses that could perform excitation over a broad range of resonant frequencies with a high degree of tolerance to RF field inhomogeneity[1]. Adiabatic pulses could produce broadband excitation and inversion even in the highly inhomogeneous B_1 field, and, unlike the conventional constant frequency pulses, their bandwidth is no longer defined by pulse duration. For a frequency-swept pulse, the excitation bandwidth is no longer defined by the pulse length but can be optimized independently for the needs of the current experiment. These properties proved themselves useful in broadband NQR and pulsed EPR excitation [2, 3] for sensitivity enhancement. Other applications include NMR tomography, where measurements are performed in a large gradient of B_0 field. NMR in magnetic materials is another field of magnetic resonance spectroscopy that deals with very broad spectra up to hundreds of MHz. Because of the intrinsic properties of magnetic materials, spin dynamics of nuclei in domain walls is complex, and conventional NMR concepts as 90° or 180° pulse are not usually applicable for the design of such kind of experiments.

The series of experiments were performed at room temperature with a bulk polycrystalline Co_2FeGa sample at ^{61}Co frequency of 180 MHz with a Tecmag

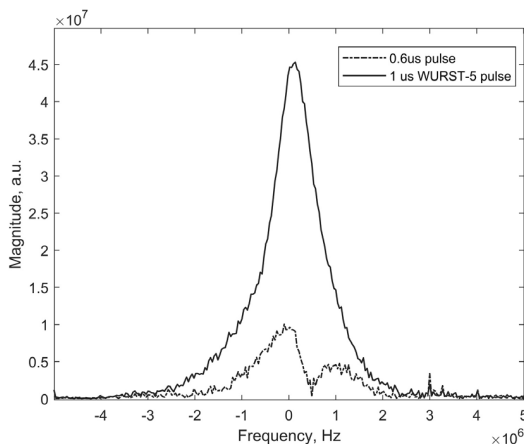


Fig. 1. Fourier spectra of echo signals in Co_2FeGa , obtained with conventional and adiabatic WURST-5 pulses.

Redstone NMR spectrometer. A solid echo NMR sequence with 1 μs WURST-5 adiabatic pulses with 64 points of phase modulation and 0.6 μs common rectangular pulses were used. Experimental time, amplifier attenuation, and the number of scans were the same for every two sets of experiments. The improvement in signal power, using adiabatic excitation, was at least three times higher compared to conventional excitation with rectangular pulses. Optimal excitation power at room temperature for WURST-5 pulses was roughly the same in comparison to conventional excitation.

There are two causes of such an improvement of the echo signal power. First, a compensation of the gradient of excitation field in domain walls, caused by the dispersion of enhancement factor. Second, to a lesser degree, a compensation of the magnetic field gradient inside the coil (caused by the imperfections of the coil and distortion of the field by the high magnetic susceptibility of the sample).

The experimental results show that compensation of effective B_1 excitation field in domain walls leads to an improvement of echo signal magnitude at a reasonable level of excitation power. However, the positive effect might depend on the overall magnetic susceptibility of the sample, the width of domain walls, and other factors. Phase and magnitude distortion of echo signal with adiabatic pulses was negligible at optimal pulse power. This effect could be used to improve the sensitivity of the NMR spectroscopy in magnetic materials, which is important for the experiments with low natural abundance isotopes (^{53}Cr , ^{57}Fe , ^{61}Ni).

Financial support. The work was supported by Ministry of Education and Science of Russia and DAAD foundation, project №2261-21.

1. Garwood M., DelaBarre L.: J. Magn. Reson. **153**, 155 (2001)
2. Rossini A.J., Hamaed H., Schurko R.W.: J. Magn. Reson. **206**, 32 (2010)
3. Baum J., Tycko R., Pines A.: Phys. Rev. A **32**, 3435 (1985)

Pulse X-band EPR-spectrometer with microwave digital synthesizer, 300 W solid-state power amplifier, and AWG unit

**K. Lomanovich¹, E. Bagryanskaya¹, S. Veber^{1,2}, N. Isaev^{1,3},
A. Melnikov^{1,2,3}, M. Dugin⁴, M. Bowman^{1,5},
M. Ivanov^{1,2}, D. Polovyanenko¹**

¹N.N. Vorozhtsov Novosibirsk Institute of Organic Chemistry SB RAS, Novosibirsk 630090, Russia, lomanovich@nioch.nsc.ru

²International Tomography Center of SB RAS, Novosibirsk 630090, Russia

³Voevodsky Institute of Chemical Kinetics and Combustion SB RAS, Novosibirsk 630090, Russia

⁴Micran, 634041, Russia

⁵Department of Chemistry & Biochemistry, University of Alabama, AL 35487-0336, USA

Pulse EPR spectroscopy is a powerful tool for studying unpaired electron spin local environment. To measure pulse EPR one requires a spectrometer, which would create MW pulses of 100–1000 W (at X-band) to excite an electron spin system and to detect spin echo or FID at the level of nW shortly, 80–100 ns, after reflected pulse comes to the detector.

A new EPR spectrometer with X-band microwave bridge based on modern elements and modules, developed at the Laboratory of Magnetic Resonance of Biomolecular Systems (NIOCH SB RAS), is presented. To control the spectrometer was used computer with installed modules: pulse blaster, digitizer and AWG. The software “Atomize” is specially created and used to control the spectrometer.

A digital frequency synthesizer was used as a microwave signal source, which allows the bridge to operate in the frequency range 8.5–12.0 GHz. A 300-watt solid-state semiconductor power amplifier was used, which has some advantages with comparison with lamp amplifier: it has a stable output power and a stable phase of pulse, regardless of the operating modes of the microwave bridge. The bridge doesn't content a CW low power module, which is usually necessary for spectrometer tuning (switching keys add noise to signal), tuning is done in pulse mode. The microwave bridge can operate in two modes: with rectangular pulses with a minimal duration 12 ns, or with arbitrary waveforms. The low-noise amplifier in receiving path contains a 3-stage pulse protection with attenuation 70 dB.

The broadband EPR dielectric resonator was developed to fit the requirements for AWG experiments with chirp pulses. The resonator was installed in a flow-through gel cryostat, which made it possible to operate at temperatures from 80 °K with liquid nitrogen and 4 °K with liquid helium to 300 °K.

The spectrometer capabilities were demonstrated with both rectangular and AWG pulse experiments.

This work was supported by the Ministry of Science and Higher Education of the Russian Federation (grant 14.W03.31.0034).

A new player in the EPR spectroscopy market: high-tech solutions for X- and W-band from ZHONGTAI

M.L. Kuklinov, A.S. Petrov, A.I. Chazov

Element company – Gold Sponsor of the conference

In 2022, a new player appeared on the EPR spectroscopy market: ZHONGTAI (China), in a partnership with its official authorized partner, company ELEMENT, for the first time in Russia, presents a line of desktop and floor standing EPR spectrometers of the ZT series. Production of modern high-tech spectrometers of electron paramagnetic resonance on par with well-known American and Japanese brands, is one of the significant activities of the company. The company's work is based on high-precision quantum measurement technologies, the source of which since 2000 is the leading laboratory of microscale magnetic resonance of the Chinese Academy of Sciences at the University of Science and Technology of China. This laboratory focuses on the research of spin quantum control and its applications in novel quantum technologies, with various experimental routes including nuclear magnetic resonance (NMR), electron spin resonance (ESR), optically-detected magnetic resonance (ODMR), magnetic resonance force microscopy (MRFM), and electrically-detected magnetic resonance (EDMR) [1, 2].

The range of X-band EPR spectrometers includes the ZT6500 benchtop EPR spectrometer, the ZT15C research grade floor standing EPR spectrometer, and the ZT15P research grade pulsed EPR spectrometer. The ZT60W high-frequency W-band EPR spectrometer is also available in the line.

The model of the desktop spectrometer ZT6500 has worthy characteristics for its class of instruments: sensitivity $5 \cdot 10^9$ spin/G, signal:noise ratio at the level of 600:1, modulation frequency 10/50/100 kHz and small overall dimensions and weight. This spectrometer was used to study $W_{18}O_{49}$ as an oxygen-deficient drug delivery system [3] and $ZnSn(OH)_6$ with hydroxyl vacancies at ultralow temperature (6 K) [4].

ZT15C research class floor standing EPR spectrometer with the following characteristics: sensitivity $3 \cdot 10^9$ spin/G, magnetic field range $-0.1 \sim 1.8$ T, as well as the possibility of using cooling systems based on liquid helium and



Fig. 1. ZHONGTAI X-band EPR spectrometers.

nitrogen. This spectrometer was used to determine the stability of the radical cation [6]CPP \subset [12]CPP [5] and to study the structure of the H₂ADC ligand [6].

The research-grade pulsed EPR spectrometer ZT15P, in addition to the CW mode with characteristics similar to ZT15C, has decent performance for the pulsed mode: the microwave source pulse time resolution is 50 ps, the maximum output power of the solid-state power amplifier is 450 W, the microwave pulse phase stability is less than 3° in 1 ms, the maximum duration of the microwave pulse is 3 ms and up to 20,000 pulses per channel. An example of the use of such a device can be the study of the effect of an oxygen vacancy on the valence and chemical state of Co in the compound Co₃O₄ [7].

In less than 5 years of production, ZHONGTAI has delivered about 30 competitive EPR spectrometers of high level of reliability and quality to the China market. Given the accumulated knowledge and experience, the company highly appreciates the growth opportunities in international markets, including the market of the Russian Federation.

1. Yudi Ma, Ruijuan Liu, Lingjing Ji, Liyang Qiu, Saijun Wu, Dianqiang Su, Yanting Zhao, Ni Yao, Wei Fang: “Composite picosecond control of atomic state through a nanofiber interface”, arXiv preprint arXiv: 2203.06716 (2022), <https://doi.org/10.48550/arXiv.2203.06716>
2. Yue Li, Zhi-Cheng He, Xinxing Yuan, Mengxiang Zhang, Chang Liu, Yi-Xuan Wu, Mingdong Zhu, Xi Qin, Zheng-Yuan Xue, Yiheng Lin, Jiangfeng Du: “Experimental Demonstration of Swift Analytical Universal Control over Nearby Transitions”, arXiv preprint arXiv: 2201.06246 (2022), <https://doi.org/10.48550/arXiv.2201.06246>
3. Zhihuan Zhao, Shasha Yang, Pengfei Yang, Jianying Lin, Jimin Fan, Bing Zhang: “Study of oxygen-deficient W18O49-based drug delivery system readily absorbed through cellular internalization pathways in tumor-targeted chemo-/photothermal therapy”, *Biomaterials Advances*, Volume 136, 2022, 212772, ISSN 2772-9508, <https://doi.org/10.1016/j.bioadv.2022.212772>.
4. Yuhan Li, Bangfu Chen, Ping Ouyang, Youyu Duan, Wee-Jun Ong, Fan Dong: “Engineering ZnSn(OH)₆ with ternary active sites-directed hydroxyl vacancies for robust deep C6H6 photo-oxidation: Experiment and DFT calculations”, *Chemical Engineering Journal*, Volume 451, Part 2, 2023, 138695, ISSN 1385-8947, <https://doi.org/10.1016/j.cej.2022.138695>.
5. Chong Zhao, Fupin Liu, Lai Feng, cMingzhe Nie, Yuxi Lu, Jie Zhang, Chunru Wang, Taishan Wang: “Construction of a double-walled carbon nanoring”, *Nanoscale*, 2021, 13, 4880-4886, <http://dx.doi.org/10.1039/D0NR08931A>.
6. Hu, JX., Li, Q., Zhu, HL. et al.: “Achieving large thermal hysteresis in an anthracene-based manganese(II) complex via photo-induced electron transfer”, *Nat Commun* 13, 2646 (2022). <https://doi.org/10.1038/s41467-022-30425-1>
7. Dongfang Chen, Lyuming Pan, Pucheng Pei, Shangwei Huang, Peng Ren, Xin Song: “Carbon-coated oxygen vacancies-rich Co₃O₄ nanoarrays grow on nickel foam as efficient bifunctional electrocatalysts for rechargeable zinc-air batteries”, *Energy*, Volume 224, 2021, 120142, ISSN 0360-5442, <https://doi.org/10.1016/j.energy.2021.120142>.

SECTION 10

ELECTRON SPIN BASED METHODS
FOR ELECTRONIC AND SPATIAL STRUCTURE
DETERMINATION IN PHYSICS, CHEMISTRY AND
BIOLOGY

Spin-dependent afterglow of irradiated crystals: an ODMR study

N.G. Romanov

Ioffe Institute, Saint Petersburg 194021, Russia,
nikolai.romanov@mail.ioffe.ru

Ionic crystals and wide-gap semiconductors exposed to ionizing radiation can produce luminescence that persists at low temperatures for a long time (up to many hours) after the end of irradiation. Such an afterglow is due to a tunneling recombination between nearby trapped electrons and holes. In nonmagnetic media, there is a strong decrease in the intensity of the afterglow caused by partial polarization of the electron spins of defect pairs in an external magnetic field as was first reported in ref. 1. The application of a resonant microwave field tends to compensate the magnetic field effect and allows the optical detection of EPR of the centers responsible for the afterglow process (see [2], [3] and references therein).

This paper presents an overview of studies of spin-dependent afterglow by optically detected magnetic resonance (ODMR) at the Ioffe Institute.

The following topics will be covered:

1. Effect of a magnetic field on the spin-dependent recombination afterglow in nonmagnetic matrices. ODMR identification of recombination centers in ionic crystals, as well as in bulk crystals and nanocrystals of wide-gap semiconductors.
2. Energy transfer from the matrix to embedded self-organized CsPbBr₃ and CsEuBr₃ nanocrystals in irradiated CsBr:Pb and CsBr:Eu crystals.
3. Peculiarities of spin-dependent recombination in irradiated magnetic crystals. Stimulation of the afterglow by magnetic field in cerium doped gadolinium garnet.

The financial support of the Russian Science Foundation (grant 20-12-00216) is gratefully acknowledged.

1. Delbecq C.J., Yuster P.H.: *Phys. Status Solidi B* **68**, K21 (1975)
2. Baranov P.G., Veshchunov Yu.P., Romanov N.G.: *Sov. Phys. Solid State* **22**, 2186 (1980)
3. Babunts R.A., Romanov N.G., Tolmachev D.O., Badalyan, A.G., Khramtsov V.A., Baranov P.G., Rauh D., Dyakonov V.: *Phys. Sol. State*, **51**, 2437 (2009)

EPR spectroscopy of Ytterbium dimer associates in synthetic forsterite Mg_2SiO_4

**V. Tarasov¹, A. Sukhanov¹, K. Salikhov¹, E. Zharikov², K. Subbotin²,
V. Dudnikova³**

¹Zavoisky Physical-Technical Institute, FRC Kazan Scientific Center of RAS, Kazan 420029, Russia, tarasov@kfti.knc.ru

²Laser Materials and Technology Research Center, Prokhorov General Physics Institute, Moscow 119991, Russia

³Faculty of Geology, Moscow State University, Moscow 119991, Russia

Rare earth impurity ions in crystals are widely studied as possible material basis for practical implementation of information technologies based on the laws of quantum mechanics. Among them, they are quantum calculations, quantum telecommunications and quantum memory. We used ELEXSYS E680 spectrometer with a cylindrical dielectric resonator ER4118MD5-W1 for continuous wave and pulse electron paramagnetic resonance (EPR) spectroscopy to determine structure, magnetic and relaxation properties of impurity ytterbium ions in forsterite (Mg_2SiO_4) single crystal. Crystal was grown by the Czochralski technique in nitrogen atmosphere from the melt containing 0.15 at.% of ytterbium in respect to Mg^{2+} .

Three structurally different paramagnetic centers formed by the ytterbium ions in forsterite were observed and studied. They are single Yb^{3+} ion substituting Mg^{2+} ion in the M1 site and two dimer associates of Yb^{3+} ions substituting Mg^{2+} ions in two M1 sites. At that, concentrations of dimer associates were several orders of magnitude higher than the concentration of associates formed randomly at the statistical distribution of impurity ions over the crystal. The first dimer consists of two ytterbium ions and magnesium vacancy between them substituting three magnesium ions in the M1 sites forming a chain parallel to the *c* crystallographic axis [1]. The second dimer is formed by Yb^{3+} ions in two nearby M1 sites with magnesium vacancy in adjacent M2 site [2].

1. Tarasov V.F., Sukhanov A.A., Dudnikova V.B., Zharikov E.V., Lis D.A., Subbotin K.A.: JETP Letters, **106**, 92 (2017)
2. Tarasov V.F., Sukhanov A.A., Zharikov E.V., Subbotin K.A., Lis D.A.: Appl. Magn. Reson., Publ. online 29.11.2021. DOI: <https://doi.org/10.1007/s00723-021-01453-9>

Graphene oxide membranes: the connection between inner structure and sorption properties

A. Rebrikova¹, A. Kaplin¹, M. Matveev¹, N. Chumakova², M. Korobov¹

¹M.V. Lomonosov Moscow State University, Chemistry Department, Leninskiye Gory, 1/3, Moscow 119991, Russia, niccolumtesla@mail.ru

²N.N. Semenov Federal Research Center for Chemical Physics, Russian Academy of Science, Kosygin St. 4, Moscow 119991, Russia

Graphite oxide (GO) is a multilayered material that can easily sorb polar molecules and be dispersed in polar liquids with the formation of stable suspensions. The graphite oxide suspensions are used to manufacture of graphene oxide membranes (GOMs) which were found to possess unique selective permeability for polar substances. It is considered that the reason for the selectivity is the difference in sorption by membranes of various polar molecules. It was also experimentally shown that permeability of GOMs is connected with their inner structure, specifically, with the orientational order of the graphene oxide layers [1]. Considering the foregoing, it is necessary to establish a connection between inner structure of GOMs and their sorption properties.

At present work the data on sorption of acetonitrile and water by GO powder and two GOMs, manufactured from this powder, was obtained, and compared with the orientational order of GOMs. Ordering of the graphene oxide layers in the membranes was determined using spin probe technique according to the method which was worked out in our scientific group [2]. GOM, manufactured by evaporation of GO suspension, turned out to be practically not aligned; and sorption of acetonitrile and water by this GOM and GO powder was the same. GOM, manufactured by filtration of GO suspension, was oriented with the order parameter $P_{20} = 0.21$; sorption of water by this GOM was the same as by GO powder, but sorption of acetonitrile was zero.

Based on the experimental data, the following conclusions can be made. Firstly, the orientational order of GOM depends on manufacturing method. Secondly, sorption seems to be in connection with orientational order of GO layers inside the membrane.

The work was supported by RSF (grant 21-73-00124).

1. Akbari A., Sheath P. et al.: Nature Communication **7**(1), 1–12 (2016)
2. Chumakova N.A. et al.: J. Phys. Chem. C **122**, 22750–22759 (2018)

Room temperature coherent control of negatively charged NV defect in silicon carbide

K. Sannikov, I. Gracheva, G. Mamin, F. Murzakhanov, V. Soltamov

Institute of Physics, Kazan Federal University, Kazan 420008, Russia,
p8376272@gmail.com

The unique properties of SiC, such as high thermal conductivity, high breakdown voltage and wide bandgap, have made it one of the most prominent materials for high-power and high-temperature electronic devices. Various mature fabrication methods originating from silicon technology have been applied to SiC and fabrication of sophisticated nanostructures has been demonstrated [1]. By combining this with a unique property of SiC – that is, a wide bandgap for broadband optical access across the visible to infrared – SiC has also

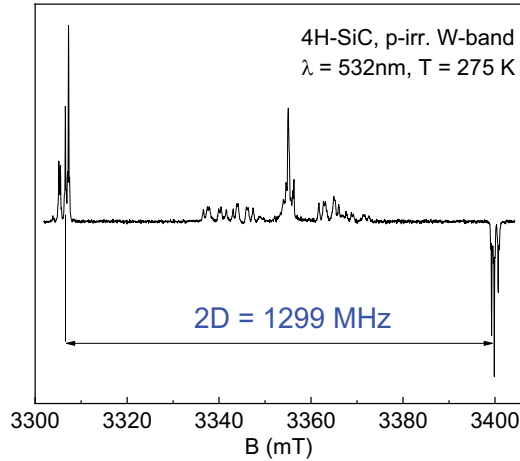


Fig. 1. EPR spectra of NV centers in SiC relaxation times [2].

become a promising platform for nanophotonics. Most recently, defects in SiC have attracted attention as potential hosts for quantum spin systems. The weak spin-orbit coupling gives it the potential to give long spin relaxation times [2].

In this work, we studied the silicon carbide ($^4\text{H SiC}$) irradiated by a flow of high-energy protons $E = 12$ MeV, which lead to the formation of defects in the structure. We succeeded in registering photoinduced EPR (Fig. 1) and ENDOR signals at a constant temperature in the high-frequency range of the spectrometer. The excitation was carried out by optical pumping by laser sources with a wavelength of 532 nm. Having established the optimal experimental conditions, the relaxation times were measured $T_1 = 105(5)$ μs and $T_2 = 13.8(4)$ μs . By ENDOR results the hyperfine and quadrupole interaction values were determined to approved the nature of NV_{kk} and NV_{hh} defects.

The work is carried out in accordance with the Strategic Academic Leadership Pro-gram “Priority 2030” of the Kazan Federal University of the Government of the Russian Federation.

1. Widmann, M. et al.: Nature materials **14**, 164–168 (2015)
2. Murzakhanov F.F., Yavkin B.V., Mamin G.V.: Phys. Rev. B **103**, 245203 (2021)

Manganese impurity dynamic polar centres in SrTiO₃

**B. Gabbasov¹, R. Yusupov¹, D. Zverev¹, A. Rodionov¹, L. Jastrabik²,
V. Trepakov³**

¹Kazan Federal University, Kremlevskaya 18, Kazan 420008, Russia
BFGabbasov@kpfu.ru

²Institute of Physics, Na Slovance 2, 18221, Prague 8, Czech Republic

³Ioffe Physical-Technical Institute RAS, St. Petersburg 194021, Russia

Pure strontium titanate SrTiO₃ (STO) is a so-called quantum paraelectric which means that the transition to a ferroelectric state at low temperatures is prohibited by quantum fluctuations. However, such transition may be induced by application of the electric field, uniaxial pressure, illumination with the UV-light or doping with the appropriate off-centre impurities. One of the interesting examples of the impurity-induced ferroelectricity in STO is the case of its doping with manganese.

Electron paramagnetic resonance (EPR) studies of the manganese-doped STO (STO:Mn) at the temperatures above 100 K reveal the spectra of cubic Mn⁴⁺ and Mn²⁺ centers, several axial Mn³⁺ centers associated with oxygen vacancies, Mn⁴⁺-Mn⁴⁺ pairs. An on-going intense discussion is related to the substitutional position of the Mn²⁺ ions: whether these species replace the octahedral Ti⁴⁺ or 12-fold-coordinated Sr²⁺ sites and whether these species possess center of symmetry or not. We report on the new results of the X-band (9.4 GHz) EPR studies of the high-quality Verneuil-grown STO:Mn single crystals from Furuuchi Chemical Corporation. In the EPR spectra the peculiar transformation of the $S = 5/2$ Mn-related signal is observed. While at room temperature and above it reveals an ideal cubic symmetry, on cooling down, the spectrum broadens significantly and can hardly be identified below 100 K. At $T \sim 10$ K the spectra of the two low-symmetry $S = 5/2$ Mn-related centres appear and grow steeply in intensity on temperature decrease.

One centre is almost axial, with the principal axis tilted by ~ 12 degrees from the quasi-cubic [001] direction in the (100) or (010) plane (Fig. 1). Angular variation of the spectrum is well described by the spin-Hamiltonian with the parameter values of $g_{zz} = 2.0155$, $g_{xx} = g_{yy} = 2.0059$, $D = 3/2$, $D_{zz} = 645$ MHz and $E = 1.2(D_{xx} - D_{yy}) = 31$ MHz. This centre's point symmetry is monoclinic C_s .

Another centre is of the rhombic C_{2v} symmetry and its principal directions are along the quasi-cubic $\langle 011 \rangle$ crystal axes (Fig. 1). Angular variation of the spectrum is also described by an $S = 5/2$ spin-Hamiltonian with the following parameters: $g = 2.0032$, $D = 3/2$, $D_{zz} = 1445$ MHz, $E = 1/2(D_{xx} - D_{yy}) = 140$ MHz. Spectra of both centres reveal almost identical temperature dependences and very close hyperfine splittings due to the interaction with $I = 5/2$ manganese nuclear spin ($A = 243$ MHz). The ratio of the two spectra intensities varies strongly from sample to sample.

Ab initio calculations [1] indicate several possibilities of the axial $S = 5/2$ Mn-related centre formation. Among the proposed models there are off-centre Mn²⁺ ions at the Sr-site with the C_{4v} symmetry and complex centres that involve

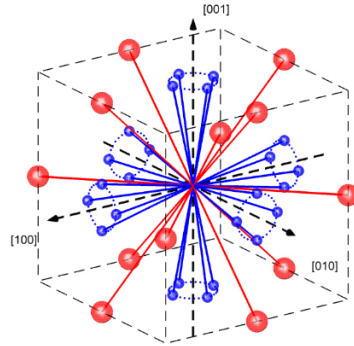


Fig. 1. Principal axes directions of the impurity Mn^{2+} -ion centers in SrTiO_3 crystals with monoclinic (blue segments) and rhombic (red segments) symmetry.

the Mn^{3+} ion at the Ti-site and an electron either localized at one of the nearest Ti-ions (C_{4v}) or delocalized within two of them (C_{2v}). All the proposed structures imply a nonzero electric dipole moment that may be a source for the observed low-temperature dielectric phenomena in STO:Mn .

Also, we present the results of the electric field effect studies in the EPR spectra of Mn^{2+} ions in STO in order to test the hypothesis of their noncentrosymmetric position. An observation of splitting of the spectrum components suggests that inversion-nonequivalent centers of Mn^{2+} ions of orthorhombic symmetry are found. This, in turn, provides the grounds to claim unambiguously that the Mn^{2+} ions occupy the off-centre position in the case of the orthorhombic-symmetry center. Accordingly, such centers have a nonzero electric dipole moment and, with a high probability, namely these centers are responsible for a local transition of strontium titanate to a polar state, which in turn causes the low-temperature dielectric hysteresis loops in manganese-doped strontium titanate.

The work is supported by RSCF, research project No. 22-72-00132.

1. Kvyatkovskii O.E.: Ab initio calculations of neutral and charged impurity centers of manganese and chromium in strontium titanate, *Physics of the Solid State* **54**, 1397–1407 (2012)

SECTION 11

OTHER APPLICATIONS OF MAGNETIC RESONANCE

Experimental manifestation of spin polariton in dilute solutions of nitroxyl radicals

K.M. Salikhov, M.M. Bakirov, R.B. Zaripov, I.T. Khairutdinov

Zavoisky Physical-Technical Institute, FRC Kazan Scientific Center of RAS, Kazan 420029, Russia

Recently, one of us proposed a new paradigm in a scientific discipline known as spin exchange in dilute solutions of paramagnetic particles [1–3]. The new paradigm of spin exchange predicts that due to the “recoil” of quantum coherence in a course of collisions of paramagnetic particles collective excitations of spins, i.e. spin excitons, are formed. According to the new paradigm, the frequencies of spin excitons should depend on the power of the microwave field. On this basis, it was concluded that, by analogy with “dressed atoms”, we are dealing with “dressed” spin excitons. They were called spin polaritons.

In this report, we will present the experimental data obtained by us when studying EPR spectrum for dilute solutions of ^{15}N containing nitroxide radicals. The results obtained confirm the frequency shift of spin excitons caused by the interaction of spins with an alternating field. Moreover, that shift is in a quantitative agreement with theoretically predicted value.

1. Salikhov K.M.: Fundamentals of spin exchange. Story of a paradigm shift. Springer (2019)
2. Salikhov K.M.: Current state of the theory of the spin exchange in dilute solutions. New paradigm of spin exchange and its manifestation in EPR spectroscopy. *Uspekhi Physics* **189**, 1017–1043 (2019)
3. Salikhov K.M.: Peculiar features of the spectra saturation effect when the spectral diffusion operates. System with two frequencies. *Appl. Magn. Reson.* **5**, 49, 1417–1430 (2018)
4. Salikhov K.M.: New information about manifestations of spin exchange in the EPR spectra of solutions of paramagnetic particles under saturation conditions. *Appl. Magn. Reson.* **52**, 1063–1091 (2021)

Gyroscope based on NV color center in diamond

**V.V. Soshenko^{1,2}, S.V. Bolshedvorskii^{1,2}, O.R. Rubinas^{1,2,4}, I.S. Cojocar^{1,2,4},
V.N. Sorokin^{1,2}, A.N. Smolyaninov², A.V. Akimov^{1,2,4,5}**

¹PN Lebedev Institute RAS, Moscow 119991, Russia, akimovwork@mail.ru

²LLC Sensor Spin Technologies, Moscow, Russia, leshakimopv@gmail.com

³Russian Quantum Center, Moscow 143025, Russia

⁴Moscow Institute of Physics and Technology, Dolgopudnii, Moscow Region 141701, Russia

⁵National University of Science and Technology, Moscow 119049, Russia

A rotation sensor is one of the key elements of inertial navigation systems and compliments most cellphone sensor sets used for various applications. Currently, inexpensive and efficient solutions are mechano-electronic devices, which nevertheless lack long-term stability. The lack of such stability comes from the ageing of the device and degradation/change of the artificially created features of micromechanical device. Much like it was done in case of frequency measurements, length and mass, there is need it creating device base on properties of elementary particles. Such a device may become a drift-free alternative to micromechanical devices. Here, we carry out a proof-of-concept experiment, demonstrating rotation measurements on a rotating setup utilizing nuclear spins of an ensemble of NV centers as a sensing element with no stationary reference. The measurement is verified by a commercially available MEMS gyroscope.

NQR detection system of nitrogen compounds in large inspection volumes

**G.V. Mozzhukhin¹, E. Doğan¹, A.F. Cakal¹, B. Colak¹, P. Kupriyanov^{1,2},
R. Khusnutdinov³, B. Rameev^{1,3,4}**

¹Gebze Technical University, 41400 Gebze/Kocaeli, Turkey, mgeorge@gtu.edu.tr

²St. Petersburg State University, St. Petersburg 199034 Russia

³Zavoisky Physical-Technical Institute, FRC Kazan Scientific Center of RAS, Kazan 420029,
Russia

⁴Kazan State Power Engineering University, Kazan, Russia

Nuclear Quadrupole Resonance (NQR) detection of nitrogen compounds has important applications in industry and security [1]. The main problem of ^{14}N NQR is an inherently very small signal-to-noise ratio in comparison with other magnetic resonance techniques. Recently use of ammonium nitrate (AN, NH_4NO_3) became an important problem for safety and security because this substance can be used as a component of improvised explosives and it is broadly used as a nitrogen fertilizer. It is usually used in large quantities, because the explosion power of ammonium nitrate is somewhat lower comparing with other explosives and it is preferred for use in car and under-road bombs. Therefore, a problem of designing of an RF probe with a large inspection volume and auxiliary units for the detection of AN appears.

In this report, we describe the design of the sensing system for the NQR detection of AN. It consists of Tecmag Scout NQR console, Tomco pulse amplifier (1 kWt), a couple of Hemholtz-like transmitting coils with a size of $65 \times 65 \text{ cm}^2$, 1 receiving planar gradiometer ($25 \times 55 \text{ cm}^2$) and a system for manipulation of the quality (Q) factor of the RF probe. For the detection of NQR signal the ^{14}N resonance frequency of near 497 kHz has been used. The detection of AN for the case of luggage scanner has been demonstrated with use of a large solenoidal RF probe inside an RF shielded volume [2]. However, it has been shown

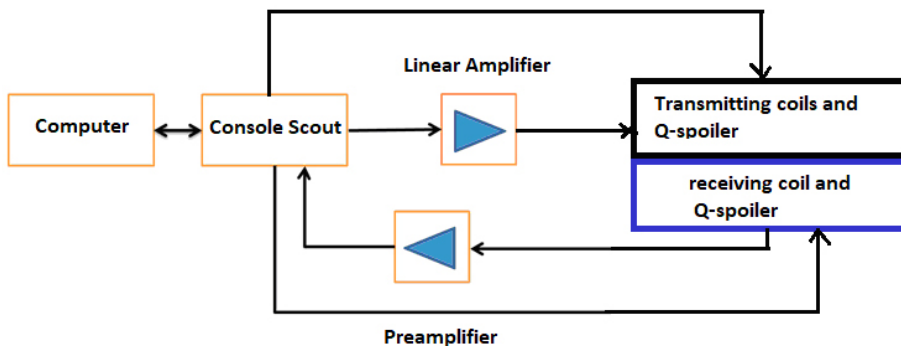


Fig. 1. Diagram of the AN detection system.

that the detection of AN in the case of large objects (e.g. cars) is also feasible although this task is more challenging [3]. It has been shown that the detection of 250 kg of AN is possible with use of specially designed RF probe. In our work we applied approach based on use of separate transmitting and receiving RF probes. A model laboratory setup has been assembled as shown in Fig. 1.

The receiving coil is a planar gradiometric coil made of copper wire with diameter of 2 mm and lateral sizes of $25 \times 55 \text{ cm}^2$. Every part of gradiometer consisted of 12 turns [4]. This planar coil can be easily positioned in any place near the inspected object, therefore it is movable with respect of a transmission probe. It should be noted that the distance between of transmitting coils (of square shape of $65 \times 65 \text{ cm}^2$) was not equal to their half-size but to their full size. Two Q-spoiler units connected to the resonance RF probes have been used. The first one is to decrease the transition process in the receiving RF probe, while the second one is to exclude the mutual influence of transmitting and receiving coils during the processes of irradiation of the sample at transmission stage as well as at the stage of receiving the NQR signal. This laboratory setup has been placed in a special RF shielding room to attenuate the outside noise ($\sim 30 \text{ dB}$). The use of gradiometric receiving coil allows decreasing outside interference for additional 20 dB.

This research was supported by the grant of technological transfer office (TTO) of Gebze Technical University.

1. Miller JB, Barrall G.A.: Explosives detection with nuclear quadrupole resonance. *Am. Scientist* **93**(1), 50–57 (2005)
2. Mozhukhin G.V., Molchanov S.V., Kupriyanova G.S., Bodnya A.V., Fedotov V.V., Hao Guoxin, Jin Yanbo, Ren Tianliang, Zhang Guojin, In book: *Explosives Detection using Magnetic and Nuclear Resonance Techniques*. Series: NATO Science for Peace and Security Series. Springer 231–244 (2009)
3. Barras J., Gaskell M.J., Hunt N., Jenkinson R.I., Mann K.R., Pedder D.A.G., Shilstone G.N., Smith J.A.S.: Detection of ammonium nitrate inside vehicles by nuclear quadrupole resonance. *Appl. Magn. Reson.* **25**, 411–437 (2004)
4. Mozhukhin G., Colak B., Mamadazizov S., Mershev I., Kupriyanova G.S., Rameev B.: “Sensing System for ^{14}N NQR Remote Detection of Explosives”, *Photonics & Electromagnetics Research Symposium (PIERS)*, , pp. 2947–2952 (2021)

Molecular structure and parameters of magnetic interactions in Ni-F_{int} paramagnetic centers synthesized in BaF_2 crystal: EPR data

R.B. Zaripov, V.A. Ulanov, I.V. Yatsyk, G.S. Shakurov

Zavoisky Physical-Technical Institute, FRC Kazan Scientific Center of RAS, Kazan 420029, Russia, zaripovruslan@gmail.com

BaF_2 crystals belong to the group of crystals with the fluorite structure. Their crystal lattice is not densely packed and contains so-called “octahedral holes”. It is known that when crystals of the fluorite group are grown in an atmosphere containing fluorine, defects in the interstitial fluorine ion appear in their lattice, localized in the volumes of “octahedral holes”. Since such defects carry an uncompensated negative charge, their presence stimulates the incorporation of cations with an excess positive charge (Me^{3+}) into the lattice. In the case of doping a BaF_2 crystal with impurities of polyvalent transition metals (for example, nickel), the presence of excess fluorine in the crystal lattice makes it possible to obtain new associative defects.

This work is devoted to the EPR study of the structure and magnetic properties of the “ $\text{Ni}^{3+}\text{-F}_{\text{int}}^-$ ” associative centers formed in $\text{BaF}_2\text{:Ni}$ crystals during their growth in a helium atmosphere containing a small amount of fluorine.

The recorded spectra corresponded to the tetragonal symmetry of the center under study with $S = 3/2$ and contained super hyperfine structure (SHFS) lines from the nine fluorine nuclei (see Fig. 1). The spin moment of the center $S = 3/2$ indicated that the nickel ion in this center is in the Ni^{3+} state. The parameters of the spin Hamiltonian of the “ $\text{Ni}^{3+}\text{-F}_{\text{int}}^-$ ” center were calculated and its molecular structure was established. These centers have not been considered in the literature so far, although they are of interest due to the fact that they should have a significant electric dipole moment and the ability to reorient by diffusion hops of interstitial fluorine into neighboring (equivalent to the Ni^{3+} ion) “octahedral holes”.

The authors acknowledge the financial support from the government assignment for FRC Kazan Scientific Center of RAS for supporting of this research activity and the CSF-SAC FRC KSC RAS for providing necessary facilities to carry out this work.

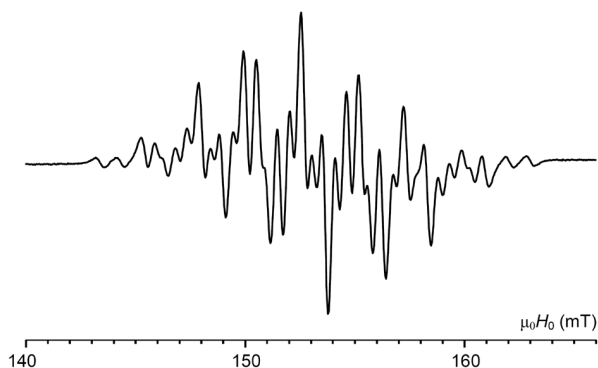


Fig. 1. EPR spectrum of the $\text{BaF}_2\text{:Ni}$ single crystal recorded in the orientation $H_0 \parallel \langle 100 \rangle$ at a frequency $f = 9.4$ GHz and $T = 10$ K.

Voice diseases diagnostics using 3T dynamic MRI and original vocal tests

**M. Fattakhova¹, R. Khabipov¹, V. Krasnozhon², V. Fedorova²,
E. Bekmacheva³, A. Akhatov³**

¹Zavoisky Physical-Technical Institute, FRC Kazan Scientific Center of RAS, Kazan 420029, Russia, mariam.fattakhova@gmail.com

²Kazan State Medical Academy – Branch Campus of the FSBEIFPE RMACPE MOH Russia, Kazan 420012, Russia, vn_krasnozhon@mail.ru

³BarsMed LLC, Kazan, 420138, Khusain Mavlyutova st., 2, becmacheva@yandex.ru

Magnetic resonance imaging was performed on a Siemens Verio with magnetic field induction 3.0 both in the mode of traditional stationary tomography and in the mode of dynamic tomography. The total examination time of the patient was about 46 minutes. In our experiments 23 pulse sequences and their modifications were used. The survey time ranged from 2–3 minutes for traditional shooting modes such as T2-weighted turbo spin echo to 20–30 seconds for dynamic modes. During dynamic studies, for example, for 22 seconds, 73 images of the patient’s vocal organs were obtained, that is, with a period of 300 ms.

One of patients was 78 years old, with several very complex diseases. She underwent surgery on suspicion of cancer. Her voice was gone. We started rehabilitation. But then she got sick with a COVID-19. We had to start over. Complex problems with the voice required the combination of three methods for diagnosis and subsequent rehabilitation.

The “Evenness measurement” test is used for vocalist patients, as it simultaneously reveals the register evenness of the voice, the quality of the sound attack, the ability to exhale the residual breath and take new phonatory breathing, regulate the subglottic pressure by the work of the diaphragm and smooth muscles of the trachea and bronchi, prepare the form of an oropharynx for attacks. The ability to accurately hit the notes in the presence of voice pathology can worsen or completely disappear from voice professionals even with twenty years of experience, since singing is a complex process of coordination of hearing, brain activity, muscle coordination, sound–muscle-motor representation of the sound of the voice and its muscle-coordination implementation. And in the presence of one or another pathology coordination of hearing and voice suffers significantly.

Using MRI and spectral voice analysis it is shown that the “Evenness measurement” test is especially effective for diagnostics of vocalist patients.

Spin and valence states of ions in nanosized bimetallic coordination compounds and their changes upon immobilization in polymer matrix

V.R. Polishchuk, A.M. Ziatdinov

Institute of Chemistry, Far Eastern Branch of the RAS, Vladivostok 690022, Russia,
ziatdinov@ich.dvo.ru

Bimetallic Prussian blue analogs of (PBA) with the general formula $M_xA_y[B(CN)_6]_b \cdot nH_2O$ (where M is an alkali metal cation, A and B are transition metal ions) – one of the oldest studied families of coordination compounds, which have several important fundamental properties and numerous applications in engineering [1–3].

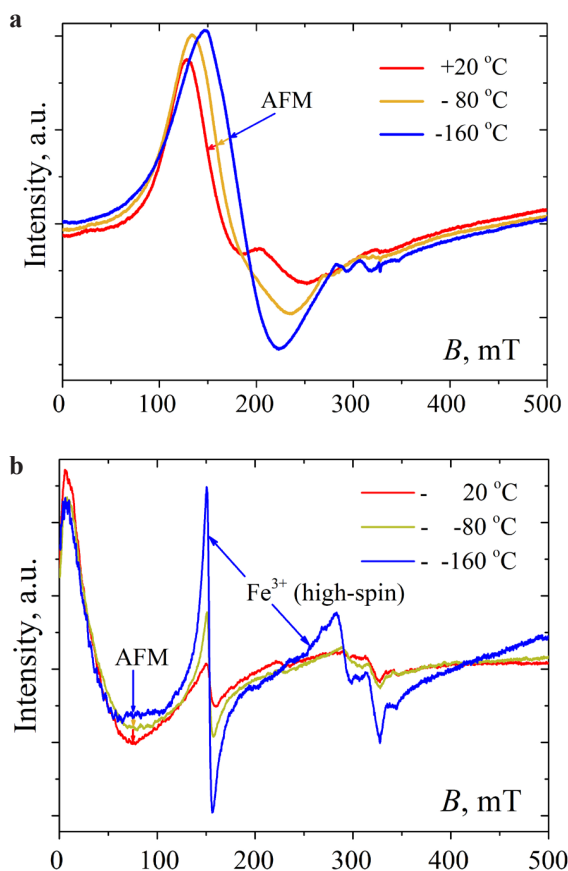


Fig. 1. EMR spectra of powders of **a** zinc ferrocyanide nanosized particles and **b** zinc ferrocyanide nanosized particles immobilized in polyethyleneimine. AFM – the antiferromagnetic resonance spectra.

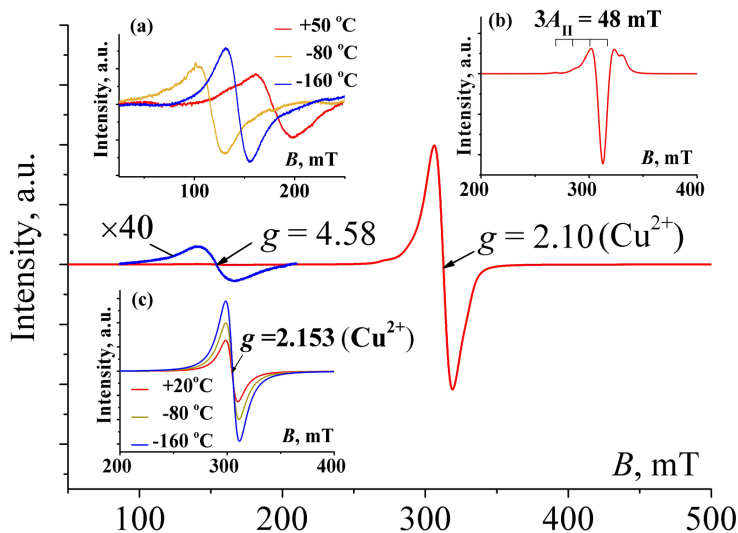


Fig. 2. EPR spectrum of a nanocomposite PEI/Cu₂[Fe(CN)₆] at -160°C. The insets (a), (b), and (c) show the temperature dependence of the low-intensity component of the spectrum, the second derivative of the mean line of the spectrum, and the EPR spectrum of Cu²⁺ in nanodispersed zinc ferrocyanide powder, respectively.

This report presents the results of studies by the electron magnetic resonance (EMR) method of some features of spin interactions in nanoscale bimetallic PBA. The objects of our research were: zinc ferricyanide, (Zn₃[Fe(CN)₆]₂), copper ferricyanide (Cu₃[Fe(CN)₆]₂) and copper ferrocyanide (Cu₂[Fe(CN)₆]). We also studied the changes in the spin and valence characteristics of PBA nanoparticles at their immobilization in polyethyleneimine (PEI), as well as at temperature variation and exposure to ultraviolet irradiation.

In the studied bimetallic PBA, the spin states of the magnetic ions of each subsystem of metals were determined, and the forms of interaction of spins in a given subsystem of magnetic metals and between the spins of magnetic metals of different subsystems were also established. In particular, it was found that in copper ferricyanide, magnetic ions of metals of different subsystems combine into exchange-coupled ferromagnetic pairs (dimers).

It has been established that during the immobilization of nanoparticles of the studied bimetallic PBA in PEI, the characteristics of the magnetically ordered phase of the iron subsystem vary, while a small part of the ions of this subsystem changes their spin and/or valence state (Fig. 1, 2). Upon immobilization of copper ferricyanide nanoparticles in PEI, the exchange-coupled ferromagnetic pairs (dimers) “copper-iron” are destroyed.

Using computer simulation, it is shown that the EMR spectrum that occurs upon ultraviolet irradiation of a zinc ferricyanide nanocomposite with PEI can be represented as a superposition of three types of spectra corresponding to 1) proton-containing radicals, 2) nitrogen-containing radicals, and 3) electrons localized on structural defects (Fig. 3).

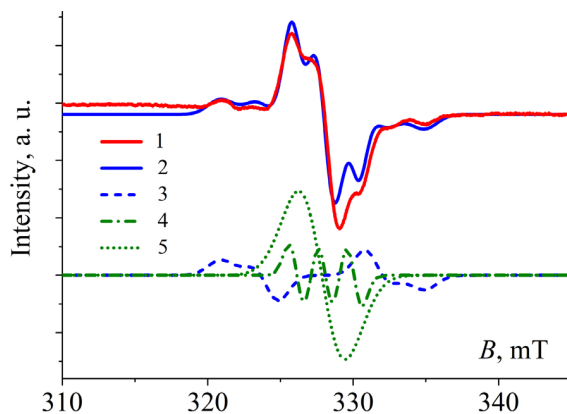


Fig. 3. EPR spectrum of a nanocomposite $\text{PEI}/\text{Zn}_3[\text{Fe}(\text{CN})_6]_2$ exposed to ultraviolet irradiation. 1 – experimental spectrum, 2 – simulated spectrum, 3, 4 and 5 – components of the simulated spectrum, corresponding to proton-containing radicals, nitrogen-containing radicals and F-centers, respectively.

Acknowledgments. The authors are grateful to the Corresponding member of the RAS Bratskaya S.Yu. for providing samples for research; Malakhova I.A. for the synthesis of studied samples. The investigations have been financially supported by the Ministry of Science and Higher Education of the Russian Federation (State assignments No. FWFN(0205)-2022-0002 and FWFN(0205)-2022-0003).

1. Yi H., Qin R., Ding S. et al.: *Adv. Funct. Mater.* **31**, 2006970 (2021)
2. Dujardin E.; Mann S.: *Adv. Mater.* **16**, 1125 (2004)
3. Polishchuk V.R., Ziatdinov A.M.: Sixth Asian School-Conference on Physics and Technology of Nanostructured Materials (Vladivostok, April 25–29, 2022) Proceedings. Vladivostok: Dalnauka. 2022. P. 195–196.

SECTION 12

MODERN METHODS OF MAGNETIC RESONANCE

Development of sensors for the study of agricultural objects in an MRI system with a field of 0.4 T

A. Bayazitov, A. Fakhрутдинov, Ya. Fattakhov, V. Odivanov, V. Shagalov

Zavoisky Physical-Technical Institute, FRC Kazan Scientific Center of RAS, Kazan 420029, Russia, alfigdi5s5d@yandex.ru

The work is devoted to the receiving and transmitting system of a small-sized specialized traumatological magnetic resonance imaging system with a magnetic field induction of 0.4 T. When developing a sensor for these types of MRI scanners, the features of the small gap between the poles of the magnet should be taken into account. Region of interest (ROI) of the MRI scanner is a space of homogeneity $200 \times 180 \times 180$ mm. The gap (and, accordingly, the size of the receiving and transmitting system) does not exceed 206 mm. The working areas of the sensors are $200 \times 95 \times 63$ and $200 \times 110 \times 19$ mm. The sensor includes a receiving circuit, a transmitting circuit and an external shield. The general principles of contour shielding are described in [1]. The axis of the receiving circuit is directed along the X axis of the magnetic system. The coil of the contour is made of copper tape. To increase the signal-to-noise ratio, the dimensions of the sensors were approximated to the dimensions of the studied objects. Sequential winding of the circuit is used to achieve the maximum signal.

Two specialized sensors “Root” have been developed to study the root system of plants in the soil. The sensor allows us to clearly distinguish the root system with a root diameter of 0.5–1 mm. In this sensor, when using the T1W and T2W methods, the roots are clearly distinguishable against the background of moist soil. An experiment was conducted to track the dynamics of fluid redistribution in the root system.

A specialized sensor “Fetus” has also been developed to study the embryos of domestic birds. The sensor will allow, for example, to more accurately determine the fertilization of eggs and the degree of development of embryos.

A comparison of the images obtained by the described sensors and by the a standard sensor of a larger size was carried out.

1. Polonskij N.B. Konstruirovaniye elektromagnitnyh ekranov dlya radioelektronnoj appa-ratury. M.: Sovetskoe radio (1979), 216 p. (In Russian)

Formation of nutation line in powerful non-uniform field in nuclear magnetic measurers with flowing liquid

I. Kochetkov¹, V. Davydov^{2,3}, R. Davydov^{3,4}

¹Higher School of Applied Mathematics and Computational Physics, Peter the Great St. Petersburg Polytechnical University, St. Petersburg 195251, Russia, temiy.goldberg@mail.ru

²Higher School of Applied Physics and Space Technologies, Peter the Great St. Petersburg Polytechnical University, St. Petersburg 195251, Russia, davydov_vadim66@mail.ru

³Department of biology, All Russian Research Institute of Phytopathology, Moscow Region, 143050, Russia, davydov_vadim66@mail.ru

⁴Department of Higher Mathematics, Peter the Great St. Petersburg Polytechnical University, St. Petersburg 195251, Russia, romanvproze@gmail.com

The nutation line is the main characteristic of NMR flowmeters and nutation NMR magnetometers with a flowing liquid for measurements [1]. It should be noted that the nutation coil, in which the direction of the magnetization of the flowing liquid changes to form the nutation line, is located at some distance from the magnetic systems of the polarizer magnet and analyzer magnet [1, 2]. At present, there are more and more various tasks to control the structure and characteristics of a magnetic field with an induction of more than 1T and an inhomogeneity of more than 0.1 cm^{-1} under various conditions: under strong electromagnetic interference, increased radiation exposure, where the use of optical sensors and other types of magnetometers is difficult. For example, in the area of a particle accelerator or a high-resolution spectrometer, near voltage converters of a power plant at offshore facilities with a nuclear reactor. Under these conditions, we need to control the field parameters at least with an error of 2%.

The design features of nutation nuclear magnetic magnetometers with a flowing medium [1, 2] make it possible to measure the induction and inhomogeneity of the magnetic field under such harsh conditions with an error of no more than 2%. The design of the magnetometer makes it possible to place the nutation coil, which is used to determine the parameters of the magnetic field, at more than 100 m from the location of other blocks of the nutation NMR magnetometer. The decoupling between the zone for measuring the parameters of the magnetic field and the device for recording the NMR signal is provided by a flowing liquid in which the magnetization inversion is implemented. Because the registration of the NMR signal is carried out in a non-contact way, the decoupling can be considered complete. Information about the parameters of the magnetic field from the nutation coil to the registration system is transferred by a rapidly flowing liquid with magnetization inversion. This makes it possible to place the NMR signal recording device in an area where the influence of electromagnetic interference is the least, and there is no radiation exposure. Our studies have shown that the structure of the nutation line is determined only by the inhomogeneity of the magnetic field in the area where the nutation coil is located and depends on its parameters (dimensions, range of the magnetic field in its cross-section). Therefore, when designing or upgrading a magnetometer, it is essential to calculate the optimal parameters of the nutation coil and the

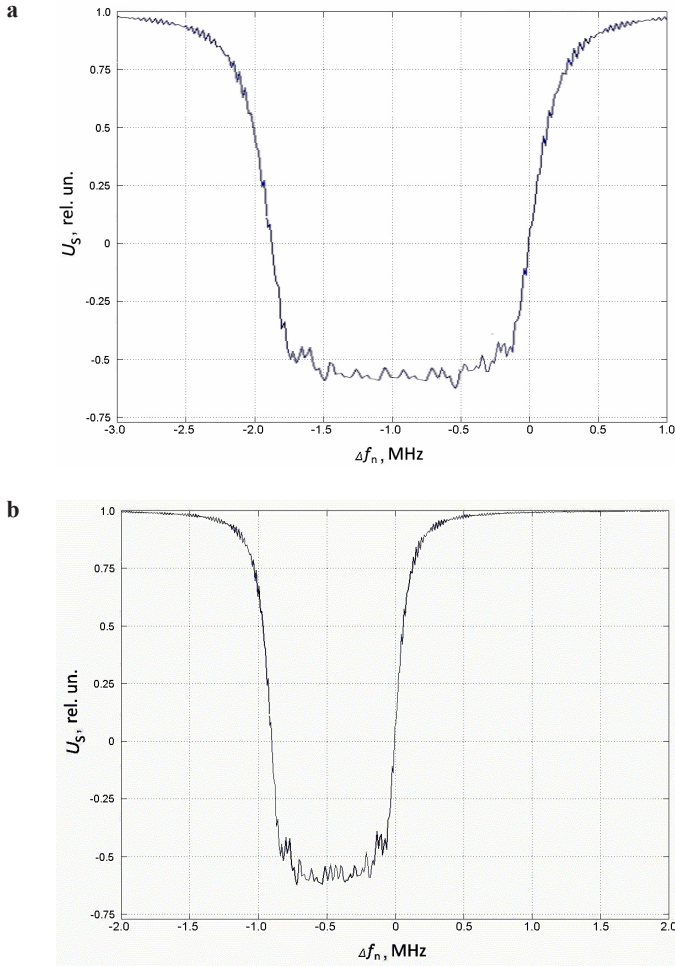


Fig. 1. The calculated nutation line for the parameters of the liquid medium $T_1 = 1.25$ s, $T_2 = 1.18$ ms and the magnetic field strength $H_0 = 899670.86$ A/m. Graph **a** and **b** correspond to the value of H_1 in A/m and the magnetic field's inhomogeneity in the nutation coil area in cm^{-1} : 10.22, 0.0121; 12.01, 0.0302.

electronic units connected to it. Our experiments have shown that the Bloch equations currently used to describe the nutation kinetics do not reflect the natural physical processes in the experiment. Therefore, we supplemented the Bloch equations with new coefficients:

$$dM_x/dt + M_x/T_2 + (\Delta\omega + (\Delta B_0/t_n) \cdot \gamma \cdot t) M_y = 0$$

$$dM_y/dt + M_y/T_2 - (\Delta\omega + (\Delta B_0/t_n) \cdot \gamma \cdot t) M_x + \gamma \cdot H_1 M_z = 0$$

$$dM_z/dt + M_z/T_1 - \gamma \cdot H_1 M_y - M_0/T_1 = 0$$

where t_a is the time of action of the H_1 nutation coil field on the current medium.

Figure 1 shows, as an example, the calculated lines from various values of the magnetic field inhomogeneity in the area where the nutation coil is located. An analysis of the obtained data showed that an increase in the value of inhomogeneity ΔB_0 leads to an increase in the width of the nutation line Δf_n . Also, as in the experiment, it is possible, in a certain range of increasing ΔB_0 , to compensate for the decrease in amplitude for the NMR signal with magnetization inversion by changing H_1 . In the case of creating optimal values of the H_1 field in the nutation coil, corresponding to the maximum of the S/N ratio, the amplitudes of the NMR signals hardly change. This situation is observed during experiments.

The results of modelling the processes of nutation kinetics showed that the system of equations we developed allows us to consider problems and obtain their solutions for any value of the magnetic field inhomogeneity in zone of nutation coil. The parameters of the nutation coil were previously selected mainly by experience, which made it much more difficult to solve many problems.

1. O'Neill K.T., Brancato L., Stanwix P.L., Fridjonsson E.O., Johns M.L.: *Chemical Engineering Science* **202**, 222–237 (2019)
2. Davydov V.V., Dudkin V.I., Karseev Y.Yu.: *Instruments and Experimental Techniques* **58**, 787–793 (2015)

Features of longitudinal relaxation time T_1 measuring in condensed media by nuclear magnetic resonance method with using a modulation technique in weak magnetic fields

M. Davydov¹, V. Davydov^{2,3}, A. Goldberg⁴, R. Davydov⁵

¹Higher Engineering Physics School, Peter the Great St. Petersburg Polytechnical University, St. Petersburg 195251, mdavydov2010@mail.ru

²Higher School of Applied Physics and Space Technologies, Peter the Great St. Petersburg Polytechnical University, St. Petersburg 195251, Russia, davydov_vadim66@mail.ru

³Department of biology, All Russian Research Institute of Phytopathology, Moscow Region, 143050, Russia, davydov_vadim66@mail.ru

⁴Higher School of Applied Mathematics and Computational Physics, Peter the Great St. Petersburg Polytechnical University, St. Petersburg 195251, Russia, artemiy.goldberg@mail.ru

⁵Department of Higher Mathematics, Peter the Great St. Petersburg Polytechnical University, St. Petersburg 195251, Russia, romanvproze@gmail.com

One of the tasks of nuclear magnetic resonance (NMR) in studying condensed matter is determining the times of longitudinal T_1 and transverse T_2 relaxation [1]. It is most important when using small-sized NMR relaxometers for express control of the state of condensed media [2]. In the case of express control, the registration of the NMR signal is carried out in a weak magnetic field with $B < 100$ mT (restrictions on the weight of the device design) using an independent power source. It creates problems using pulsed methods (Hann and Carr-Purcell spin echo) in small portable NMR relaxometers to measure T_1 and T_2 [1]. A gap between the magnet poles of at least 80 mm is required to implement these methods to accommodate the coil system, which increases the weight of the device and the impulse voltage of several hundred volts (restrictions on battery charge) [2]. Therefore, measurements of T_1 and T_2 in small-sized NMR relaxometers record the signal using a modulation technique. In this case, the NMR signal is obtained in the form of damped non-periodic oscillations (“wiggles”). Figure 1 shows the recorded NMR signal from tap water at $T = 290.2$ K. The time T_2 is determined from the envelope’s decay constructed from the tops of the peaks. The inhomogeneity of the magnetic field is considered in the area where the registration coil is located [1]. Difficulties arise with the measurement of T_1 . Experimental studies have shown that it is extremely difficult to use the frequency measurements of the Giulotto method [3] to determine T_1 in the design of a small-sized NMR relaxometer.

In a weak magnetic field B , the resonant frequencies, when the modulation frequency of the magnetic field B changes, differ from each other by fractions of a hertz. Recording these frequencies requires high resonance tuning accuracy, which can only be achieved under laboratory measurement conditions. In the case of using the device in the field, such a measurement mode is challenging to implement. In addition, the formula for determining T_1 in the Giulotto method [3] was obtained from the Bloch equations without considering the features of recording the NMR signal in a weak magnetic field using the modulation technique [2]. Also, Bloch’s equations did not consider the effect of magnetic

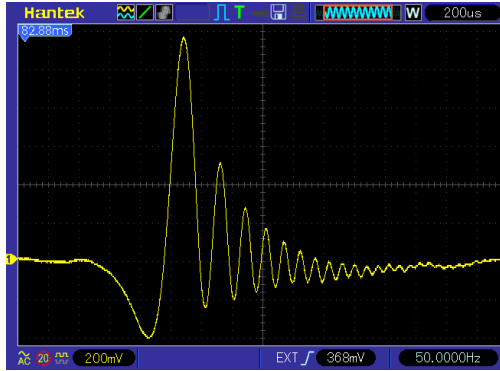


Fig. 1. NMR signal from tap water.

field modulation on the magnetization of the condensed medium. Therefore, considering all the factors in the Bloch equations, we obtained a formula for determining T_1 from two measurements of the NMR signal amplitude at different modulation frequencies τ .

$$M = M_0 [1 - (1 - \exp(-\tau/T_1)) / (1 + \exp(-\tau/T_1))] , \quad (1)$$

The value of M in formula (1) is proportional to the amplitude of the registered NMR signal, $M_0 = \chi_0 B_0$ is the value of the magnetization of the condensed medium in the absence of magnetic field modulation, where χ_0 is the static nuclear magnetic susceptibility. The studies have shown that when using (1) to determine T_1 , several features arise related to the relationship between the values of τ , the modulation amplitude, and the conditions for recording the NMR signal using the modulation technique. It has been established that the modulation frequencies τ during the measurement of T_1 should differ by at least ten times at the maximum modulation depth. In this case, the signal-to-noise ratio of the registered NMR signal should not be less than 1.3. If these conditions are not fulfilled, it is impossible to determine T_1 from (1).

1. Leshe A.: Nuclear induction. Veb Deutscher Verlag Der Wissenschaften, Berlin (1963)
2. Davydov V.V., Dudkin V.I., Vysoczky M.G., Myazin N.S.: Applied Magnetic Resonance **51**, 653–666 (2020)
3. Giulotto L., Lanzi G., Tosca L.: Journal of Chem. Physics **24**, 632 – 644 (1956)

Experimental investigation of free induction decay in zigzag spin chains of hambergite in multiple quantum NMR

S.G. Vasil'ev, G.A. Bochkin, E.B. Fel'dman, D.P. Kiryukhin, P.P. Kushch

Institute of Problems of Chemical Physics of RAS, Moscow Oblast, Chernogolovka 142432, Russia,
viesssw@mail.ru

NMR line shape and its Fourier transform, free induction decay (FID) are essential sources of structural and dynamic information in diverse materials [1]. Multiple quantum NMR spectroscopy [2] created new possibilities for the problem under consideration, both experimental and theoretical [3]. Recently we have shown [4] that proton zigzag chains in single crystals of hambergite can be considered as isolated one-dimensional systems. The dipole-dipole interaction (DDI) coupling constants of the nearest neighbors in hambergite can be equal or alternate, taking two different values, depending on the orientation of the crystal. Investigation of the one-dimensional spin systems is beneficial since there exist exactly solvable theoretical models, in particular [3]. Earlier we have investigated the MQ dynamics in homogeneous quasi-one-dimensional spin chains in fluorapatite (FAP) [5]. The regularity of the FAP crystal lattice creates identical dipolar couplings among the nearest spins in the chain while the interactions with other spins are significantly smaller and can be ignored, at least in the first approximation. In the present study we investigate the MQ dynamics in the inhomogeneous quasi-one-dimensional spin chains of protons in hambergite. The zig-zag arrangement of the spins in the chains causes the dipolar coupling constants to alternate between two values when passing along the chain.

The experiments were performed on a Bruker Avance III spectrometer at 400 MHz ^1H frequency using a 2.5 mm solenoidal coil probe. The duration of 90° pulses was 1.2 μs . The 8-pulse Baum-Pines sequence of 26.4 μs length was used to create the two-spin double quantum Hamiltonian, which was incremented to obtain the desired preparation time. Two samples (S1 and S2) of the hambergite crystal were cut from the larger piece of single crystal and shaped into cylinders to fit the dimensions of the probe. The axes of the cylinders were cut perpendicular to the chain axis such that the rotation of the crystal changes the angle between the chain axis and the external magnetic field. The ratio of the dipolar coupling constants depends on the orientation of the crystal (it can equal 1, meaning that the chain is homogeneous) and thus can be adjusted to some extent. The axes of the two cylindrical samples were perpendicular which allowed to perform rotations in the plane of zigzag (S1) and in the perpendicular direction (S2). The samples were exposed to ^{60}Co γ -radiation on a "Gammatok-100" apparatus [6] to shorten the spin-lattice relaxation time which otherwise was unacceptably long [4]. The obtained MQ FIDs are shown in Fig. 1. The initial parts of the decays were made to coincide on the plot by normalizing the amplitudes and multiplying the preparation time by the values specified in Fig. 1. Due to the

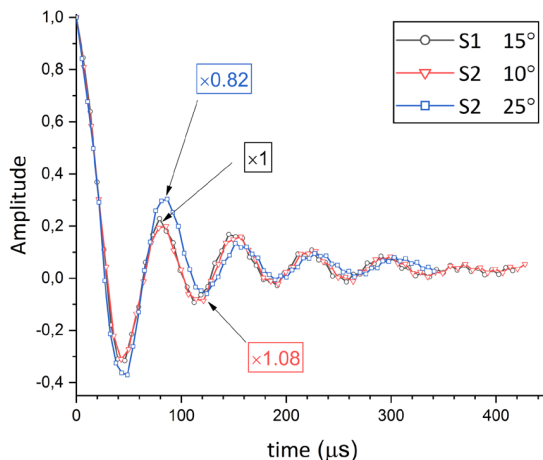


Fig. 1. MQ FIDs for different orientations of hambergite with respect to the magnetic field.

planar nature of the zigzag the rotations of the two crystals are not equivalent. In the case of S2 the ratio of the dipolar constants changes less with the rotation of the sample compared to the case of S1, where the maximum difference between the constants can be achieved. The curves are almost identical for S1 inclined at 10° and S2 inclined at 15° , though some divergence is observed at later times. These two examples correspond to the case of inhomogeneous spin chains. Most noticeable difference is observed for S2 inclined at 25° . In this orientation the isolation of the chain from the neighbors is still good but the values of the nearest neighbor DDI constants are significantly reduced and reach similar values converting the chain into a homogeneous one. The obtained experimental results show the difference in MQ dynamics between homogeneous and inhomogeneous quasi-one-dimensional spin chains confirming the predictions of the theory [3].

The work was performed as a part of a state task, State Registration No. AAAA-A19-119071190017-7. This work was partially supported by the Russian Foundation for Basic Research (project No. 20-03-00147).

1. Abragam A.: The Principles of Nuclear Magnetism. Oxford, Clarendon press, 1970.
2. Baum J., Munowitz M., Garrowsay A.N.: A. Pines, J. Chem. Phys. **83**, 2015 (1985)
3. Vasil'ev S.G., Fedorova A.V., Fel'dman E.B.: Appl. Magn. Res. **52**, 831 (2021)
4. Bochkin G.A., Fel'dman E.B., Kuznetsova E.I., Lazarev I.D., Vasil'ev S.G., Volkov V.I.: J. Magn. Reson. **319**, 106816 (2020)
5. Bochkin G.A., Fel'dman E.B., Vasil'ev S.G.: Phys. Lett. A **383**, 2993 (2019)
6. Kiryukhin D.P., Kichigina G.A., Allayarov S.R., Badamshina E.R.: High Energy Chem. **53**, 228–237 (2019)

WORKSHOP

SENSING AND QUANTUM INFORMATION
IN FLUORISCENT NANOMATERIALS

Opportunities for biosensing with fluorescent diamond and phosphor nanoparticles

P.R. Hemmer

Electrical & Computer Engineering Department, Texas A&M University, College Station, Texas,
77843, USA, prhemmer@ece.tamu.edu

Diamond and phosphor nanoparticles can probe biological processes on the nanoscale, sometimes with the potential for quantum-enhanced sensing. However, there are issues that must be addressed to enable widespread application.

In the case of nanodiamond the main problem is a lack of physical understanding of diamond growth, especially of nucleation. This leads to a tradeoff in the ability to dope the diamond with sensing defects, without sacrificing the overall material quality, thereby degrading sensing performance. For example, in the case of magnetic sensing it is desirable to have as many nitrogen-vacancy (NV) color center as possible. Yet the nitrogen atoms are a source of spin noise that rapidly degrades magnetic sensitivity. In addition, for nanoscale magnetic sensing, it is necessary to get NVs close to the surface to improve sensitivity yet ensure that the surface quality is sufficiently good so as to suppress spin noise from surface defects.

In the case of phosphor nanoparticles, the ubiquitous biofluorescence background can be suppressed by upconversion, even for excitation laser intensities comparable to single-photon transitions. In particular I will discuss new opportunities to combine diamond and phosphor nanoparticles, for example as heterogeneous core-shell structures, that promise the best of both.

Optical magnetometry with home-synthesized fluorescent nanodiamonds

**A.V. Leontyev¹, D.K. Zharkov¹, A.G. Shmelev¹, V.G. Nikiforov¹,
V.S. Lobkov¹, E.O. Mityushkin², M.H. Alkahtani³**

¹Zavoisky Physical-Technical Institute, FRC Kazan Scientific Center of RAS, Kazan 420029, Russia

²Kazan Federal University, Institute of Physics, Kazan, 420008, Russia

³National Center for Laser and Optoelectronics, Riyadh, Saudi Arabia

Fluorescent nanodiamonds have a number of advantages compared to other fluorescent nanoprobe types, including biocompatibility and photostability. We report the results on the creation of optically active nanodiamonds sensitive to magnetic fields. Fluorescent nanodiamonds were grown at high pressure from a mixture of diamondoid seed molecules and carbon-hydrogen compounds.

Experiments on the optical detection of magnetic resonance in synthesized nanodiamonds clearly show the presence of negatively charged nitrogen-vacancy color centers sensitive to an external magnetic field. The results demonstrate the possibility of applications as nanosensors of weak magnetic fields. We acknowledge the support from Ministry of Education and Science of the Russian Federation in the frame of Agreement No. 075-15-2021-623 with the FRC Kazan Scientific Centre of RAS.

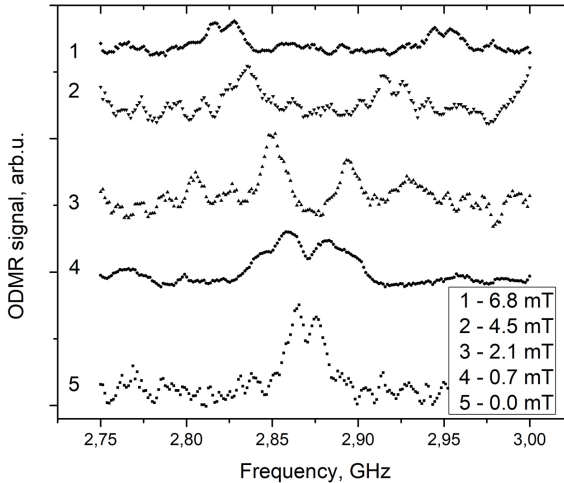


Fig. 1. ODMR signal from NV color centers in home-grown fluorescent nanodiamonds in external magnetic field.

YVO₄:Yb, Er UCNP – insight to the nano thermosensor

**A.G. Shmelev¹, D.K. Zharkov¹, A.V. Leontyev¹, V.G. Nikiforov¹,
D.N. Petrov², M.F. Krylov², J.E. Clavijo², E.O. Mityushkin², V.S. Lobkov¹**

¹Zavoisky Physical-Technical Institute, FRC Kazan Scientific Center of RAS, Kazan 420029,
Russia

²Institute of Physics, Kazan Federal University, Kazan 42008, Russia

YVO₄-based nanoparticles doped with Yb and Er have been synthesized by the thermal decomposition in Ar-atmosphere method and by solvo-thermal method. The UCNPs are demonstrating a strong luminescence upconversion in 510–560 nm range. The dependence of the luminescence intensities was studied in wide range of temperatures.

Different synthesis method leads to the different spectral lines relative intensities. But a temperature dependency was found in both cases.

The origin of the difference in the relative spectral lines intensity and the fluorescence spectra peculiarities is discussing. The strategy of the UCNP-based nano-thermosensor developing was suggested. Key parameters of the UCNP for nanosensing applications are crystal parameters uniformity. The ideal UCNPs will be a uniform defect-free nanocrystals, shielded from the solvents and round shaped with ligands or the hard shell.

The work supported by Ministry of Education and Science of the Russian Federation in the frame of Agreement No. 075-15-2021-623 with the FRC Kazan Scientific Centre of RAS.

Highly efficient broadband superconducting quantum memory

A.R. Matanin^{1,2}, K.I. Gerasimov³, E.S. Moiseev³, N.S. Smirnov^{1,2},
 A.I. Ivanov^{1,2}, E.I. Malevannaya^{1,2}, V.I. Polozov^{1,2}, E.V. Zikiy²,
 A.A. Samoilo^{1,2}, I.A. Rodionov^{1,2}, S.A. Moiseev³

¹FMN Laboratory, Bauman Moscow State Technical University, Moscow 105005, Russia

²Dukhov Automatics Research Institute (VNIIA), Moscow 127030, Russia

³Kazan Quantum Center, Kazan National Research Technical University, Kazan 420111, Russia

Quantum memory promises advanced capabilities for noisy intermediate-scale quantum computers [1–5]. Existing approaches to quantum memory lack complete combination of high efficiency, long storage time, noiselessness and multi-qubit capacity. Here we demonstrate a record-breaking broadband two-mode multi-

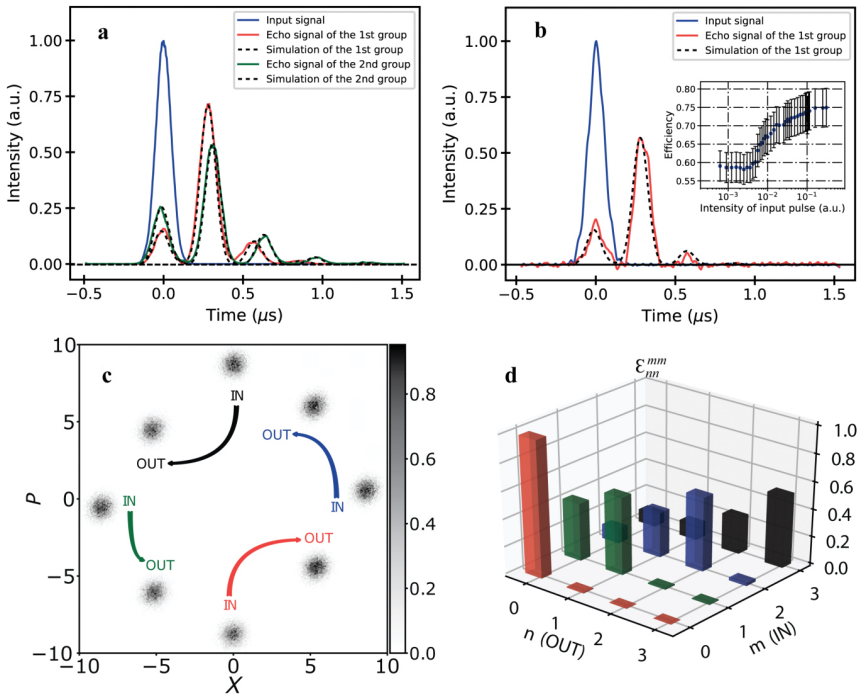


Fig. 1. **a** The signals from the first (red solid line) and second (green solid line) memory cells at high power with large average photon number. **b** The signals from the first memory cell (red solid line) at single photon level input pulse intensities. The signals are normalized to the maximum intensity of the input Gaussian-shaped coherent pulse (blue solid line). The black dashed and dotted lines are theoretical simulations. Efficiency dependence for input pulse intensity is shown in the inset. **c** Four pairs of experimentally acquired phase space distribution for input pulses ('IN') and the corresponding memory's response ('OUT'). Single color and arrow indicate a single pair of phase space distributions of conjugate position X and momentum P for state of the mode being sent into the memory and recalled state. **d** Diagonal elements of the reconstructed quantum process tensor.

resonator quantum memory with strongly suppressed quantum noise and show real ways to increase its efficiency close to 100%. The memory stores two spectral modes of single photon level radiation in on-chip system of eight coplanar superconducting resonators. Single mode storage shows a power efficiency of up to 60% at single photon energy and more than 73% at higher intensity. The demonstrated efficiency is an order of magnitude larger than the previously reported multimode microwave quantum memory. The noiseless character of the storage is confirmed by coherent state quantum process tomography.

We presented noiseless two-mode on-chip quantum memory for microwave photons that is compatible with superconducting cQED architecture. Among different photon storage experiments in frequency-comb media, such as rare-earth ions for optical storage [6] and nuclear transitions for gamma-photon storage [7], the presented results demonstrate the highest efficiency. The obtained experimental results agree well with the theory, which predicts a further considerable increase of efficiency towards 100%. It will open an avenue for a practical multi-qubit memory with arbitrary temporal and spectral mode multiplexing with a range of applications in superconducting quantum processing.

Device was fabricated at the BMSTU Nanofabrication Facility (Functional Micro/Nanosystems, FMNS REC, ID 74300). The work of S.A.M., K.I.G and E.S.M. were carried out with financial support of the Ministry of Education and Science of Russia, Reg. number NIOKRT 121020400113-1.

1. Kimble H.J.: *Nature* **453**, 1023 (2008)
2. Lvovsky A.I., Sanders B.C., Tittel W.: *Nat Photon* **3**, 706 (2009)
3. Wehner S., Elkouss D., Hanson R.: *Science* **362**, 9288 (2018)
4. Blais A., Grimsmo A.L., Girvin S.M., Wallraff A.: *Rev. Mod. Phys.* **93**, 025005 (2021)
5. Mariani M., Wang H., Yamamoto T., Neeley M., Bialczak R.C., Chen Y., Lenander M., Lucero E., O'Connell A.D., Sank D., Weides M., Wenner J., Yin Y., Zhao J., Korotkov A.N., Cleland A.N., Martinis J.M.: *Science* **334**, 61 (2011)
6. Sabooni M., Li Q., Kroll S., Rippe L.: *Phys. Rev. Lett.* **110**, 133604 (2013)
7. Zhang X., Liao W.-T., Kalachev A., Shakhmurov R., Scully M., Kocharovskaya O.: *Phys. Rev. Lett.* **123**, 250504 (2019)

Atomic frequency comb memory for polarization state of light in a $^{153}\text{Eu}:\text{Y}_2\text{SiO}_5$ crystal

R.A. Akhmedzhanov, L.A. Gushchin, N.A. Nizov, V.A. Nizov,
D.A. Sobgayda, I.V. Zelensky

Institute of Applied Physics of the Russian Academy of Science, Nizhny Novgorod 603950,
Russia, rinat@ipfran.ru

Quantum communication is one of the most well developed areas of quantum technologies with many potential practical applications. Perhaps the most interesting application is the possibility of enabling absolutely secure communication via quantum key distribution (QKD). Even though commercial QKD systems that utilize existing optical fiber networks to connect users are already available, due to optical fiber losses and the no cloning theorem the range of such devices is limited and the effective key distribution rate decays exponentially with distance. In order to increase the range of quantum communication and eventually create the global quantum network it is suggested to use intermediary nodes, either trusted or untrusted (quantum repeaters).

One of the main difficulties on the path towards creating a working quantum repeater is the lack of a quantum memory that has all the necessary characteristics including high efficiency, long storage times and high bandwidth in one device. Among the more promising media for implementing quantum memories are inorganic crystals doped with rare earth ions. Their advantages include good coherence properties, high potential for spectral or temporal multiplexing due to the existence of large inhomogeneous broadening, and the possibility of working with large ensembles of ions in the crystal lattice which increases the interaction strength.

In the present work we used a $^{153}\text{Eu}:\text{Y}_2\text{SiO}_5$ crystal which is noteworthy due to its long coherence times, reaching up to 6 hours on the spin transition with the help of dynamic decoupling pulse sequences[1]. Using control pulses that transferred optical coherence to the spin transition, an on-demand memory with a storage time of about an hour was demonstrated [2].

While single photon qubits can be encoded using various degrees of freedom (such as time, frequency or polarization), polarization qubits are widely used in quantum communication due to the simplicity of implementing single-qubit gates and projection measurements.

However, storing arbitrary polarization in such a crystal is a nontrivial task since absorption is highly anisotropic. Eu ions exhibit maximum absorption when the light is polarized along the D_1 crystal axis and absorption becomes a few times lower for the D_2 axis that is perpendicular to D_1 . In addition, the crystal has birefringent properties with axes D_1 and D_2 being principal axes. As a result, an arbitrary polarization sent into the crystal will be decomposed into two rays that propagate at different speeds and the resulting polarization after the crystal will be changed. In order to store polarization states in such

anisotropic media, there are several possible approaches [3, 4]. We chose to implement setups with multiple passes through the crystal with intermediary rotation of polarization. In the two-pass case, after the first pass through the crystal the light was sent through a halfwave plate with fast axis oriented at 45 degrees to the crystal axes. The light was then sent through the crystal again and the resulting absorption was polarization independent, which was confirmed by optical depth measurements for different polarizations. A similar setup but with four passes through the crystal was implemented where the halfwave plate was placed after the second pass. This allowed us to increase the optical depth and, consequently, the memory efficiency.

Afterwards, we implemented the atomic frequency comb memory protocol. The comb burning sequence was sent into the crystal with polarization oriented at 45 degrees to the crystal axes so that the comb was created on all passes through the crystal (the passes were spatially separated). The efficiency obtained in the four-pass setup was around 25% with the storage time of around 165 ns.

To determine the memory fidelity and show that it could be used to faithfully store polarization states of light, we performed polarization tomography of the memory [5]. In order to analyze the performance of the memory as a quantum process, we compared input and echo pulses. Four different basis input polarizations (vertical, horizontal, diagonal and circular) were created and each echo was projected onto the same four basis states. As a result, χ -matrix of the quantum process was calculated and the memory fidelity was determined to be above 85%.

This work was supported by the Russian Railways joint stock company.

1. Zhong M. et al.: Nature **517**, 177(2015).
2. Ma Y. et al.: Nat. Comm. **12**, 2381(2021).
3. Laplane C. et al.: New J. Phys. **18**, 013006(2015).
4. Clausen C. et al.: Phys. Rev. Lett. **108**, 190503(2012).
5. Zhu T.-X. et al.: Phys. Rev. Lett. **128**, 180501(2022).

Photonic crystal cavities for GeV&SnV diamond

A.V. Akimov

Russian Quantum Center, Business center "Ural", Skolkovo, Moscow 143025, Russia
P.N. Lebedev Institute RAS, Moscow, 119991 Russia.
National University of Science and Technology MISIS, Moscow 119049, Russia

Color centers in diamond attract a lot of attention due to unique properties of diamond, such its optical and chemical purity, low concentration of nuclear spins in diamond matrix and also its physical and chemical inertness. Germanium-vacancy (GeV) and tin-vacancy (SnV) are interesting centers, since they do not have much of sensitivity to the electric field, and therefore defects created during nanofabrication. To the contrary to the similar silicon-vacancy center these centers have mostly radiative decay and larger splitting of the ground state. The large splitting of the ground state help reduction of the interaction with phonons, which are the main source of decoherence of the spin states in these color centers.

This opens unique opportunity to use this color centers with nanostructures photonic. It been already successfully demonstrated that silicon-vacancy color center containing nanocavities may significantly advance performance of the color centers, making many tasks of quantum information processing possible. In our work we are trying to make the next step in the development for such a device by integrating nanodiamonds, containing GeV/SnV color center with photonics devices out of more conventional for industry materials. In particular, we are trying to implement fast, GHz range quantum memory utilizing SnV color centers. Such a memory is based on multifrequency electromagnetic induced transparency and should allow significantly increase bandwidth of future quantum memory devices.

Quantum memory in nanodiamonds with color centers

A.D. Berezhnoi, A.A. Kalachev

Zavoisky Physical-Technical Institute, FRC Kazan Scientific Center of RAS, Kazan 420029,
Russia, alex.berezhnoi@mail.ru

Recently, in our work [1], a theoretical model was developed that describes the recording and amplification of weak light pulses by means of nonresonant Raman and absorption photon emission in an ensemble of SiV centers. The numerical results measure that the signal-to-noise ratio can significantly increase the density for different single-photon input pulses if the orbital splitting of the center state levels significantly increases the strain count. However, this significantly reduces the coherence time for this transition, which limits the possibility of using it to store information. Probably, the relaxation time in this case is determined by the electron-phonon interaction; the control of the phonon spectrum measures a significant change in the coherence time of both the orbital and spin qubits in the considered color centers. A promising approach to solving the problem is the use of nanodiamonds with acoustic resonators [2, 3]. A similar idea underlies the increase in the optical lifetime based on the long-lived photon echo in impurity memory crystals [4].

In summary, we have analyzed the possibility of increasing the storage time in quantum memory devices based on SiV-centers in diamond by using diamond nanoparticles instead of the bulk matrix. The numerical results show that direct one-phonon orbital relaxation rate can be reduced three orders of magnitude for a spherical nanoparticle that is in weak mechanical contact with a substrate and surrounded by vacuum. As a result, both orbital and spin coherence times, which are limited by this relaxation process, can be increased significantly.

This work supported by Ministry of Education and Science of the Russian Federation in the frame of Agreement No. 075-15-2021-623 with the FRC Kazan Scientific Centre of RAS.

1. Kalachev A. et al.: *Laser Physics* V. **29**, no 10, 104001 (2019).
2. Jahnke K.D. et al.: *New J. Phys.* **17**, 043011 (2015).
3. Pingault B., Jarausch D.D., Hepp C. et al.: *Nature commun.* **8**, no. 1, 1 (2017).
4. Kalachev A.A., Vlasova D.D.: *Proceedings of SPIE* **7024**, 702401 (2008).

POSTERS

W-band EPR and quantum-chemical calculation of radicals in calcium gluconate

**M.M. Akhmetov¹, G.G. Gumarov¹, R.B. Zaripov¹, G.N. Konygin²,
D.S. Rybin²**

¹Zavoisky Physical-Technical Institute, FRC Kazan Scientific Center of RAS, Kazan 420029, Russia, mansik86@mail.ru

²UdmFRC Ural Branch of RAS, Izhevsk 426067, Russia, dsrybin@mail.ru

Previously, using various methods of pulsed EPR in combination with quantum chemical calculations, a set of structures of radicals formed during mechanochemical activation of calcium gluconate (CG) was proposed [1], but a complete description of the structure of radicals, as our studies have shown, turned out to be incomplete. Moreover, the final structure of the radical has not been established. The proposed radical R2 ($C_6H_{11}O_7Ca^*$) [1] contains a calcium ion, and the unpaired electron of this radical is delocalized on calcium and oxygen atoms. It is known that the interaction of radicals arising during mechanical activation with environmental components can significantly affect their appearance and stabilization [2]. To study structural transformations, it is necessary to use a wide range of physical methods; in this respect, radiospectroscopy methods are the most sensitive and informative. One of such method is W-band EPR spectroscopy, which was used in this work. Modern methods of quantum chemistry make it possible to establish a relationship between the structure of a molecule and the parameters of EPR spectra.

CG monohydrate produced by the Tyumen Chemical-Pharmaceutical Plant was used as the initial samples. The mechanoactivation of the samples was carried out on a LAIR ball mill at the Udmurt Federal Research Center of the Ural Branch of the Russian Academy of Sciences. The W-band EPR spectra

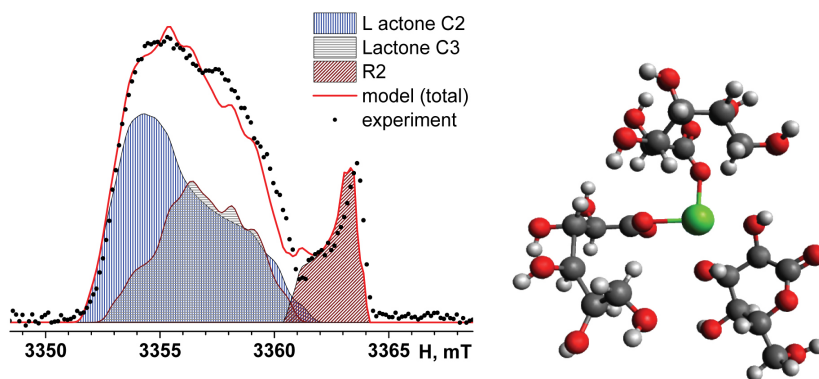


Fig. 1. W-band EPR spectra of MACG and the molecular structure of the radical Lactone-C2.

measurements were carried out in a pulsed mode, the duration of the 90°-pulse was 80 ns, the temperature was 80 K (Bruker Elexsys spectrometer). Both the g -tensor and hyperfine-tensor components of radical are computed by unrestricted Kohn–Sham density functional (UB3LYP) techniques using the Orca program [3].

It should be noted that the EPR spectrum in the X-band looks like asymmetric single line, while spectrum in W-band is split (Fig. 1). The EPR spectrum in the W-band consists of two parts. When comparing width of the spectra in two ranges, it can be seen that there is anisotropy of the g -factor. The corresponding EPR spectrum was calculated using the Easyspin software package. π -radicals of δ -gluconolactone formed as a result of proton abstraction from C2 and C3 carbon atoms were named Lactone C2 and Lactone C3.

As can be seen from Fig. 1, the W-band EPR spectrum of mechanically activated calcium gluconate can be described by three components (Lactone C2, Lactone C3 and R2). In addition, the available data on the concentration of radicals and its dependence on the time of mechanoactivation indicate that the most intense part of the EPR signal is associated with δ -gluconolactone. Quantum-chemical calculation of radicals for this compound gives noticeably low values of the g -tensor. It is known that the calcium atom in gluconates coordinates a large number of oxygen atoms; therefore, molecular structures were considered in which the calcium atom is coordinated by 4 oxygen atoms: two from gluconate anions and two from lactone hydroxyl groups. This calculation gives values of the g -tensor that are close enough to those determined on the basis of fitting to experimental spectra. In addition, for all radicals, the lactone part of the molecular structures turns out to be exactly the same, only the location of the radical changes. It should be noted that the fitting indicates the Gaussian nature of the line broadening. However, this broadening is very small – for the radical R2 (this is indicated by the almost sheer boundary of the right side of the EPR spectrum). This trend also indicates the existence of a stable and energetically favorable configuration of atoms, possibly related to the previously established high therapeutic efficacy of mechanoactivated CG.

1. Zaripov R.B., Aminova R.M., Salikhov K.M.: *Appl. Magn. Res.* **35**, 337–358 (2008)
2. Nonhebel D.C., Walton J.C.: *Free-Radical Chemistry*, Cambridge University Press (1974)
3. Schafer A., Horn H., Ahlrichs R.: *J. Chem. Phys.* **97**, 2571–2577 (1992)

EPR study of the content of nitric oxide and copper in the hippocampus of rats after brain injury and hemorrhagic stroke

**V.V. Andrianov^{1,2}, G.G. Yafarova², A.S. Zamaro³, Y.P. Tokalchik³,
L.V. Bazan¹, T.Kh. Bogodvid^{2,4}, V.S. Iyudin¹, V.A. Kulchitchky³,
Kh.L. Gainutdinov^{1,2}**

¹Zavoisky Physical-Technical Institute, FRC Kazan Scientific Center of RAS, Kazan 420029, Russia

²Institute of Fundamental Medicine and Biology of Kazan Federal University, Kazan 420008, Russia

³Institute of Physiology of Nat. Acad. of Sci. of Belarus, Minsk 220072, Belarus

⁴Volga Region State Academy of Physical Culture, Sport and Tourism, Kazan 420010, Russia, andrianov.neuro@yandex.ru

Traumatic and ischemic brain injuries continue to be one of the most difficult problems of modern medicine. The study of the mechanisms of neurodegeneration and the development of new methods for the restoration of neuronal structures are of great importance for the development of new therapeutic and rehabilitation strategies. Hypoxia occurs when there is insufficient supply of oxygen to the tissues of the body, when there is a state of oxygen starvation of both the whole organism as a whole and individual organs and tissues [1, 2]. Hypoxia disrupts the functioning of neurotransmitter systems, including the nitric oxide system [3]. Nitric oxide (NO) is known as one of the most important signaling molecules regulating the physiological functions of the body and cell metabolism, it is widely distributed in the nervous system [4, 5].

On the one hand, the development of cerebral ischemia and the subsequent occurrence of stroke is associated with impaired regulation of blood supply to brain tissues by the NO system [3]. On the other hand, hypoxia itself, resulting from an ischemic stroke, is accompanied by early cell death in various parts of the brain, followed by programmed late death of other cells by apoptosis [4, 5]. Brain injury damages not only neurons and glial cells, but also blood vessels. The change in blood supply to the damaged area of the brain is accompanied by an increase in destructive processes, which actually become dominant in the post-traumatic period, when the direct effect of the physical factor that caused the injury is no longer present. Behavioral changes in stroke and brain injury are similar, so the task was set to compare the dynamics of NO in these forms of pathology.

Recently, the electron paramagnetic resonance (EPR) method has become one of the most effective methods for detecting and quantifying NO in biological tissues [6, 7]. This happened thanks to a technique developed by Vanin and his collaborators, in which they used a spin capture method based on the reaction of a radical (in this case NO) with a spin trap [7]. As a result of the reaction, an adduct with a characteristic EPR spectrum is formed, when the Fe²⁺ with diethyldithiocarbamate (DETC) forms a stable triple complex (DETC)₂-Fe²⁺-NO [6, 7]. The method allows direct measurements, and is highly sensitive due

to the use of spin traps. Modelling of hemorrhagic stroke was carried out by microinjection of 500 nL of autologous blood into the brain to a depth of 5.0 mm (hippocampus) on the left side. Brain injury was performed by removing a 5.0 mm deep section of nerve tissue from the left side of the hippocampus.

A significant decrease in the NO content in the hippocampus by 36% was observed on the 3rd day after modelling hemorrhagic stroke while an inconsiderable decrease in the copper content by an average of 24% was registered. After modelling the brain injury no significant changes in the NO level in the hippocampus were found neither on the 3rd day nor on the 7th day after the injury. There was also no change in copper content.

Thus, in the experiments carried out, it was demonstrated that modelling of brain injury, in contrast to hypoxia in hemorrhagic stroke, is not accompanied by significant changes in NO production and copper content in the hippocampus of the rat brain.

Modelling ischemia supported by the Belarusian RFFR (project # B18P-227). Electron spin resonance measurements were supported by Zavoisky Physical-Technical Institute of KazSC RAS framework of a state assignment. The processing of the results has been supported by the Kazan Federal University Strategic Academic Leadership Program (PRIORITY-2030)

1. Novikov V.E., Katunina N.P.: *Rev. Clin. Pharmacol. Drug Ther.* **1**(2), 73–87 (2002)
2. Lo E.H. et al.: *Nat. Rev. Neurosci.* **4**(5), 399–415 (2003)
3. Bolanos J.P., Almeida A.: *Biochim. Biophys. Acta* **1411**, 415–436 (1999)
4. Steinert J.R., Chernova T., Forsythe I.D.: *Neuroscientist* **16**(4), 435–452 (2010)
5. Gainutdinov Kh.L., Gavrilova S.A. et al.: *Appl. Magn. Reson.* **40**, No 3, 267–278 (2011)
6. Mikoyan V.D., Kubrina L.N. et al.: *Biochim. Biophys. Acta* **1336**, 225–234 (1997)
7. Vanin A.F., Huisman A. et al.: *Methods in Enzymology* **359**, 27–42 (2003)

Experimental observation of spin polariton in dilute solutions of nitroxide radicals

M.M. Bakirov, K.M. Salikhov, R.B. Zaripov, I.T. Khairutdinov

Zavoisky Physical-Technical Institute, FRC Kazan Scientific Center of RAS, Kazan 420029, Russia, pinas1@yandex.ru

The spin polariton was first theoretically predicted by K.M. Salikhov [1] as part of a new spin exchange paradigm published in 2019. Spin exchange in dilute solutions of paramagnetic particles manifests itself in the spectrum of electron paramagnetic resonance (EPR). The new paradigm predicts the formation of compound quasiparticles, which have been called spin polaritons. They are formed as a result of the interaction of collective excitations of a system of spins (spin excitons) with a microwave field. The excitation frequencies of spin polaritons depends on the power of the microwave field [2]. In this work, experimental confirmation of the theoretical prediction about the dependence of the EPR resonant frequencies on the power of the microwave field in the presence of spin exchange was obtained (Fig. 1). This experimental result was obtained from the analysis of the EPR spectra of solutions of the nitroxyl radical Tempol ^{15}N (4-hydroxy-2,2,6,6-tetramethylpiperidine-1-oxyl – ^{15}N) in toluene.

The authors acknowledge the financial support from the government assignment for FRC Kazan Scientific Center of RAS for supporting of this research activity. The authors are grateful to V.F. Tarasov, G.B. Teitelbaum, B. Bales, M. Bowman, R. Schwartz for discussions of the problem of spin polaritons.

1. Salikhov K.M.: Fundamentals of spin exchange. Story of a paradigm shift, p. 265. Springer International Publishing (2019)
2. Salikhov K.M.: Appl. Magn. Reson. **52**, 1063 (2021)

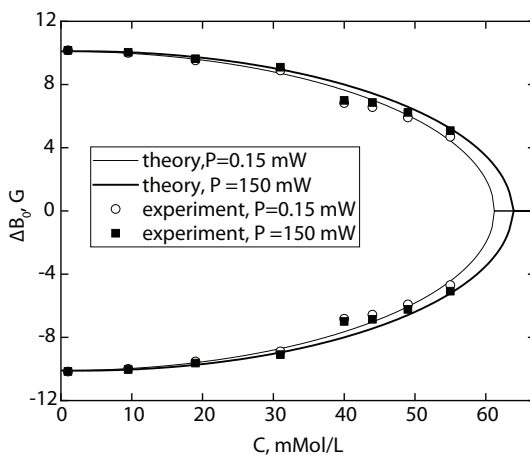


Fig. 1. Experimental and calculated values of the resonant positions of the nitrogen components depending on the spin exchange rate at different values of the microwave field power.

Electron spin dynamics of photoexcited bodipy dimers

H. Cao¹, A.A. Sukhanov², M.M. Bakirov², Yu.E. Kandrashkin²,
J. Zhao¹, V.K. Voronkova²

¹State Key Laboratory of Fine Chemicals, Dalian University of Technology,
Dalian 116024, China

²Zavoisky Physical-Technical Institute, FRC Kazan Scientific Center of RAS, Kazan 420029,
Russia, pinas1@yandex.ru

Time-resolved electron paramagnetic resonance (TREPR) spectroscopy is a powerful tool to characterize structurally close transient paramagnetic states formed after the excitation of dimers [1]. Two Bodipy dimers were prepared (BDP-BDP and BDP-BDP-I₂), with phenyl unit as the linker between two Bodipy moieties (Fig.1). TREPR measurements of Bodipy dimers in polar and not polar solvents were performed. The time-resolved data of the BDP-BDP-I₂ in frozen solution are presented in Fig. 2a. No signal for BDP-BDP dimer has been observed. At low temperature (80–140 K), three types of triplet signals were observed for BDP-BDP-I₂, which are assigned to two subunits (BDP-I₂ and BDP-Ph₂) and the charge transfer state. Time-resolved EPR spectra are simulated by the Spin-Hamiltonian including the Zeeman interaction and zero-field splitting

$$H_{i=1,2}/\hbar = \omega_i S_{i,z} + D_i(\tilde{S}_{i,z}^2 - \mathbf{S}_i^2/3) + E_i(\tilde{S}_{i,x}^2 - \tilde{S}_{i,y}^2) \quad (1)$$

Here, \mathbf{S}_i is the spin vector operator, index i refers to subunit ($i = 1$ for BDP-I₂, $i = 2$ for BDP-Ph₂). The best-fit zero field splitting parameters, found for

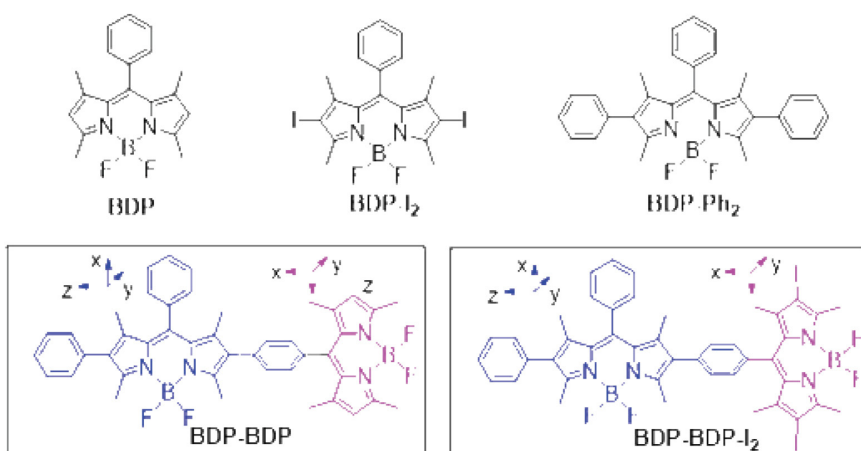


Fig. 1. Molecular structure of the Bodipy Dimers.

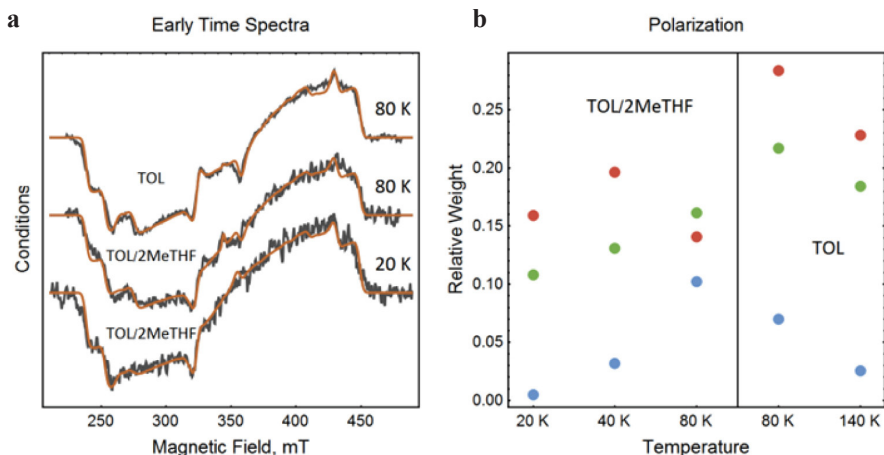


Fig. 2. (a) Normalized spectra of BDP-BDP-I₂ at 0.1 μ s after the laser flash at different experimental conditions. (b) The relative weights of the polarization patterns of BDP-Ph₂ subunit at 0.1 μ s after the laser flash: p_2/p_1 (red points), p_3/p_1 (green points), and p_4/p_1 (blue points) derived from the fitting of the experimental data detected at different conditions.

BDP-I₂ and BDP-Ph₂ equal: $D_1 = -105.3$ mT, $E_1 = 24$ mT and $D_2 = -82.8$ mT, $E_1 = 17$ mT. Experimental data are fitted by the weighted patterns simulated for different types of the polarization: 1) the axial part of the multiplet polarization of BDP-I₂, 2) the axial and 3) the non-axial parts of the multiplet polarization of BDP-Ph₂, and 4) net polarization of BDP-Ph₂. The corresponding density matrices are given as Eq. 2:

$$\begin{aligned}
 \rho_1 &= -p_1(\tilde{S}_{1,z}^2 - \mathbf{S}_1^2/3) \\
 \rho_2 &= p_2(\tilde{S}_{2,z}^2 - \mathbf{S}_2^2/3) \\
 \rho_3 &= p_3(\tilde{S}_{2,x}^2 - \tilde{S}_{2,y}^2) \\
 \rho_4 &= p_4 S_{2,z}
 \end{aligned} \quad (2)$$

The local equilibrium between three metastable states observed within ca. 1 μ s after the laser flash is sensitive to the temperature and the polarity of the solvent. The observed properties imply the presence of the energy and electron transfer pathways between two moieties of the studied dimers [2].

1. Imran M., Zhang X., Wang Z., Chen X, J. Zhao, Barbon A., Voronkova V.K.: "Electron Spin Dynamics in Excited State Photochemistry: Recent Development in the Study of Intersystem Crossing and Charge Transfer in Organic Compounds", *Phys. Chem. Chem. Phys.* **23**, 15835–15868 (2021)
2. Cao H., Sukhanov A.A., Bakirov M.M., Kandrashkin Y.E., Zhao J., Voronkova V.K.: "Intersystem Crossing and Electron Spin Dynamics of Photoexcited Bodipy Dimers", *J. Phys. Chem. C* **126**, 12, 5473–5482 (2022)

Development of sensors for the study of small animals in an MRI system with a field of 0.4 T

A. Bayazitov, A. Fakhruddinov, Ya. Fattakhov, V. Odivanov, V. Shagalov

Zavoisky Physical-Technical Institute, FRC Kazan Scientific Center of RAS, Kazan 420029,
Russia, alfigdi5s5d@yandex.ru

The work is devoted to the receiving and transmitting system of a small-sized specialized traumatological magnetic resonance imaging system with a magnetic field induction of 0.4 T. The sensor includes a receiving circuit, a transmitting circuit and an external shield. The general principles of contour shielding are described in [1]. Region of interest (ROI) of the MRI scanner is a space measuring 200×180×180 mm. The working area of the sensor is a space of 200×120×60 mm. The axis of the receiving circuit is directed along the X axis of the magnetic system. The contour is made of copper tape.

Taking into account the results of early works [2, 3], mathematical modeling of the transmitting part of the solenoid-shaped sensor is carried out in this work. The paper considered a variant with parallel inclusion of coils with special power supplies optimized to improve the uniformity of the RF field formed by the transmitting circuit. This transmission circuit can be considered additionally as an electromagnetic shield.

The purpose of shielding is to decrease the coupling between the receiving circuit and the gradient coils in order to maintain a high Q-factor of the receiving circuit.

The paper also describes the receiving system and its characteristics. Test images of laboratory animals were obtained.

1. Polonskij N.B.: *Konstruirovaniye elektromagnitnykh ekranov dlya radioelektronnoy apparatury*. M.: Sovetskoe radio (1979), 216 p. (In Russian)
2. Bayazitov A.A., Fattakhov Ya.V., Khundiryakov V.E.: *J. Nauchnoe priborostroenie* **29**, no. 1, 92 (2019)
3. Bayazitov A.A., Fattakhov Ya.V., Fakhruddinov A.R., Shagalov V.A.: *Instruments and Experimental Techniques* **63**, no. 6, 89 (2020)

Determination of the zero field splitting parameters of the cobalt(II) ion in diamagnetically diluted samples using circularly polarized radiation

A.V. Borodulina^{1,2}, A.R. Melnikov^{1,2}, S.L. Veber^{1,2}

¹International Tomography Center SB RAS, Novosibirsk, Russia

²Novosibirsk State University, Novosibirsk, Russia, a.borodulina@g.nsu.ru

Cobalt(II)-based compounds can be considered as useful high-spin systems for studying magnetic properties of single-molecule magnets (SMMs), demonstrating an energy barrier between states with different magnetization. Zero field splitting (ZFS) energy is one of the fundamental characteristic of such compounds. One of the most important properties of SMMs for practical applications is slow relaxation of magnetization. The relaxation time usually depends on surroundings of magnetic center. Therefore, study of diamagnetically diluted compounds, where magnetic ions are partially replaced by diamagnetic analogs, is of current interest. However, diamagnetic dilution sometimes affect not only the mechanisms of magnetic relaxation, but also change the value of ZFS energy [1]. Thus, development of methods for determining ZFS energy in diamagnetically diluted samples, including different types of THz EPR spectroscopy, is of great importance in the study of SMMs.

This paper presents the results of determining ZFS energy using circularly polarized radiation for samples of the $\text{Co}(\text{L}(\text{III}))_2$ compound with various degrees of diamagnetic dilution by Zn (100%, 30%, 10%, 3% $\text{Co}(\text{L}(\text{III}))_2$). The method is based on the possibility of selective excitation of transitions between states of cobalt(II) system in a weak external magnetic field using right- and left-handed polarized radiation [2]. It allows one to distinguish magnetic dipole transitions with energies lie in the far IR range from electric dipole transitions and determine values of ZFS energy from the result of dividing spectra of right- and left-handed circular polarization. The experiments were carried out on an FTIR spectrometer with an optical cryostat at temperatures around 5 K. Automatization of the experiment was performed to increase the signal-to-noise ratio of the obtained spectra. As a result, for the samples under study, obtained values of ZFS energy lie in the range of 43.6–43.4 cm^{-1} .

This research was funded by the Russian Science Foundation, grant number 22-13-00376. Authors also thank Dr. D. A. Safin for the samples provided.

1. Nehr Korn J., Valuev I.A., Kiskin M.A., Bogomyakov A.S., Suturina E.A., Sheveleva A.M., Ovcharenko V.I., Holldack K., Herrmann C., Fedin M.V., Schnegg A., Veber S.L.: *J. Mater. Chem. C* **9**, 9446 (2021)
2. Maryasov A.G., Bowman M.K., Fedin M.V., Veber S.L.: *Materials* **12**, 3865 (2019)

Photoresistivity of the film heterostructure $\text{Ba}_{0.8}\text{Sr}_{0.2}\text{TiO}_3/\text{Ba}_{0.8}\text{Sr}_{0.2}\text{TiO}_3$ on MgO substrate

A.O. Chibirev, A.V. Leontyev, N.N. Garif'yanov, R.F. Mamin

Zavoisky Physical-Technical Institute, FRC Kazan Scientific Center of RAS, Kazan 420029, Russia, chibirev12@mail.ru

Properties of functional materials are achieved due to the effects associated with the complex composition of the heterostructure. A high-mobility electron gas has been discovered at the interface between two oxide insulators LaAlO_3 (LAO) and SrTiO_3 (STO) [1]. Previously the effect of infrared, green, and ultraviolet laser radiation on the electrical resistance of the heterostructure $\text{Ba}_{0.8}\text{Sr}_{0.2}\text{TiO}_3/\text{LaMnO}_3$ was investigated here [2].

Here the dependences of the electrical resistance on temperature were studied for $\text{Ba}_{0.8}\text{Sr}_{0.2}\text{TiO}_3/\text{LaMnO}_3/\text{Ba}_{0.8}\text{Sr}_{0.2}\text{TiO}_3$ heterostructure on MgO-substrate. An unfocused laser beam with a diameter of 4 mm, with a Gaussian shape, irradiated the space between the contact pads through the optical window of the cryostat. We observed an increase when in resistance when 170 K range this transient component is $\sim 20\text{--}200$ s. the response to green light exposure was the most prominent. It was found that when illuminated with light of different wavelengths, there was a cumulative effect, a change in resistance over several on/off cycles green and infrared light. The observed effect cannot be explained by direct heating of the sample by laser pulses, because the laser pulse repetition rate is low and, therefore, the cumulative thermal effects should be negligible. This example shows that quasi-two-dimensional high conductance at ferroelectric/dielectric interfaces can be controlled by a light.

The reported study was funded by Russian Science Foundation according to the research project No. 21-12-00179.

1. Ohtomo A., Hwang H.Y.: Nature **427**, 423 (2004)
2. Chibirev A.O. et al.: JETP Letters **114**, 757–762 (2021)

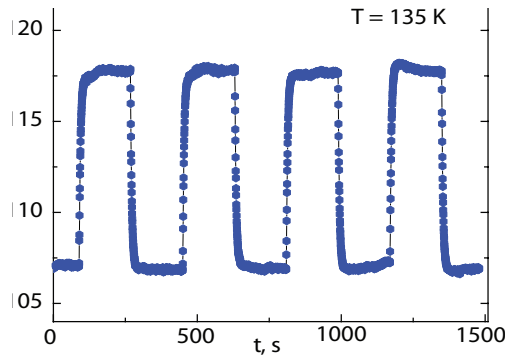


Fig. 1. Multiple on-off switching of electrical resistance of the $\text{Ba}_{0.8}\text{Sr}_{0.2}\text{TiO}_3/\text{LaMnO}_3/\text{Ba}_{0.8}\text{Sr}_{0.2}\text{TiO}_3$ heterostructure at 135 K by green illumination.

Anisotropic rotation of nitroxide radical in the pore system of metal-organic framework induced by guest solvents

A.A. Efremov^{1,2}, A.S. Poryvaev¹, D.M. Polyukhov¹, M.V. Fedin^{1,2}

¹International Tomography Center SB RAS, Novosibirsk, 630090, Russia,
a.efremov@tomo.nsc.ru

²Novosibirsk State University, Novosibirsk, 630090, Russia

Nitroxide radicals, encapsulated into the cavities of metal-organic frameworks (MOFs), have recently drawn attention as multifunctional spin probes. In this work we investigate the mobility of TEMPO nitroxide in MOF in the presence of various solvent molecules located in the same cavity. Fast isotropic rotation of nitroxide in MOF cavity under vacuum can be changed to some more complicated pattern when solvent molecules are present in the same cavity. Since the cavity has its own symmetry, some constraints for the mobility might be imposed in the presence of solvents of different size and shape.

We employ simulations of continuous wave (CW) EPR spectra to reveal anisotropic rotation of radical. It is shown that the largest anisotropy of rotation occurs for MOF impregnated with alcohols: it is most pronounced at low temperatures, but also manifested at room temperatures. It can be caused by non-covalent interactions between alcohol molecules: hydrogen bonding in alcohol molecules can form a specific structure in cavity. Linear alkanes do not indicate any significant effect onto the rotation anisotropy of TEMPO, while various benzene derivatives show more complicated trends caused by their bulkier shapes and different number of molecules occupy the cavity, caused by small changes in structure of solvents, thus creating different 'packing' and unobvious trends. This means, that solvent molecules are ordered in the cavity in specific way, making it asymmetric and imposing restrictions on the rotation of a nitroxide

With a number of examples, we demonstrate the ability of CW EPR analysis to disclose effects of solvent ordering in MOFs via anisotropic rotation of encapsulated spin probe. We assume that such specific ordering has to be accounted for when performing target reactions in MOFs.

Acknowledgments. This work was supported by the Russian Science Foundation (22-73-10239).

ESR of Dy^{3+} ion at cubic sites in Cs_2KYF_6 crystals

M.L. Falin¹, V.A. Latypov¹, N.M. Khaidukov²

¹Zavoisky Physical-Technical Institute, FRC Kazan Scientific Center of RAS, Kazan 420029, Russia, falin@kfti.knc.ru

²Institute of General and Inorganic Chemistry, Moscow 119991, Russia

Fluoroelpasolites $A_2^+B^+C^3+F_6^-$ ($A = Cs, B = Na, C = Y, Sc$) having the cubic structure in the wide temperature interval are perfect model systems in which the isomorphous substitution of cations by trivalent rare-earth ions provides an opportunity to study optical and magnetic properties of dopants in a wide concentration range.

Crystals of cubic elpasolites A_2BCF_6 doped with rare-earth ions were grown under hydrothermal conditions. Under these conditions, spontaneously nucleated crystals of up to 0.5 cm^3 were grown in the upper crystallization zone of the autoclave for 200 h.

EPR experiments were carried out using an X-band spectrometer ERS-231 (Germany) at $T = 4\text{ K}$.

The parameters of the corresponding spin Hamiltonians, the ground states and their wave functions were determined. Structural model of the observed complex was proposed. The experimental results were analyzed in comparison with those for the same paramagnetic ion in other hosts [1-3].

This work was supported by Ministry of Science and Higher Education of the Russian Federation in the frame of Agreement No. 075-15-2021-623 with the FRC Kazan Scientific Centre of RAS.

1. Falin M.L., Latypov V.A., Khaidukov N.M.: Appl. Magn. Reson. (2022) (in press)
2. Falin M.L., Latypov V.A., Bill H., Lovy D.: Appl. Magn. Reson. **14**, 427 (1998)
3. Abraham M.M., Finch C.B., Kolopus J.L., Lewis J.T.: Phys. Rev. B **3**, 2855 (1971)

An estimate of the activation energy of the solid-phase recrystallization of ion implanted Si (111) by an optical diffraction method

B.F. Farrakhov, Ya.V. Fattakhov

Zavoisky Physical-Technical Institute, FRC Kazan Scientific Center of RAS, Kazan 420029, Russia, bulat_f@mail.ru

The results of estimates of the activation energy of the solid-phase recrystallization (SPR) of ion implanted Si (111) by an optical diffraction method directly during a pulse light annealing (PLA) procedure are presented. This technique is based on registration of Fraunhofer diffraction picture change from special periodic structures. For this purpose, two measuring diffraction gratings (DG) were preliminarily formed on the surface of a silicon wafer: a phase grating and an amplitude grating.

KDB-1 single-crystal silicon wafers with the (111) surface orientation and a thickness of 0.4 mm were chosen as the objects of study. The ion implantation of P⁺ ions samples through the grid was performed in the chamber of an ILU-3 ion-beam accelerator. Thus, an amplitude DG with a 50- μm period was formed (Fig. 1a). The ion implantation with energies of 25, 50 keV and doses of $3.12 \cdot 10^{15}$, $6.2 \cdot 10^{15}$, and $1.9 \cdot 10^{16} \text{ cm}^{-2}$ was performed. A phase DG with a 4- μm period that was formed near the amplitude DG was used to record the temperature of the silicon wafers [1].

Figure 2 shows the signal of a change in the diffraction efficiency and temperature dynamic.

During the epitaxial SPR, amorphous-crystalline interface moves toward the surface. From a diffraction efficiency change signal (change of the first diffraction maximum of the intensity) the time (t) of position (d) this interface

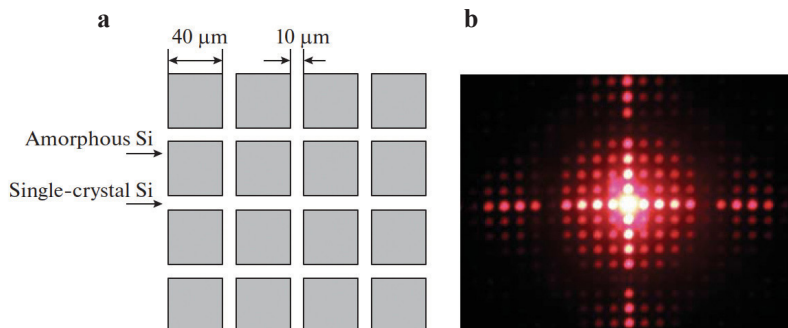


Fig. 1. **a** The structure of the amplitude diffraction grating on the sample surface and **b** the diffraction pattern that was obtained when probing this grating with a He-Ne laser ($\lambda = 0.6328 \mu\text{m}$).

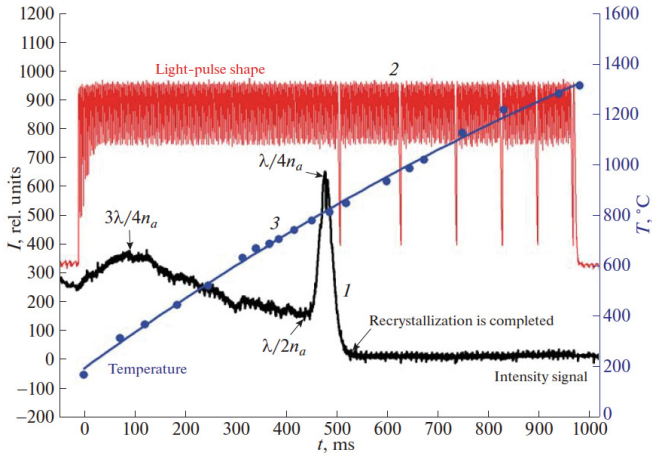


Fig. 2. (1) A signal of the intensity of the first diffraction maximum, obtained under irradiation with (2) a light pulse with a duration of 970 ms and a power density of 140 W/cm², and (3) the temperature dynamics. The sample is (111) silicon implanted with P⁺ ions with an energy of 50 keV and a dose of 3.12 · 10⁻¹⁵ cm⁻².

Table 1. An SPR activation energy for several implantation and PLA regimes.

E_{imp} , keV	P , W/cm ²	V_p , ×10 ⁻⁶ m/s	T , °C	E_a , eV
25	140	1.6	1020	2.02
25	530	2.8	1030	2.19
50	140	1.86	1100	2.16
50	530	3.72	1180	2.25

to surface was obtained [1]. A temperature from a diffraction angle change of 5th other diffraction beam was obtained [1].

An SPR activation energy is obtained by equation:

$$E_a = kT(P, t) \ln(V_0/V_p), \tag{1}$$

where are, k – Boltzmann constant, $T(P_0, t)$ – temperature, P_0 – light pulse density, t – time, $V_0 = 1.55 \cdot 10^4$ m/s, $V_p = d/t$ – SPR average velocity obtained from a signal of the intensity.

Several results are showing in Table 1.

1. Farrakhov B.F., Fattakhov Ya.V.: Pribory i Tekhnika Eksperimenta **2**, 93 (2019)

Effect of the anion nature on the spin properties of new Fe (III) complexes with tridentate ligands

E. Frolova, A. Sharipova, L. Bazan, O. Turanova, I. Ovchinnikov

Zavoisky Physical-Technical Institute, FRC Kazan Scientific Center of RAS, Kazan 420029, Russia, fro-e@yandex.ru

It is known that differences in the size and shape of counterion in spin-crossover (SCO) systems often cause differences in the crystal packing and changes in the cooperative properties of the complexes. So it seems possible to tune the properties of the spin crossover by changing the size of the counterion. However, it is difficult to establish general patterns in different ligand series. For example, for Fe (III) complexes with quinolylsalicyladimine (HQsal) – tridentate NNO donor ligands, it was found that small anions stabilize the low-spin state (LS, $S = 1/2$), while large anions stabilize the high-spin (HS, $S = 5/2$) state. Nevertheless, in the case of other ligand systems, the opposite trend was observed.

For the purpose of creating a controlled spin transition compounds, Fe (III) complexes with a 1-phenyl-3-(quinolin-8-ylamino)prop-2-en-1-one (HQAVK) tridentate NNO donor ligand is obtained for the first time. Here we present boron containing Fe (III) compounds of general formula $[\text{Fe}(\text{QAVK})_2]\text{BX}_4 \cdot n\text{H}_2\text{O}$ (here X = phenyl or F, $n = 0, 1$) that allow a direct evaluation of the impact of anion size and solvent effects on SCO properties. Counterions were chosen based on the volume difference [1]: the smallest BF_4 (38 \AA^3) and largest BPh_4 (323 \AA^3) sizes of anions were used.

The composition and structure of the synthesized compounds are confirmed by analytical data and UV-Vis spectroscopy. The magnetic properties are studied by the EPR method. Data on the electronic structure of complexes in vitrified solutions are obtained. For powder samples, it is found that the compounds are mainly LS and the spin transition is not complete in the available temperature range. It is shown that crystal packing has a critical effect on the implementation of the SCO and its characteristics.

1. Michael D., Mingos P., Rohl A.L.: *Inorg. Chem.* **30** (19), 3769 (1991)

W-band EPR investigation of mechanoactivated and γ -irradiated calcium gluconate

**A.R. Gafarova¹, G.G. Gumarov¹, R.B. Zaripov¹, D.S. Rybin²,
G.N. Konygin²**

¹Zavoisky Physical-Technical Institute, FRC Kazan Scientific Center of RAS, Kazan 420029, Russia, albina-gafarova@mail.ru

²UdmFRC Ural Branch of RAS, Izhevsk 426067, Russia, dsrybin@mail.ru

Recent interest in the study calcium gluconate has been associated with the development of its mechanically activated form (MACG), the efficiency of which is much higher [1]. The high bioavailability of MACG associated with stereochemical changes in the molecule calcium gluconate. In this regard, it is attractive to use EPR spectroscopy and quantum chemical methods. In this work, an attempt was made to use gamma radiation to create radical centers and obtain more detailed information about such structural transformations.

The starting material was a CG powder from Sigma Aldrich (SA). The mechanoactivation of the samples was carried out on a LAIR ball mill. The samples were irradiated on a Rokus apparatus by 1.25 MeV photons with dose 400 Gy.

The shape of the EPR spectrum of a mechanically activated SA GC (Fig. 1) indicates the anisotropy of the g -factor, as well as a small linewidth. Subsequent irradiation leads to a significant transformation and shift of the spectrum. It is quite remarkable that these two spectra together give a spectrum corresponding to mechanically activated CG produced by industry and containing excipients (Fig. 1). By quantum chemical calculations, it was found that the observed lines correspond to the same molecular structure containing δ -gluconolactone and a calcium gluconate molecule. Apparently, irradiation only leads to the displacement of the radical center without destroying the molecular complex. This confirms the previously stated assumption about the formation of a stable structure.

Funding. The reported study was funded by RFBR, project number 20-31-70001.

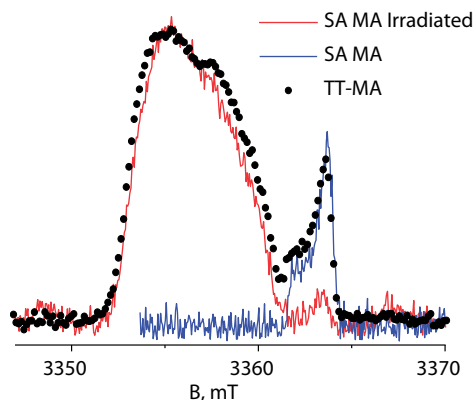


Fig. 1. EPR spectra of pure CG from Sigma Aldrich and of CG with excipients from Tyumen Chemical-Pharmaceutical Plant (TT).

Reversible intercalation of lithium ions into the structure of $\text{Li}_3\text{V}_2(\text{PO}_4)_3$ cathode material for lithium-ion batteries: ESR measurements

**T.P. Gavrilova¹, I.V. Yatsyk¹, J.A. Deeva², T.I. Chupakhina²,
N.M. Suleimanov¹, S.M. Khantimerov¹**

¹Zavoisky Physical-Technical Institute, FRC Kazan Scientific Center of RAS, Kazan 420029, Russia

²Institute of Solid State Chemistry of RAS (UB), Ekaterinburg 620990, Russia

Nowadays, many researches in the field of modernization of Li-ion batteries (LIB) are devoted to the developing of the high energy density materials for the so-called “post-lithium-ion batteries”. Among others oxides, the phosphorus-containing materials as the potential electrodes materials for LIB are of particular interest, e.g. orthophosphate vanadates as the cathode materials in the form of a composite or the partially substituted composition.

Here we present the investigations of magnetic and electrochemical properties of $\text{Li}_3\text{V}_2(\text{PO}_4)_3$ -based composites, including $\text{Li}_3\text{V}_2(\text{PO}_4)_3/\text{Li}_3\text{PO}_4$ (LVPO/LPO) and $\text{Li}_3\text{V}_2(\text{PO}_4)_3/\text{C}$ (LVPO/C). LVPO/LPO solid solutions were obtained by the thermal hydrolysis method [1] or hydrothermal method with the subsequent annealing in Ar atmosphere. In comparison, the mesoporous sample of LVPO/C was synthesized by the soft-template method [2]. Magnetic properties of LVPO/LPO and LVPO/C composites (including as-prepared samples and samples after Li deintercalation and intercalation processes) were investigated using the electron spin resonance (ESR) method. The complete reduction of vanadium ions to the initial valence state V^{3+} after the first charge/discharge cycle was determined indicating the reversible intercalation of all lithium ions to the structure during the first delithiation/lithiation cycle in the investigated objects.

The reported research was funded by Russian Science Foundation (grant No 19-79-10216), <https://rscf.ru/project/19-79-10216/>.

1. Gavrilova T., Khantimerov S., Cherosov M. et al.: *Magnetochemistry* **7**, 64 (2021)
2. Gavrilova T.P., Khantimerov S.M., Fatykhov R.R. et al.: *Solid State Commun.* **323**, 114108 (2021)

Features of the temperature behavior of the ESR spectra of Cr³⁺ ions in the 3D Dirac semimetal Cd₃As₂

Yu. Goryunov¹, A. Nateprov²

¹Zavoisky Physical-Technical Institute, FRC Kazan Scientific Center of RAS, Kazan 420029, Russia, goryunov@kfti.knc.ru

²Institute of Applied Physics, Chisinau, MD-2028, Moldova, nateprov@ifa.md

A possibility of doping Dirac topological semimetals with both rare earth and iron-group ions makes them attractive from the point of view of magnetism, since the interaction of two electronic subsystems (localized and free electrons) results in a number of specific features. Very rich physics is expected for impurity of chrome in 3D topological semimetal Cd₃As₂. The influence of Cr impurities on the properties of 3D topological Dirac semimetal Cd₃As₂ has been studied by the electron spin resonance (ESR). We have fabricated sample and studied the temperature behavior of its ESR spectra. Cd₃As₂ ingots alloyed with 0.5 at.% Cr were synthesized at 1023 K by both direct reaction of components, Cd (purity 99.999%), As (99.9999%), and Cr (99.99%), and via Cd–Cr alloys in glass–graphite crucibles placed in evacuated sealed-off quartz ampoules. The crystal structure and stoichiometry was verified by EDX analysis and powder X-ray diffraction (PXRD). The ESR were measured on a standard Bruker modulation ESR spectrometer in the X range (9.3 GHz). ESR signals from Cr³⁺ ions were observed in the temperature range of 10–300 K. A central ESR signal had a distorted almost symmetric shape. This signal had few weak satellites, which one could interpret as the signs of a fine or hyperfine structure. However for right interpretation of spectra one need to decide the main question, which arises in this investigation, is question about valence (charge) state of Cr impurities. Chromium may be have valence state +1, +2, +3, +4. Substituting bivalent cadmium in a tetrahedral positions of a substitution or insertion, also as in case of iron, chromium have valence +2. In a tetragonal crystal field, the ground level of the Cr²⁺ ion is an orbital singlet split by the second order spin-orbit interaction into five ($S = 2$) spin sublevels (one singlet and two doublets). Observation of EPR in such systems is impossible [1], since the energy states between which resonant transitions are allowed are separated by an energy gap many exceeding the quanta of the radio-frequency field for a frequency of X-band spectrometers. Therefore, we conclude that we observe signals from a small number of trivalent chromium ions located in substitutional or interstitial positions.

The Cr³⁺ ion has 3d³ electronic configuration and the ground state with $L = 3$, $S = 3/2$ (4F term). This state is split in the crystalline field so that an orbital singlet has the lowermost energy. This singlet consists of two Kramers doublets which are split in the crystalline field with the low symmetry on four levels. The transitions between the levels of such quartet corresponding to the selection rule $D_{ms} = \pm 1$ are observed in the X-band ESR.

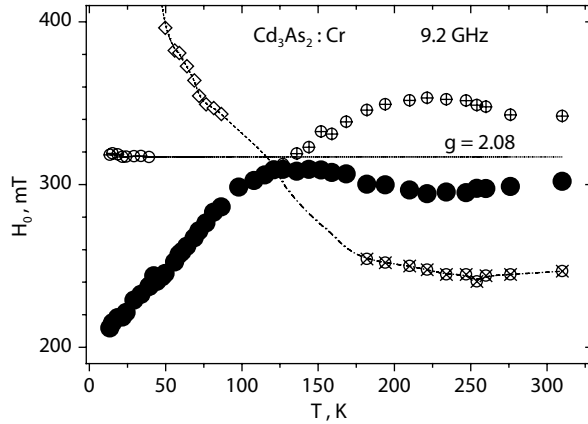


Fig. 1. Temperature dependences of the re-sonance fields of lines in the ESR spectra. Full symbol – main intensive line, open symbols – weak lines, diamond – step on spectra.

Thus, we observe ESR on inclusions of Cr^{3+} ions located in the magnetic system of impurity Cr^{2+} ions and indicating the processes occurring in this system. The temperature dependences of the position of the lines in the ESR spectra of this system (see Fig. 1) indicate an increase in the exchange narrowing of the ESR spectrum and the presence of a magnetic phase transition near $T \sim 120$ K. A similar phase transition was observed in the system of magnetic impurities of bivalent europium at close temperatures [2]. It should be emphasized that in the case of Cr^{3+} ions the value of g -factor is also anomalously high, as in the case of europium ions. We attribute this anomaly to the interaction of localized magnetic moments with conduction electrons, which have extremely large g -factor in the Cd_3As_2 matrix.

1. Avanesov A.G., Badikov V.V., Shakurov G.S.: Phys.Solid State **45**, 1451 (2003)
2. Goryunov Yu.V., Nateprov A.N.: Phys. Solid State **60**, 68 (2018)

Synthesis and investigation of magnetic properties of thin film systems Fe_3Al and $\text{Fe}_3\text{Al}/\text{Pt}$

A.Hh. Kadikova

Kazan Federal University, anelyakadikova11@gmail.com

One of the most promising types of dynamic memory is magnetoresistive random access memory (MRAM). The main advantage of this type of memory is its non-volatility, i.e. the ability to store the recorded information when disconnected from the power supply, and high recording density. MRAM is based on heterostructures with layers of ferromagnetic (F) and normal (N) metals. The resistivity of a three-layer F/N/F heterostructure, for example, depends on the magnetization arrangement of the two F-layers (giant magnetoresistance effect and tunnel magnetoresistance). Therefore, the “0” and “1” states of the simplest MRAM cell differ in the resistance values. Switching the magnetization between two opposite directions provides information recording. The spin Hall effect is a promising phenomenon for rapid magnetization direction switching. This effect occurs in F/N-type heterostructures, where N is heavy non-magnetic metal with large spin-orbit coupling.

We present results of the synthesis and magnetic properties studies of the ferromagnetic alloy thin films of Fe_3Al and of the F/N heterostructure based on it, where platinum is used as a heavy normal metal. The Fe_3Al thin films were grown by molecular beam coprecipitation (MBE) in an ultrahigh vacuum chamber manufactured by SPECS (Germany). Deposition rates of iron and aluminum from two high-temperature cells were set at their temperatures and the deposition rate of each element was calibrated using a quartz sensor. The substrates were the single crystal plates of MgO compound with orientation (001) with a roughness of less than 0.5 nm (epi-ready grade).

A Fe_3Al thin film served as a sample for the study of magnetic properties. A platinum layer was deposited on half of the sample area. To prevent oxidation, the area of the samples was covered with a aluminum capping layer. Epitaxy of growth was investigate by low-energy electron and X-ray diffraction which shows that the Fe_3Al film is single-crystalline with the $[110]_{\text{Fe}_3\text{Al}} \parallel [100]_{\text{MgO}}$ epitaxy character. By the AFM method it was established the Fe_3Al film have an island morphology.

Magnetic properties were studied at room temperature by the vibration sample magnetometry of the PPMS-9 system by Quantum Design (USA). Magnetic hysteresis loops were studied under the magnetic field applied either in the film plane or along the film normal. It is shown that saturation magnetization of the $\text{Fe}_3\text{Al}/\text{Pt}$ heterostructure exceeds that of the Fe_3Al film by ~6% indicating the induced magnetism of the Pt-layer. We found differences in the ferromagnetic resonance (FMR) spectra of these two samples. The FMR line of the $\text{Fe}_3\text{Al}/\text{Pt}$ heterostructure has a larger width than the Fe_3Al thin film line. In our opinion, the increase in the line width is associated with the occurrence of the reverse

spin Hall effect and, accordingly, with losses arising from the generation of charge currents in the platinum layer under spin pumping conditions. Peculiar FMR lineshape transformation observed under sample rotation within 10 degrees from the normal are observed that we assign presumably to the resonance specific for a ferromagnetic film with an island morphology.

Study of the features direction of the magnetization vector in two-layer system Fe/LiNbO₃

A.A. Kamashev, A.V. Leontyev, R.F. Mamin, I.A. Garifullin

Zavoisky Physical-Technical Institute, FRC Kazan Scientific Center of RAS, Kazan 420029,
Russia, kamandi@mail.ru

To date, the control of superconducting current under the action of an external magnetic field in SSV structures has reached the maximum efficiency. Now is necessary to investigate new heterostructures with non-standard approaches. One of such approaches can be the study of superconducting spin valve (SSV) structures based on ferroelectric substrates. This will make it possible to control the superconducting current using an electric field in the SSV structures.

In the general case, to implement the SSV model based on a ferroelectric substrate, it is necessary to solve the main problem. It is necessary to implement and debug the mechanism for controlling the direction of the magnetization vector of a ferromagnetic layer in a two-layer ferromagnet/ferroelectric heterostructure due to the magnetoelastic effect. The magnetoelastic effect in this system arises due to deformations of the ferroelectric substrate caused by the inverse piezoelectric effect when an external electric field is applied to the ferroelectric substrate. Deformations in the ferroelectric substrate cause stresses in the ferromagnetic layer due to the contact of the ferromagnet and the ferroelectric, that is, due to the ferromagnet/ferroelectric proximity effect. This, in turn, manifests itself in the appearance of additional magnetic anisotropy, which, with a certain construction of the system, can lead to a change in the direction of the magnetization vector of the ferromagnetic layer.

In this work, we studied two-layer ferromagnet/ferroelectric heterostructures, where iron was used as the ferromagnetic layer and 41°Y-cut lithium niobate was used as the ferroelectric substrate. We will show that when an electric field in the region of 50 V is applied to a ferroelectric lithium niobate substrate, changes in the direction of the magnetization vector of the ferromagnetic layer are reliably recorded using the Kerr effect.

The reported study was funded by Russian Science Foundation according to the research project No. 21-72-10178.

Phase transformation in the system “Brodie graphite oxide-acetonitrile” according to EPR and XRD data

**A.V. Kaplin^{1,2}, N.A. Chumakova^{1,2}, D.S. Popov², A.T. Rebrikova²,
M.V. Korobov², O.N. Khrykina³**

¹N.N. Semenov Federal Research Center for Chemical Physics, Russian Academy of Science, Kosygin St. 4, Moscow 119991, Russia

²M.V. Lomonosov Moscow State University, Chemistry Department, Leninskiye Gory, 1/3, Moscow 119991, Russia

³Shubnikov Institute of Crystallography, Federal Scientific Research Centre ‘Crystallography and Photonics’ of Russian Academy of Sciences, 59 Leninskiy prospect, Moscow 119333, Russia

Graphite oxide is a layered material obtained by oxidation of graphite in an acidic environment. There are two main ways to obtain graphite oxide – Hammers’ and Brodie’s methods. The materials obtained by these methods (HGO and BGO) differ in degree of oxidation, composition of the oxygen-containing groups as well as ability to swell in polar liquids; HGO swells more easily compared to BGO. The membranes based on graphite oxide capable of retaining gases and sorbing, separating, and purifying many polar liquids.

In the systems “BGO–polar liquid” for acetonitrile, DMFA and alcohols the reversible phase transformations were observed with release of part of the sorbed liquid and decrease of the inter-plane distance. The aim of the present work was to establish the dependence of the phase transformation in the system “BGO–acetonitrile” on the oxidation level of the material. Figure 1 shows the temperature dependence of the rotational mobility of the nitroxide spin probe

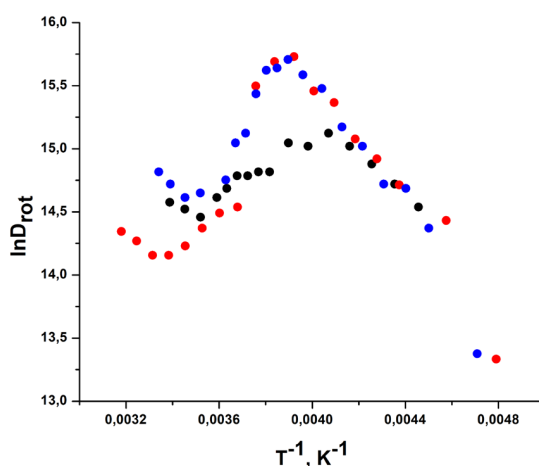


Fig. 1. Temperature dependence of the rotational mobility of the nitroxide spin probe sorbed on inner surface of BGO1 (black points), BGO2 (red points) and BGO3 (blue points).

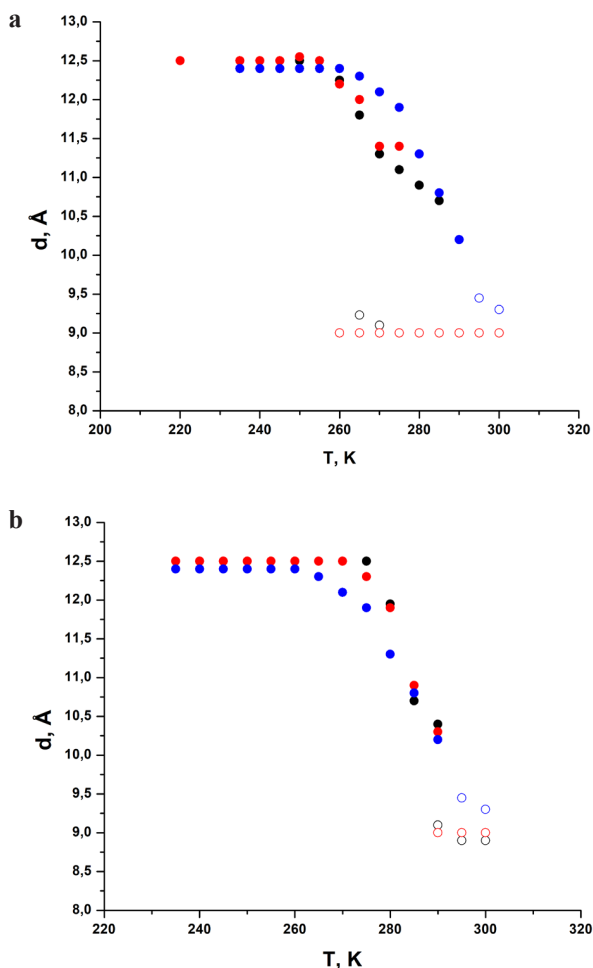


Fig. 2. Temperature dependence of the inter-plane distance for the systems “BGO1–acetonitrile” (black points), “BGO2–acetonitrile” (red points), and “BGO –acetonitrile” (blue points) recorded with decreasing (a) and increasing temperature (b). Colored points – inter-plane distance in low-temperature phase. Hollow points - inter-plane distance in high-temperature phase.

TEMPOL sorbed on inner surface of BGO for one-stage (BGO1), two-stage (BGO2) and three-stage (BGO3) oxidized materials. In all cases the anomaly at the temperature dependency of the rotational diffusion coefficients is observed in the range 255–280 K which reflects the phase transformation in the system. Hence, the phase transformation takes place for BGO with different oxidation level.

The phase transformations in all systems under study were also observed using temperature programming XRD. In Figure 2 there is the temperature dependence of the inter-plane distance for the systems “BGO1–acetonitrile”, “BGO2–acetonitrile”, and “BGO3–acetonitrile” recorded with decreasing (Fig. 2a) and increasing temperature (Fig. 2b).

This work was supported by RSF (grant 21-73-00124).

Phase cycling sequences designing in CPMG method to eliminate unwanted echoes

I.T. Khairutdinov, R.B. Zaripov, M.M. Bakirov, M.Yu. Volkov

Zavoisky Physical-Technical Institute, FRC Kazan Scientific Center of RAS, Kazan 420029, Russia, semak-olic@mail.ru

The Carr-Purcell-Meiboom-Gill (CPMG) pulse sequence is useful to minimize the influence of decoherence processes on the spin system [1, 2]. These processes are characterized by spin-spin (T_2) and spin-lattice (T_1) relaxation times. EPR spectrum line width usually is one order or larger than the microwave field amplitude B_1 . This is called the case of selective excitation. In this case the magnetization will be particularly on longitudinal direction along external magnetic field B_0 . This

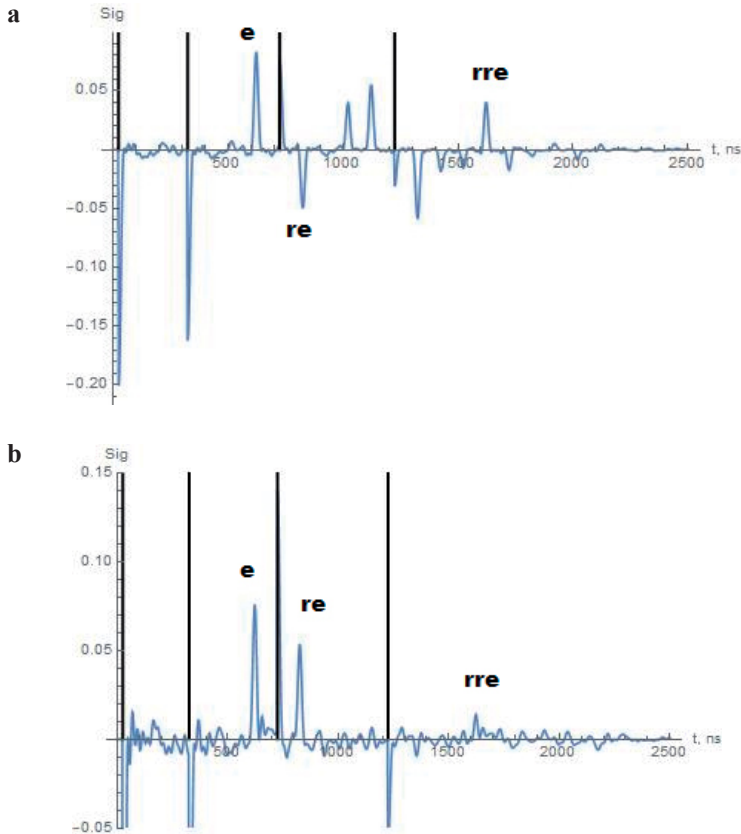


Fig. 1. Simulation of four pulse echo train sequence with unequal delays between pulses $\tau_1 \neq \tau_2 \neq \tau_3$. **a** Pulse sequence without phase cycling. **b** Pulse sequence with phase cycling. In classical CPMG it would be $2\tau_1 = \tau_2 = \tau_3$.

leads to a large number of echo signals. These signals have own magnitude and decay time. Time decay of echo signals looks like exponential combination of relaxation times T_1 and T_2 in different proportions. Appearance of stimulated and other unwanted echoes can be a drawback in practice because they may interfere with the refocused primary echo (Hahn echo). This signal mixing makes it very difficult to obtain T_1 and T_2 relaxation times from CPMG experiments.

In this work we describe way to build CPMG phase cycle sequences taking into account the selectivity of pulses. Phase cycling allows us to eliminate unwanted echo signals and increase the desired ones against their background. For the N -pulse sequence the number of necessary cycles increases to 2^N and thus for large N values the measuring times become unrealistically long. Analytical expressions for all echo signals in 4 pulse sequence within the spin density matrix formalism were obtained and analyzed. We performed numerical simulation of CPMG experiment for different relations between inter pulse delays and relaxation times values. Numerical simulations were compared with experimental data.

The Fig. 1 shows sequences of 4 pulses with incomplete excitation of the inhomogeneous width of the EPR spectrum. To determine the time T_2 from a monoexponential decay, signals such as the Hahn echo (**e**) and its refocused signals (**re**, **rre**) are needed. It can be seen from the Fig. 1a that in the case of incomplete excitation, unwanted echo signals appear. These unwanted signals overlap in the classical CPMG method and make it difficult to determine T_2 . The Fig. 1b shows a sequence with phase cycling, which removes all unwanted signals for 4 pulses. One can determine the time T_2 in this case directly from the monoexponential decay in CPMG pulse train.

The reported study was funded by RSF according to the research project № 22-72-10063.

Web: <https://rscf.ru/en/project/22-72-10063/>

1. Carr H.Y., Purcell E.M.: Phys. Rev. **94**, 630 (1954)
2. Meiboom S., Gill D.: Rev. Sci. Instrum. **29**, 688 (1958)
3. Song Y.-Q.: Journal of Magnetic Resonance **157**, 82–91 (2002)

Spin-orbit interaction in GaN/AlGaN heterojunctions probed by ESR

**R. Khisameeva¹, A.V. Shchepetilnikov¹, V.V. Solovyev¹, T. Mikolajick³,
A. Großer², S. Schmult³, I.V. Kukushkin¹**

¹Institute of Solid State Physics RAS, 142432 Chernogolovka, Moscow district, Russia,
akhisameeva@issp.ac.ru

²NaMLab gGmbH, Nöthnitzer Str. 64, 01187 Dresden, Germany

³TU Dresden, Electrical and Computer Engineering, Institute of Semiconductors and Microsystems

The spin-orbit interaction was extensively studied with the aid of electron spin resonance technique in GaN/AlGaN heterojunctions containing high quality two-dimensional electron system. The spin resonance technique was used to perform accurate measurements of the single-particle g factor that experiences substantial modification induced by the coupling between the spin degree of freedom and the quantized orbital motion of an electron in the quantum Hall regime. Analysis of this filling factor dependent variation of g allowed us to extract the constant α of the Rashba spin-orbit interaction in several GaN/AlGaN heterojunctions with varying electron sheet density. The electron concentration n in the samples was varied by several essentially distinct methods, namely, by optical pumping, by applying external gating, and by changing the Al composition in the barrier region. The extracted value of α demonstrated almost no dependence neither on the electron density, nor on the way n was varied. This striking finding may be explained if the cubic term in the in-plane wave vector of the spin-orbit interaction is taken into account. Theoretical calculations reveal that this term diminishes the effective Rashba constant with rising n and effectively cancels out the amplification of α due to the change in the quantum well form. Lastly, the Rashba constant was extracted from the weak antilocalization observed in the longitudinal resistance of the samples at low magnetic fields. The values of α extracted both from the spin resonance and antilocalization measurements compared well with each other.

The ESR experiments, data analysis and theoretical modelling was supported by Russian Science Foundation (Grant No. 20-72-10097).

Creation of new methods of mid-field magnetic resonance imaging

**A. Kolesova¹, T. Islamov¹, I. Sidorov¹, V. Skirda¹, A. Alexandrov¹,
D. Melnikova¹, Ya. Fattakhov², V. Odivanov²**

¹Institute of Physics, Kazan (Volga Region) Federal University, Kazan 420008, Russia,
akolesova0707@mail.ru

²Zavoisky Physical-Technical Institute, FRC Kazan Scientific Center of RAS, Kazan 420029,
Russia

The use of mid-field tomography is much cheaper in purchase and during operation, in contrast to high-field tomography. The spread of mid-field installations will increase the use of tomography in emergency rooms and medical institutions in small towns. There are limitations to the use of all known tomography techniques due to some features of such installations. This makes the development of new measurement techniques for mid-field tomographs topical.

The value of the magnetic field of mid-field MRI is in the range from 0.3 to 0.5 T. New methods of tomography make it possible to bring the quality of diagnostics of mid-field tomographs closer to the level of tomographs by 1.5 T. That is, new methods of magnetic resonance imaging can increase sensitivity and reduce the time of examination of patients on mid-field devices.

A technique has been developed to obtain more information in standard time. The technique is based on the Carr-Purcell and Meiboom-Gill sequences. It allows you to get a complete relaxation decay in T_2 in one measurement cycle. In this case, the spin echo signal is recorded several times in one run. As a result, we get an image for each signal.

It is possible to apply digital filters with adjustable parameters to multicomponent decays. Thus, we obtain images with contrasting of various pathologies at different stages of diseases. The advantage is that data from a single survey are used.

The developed techniques make it possible to obtain a larger amount of information during the usual scanning time. This ensures that more pathologies are detected during subsequent data processing. Also, new techniques can significantly reduce the time of examination of patients. At the same time, the quality of the resulting images is maintained. New methods will expand the capabilities of diagnostic centers and departments of medical institutions. They will allow timely detection of diseases and injuries of the joints.

Lipid peroxidation processes involving thiosemicarbozones

V. Koshman^{1,2}, E. Shelepova^{1,2}, O. Selyutina², N. Polyakov²

¹Physics department, Novosibirsk State University, Novosibirsk 630090, Russia

²Voevodsky Institute of Chemical Kinetics and Combustion SB RAS, Novosibirsk 630090, Russia, admin@kinetics.nsc.ru

Thiosemicarbozones (TSCs) have a wide range of biological activities, including anticancer, and are of great interest to scientists from various fields of science. Their anticancer activity has long been attributed to their ability to inhibit ribonucleotide reductase. However, recent studies indicate a significant role of oxidative stress in the anti-tumor activity of TSCs. This aspect of their biological activity is currently very poorly understood and is of great interest to medicinal chemistry [1].

In this work, the processes of lipid peroxidation involving chelate complexes with iron and copper ions were studied using the thiosemicarbozones di-2-pyridylketone-4,4-dimethyl-3-thiosemicarbazone (Dp44mT), di-2-pyridylketone 4-cyclohexyl-4-methyl-3-thiosemicarbazone (DpC) and novel thiosemicarbazone AOBP as examples. The interaction of chelate complexes with the lipid bilayer and their role in the lipid peroxidation reaction were studied on model systems by ¹H NMR methods and molecular dynamic simulation using GROMACS software.

Experiments were performed in model systems (linoleic acid micelles and DHPC/DLPC bicelles). The redox properties of Dp44m, DpC, and AOBP complexes with iron and copper in the lipid peroxidation reaction and the role of the natural antioxidant ascorbic acid in this process were studied. The interaction of TSCs complexes with the lipid membrane was also studied. It was found that complexation of Dp44mT with iron almost completely inhibits the peroxidation reaction, while complexes with copper retain oxidative activity. At the same time, in the presence of ascorbic acid, the activity of Dp44mT complexes with iron significantly increases. It was revealed that the complexation of Dp44mT with iron ions inhibits the formation of the OH-radical in the Fenton reaction. In the presence of ascorbic acid, OH-radical formation was observed. The increase in the oxidative activity of Dp44mT complexes with iron ions in the presence of ascorbic acid is due to the cyclic oxidative-reductive reaction with Dp44mT complexes. Complexation of iron with DpC also inhibits lipid peroxidation.

1. Lu B., Chen X., Ying M., He Q., Cao J., Yang B.: *Frontiers in Pharmacology* **8**, 992 (2018)

Polarizing insensitive nuclei at ultralow magnetic fields using parahydrogen: a facile route to optimize adiabatic magnetic field sweeps

V.P. Kozinenko, A.S. Kiryutin, A.V. Yurkovskaya

International Tomography Center, Novosibirsk 630090, Russia;
Novosibirsk State University, Novosibirsk 630090, Russia
vitaly.kozinenko@gmail.com

Over the last decade, parahydrogen-induced polarization (PHIP) has been accepted as an exceptionally powerful method of NMR signal enhancement. This is due to its ability to effectively hyperpolarize molecules relevant for biomedical research while using low-cost experimental procedures. NMR signal enhancement in PHIP method derives from the non-equilibrium population of nuclear spin states in parahydrogen molecule, i.e. dihydrogen with proton spins being in singlet spin state. The majority of practical applications require transferring PHIP from protons to low-gamma nuclei (^{13}C , ^{15}N , and others) since they are less susceptible to relaxation and allow background-free signal detection.

One of the most commonly used routes for PHIP transfer exploits adiabatic sweeping of the external magnetic field in the range of several micro tesla, where coherent spin mixing of protons and heteronuclei occurs [1]. This approach, often referred to as magnetic field cycling, or MFC, becomes even more effective, when instead of linear profile of field sweep one utilizes the optimal one [2]. However, calculation of such profiles becomes laborious and impractical for complex spin systems, which is often a case for PHIP with non-isotopically labeled substrates.

We propose a facile route for the optimization of field profile in experiments on magnetic field cycling, exploiting the field dependence of average ^{13}C polarization in PHIP transfer experiment. Both experimental detection and numerical simulation of such field dependence are straightforward even for complex multi-spin systems. We demonstrate the validity of our approach by conducting comprehensive MFC experiments with allyl pyruvate. This molecule has a potential as a biologically relevant PHIP target and yields an intricate multi-spin system. The proposed optimization method allows straightforward calculation of field profile for this molecule and provides higher levels of ^{13}C signal enhancement as compared to the linear profile.

The work was supported by Russian Scientific Foundation - Grant № 20-62-47038.

1. Eills J. et al.: *J. Chem. Phys.* **150** (2019)
2. Rodin B.A. et al.: *Phys. Chem. Chem. Phys.* **23** (2021)

Effect of transition metal ions to hydrodynamic behavior of human serum albumin

A.M. Kusova¹, K.R. Mirsalimova¹, A.N. Turanov², Yu.F. Zuev¹

¹Kazan Institute of Biochemistry and Biophysics, FRC Kazan Scientific Center of RAS, Kazan, Russia, alexakusova@mail.ru

²Zavoisky Physical-Technical Institute, FRC Kazan Scientific Center of RAS, Kazan 420029, Russia

In this work we have studied the HSA molecular association in the presence of metal ions (Cu^{2+} , Mg^{2+}) using two complementary diffusion techniques (DLS and PFG-NMR). We analyzed the self- and collective diffusion data with a focus on HSA oligomerization process. It was shown that these diffusion regimes are complementary and sensitive differ to a polydispersity of sample. The PFG NMR probes molecular translational diffusion in the long-time regime (self-diffusion) and yields an averaged self-diffusion coefficient. The DLS allows to observe diffusion in short-time regime via the collective diffusion coefficient. We clearly observed HSA monomers together with big oligomers using short-time collective diffusion, while the long-time self-diffusion shows time-averaging over all protein states, which is displayed in small apparent increase of protein size. It was assumed that the oligomer exchange time of HSA lies within the characteristic time scale of PFG NMR and DLS methods.

For a theoretical description of concentration dependence of the HSA self- and collective diffusion coefficients, the phenomenological approach based on the frictional formalism of nonequilibrium thermodynamics was used (Vink theory), which allows the analysis of solvent–solute and solute–solute interactions in protein solutions. In the presence of metal ions a significant increase of the HSA solute-solute friction coefficient was shown which can be associated with the protein-protein interactions occurring during formation of HSA oligomers. Based on theoretical analysis of collective diffusion data, positive values of second virial coefficients A_2 were obtained for all HSA solutions. This allowed us to conclude that the most pronounced deposit to the protein-protein interaction for different forms of HSA is determined by the electrostatic repulsion.

This work was performed with financial support from the Russian Foundation for Basic Research, Grant № 20-04-00157.

Electron spin resonance of ^{51}V ions in scandium orthosilicate monocrystal

R.F. Likеров, I.V. Yatsyk, R.B. Zaripov, K.B. Konov, V.A. Shustov, R.M. Eremina

Zavoisky Physical-Technical Institute, FRC Kazan Scientific Center of RAS, Kazan 420029, Russia, rodionlikеров@gmail.com

Active search for suitable materials has a significant role in the quantum communications development. Such materials will be used as a medium for quantum memory devices. Key requirements for these devices are long phase memory time enough to complete manipulations with the quantum information and simplified method of interaction with the quantum memory through various protocols.

For example, scandium and yttrium orthosilicate (YSO, SSO) monocrystals doped with monoisotopic rare-earth ions such as ^{143}Nd , ^{145}Nd , ^{171}Yb were studied for quantum memory applications [1, 2]. In this work we study scandium orthosilicate monocrystal with monoisotopic Si ($\text{Sc}_2^{28}\text{SiO}_5$) and doped with monoisotopic ^{51}V ions (0.001 at.%).

We measured CW ESR spectra and orientational dependencies of the ESR transitions from the rotation angle in the external magnetic field in X-band at the temperature $T = 15$ K (Fig. 1). On spectra we observed the group of lines from paramagnetic centers of vanadium ions V^{4+} ($3d^1$).

Since there is only 1 electron on the d-shell responsible for one ESR transition and the nuclear magnetic moment of ^{51}V isotope is $I = 7/2$ resulting in

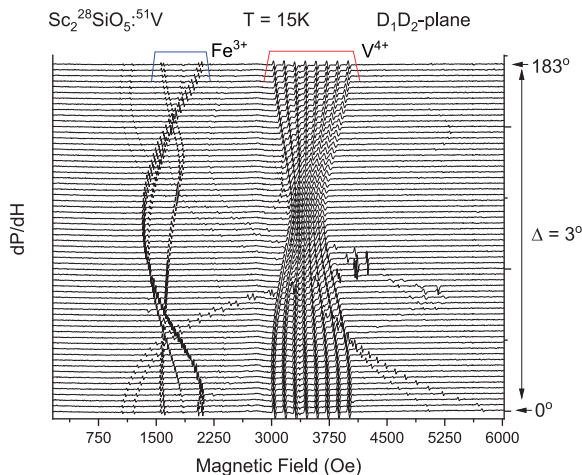


Fig. 1. Orientational dependence of ESR spectra for $^{51}\text{V}:\text{Sc}^{28}\text{SiO}_5$ (0.005 at.%) measured at $T = 15$ K with $B_0 \parallel D_1D_2$.

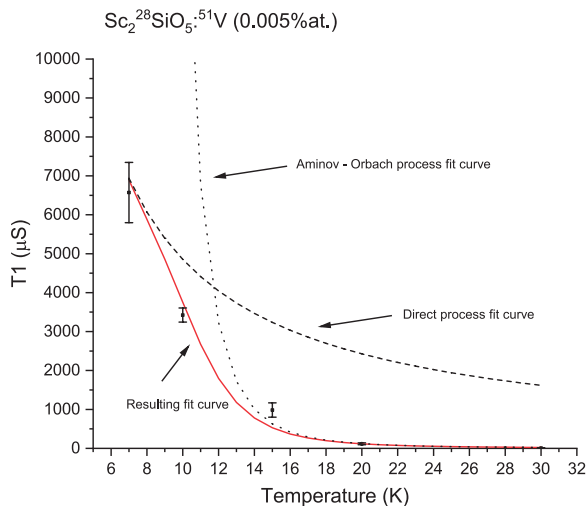


Fig. 2. Temperature dependence of the spin-lattice relaxation time for $^{51}\text{V}:\text{Sc}_2^{28}\text{SiO}_5$ (0.005 at.%) measured with inversion recovery method.

$2I + 1 = 8$ lines of hyperfine structure. The group of lines in the 1000–2250 Oe magnetic field range belongs, presumably to Fe^{3+} ions, which are presented in the crystal as unwanted impurity.

We also measured spin dynamics by pulsed ESR methods, such as spin-lattice and phase coherence times and their temperature dependencies. The temperature dependence for spin-lattice relaxation time of V^{4+} centers is shown at Fig. 2. The experimental points were approximated by the sum of direct phonon relaxation process and Aminov-Orbach process. The spin-lattice relaxation time $T_1 \approx 6.5$ ms.

1. Sukhanov A.A. et al.: Journal of Magnetic Resonance **295**, 12–16 (2018)
2. Likеров R.F. et al.: Magn. Reson. Solids **22**, 20201 (2020)

Strategy of simulation of the EPR spectra angular dependence for nitroxide spin probes in graphene oxide membranes

M. Matveev

Chemistry Department, MSU, Moscow 119991, matveev2002@yandex.ru

Graphite oxide (GO) is a layered material composed of graphene planes which are randomly decorated with oxygen-containing groups. Membranes formed from graphite oxide (GOM) possess selective permeability for liquids and gases. The ordering of the graphene planes is one of the factors determining permeability. At present, spin probe method is the only experimental technique which allows the quantitative determination of the ordering of graphene planes in GOM. Orientational order parameters of the spin probe in the membrane are determined by simulation of a series of EPR spectra recorded at different orientation of the membrane relative to magnetic field lines of the spectrometer. The most perspective spin probes for GOM analysis were found to be stable nitroxide radicals.

Graphite oxide has a native EPR signal which overlaps with central part of the nitroxide signal, so the analysis of the EPR spectra angular dependence is much more difficult. Moreover, the amplitude and width of the GO signal depends on orientation of the membrane in magnetic field and the concentration of the paramagnetic probe. Hence, we cannot subtract this signal from the spectra and have to describe every spectrum as a sum of the signals of nitroxides and GO.

In the present work the strategy of simulation of the EPR spectra angular dependence for nitroxide spin probes in GOM is proposed. Usually, the simulation of EPR spectra is performed according to the principle of minimization of the discrepancy between the theoretically calculated spectra and the experimental ones in the given number of points. Each point can be assigned with the weight coefficient that changes contribution of this point to the total discrepancy. For

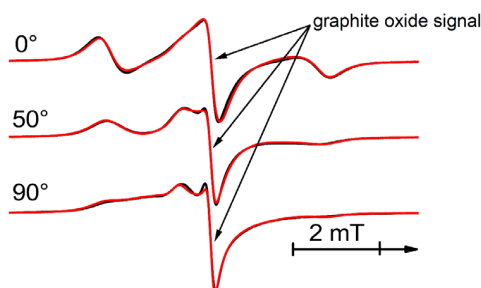


Fig. 1. Angular dependence of EPR spectra of TEMPOL in GOM; black lines – experimental spectra, red lines – result of simulation.

better description of the low-field and high-field components of EPR spectra of nitroxide spin probe in GOM, which are not overlapped with GO signal, higher weight coefficients for these parts of the spectra are needed. For satisfactory description of the central parts of the spectra, the simulation must be performed in several stages:

- a) rough approximation;
- b) simulation with the weight coefficients leading to the accurate description of the low-field and high-field components;
- c) simulation without the weight coefficients with fixed values of the order parameters obtained at stage b;
- d) repetition of stages b) and c) until the convergence of the result.

Figure 1 illustrates the result of simulation of the angular dependence of EPR spectra of spin probe TEMPOL sorbed on the inner surface of GOM. It is seen that the proposed procedure leads to good description as low-field and high-field components of TEMPOL spectra and intensive GO signal.

The work was supported by Foundation for Basic Research (grant 18-29-19120).

Dual-compensated composite pulses for nuclear quadrupole resonance spectroscopy

I. Mershiev, G. Kupriyanova

Institute of Physics and Technology, Immanuel Kant Baltic Federal University, Kaliningrad 236041, Russia, IMershiev@kantiana.ru

In NMR spectroscopy, a composite pulse in general case is a series of radiofrequency pulses with phase modulation, tuned for compensation of instrumental imperfections. Composite pulses for NQR can be optimized in a similar way for compensation of frequency offset and effects of powder averaging. One of the most straightforward and computationally effective ways to describe composite rotations and design composite pulses is using quaternions [1].

In NQR in powders, unlike in NMR, nutation oscillations are heavily damped because of effects of powder average. In this case, the dependency of signal magnitude on pulse length is non-periodic. Consequently, the popular approach of using quaternion fidelity function as a measure of similarity of result of composite rotation to a perfect predefined rotation will be not valid for NQR.

Still, NQR composite pulses fall into the category B3 according to M. Levitt classification, where composite quaternion rotation can be designed for maximizing transverse magnetization while ignoring its phase [2]. Experimental results show that numerically optimized composite pulses in presence of frequency offset can produce signal with intensity comparable to on-resonance excitation for the wide range of effective pulse lengths.

1. Blümich B., Spiess H.W.: J. Magn. Reson. **61**, 356 (1985)
2. Levitt M.H.: Prog. Nucl. Magn. Reson. Spectrosc. **18**, 61 (1986)

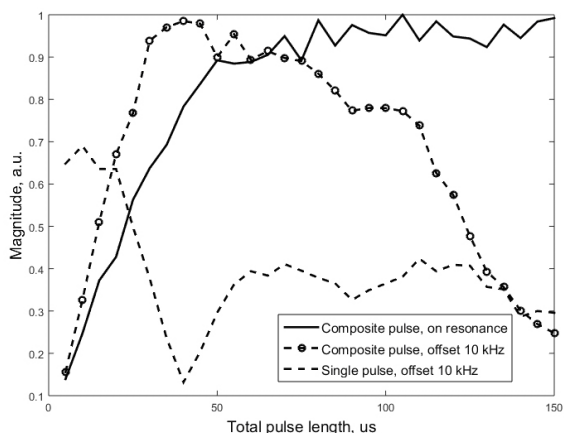


Fig. 1. Nutation experiments for single 90° pulse and $(0,430)0^\circ-(0,30)180^\circ-(0,270)90^\circ$ composite pulse (NaNO_2 powder sample, 3.608 MHz).

Determining patient compliance with low-dose aspirin therapy using $^1\text{H-NMR}$

I. Mershiev, G. Kupriyanova, V. Rafalskiy, E. Moiseeva

¹Institute of Physics and Technology, Immanuel Kant Baltic Federal University, Kaliningrad 236041, Russia, emoiseeva@kantiana.ru

Introduction. Appropriate prescription of antiplatelet therapy is fundamental to the secondary prevention of cardiovascular complications. Continued adherence to long-term prophylactic aspirin intake is extremely important for patients with cardiovascular disease. It has been shown that patients often stop taking their medication in 12 months after prescribed [1]. In this regard, it is important to have a tool to objectively determine whether a patient is taking aspirin or has stopped taking the drug.

In this paper, we investigated the possibility of using urinary aspirin metabolites by $^1\text{H-NMR}$ -spectroscopy for monitoring patients' adherence to long-term use of the drug. Such an approach is justified in view of the short half-life of aspirin in serum and the high concentration of aspirin metabolites in urine [2]. The advantages of this method are shortened preanalytical preparation time and the possibility of simultaneous detection and quantification of drug conjugates and drug metabolites.

Materials and methods. The study involved patients with cardiovascular disease. The first group consisted of 15 patients with coronary heart disease receiving a 75–100 mg prophylactic dose of aspirin. The second group included eight patients who had hypertension but were not receiving aspirin. Freshly collected urine was centrifuged for 10 minutes at 7000 rpm (2000 g) to remove any solids, after which the supernatant was collected and passed through a sterile syringe filter with an average pore diameter of 0.2 μm and membrane diameter of 28 mm (cellulose acetate, glass).

Then a 100–200 mM phosphate buffer solution (K_2HPO_4) was added to the urine sample to avoid changes in chemical shifts and stabilize the solution for several hours. The urine pH was corrected to 7.2–7.4. Next, 540 μl of the sample was placed in a standard 5 mm tube for NMR experiments. The total sample volume was brought to 600 μl by adding 60 μl of a 0.1% solution of DSS (4,4-dimethyl-4-silapentane-1-sulfonic acid) in D_2O . DSS is an NMR calibration standard used for both quantitative measurements and obtaining the chemical shift reference signal.

The tube with the sample was placed in the sensor inside the magnet of a Varian 400MR NMR spectrometer with a magnetic field strength of 9.4 Tesla and a proton resonance frequency of 400 MHz. NMR signals were recorded at 25 degrees Celsius using a WATERGATE excitation sequence with water signal suppression. After transforming the signals into a frequency representation using the Fourier transform, the sections of the spectrum in the 4 ppm and 7–8

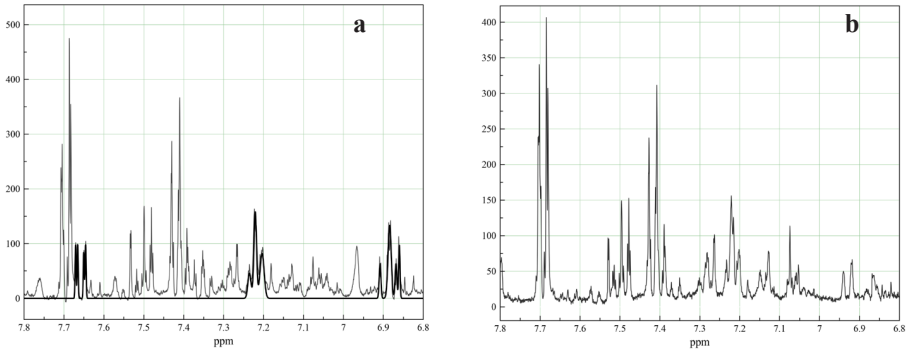


Fig. 1. **a** ^1H NMR spectrum of urine of a patient receiving aspirin, **b** ^1H NMR spectrum of urine of a patient not receiving aspirin.

ppm chemical shift regions were examined for the presence of aspirin metabolic products, particularly for salicylic acid.

Results. Urine samples from cardiac patients without aspirin and after administration of 75–100 mg prepared as described above were analyzed by ^1H NMR using the water suppression method. We could clearly see the appearance of intense overlapping signals in the region between 6.8 and 6.9 ppm, as well as well-defined triplet and overlapping signals in the regions between 7.4 and 7.2 ppm and between 7.7 and 7.6 ppm. As an example, Figure 1 shows two fragments of ^1H NMR spectra from the urine of patients without aspirin and after a cardiac dose.

Conclusion. ^1H NMR spectroscopy can be used for monitoring of long-time aspirin compliance in patients with cardiovascular disease. Our work shows that ^1H NMR spectroscopy is a fast and efficient non-destructive method for detection of ASA metabolites, which does not require laborious sample preparation and can serve as a basis for development of algorithms for automatic detection of ASA metabolites in urine.

Financial support. The work was supported by RFBR and Kaliningrad regional government grant, project No. 19-415-390001

1. Kulkarni S.P., Alexander K.P., Lytle B., Heiss G., Peterson E.D.: *Am. Heart J.* **151**, 185 (2006)
2. Jian-Hua L., Smith P.C.: *J. Chromatogr. B Biomed. Sci. Appl.* **675**, 61 (1996)

ESR of heterometallic Mg-Mn warwickites

A.R. Muftakhutdinov¹, R.M. Eremina², E.M. Moshkina³

¹Kazan (Volga Region) Federal University, Kazan 420008, Russia, mufta96@mail.ru

²Kazan (Volga Region) Federal University, Kazan 420008, Russia, reremina@yandex.ru

³Kirensky Institute of Physics, FRC SB RAS, Krasnoyarsk 660036, Russia, ekoles@iph.krasn.ru

Oxiborates cause scientific interest due to their rich phase diagram and low-dimensional zig-zag -chain structure. Monocrystals of $Mn_{2-x}Mg_xBO_4$ (x varies from 1 to 0.73) were synthesized by the flux method. Electron spin resonance spectra of these compounds were measured.

Angular and temperature dependencies of ESR linewidth are reported. One exchange narrowed ERP line was observed in the magnetic resonance spectrum. Angle dependence of the peak-to-peak linewidths in two orthogonal (**ab**) and (**ac**) planes are presented in Fig. 1. Temperature dependencies of ERP linewidth are shown in Fig. 2. Anisotropic exchange interactions between magnetic Mn^{2+} and Mn^{3+} ions and crystal field parameters describe the linewidth.

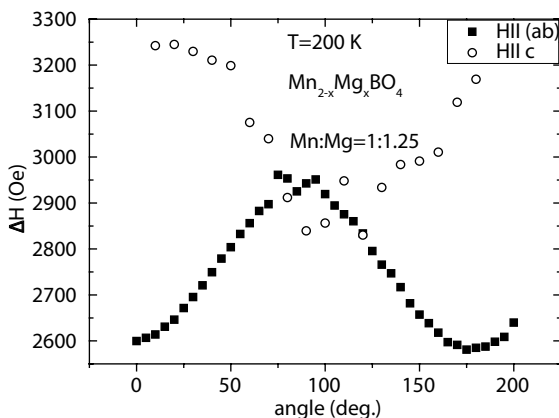


Fig. 1. Angle dependences of ΔH linewidths in **ab** and **ac** planes. $Mn_{1.11}Mg_{0.89}BO_4$ sample.

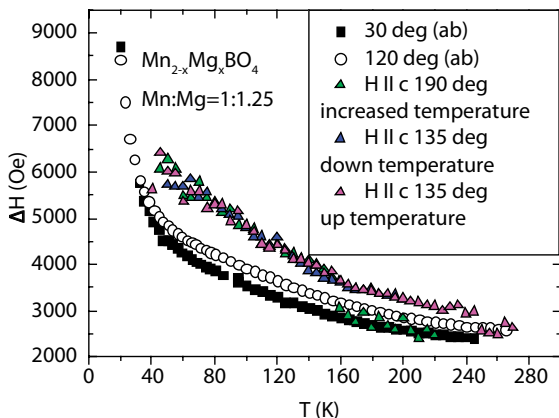


Fig. 2. Temperature dependencies of ΔH linewidths in **ab** and **ac** planes. $Mn_{1.11}Mg_{0.89}BO_4$ sample under different angles.

Base-pair opening and closing kinetics in DNA duplex containing oxoG:A mismatch

**D. Nasonov^{1,3}, S. Ovcherenko^{1,3}, A. Shernyukov¹, A. Endutkin²,
D. Zharkov^{2,3}, E. Bagryanskaya¹**

¹N.N. Vorozhtsov Novosibirsk Institute of Organic Chemistry SB RAS, Novosibirsk 630090, Russia

²Institute of Chemical Biology and Fundamental Medicine SB RAS, Novosibirsk 630090, Russia

³Novosibirsk State University, Novosibirsk 630090, Russia

Chemicals, radiation, UV light, and other mutagens eventually lead to DNA damage. The common oxidative lesion of DNA is 8-oxoguanine (oxoG). When the damaged base is located opposite to adenine in a base pair, the change from oxoG anti- to syn-conformation leads to the formation of a Hoogsteen oxoG:A base pair. In human cells, oxoG is found at the background level of ~ 1 per 10^6 guanines and increases severalfold upon oxidative stress [1]. A variety of repair strategies are existing, usage any of them depends on the type of DNA lesion. For oxoG:A mismatch lesion applies base excision repair (BER). Works of BER mechanism begin with the recognition of a damaged base by repairing enzymes, namely DNA glycosylases followed by the excision of this base. There are several models of how DNA glycosylases locate a damaged base and the role of the base pair opening-closing kinetics in this process [2]. However, there is no exact match in the literature that confirms one model and refutes the others [3].

NMR spectroscopy provides the exact experimental detection of DNA base pair opening-closing rate constants at the single base pair level through the analysis of the water-iminoproton exchange rate. Iminoproton exchange with water occurs in two steps, namely opening of a base pair followed by proton exchange from the open conformation. This exchange rate is measured by transfer of magnetization

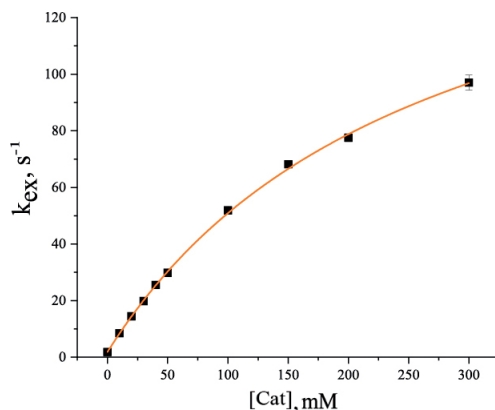


Fig. 1. Dependence of the exchange rate constant k_{ex} on the concentration of the added proton acceptor.

from water via CLEANEX pulse sequence [4]. CLEANEX pulse sequence has several advantages, the major one is compensation of internal molecule cross-relaxation and spin diffusion influence. The exchange rate constant depends on a base-pair opening (k_{op}), closing (k_{cl}) rate constants, and concentration of an added proton acceptor ($[C_{\text{at}}]$) as

$$k_{\text{ex}} = \frac{k_{\text{op}}(k_0 + \alpha k_{\text{B}}[C_{\text{at}}])}{k_{\text{cl}} + (k_0 + \alpha k_{\text{B}}[C_{\text{at}}])} \quad (1)$$

Figure 1 shows the dependency of exchange rate constant on proton acceptor concentration with the fitted curve by Eq. (1). From this dependency the opening and closing rate constants can be obtained.

In this work our objective was to obtain the kinetic parameters: base-pair opening and closing rate constants in DNA duplex containing oxoG:A mismatch. This data would provide a foundation for future experiments with the repair enzyme (DNA-formamidopyrimidine glycosylase (FPG)) to determinate its influence on kinetics of base-pair opening and closing process. All the obtained kinetic parameters of the process of opening and closing base pairs of DNA duplex will be presented and discussed.

The work was supported by the Russian Science Foundation (grant no. 21-14-00219).

1. Fromme J.C., Banerjee A., Verdine G.L.: DNA glycosylase recognition and catalysis. *Curr Opin Struct Biol* **14** (1), 43–49 (2004)
2. Cao C. et al.: Dynamic opening of DNA during the enzymatic search for a damaged base. *Nat Struct Mol Biol* **11**(12), 1230–12366 (2004)
3. Li R., Mak C.H.: A Deep Dive into DNA Base Pairing Interactions Under Water. *The Journal of Physical Chemistry B* **124** (27), 5559–5570 (2020)
4. Hwang, T.L., van Zijl P.C., Mori S.: Accurate quantitation of water-amide proton exchange rates using the phase-modulated CLEAN chemical EXchange (CLEANEX-PM) approach with a Fast-HSQC (FHSQC) detection scheme. *J. Biomol. NMR* **11** (2), 221–226 (1998)

EPR study of nitrogen P1 centers in nature and synthetic diamonds

**Yu. Bogachev¹, V. Zubkov¹, A. Nikitina¹, M. Shishkina¹,
S. Sukharzhevsky²**

¹Physics Department, St. Petersburg Electrotechnical University “LETI”,
St. Petersburg 197022, Russia, nastya_nikitina1996@mail.ru

²Magnetic Resonance Research Centre, St. Petersburg State University,
St. Petersburg 198504, Russia, stanislav.sukharzhevskii@gmail.com

The EPR of monocrystalline samples of diamond synthesized by the HTHP method and natural diamond from collection of Western Siberia was studied. The EPR measurements were carried out on ELEXSYS E580 EPR spectrometer (Bruker, Germany) in Magnetic Resonance Research Centre (St. Petersburg State University, Russia).

The observed EPR spectra consist of three groups of hyperfine structure belong to magnetically nonequivalent nitrogen P1 centers, where an unpaired nitrogen electron can be located on any of the four equivalent C-N bonds, and the symmetry axis of the hyperfine interaction with ^{14}N is parallel to any of the four $\langle 111 \rangle$ bond directions. According to various estimates, the length of the C-N bond on which the unpaired electron is localized increases by (10–30)%, which leads to the fact that the nitrogen center acquires axial symmetry C3v. When directions of vector \mathbf{B} of the polarizing magnetic field parallel to the $\langle 111 \rangle$ or $\langle 110 \rangle$ crystallographic axes, EPR spectrum of P1 centers consist of two EPR hyperfine structure lines which observed on the left and right relative to the central EPR line. Such EPR spectrum was observed for a natural diamond. If the vector \mathbf{B} is directed arbitrarily relative to the crystallographic axes, then the four magnetically nonequivalent positions of the P1 centers lead to an EPR spectrum consisting of four hyperfine structure lines on the left and right relative to the central EPR line (the EPR spectrum of synthetic diamond). A group of additional EPR lines caused by paramagnetic centers of a different nature was also observed in the EPR spectra of natural diamond.

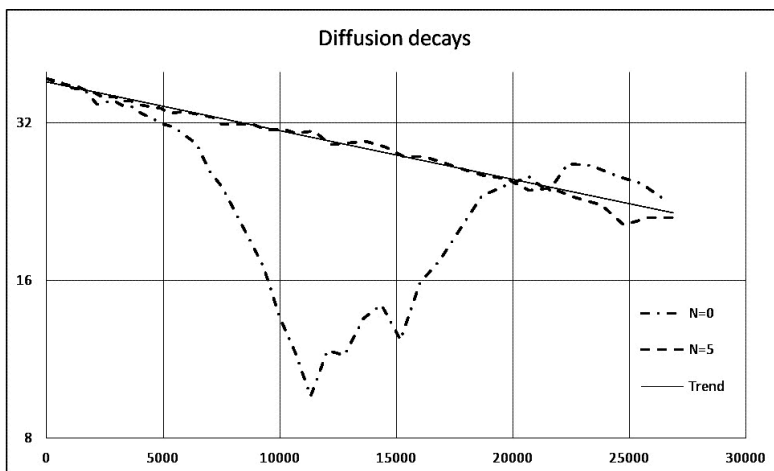
To estimate the decoherence of the quantum states of the unpaired electrons of paramagnetic centers in diamond, the spin-lattice T_1 and spin-spin T_2 relaxation times were determined by the stationary saturation method of the inhomogeneous broadened EPR lines [1].

Increasing the accuracy of diffusion parameters measurements by NMR

V. Odivanov, Ya. Fattakhov

Zavoisky Physical-Technical Institute, FRC Kazan Scientific Center of RAS, Kazan 420029, Russia, odivanov@mail.ru, fattakhov@kfti.knc.ru

Measurements of the self-diffusion parameters of various substances in the free state and inside heterogeneous structures make it possible to obtain information about both the properties of the substance and the parameters of the structure. NMR techniques are the most informative for such measurements. In many cases, for research or technological measurements, inexpensive NMR relaxometers or specialized measuring instruments are used, which allow obtaining the relaxation and diffusion parameters of the samples under study. A commonly used technique for measuring diffusion characteristics is using a pulsed magnetic field gradient [1], which measures the attenuation of the spin echo signal as a function of the amplitude of two identical gradient pulses separated by an inverting RF pulse. The first pulse dephases the spin packet according to the location of the spins along the gradient axis, and the second pulse returns it to the original phase. The movement of spins in the packet due to self-diffusion in the interval between pulses leads to the fact that some of the spins do not restore their phase, as a result of which the echo amplitude decreases. The accuracy of such measurements critically depends on the equality of the gradient pulses, especially at low values of the self-diffusion coefficient.



The graph $N = 0$ shows the diffusion decay for a sample of vacuum oil, measured on a relaxometer with a field induction of about 0.4 T in the usual manner. The distortion is due to the fact that as a result of parasitic phenomena, such as heating of the reference resistor in the gradient pulse current stabilization circuit and relaxation processes in the structural elements of the magnetic system, the gradient pulses turn out to be different in amplitude, which leads to incomplete restoration of the echo signal phase.

The patent [2] proposes a method that makes it possible to even out the effects of gradient pulses by applying a series of gradient pulses with a period and duration coinciding with a pair of pulses in the active part of the sequence before the exciting pulse. This leads to the establishment of dynamic equilibrium in the pulse shaper and the effect of active pulses is leveled out. The $N = 5$ plot shows the diffusion decay obtained with a series of 5 preliminary pulses, and the trend line corresponds to a self-diffusion coefficient of $20.5 \mu\text{m}^2/\text{s}$. Thus, it is possible to achieve a significant increase in the accuracy and measurement range without the use of multivariate compensation and expensive circuit solutions in the gradient pulse shaper.

1. Stejskal E.O., Tanner J.E.: J. Chem. Phys. **42**, no. 1, 288 (1965)
2. Pulse sequence for measuring self-diffusion parameters by the method of nuclear magnetic resonance / Aslanyan A.M. (RU), Davydov D.A. (RU), Odivanov V.L. (RU) – Patent RF No. 2517762 dated 12.09.2012.

Improving the accuracy of NMR fluid flow measurements

V. Odivanov, Ya. Fattakhov

Zavoisky Physical-Technical Institute, FRC Kazan Scientific Center of RAS, Kazan 420029,
Russia odivanov@mail.ru, fattakhov@kfti.knc.ru

There are a number of ways to measure fluid flow rate using NMR. In particular, the article [1] proposes a method based on measuring the phase shift of the spin echo signal due to the action of two identical gradient pulses separated by an inverting RF pulse. The method gives sufficient accuracy provided that the action of gradient pulses is equal. Assuming that the pulses differ in amplitude, the expression for the velocity is:

$$v = \frac{\Delta\varphi - \Delta\varphi_0}{\gamma \left[\Delta G \left(\frac{t_g^2}{2} + t_1 t_g + \tau t_g \right) - G \tau t_g \right]},$$

where t_g is the duration of the gradient pulses, t_1 is the delay of the beginning of the gradient pulse from the exciting one, τ is the interval between the gradient pulses, G is the magnitude of the gradient of the second pulse, $G + \Delta G$ is the first pulse, $\Delta\varphi$, $\Delta\varphi_0$ are the phases of the echo signal with the gradient turned on and off.

Patent [2] proposes a method for improving the accuracy of measuring self-diffusion characteristics by applying a series of gradient pulses before the exciting RF pulse, repeating their sequence in the active interval, which leads to the establishment of dynamic equilibrium and equalization of the effect of gradient pulses. This approach can be applied to NMR flow rate instruments to reduce ΔG and improve accuracy without the use of expensive components in the gradient pulse shaper and without complex compensation in software.

1. Stejskal E.O., Tanner J.E.: J. Chem. Phys. **42**, no. 1, 288 (1965)
2. Pulse sequence for measuring self-diffusion parameters by the method of nuclear magnetic resonance / Aslanyan A.M. (RU), Davydov D.A. (RU), Odivanov V.L. (RU) – Patent RF No. 2517762 dated 12.09.2012.

Spatial structure of the fibril-forming PAP(85-120) peptide in a complex with dodecylphosphocholine micelles by high-resolution NMR spectroscopy

D. Osetrina, V. Klochkov, D. Blokhin

Institute of Physics, Kazan Federal University, Kazan 420008, Russia, dblohin@kpfu.ru

HIV is one of the most dangerous diseases: since the first detecting of HIV infection in 1981 more than 25 million people have died from HIV infection and the resulting acquired immunodeficiency syndrome (AIDS) [1]. However, the HIV virus is a weak pathogen in vitro with only a small percentage (0.1–0.001%) of virions which are capable of replication in vitro [2].

Semen can be not only a passive HIV carrier, but it also contributes to the transmission of the virus [3]. HIV activity strongly correlates with the content of amyloidogenic peptides in semen which are involved in the formation of SEVI (semen-derived enhancer of virus infection) fibrils [4]. It was shown that the SEVI contains several peptides which are the proteolytic fragment of prostatic acid phosphatase (PAP) and semenogelin (SEM1 and SEM2) [5].

The PAP(85-120) peptide forms amyloid fibrils known as SEVI, which enhance attachment of the virus to the host cell via reducing the electrostatic repulsion between the membranes of the virus and the target cell. In this work, the spatial structure of the PAP(85-120) peptide in an aqueous solution in the presence of dodecylphosphocholine (DPC) micelles [6], which were chosen as a model of the lipid membrane surface was solved using nuclear magnetic resonance spectroscopy.

The purpose of our work was to determine the spatial structure of PAP(85-120)+DPC in solution by NMR spectroscopy. Assignment of ^1H , ^{13}C NMR signals was performed using 2D ^1H - ^1H TOCSY, 2D ^1H - ^1H NOESY, ^1H - ^{13}C HSQC, ^1H - ^{13}C HMBC, ^1H - ^{13}C TOCSY-HSQC experiments. Internuclear distances were determined from NOESY spectrum analysis. The spatial structure of PAP(85-120)+DPC was determined by the non-linear annealing in the XPLOR-NIH program [7]. Internuclear distances were used as input parameters for the calculation.

This work is supported by the Russian Science Foundation (D.S. Blokhin, project no. 20-73-10034).

1. Lederman M.M., Offord R.E., Hartley O.: Microbicides and other topical strategies to prevent vaginal transmission of HIV, *Nat. Rev. Immunol.* **6**, 371–382 (2006), doi:10.1038/nri1848.
2. Galvin S.R., Cohen M.S.: The role of sexually transmitted diseases in HIV transmission, *Nat. Rev. Microbiol.* **2**, 33–42 (2004), doi:10.1038/nrmicro794.
3. Castellano L.M., Shorter J.: The surprising role of amyloid fibrils in HIV infection, *Biology* **1**, 58–80, (2012), doi:10.3390/biology1010058.
4. Roan N.R., Müller J.A., Liu H., Chu S., Arnold F. et al.: Peptides released by physiological cleavage of

-
- semen coagulum proteins form amyloids that enhance HIV infection, *Cell Host Microbe* **10**, 541–550 (2011), doi:10.1016/j.chom.2011.10.
5. Ronnberg L., Vihko P., Sajanti E., Vihko R.: Clomiphene citrate administration to normogonadotropic subfertile men: Blood hormone changes and activation of acid phosphatase in seminal fluid, *Int. J. Androl.* **4**, 372–378 (1981), doi:10.1111/j.1365-2605.1981.tb00721.x.
 6. Beswick V. et al.: Dodecylphosphocholine micelles as a membrane-like environment: new results from NMR relaxation and paramagnetic relaxation enhancement analysis, *Eur. Biophys. J.* **28**(1), 48–58 (1998), doi: 10.1007/s002490050182
 7. Schwieters C.D., Kuszewski J.J., Tjandra N., Clore G.M., The Xplor-NIH NMR molecular structure determination package, *J. Magn. Reson.* **160**, 65–73 (2003), doi:10.1016/s1090-7807(02)00014-9.

Investigation of the features of translational mobility of liquid molecules in porous media by PFG NMR

D.A. Parfenova¹, D.L. Melnikova¹, A.S. Gordeev², V.D. Skirda¹

¹Department of Molecular Physics, Institute of Physics, Kazan Federal University, Kazan 420008, Russia, daryaparfenova@mail.ru

²Institute of Environmental Sciences, Kazan Federal University, Kazan 420008, Russia

Currently, substances with a porous structure are among the most promising materials. For their effective use as catalysts, it is necessary to take into account the features of porous structures and the processes occurring in them [1]. One of the most important catalysts is zeolite – crystalline aluminosilicate [2].

The purpose of current work was to study the features of translational mobility of liquid molecules in a limited environment using the example of three media: zeolite, aluminum oxide, calcined sand. In addition, the influence of the presence of biomolecules, such as xylose and rhamnolipids, on the translational mobility of water in a porous zeolite medium was studied.

Studies were carried out with a particle size distribution of 1–10 μm for zeolite and 10–100 μm for aluminum oxide and calcined sand.

The work was carried out on the equipment of the Federal Center of Shared Facilities for physical and chemical research of substances and materials (FCSF) KFU Bruker AVANCE 400 MHz spectrometer optimized for microtomography, solid state and self-diffusion.

1. Dubinin M.M.: *Advances in Colloid and Interface Science* **2**, 217–235 (1968)
2. Naber J.E., de Jong K.P., Stork W.H.J., Kuipers H.P.C.E., Post M.F.M.: *J. Studies in Surface Science and Catalysis* **84**, 2197–2219 (1994)

ESR spectroscopy of Ziegler catalytic systems

D.V. Pavlov, Yu.Yu. Titova

Irkutsk A.E. Favorsky Institute of Chemistry SB RAS, Irkutsk 664033, Russia,
pavlov@irioc.irk.ru, ytitova60@gmail.com

Previously it was shown that the formation of $\text{Co}(\text{acac})_2\text{-AlEt}_3$ based Ziegler catalytic systems leads to the formation of $\text{Co}(0)$ complexes ($g_{\perp} = 2.0185$, $g_{\parallel} = 2.051$, $g_{\parallel} = 2.332$) [1]. The aim of this study was a detailed investigation of these structures by CW ESR spectroscopy in the temperature range from 5 K to 340 K. The data obtained in combination with the results of mathematical modeling showed that the interaction of $\text{Co}(\text{acac})_2$ and AlEt_3 leads to the formation of both the $\text{Co}(0)$ complex and the aluminum complex. The percentage of these complexes in the mixture varies depending on the time from the moment of the components mixing, or in the same sample depending on the shooting temperature (see Fig. 1). A detailed study of these complexes formation in such systems will be the subject of further research.

Research completed in the framework of Contracts No. 1021051703316-6-1.4.3 and 121021000264-1 of the Program of Fundamental Research.

1. Titova Y.Y.: Sc.D Thesis. Irkutsk, **368** (2018)

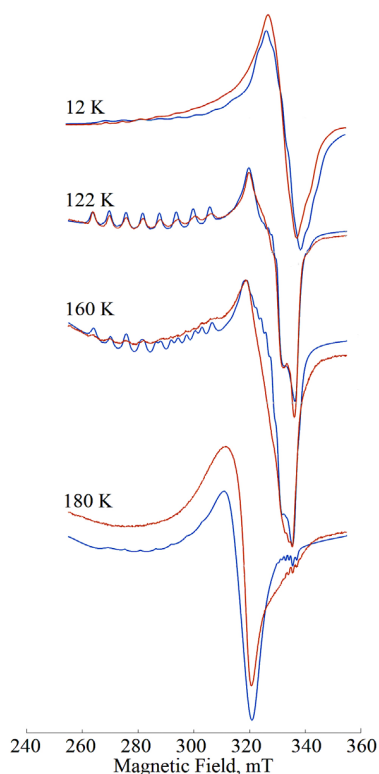


Fig. 1. Experimental (red) and simulated (blue) ESR spectra of $\text{Co}(\text{acac})_2\text{-AlEt}_3$ catalytic system,

EPR and DFT study of the radiation-induced defects in $\text{Si}(\text{OH})_4$

A.A. Petrova, A.A. Rodionov, M.R. Gafurov

Institute of Physics, KFU, Kazan 420029, Russia, Petrovaalinakfu@gmail.com

The main process of biosilification is the oligomerization of silicic acids $n(\text{SiO}_2)m(\text{H}_2\text{O})$. The influence of the environment of the silicon atom on the oligomerization process can be one of the important factors of biosilification.

In this work, quantum-chemical and EPR studies of $\text{Si}(\text{OH})_4$ powder as a model compound acting as the main oligomerization reagent were carried out. The EPR spectra of the $\text{Si}(\text{OH})_4$ powder were acquired with Bruker X-band spectrometer ESP

300. To obtain paramagnetic centers, the samples were irradiated with URS-55 X-ray setup at room temperature with the irradiation dose of 10 kGy.

As a result of X-ray irradiation, a group of lines in the EPR spectra for the g -factor of 2 appears (Fig. 1). The studies performed by the microwave saturation method showed that this group of lines belongs to at least two types of paramagnetic centers.

The easily saturated narrow EPR line with $g = 2.00$ and a shape characteristic of the axial symmetry of the center can be attributed to the so-called E^{\cdot} -centers, which are quite well studied in the literature [1]. The nature of the paramagnetic centers, to which such a spectrum of complex structure can be assigned, is the subject of further study.

The DFT method was used to calculate the EPR parameters (HFI constant and g -factor) for $\text{Si}(\text{OH})_4$, $\text{Si}(\text{OCH}_2\text{CH}_3)_4$, and model oligomers with the degree of oligomerization from 1 to 6 Si atoms using the ORCA software package [2].

The work was supported by Russian Federation State Task No. 0671-2020-0051.

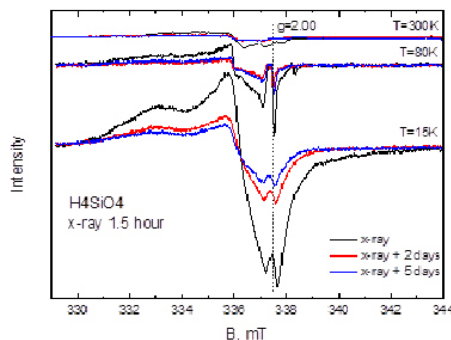


Fig. 1. EPR spectra of $\text{Si}(\text{OH})_4$ sample.

- Galukhin A. et al.: Magn. Reson. Solids **20**, 18203 (2018)
- Neese F.: Wiley Interdisciplinary Reviews: Computational Molecular Science **2**, 73 (2012)

EPR study of iron oxide magnetic nanoparticles in water suspensions

Yu. Bogachev, A. Gorbunov, A. Nikitina, E. Pobedimova, M. Shishkina

Physics Department, St. Petersburg Electrotechnical University "LETI", St. Petersburg 197022,
Russia, evapobedimova@mail.ru

The EPR of magnetic nanoparticles Fe_2O_3 and Fe_3O_4 in a dextran shell dispersed in distilled water and in aqueous physiological solutions (phosphate buffer with $\text{pH} = 7.0$) was studied. Synthesis of superparamagnetic iron oxide nanoparticles was carried out under heterophase conditions from Fe^{3+} and Fe^{2+} solutions according to the Elmore-Massart scheme. A compact EPR spectrometer of the X-band, model ESR-MINI (Resonance-M, Russia) was used for measurements.

EPR studies of suspensions of iron oxide superparamagnetic nanoparticles in aqueous solutions and physiological fluids have shown the presence of an EPR spectrum (with an effective g -factor of 2.32) consisting of two lines – narrow and wide, overlapping each other. Analysis of EPR spectra shows that the shape of spectrum depends on the size and concentration of nanoparticles, their dispersed state, and manufacturing technology.

Comparison of the results of EPR studies with the data of electron and atomic force microscopy [1], modeling of the EPR spectra of nanoparticles [2] shows the presence of a fractal structure of aggregates of polydisperse iron oxide nanoparticles and the dependence of the EPR spectra on the width of the particle size distribution, as well as the distribution features of different particles in the aggregate.

The results obtained show the possibility of using the EPR method to assess the structure of aggregates of nanoparticles formed in a magnetic field, the degree of dispersion of iron oxide nanoparticles in biological fluids.

1. Bogachev Yu.V., Gareev K.G., Ryzhov V.A., Kharitonsky P.V.: Magnetic nanoparticles based on metal oxides. Properties and application. SPb: Publishing house of SPbETU "LETI", 2015. 148 p.
2. Roldugin V.I., Dolotov S.V.: Colloids Journal (Rus.) **69**, 1, 13–17 (2007)

Magnetization, specific heat and ESR measurements of ludwigite $\text{Mn}_{1.17}\text{Co}_{1.83}\text{BO}_5$

**D.V. Popov¹, T.P. Gavrilova¹, I.V. Yatsyk¹, M.A. Cherosov³,
E.M. Moshkina², V.A. Shustov¹, R.M. Eremina¹**

¹Zavoisky Physical-Technical Institute, FRC Kazan Scientific Center of RAS, Kazan 420029, Russia, kazan-city.dvpopoff@yandex.ru

²Kirensky Institute of Physics, Federal Research Center KSC SB RAS, Akademgorodok 50, Krasnoyarsk 660036, Russia

³Institute of Physics, Kazan Federal University, Kazan 420008, Russia

Ludwigites are oxyborates with structural formula $(\text{M}^{2+})_2(\text{M}^{3+})\text{BO}_5$, with (M^{2+}) and (M^{3+}) being metallic ions of corresponding valence. These metallic ions create zigzag walls in crystal structure with four non-equivalent positions for them, therefore producing unusual magnetic properties, such as random magnetic ions distribution, mixed valence, strong electronic correlations, uncommon charge ordering, etc. Bimagnetic ludwigites are of particular interest, since one can easily observe evolution of said properties in dependence of relative concentrations of magnetic ions [1–3].

The aim of this work is investigation of magnetic properties of $\text{Mn}_{1.17}\text{Co}_{1.83}\text{BO}_5$ ludwigite. X-ray diffraction analyses were performed using DRON-7 diffractometer. Crystallographic unit parameters were obtained. Crystal has Pbam space group with $a = 9.2039(9)$ Å, $b = 12.4944(9)$ Å, and $c = 3.0732(2)$ Å. Diffractograms were fitted using Rietveld method.

Magnetization dependences from temperature and external magnetic field were measured, using PPMS-9 device in Kazan Federal University. Temperature dependences of magnetization were measured in zero field cooling (ZFC) and field

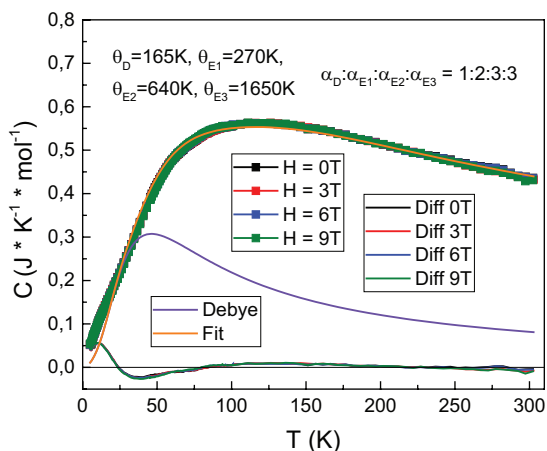


Fig. 1. ESR spectra for $\text{Mn}_{1.17}\text{Co}_{1.83}\text{BO}_5$.

cooling (FC) modes at range 2–300 K. A magnetic transition was obtained at $T = 43.9\text{K}$ in this compound. Most likely this is ferrimagnetic transition. Magnetization dependences from external magnetic field were measured in fields up to 9 T. Hysteresis loops were obtained at temperatures below 50 K in this ludwigite along a and b axis. In addition, specific heat measurements were made, using the same device. They show unusual points at temperatures, close to 50 K. One Debye and three Einstein terms were obtained via approximation with term temperatures being $\theta_D = 16\text{ K}$, $\theta_{E1} = 270\text{ K}$, $\theta_{E2} = 620\text{ K}$, $\theta_{E3} = 1650\text{ K}$ and α ratio being $\alpha_D : \alpha_{E1} : \alpha_{E2} : \alpha_{E3} = 0.92:2.04:3.02:3.02$. Figure 1 shows specific heat measurements approximation results.

EPR spectra were also measured using a Bruker spectrometer. Figure 2 shows obtained ESR spectra. The measurements were performed at temperature range from 5 to 345 K. Spectra was approximated using three Lorentz lines. With these measurements several points of interest were obtained at temperatures $T = 70\text{ K}$, $T = 114\text{ K}$ and $T = 253\text{ K}$. It is possible, that these points mark different phase and structural transitions.

Electron spin resonance measurements were performed with the financial support from the government assignment for FRC Kazan Scientific Center of RAS.

1. Popov D.V. et al.: Journal of Physics and Chemistry of Solids **148**, 109695 (2021)
2. Freitas D.C. et al.: Physical Review B **94**, 174409 (2016)
3. Heringer M.A.V. et al.: Physical Review Materials **4**, 064412 (2020)

EPR study of hydrocarbons sorption in metal-organic frameworks

A. Poryvaev¹, A. Yazikova^{1,2}, A. Efremov^{1,2}, D. Polyukhov¹, M. Fedin¹

¹International Tomography Center SB RAS, Novosibirsk 630090, Russia, poryvaev@tomo.nsc.ru

²Novosibirsk State University, Novosibirsk 630090, Russia

Metal-organic frameworks (MOFs) are porous coordination compounds consisting of metal ions and organic linkers, and demonstrating very high tunability of their porous structure. Numerous different MOFs were already addressed to solve the task of benzene/cyclohexane separation, and some of them demonstrate record values of selectivity. Such high selectivity values were achieved via fine control of diffusion by the shape of MOF pores, as well as by employing specific interactions between π -system of benzene and open metal sites. Most examples where MOFs were used for benzene/cyclohexane separation demonstrate high dynamic uptake capacity evaluated from sorption isotherms. However, in some cases high selectivity resulting from fine tuning of pores geometry does not lead to a sufficient sorption capacity. Moreover, even high capacity obtained upon single component sorption may not reflect real sorption capacity from binary mixture. This occurs because sorption from binary mixture might have a tremendous restriction imposed by chemical equilibrium between benzene dissolved in cyclohexane and benzene adsorbed by MOF. Thus, an ideal material for separation of benzene/cyclohexane mixtures has to combine high selectivity, high capacity and provide relatively low residual content of benzene in the treated mixture.

In this work we report a detailed study of benzene/cyclohexane sorption by metal-organic frameworks upon a precise control of guest penetration via EPR spectroscopy. The analysis of EPR data demonstrates that benzene molecules do penetrate into the MOF cavities, whereas cyclohexane ones do not. Such specific permeability stems from a shape of cyclohexane molecule and correlates with the observed extremely high selectivity of benzene over cyclohexane sorption.

Acknowledgments. This work was supported by the Russian Science Foundation (22-73-10239).

EPR study of LaF_3 nanoparticles doped with Er^{3+} ions

M.S. Pudovkin, R.M. Rakhmatullin, A.A. Rodionov

Institute of Physics, Kazan Federal University, Kazan 420008, Russia,
jaz7778@list.ru

Fluoride nanoparticles are very promising materials for biomedical applications, catalysis and optoelectronics [1]. These applications are based on the unique physical and chemical properties of fluoride materials such as transparency in a wide spectral range, low phonon energy, good chemical stability and low toxicity [2]. In this work EPR technique complemented with XRD and optical methods were applied to study of LaF_3 nanoparticles doped with Er^{3+} ions. The nanoparticles were synthesized via co-precipitation method with subsequent microwave treatment using a microwave oven (650 W, 2.45 GHz) for 0, 30, 90 and 180 minutes. The average particle size

estimated from XRD peaks based on the Scherrer equation was 20 nm. EPR measurements were made using a Bruker ESP-300 spectrometer operating in the X-band (~9.4 GHz). Optical measurements revealed strong dependence of spectral-kinetic characteristics on the time of treatment whereas EPR spectra have no such strong dependence. Further researches are planned on this subject.

The work is carried out in accordance with the Strategic Academic Leadership Program “Priority 2030” of the Kazan Federal University of the Government of the Russian Federation.

1. Wang G., Peng Q., Li Y.: Acc. Chem. Res. **44**, 322–332 (2011)
2. Kondratyeva E., Alakshin E. et al: Journal of Nanoparticle Research **24**(1), 1–14.

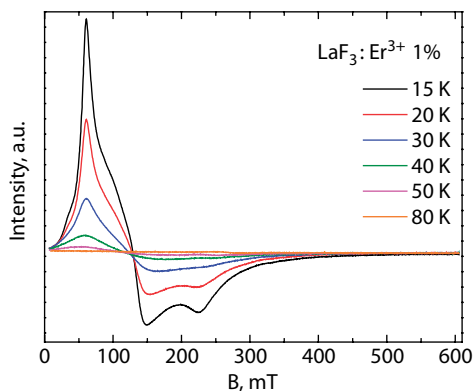


Fig. 1. EPR spectra of Er^{3+} ions in LaF_3 nanoparticles.

Two-pulse NMR responses in solids with internal molecular mobility

D.S. Ryabushkin

Physical-Technical Institute, V.I. Vernadsky Crimean Federal University, Simferopol 295007, Russia, druabushkin@cfuv.ru

There are some methods of evaluations of two-pulse NMR echo shapes in solids. For very restricted quantity of simple systems like molecule of water the problem may be solved exactly. For real systems with many particles the echo may be represented as an expansion in time but in such case the result describes only short-time behavior of spin response. Using of Liouville superoperator allows to get very useful formulae for responses of multiparticle systems [1]. If distribution of random fields on nuclei is close to Gauss' one, convenient results may be got by the method of the random local field [2].

As a rule, pulse series $90^\circ\text{-}y - \tau - 90^\circ\text{-}y,x - t$ are evaluated and investigated for various systems (τ is time interval between pulses, t is time from the first pulse). In this paper a more general case is discussed: $90^\circ\text{-}y - \tau - \beta^\circ\text{-}y,x - t$, where $\beta^\circ\text{-}y,x$ is an arbitrary angle of turn around axes y or x of rotating coordinate system. Obviously, the result allows to study angle dependences of NMR echo.

It is considered a multiparticle system with Gauss' distribution of resonance frequencies and internal molecular mobility of Markov type. The magnetic field adopted as strong. The interaction Hamiltonian was chosen in the form [1]

$$\hat{H} = \frac{1}{2} \sum_{i>j} D_{zz}^{ij} (2\hat{I}_{iz}\hat{I}_{jz} - \hat{I}_{ix}\hat{I}_{jx} - \hat{I}_{iy}\hat{I}_{jy}). \quad (1)$$

In accordance with formalism of density matrix, the response for two-pulse series will be as

$$V(t) = \text{Tr}(e^{-i\int_{\tau}^t \hat{H}(t'')dt''} \hat{R} e^{-i\int_0^{\tau} \hat{H}(t')dt'} \hat{I}_x e^{i\int_0^{\tau} \hat{H}(t')dt'} \hat{R}^{-1} e^{i\int_{\tau}^t \hat{H}(t'')dt''} \hat{I}_x) / \text{Tr}(I_x^2), \quad (2)$$

where $\hat{R} = \exp(-i\beta\hat{I}_{-y,x})$ is the operator of rotation corresponding the second pulse.

Easy to show that

$$\exp(-i\beta\hat{I}_{-y}) \hat{H} \exp(i\beta\hat{I}_{-y}) = \cos^2\beta \cdot \hat{H} + \sin^2\beta \cdot \hat{H}_{xx} + \dots, \quad (3)$$

$$\exp(-i\beta\hat{I}_x) \hat{H} \exp(i\beta\hat{I}_x) = \cos^2\beta \cdot \hat{H} + \sin^2\beta \cdot \hat{H}_{yy} + \dots, \quad (4)$$

where $\hat{H}_{xx} = \sum_{i>j} D_{zz}^{ij} (2\hat{I}_{ix}\hat{I}_{jx} - \hat{I}_{iz}\hat{I}_{jz} - \hat{I}_{iy}\hat{I}_{jy})$, $\hat{H}_{yy} = \sum_{i>j} D_{zz}^{ij} (2\hat{I}_{iy}\hat{I}_{jy} - \hat{I}_{iz}\hat{I}_{jz} - \hat{I}_{ix}\hat{I}_{jx})$.

The ellipsis in (3) and (4) means terms that may be ignored if times τ and t are short enough.

Evaluation of (2) was fulfilled using averaging of frequencies [2]

$$\langle \omega(t')\omega(t'') \rangle = \bar{M}_2 + \Delta M_2 \cdot \exp\left(-\frac{|t'-t''|}{\tau_c}\right), \quad (5)$$

where τ_c is correlation time (average life time of the system in given lattice configuration), \bar{M}_2 is the second moment of the line shape if the system is in state of intensive molecular mobility, ΔM_2 is the difference of second moments of the line shape for rigid and fast moving lattices.

As a result, the next formulae are evaluated.

1) For series $90^\circ\text{-}y - \tau - \beta^\circ\text{-}y - t$ (in-phase response):

$$G(t, \tau) = \cos\beta \cdot \exp\left(-\frac{1}{2}\bar{M}_2(t - \tau(1 - \cos^2\beta))^2\right) \cdot \exp\left[-\Delta M_2\tau_c^2\left(\frac{t-\tau}{\tau_c} - 1 + e^{-\frac{t-\tau}{\tau_c}} - \cos^2\beta \cdot \left(e^{-\frac{t}{\tau_c}} - e^{-\frac{\tau}{\tau_c}}\right) \cdot \left(e^{\frac{\tau}{\tau_c}} - 1\right) + \cos^4\beta \cdot \left(\frac{\tau}{\tau_c} - 1 + e^{-\frac{\tau}{\tau_c}}\right)\right)\right].$$

2) For series $90^\circ\text{-}y - \tau - \beta^\circ\text{-}x - t$ (echo):

$$V(t, \tau) = \exp\left(-\frac{1}{2}\bar{M}_2(t - \tau(1 - \cos 2\beta))^2\right) \cdot \exp\left[-\Delta M_2\tau_c^2\left(\frac{t-\tau}{\tau_c} - 1 + e^{-\frac{t-\tau}{\tau_c}} - \cos 2\beta \cdot \left(e^{-\frac{t}{\tau_c}} - e^{-\frac{\tau}{\tau_c}}\right) \cdot \left(e^{\frac{\tau}{\tau_c}} - 1\right) + \cos^2 2\beta \cdot \left(\frac{\tau}{\tau_c} - 1 + e^{-\frac{\tau}{\tau_c}}\right)\right)\right]$$

Easy to see that for $\beta = 0^\circ$ or 180° $G(t, \tau)$ gives the known signal of free induction decay [2]:

$$G(t, \tau) = \exp\left(-\frac{1}{2}\bar{M}_2 t^2\right) G(t), \text{ where } G(t) = \exp\left[-\Delta M_2\tau_c^2\left(\frac{t}{\tau_c} - 1 + e^{-\frac{t}{\tau_c}}\right)\right]$$

If $\beta = 90^\circ$, $V(t, \tau)$ defines the shape of solid-echo [2]:

$$V(t, \tau) = \exp\left(-\frac{1}{2}\bar{M}_2(t - 2\tau)^2\right) \cdot G(t - \tau) \cdot G(\tau) \cdot \exp\left[-\Delta M_2\tau_c^2\left(e^{-\frac{t}{\tau_c}} - e^{-\frac{\tau}{\tau_c}}\right)\left(e^{\frac{\tau}{\tau_c}} - 1\right)\right]$$

1. Sergeev N.A., Ryabushkin D.S.: Osnovi kvantovoi teorii yzdernogo magnitnogo rezonansa (in Russian): Logos, Moscow, 2013.
2. Sergeev N.A., Ryabushkin D.S.: Sluchainyye protsessyy v YMR tverdogo tela (in Russian): Buk, Kazan, 2018.

Investigation of tricalcium phosphate ceramics doped with gadolinium ions by electron paramagnetic resonance

**M.A. Sadovnikova¹, G.V. Mamin¹, A.A. Forysenkova², I.V. Fadeeva²,
F.F. Murzakhanov¹, M.R. Gafurov¹**

¹Institute of Physics, Kazan Federal University, Kazan 420008, Russia, margaritaasadov@gmail.com

²A.A. Baikov Institute of Metallurgy and Material Science, Russian Academy of Sciences, Moscow 119334, Russia

Currently there is a high demand for bone substitutes, thanks to the frequent diseases of human hard tissues, such as fractures, the consequences of surgeries, including oncological ones. Improving the quality of the patients life and increasing its duration involve the need to create new, biocompatible, non-toxic bone grafts that should be able to be resorbed in the body at the same physiological conditions. The problem of regenerating of the bone tissue can be resolved using materials based on calcium phosphates that present in the human body, for example, β -tricalcium phosphate (β -TCP, $\text{Ca}_3(\text{PO}_4)_2$), which is an osteoconductive, osteoinductive material and has high solubility and, accordingly, the fast rate of resorption [1].

In this work, synthetic nanosized samples of TCP doped with Gd^{3+} ions were studied by electron paramagnetic resonance (EPR). Gadolinium-substituted TCP powders were synthesized by wet precipitation way from aqueous solutions of salts. These compounds are promising materials for bone engineering, as contrast agents in computer and magnetic resonance imaging, since it is important to control each stage of healing and the degree of regeneration of hard tissues [2]. EPR spectra were recorded in continuous wave and pulsed modes using abilities of the Bruker Elexsys E580/680 spectrometer in the X-band microwave range

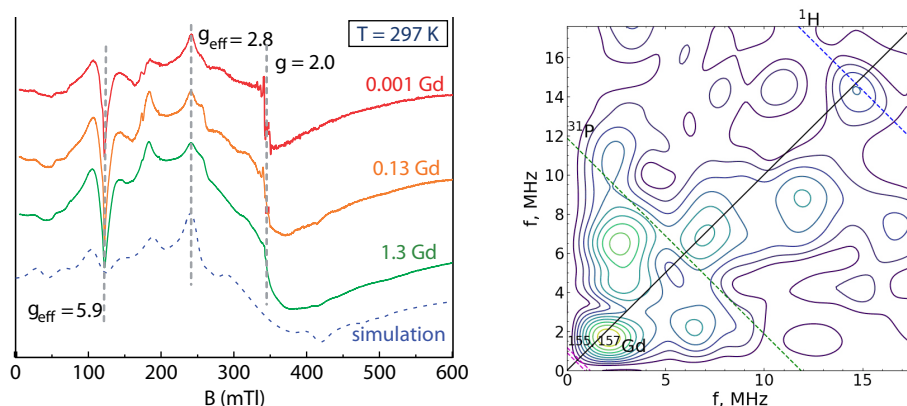


Fig. 1. EPR spectra of TCP ceramics with different Gd^{3+} ions concentration supported by simulation (left panel). HYSORE spectrum indicating the local nuclear environment (right panel).

($\nu_{\text{MW}} = 9.6$ GHz) at room temperature (297 K) and at low temperatures (25 K, 12 K) using a flowing helium cryostat. The analysis of the obtained EPR results made it possible to unambiguously establish that Gd^{3+} is embedded in the TCP crystal lattice and occupies two structurally nonequivalent positions of calcium Ca^{2+} . The main spin-Hamiltonian parameters of Gd^{3+} (zero-field splitting, hyperfine interaction values) and relaxation characteristics were studied. The analysis of the ESEEM and HYSCORE results reveals the presents at least two ionic environment with various degree of crystallinity. The low concentration values ($x = 0.001$) of Gd^{3+} ions do not lead to significant distortions of the crystal lattice and the TCP retains its spatial symmetry. The presence of paramagnetic Gd^{3+} ions affects to the dynamic (relaxation) characteristics of stable nitrogen radicals. Thus, nitrogen radicals can serve as a sensitive probe for the study of gadolinium ions in the TCP structure.

The EPR research was supported by funding allocated to Kazan Federal University for scientific activities, project No. 0671-2020-0051.

1. Bohner M., Santoni B.L.G., Döbel N.: *Acta biomater.* **113**, 23–41 (2020)
2. Liao F., Peng X.Y., Yang F., Ke Q.F., Zhu Z.H., Guo Y.P.: *Mater. Sci. Eng. C* **104**, 109999 (2019)

Paramagnetic derivatives of molecules, clusters and crystals of phenanthroline induced by ultraviolet irradiation

N.S. Saenko, A.M. Ziatdinov, A.S. Shishov, A.G. Mirochnik

Institute of Chemistry, Far Eastern Branch of the RAS, Vladivostok 690022, Russia,
saenko@ich.dvo.ru

It is well known [1] that phenanthroline ($C_{12}H_8N_2$) has two very close separated vacant molecular orbitals, which can be occupied by an additional electron. Chemists use this feature of its electronic structure to synthesize new metal coordination compounds in which phenanthroline molecules are reduced to anion-radicals and are visible in EPR experiment [2]. This paper presents the results of EPR studies of paramagnetic derivatives of molecules, clusters, and crystals of phenanthroline induced by ultraviolet (UV) irradiation.

The EPR spectrum of an initial crystalline powder of phenanthroline contains a single low-intensity resonance from its imperfections with $g = 2.006$ (Fig. 1a, spectrum 1). After ~ 5 minutes of UV irradiation, the resonance with this g -value rise by about an order of magnitude. At the same time, the spectrum of the irradiated sample has other resonances with the intensities much lower than the intensity of the considered resonance. One of them is presented in Fig. 1a (spectrum 2). The intense (main) and low-intensity resonances have significantly different relaxation times. Low-intensity resonances disappear within ~ 1 sec after turning off the UV irradiation (Fig. 1a, spectrum 3), whereas the intensity of the main resonance decreases to the value in the initial sample after ~ 23 days (Fig. 1b).

A small and abrupt (less than 1 sec) decrease in the intensity of the main resonance after turning off the UV irradiation indicates the presence of a contribution to it by a low-intensity component with a short relaxation time (Fig. 1c).

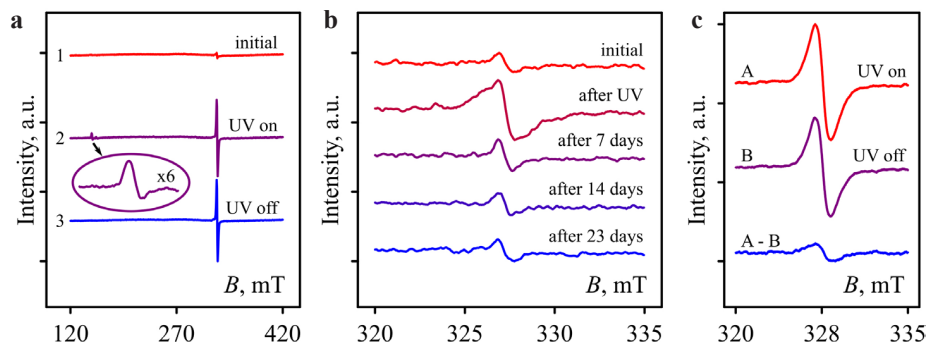


Fig. 1. **a** EPR spectrum of phenanthroline before (1), during (2) and after (3) UV irradiation; **b** relaxation of the intense resonance; **c** revealing a hidden low-intensity resonance

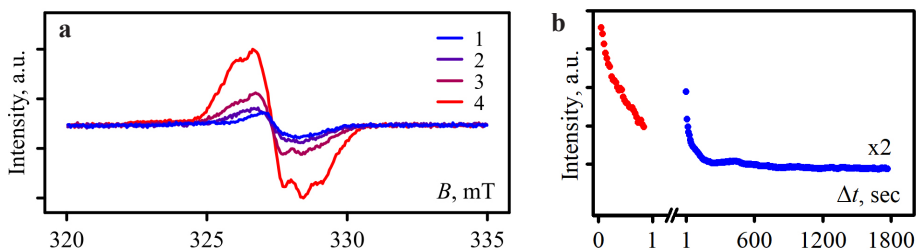


Fig. 2. **a** UV-induced EPR spectra of phenanthroline solutions in ethanol with concentrations: 0.3 M (1), 1 M (2), 2 M (3) and 3 M (4); **b** relaxation of the intensities of two different components of the UV-induced EPR spectrum of 3 M phenanthroline solution in ethanol.

The study of the effect of UV irradiation on the EPR spectra of phenanthroline solutions in ethanol at $-100\text{ }^{\circ}\text{C}$ made it possible to get additional information on the considered above resonances. All initial solutions are EPR transparent. EPR spectra of solution with a low content of phenanthroline under UV irradiation have a low-intensity asymmetric resonance with $g = 2.006$ (Fig. 2a, spectrum 1). The intensity of this resonance is halved in two minutes after switching off UV irradiation. Other resonances in EPR spectra become visible with increasing solution concentration (Fig. 2a). Important distinctive feature of different resonances is the time of their relaxation (disappearance) after turning off the UV source. For example, after turning off the UV irradiation source, the resonances in spectra observed in all studied solutions disappear within a minute or more meanwhile the resonances observed only in spectra of concentrated solutions disappear in just a second (Fig. 2b).

Based on the above data, it was concluded that the resonances with long relaxation times can be attributed to paramagnetic derivatives of phenanthroline molecules whereas the resonances with short relaxation times to paramagnetic derivatives of clusters and crystals of phenanthroline, possibly at their excited energy levels.

The investigations have been financially supported by the Ministry of Science and Higher Education of the Russian Federation (State assignments: FWFN(0205)-2022-0003).

1. Klein A., Kaim W., Waldhor E., Hausen H.-D.: J. Chem. Soc. **2**, 2121 (1995)
2. Koizumi T., Yokoyama Y., Morihashi K. et al.: Bull. Chem. Soc. Jpn. **65**, 2839 (1992)

Spin exchange interactions in nitronyl nitroxide biradical studied by X-band EPR spectroscopy

A.A. Samsonenko, M.V. Fedin, S.L. Veber

International Tomography Center SB RAS, Novosibirsk, Russia;
Novosibirsk State University, Novosibirsk, Russia

Exchange-coupled two-spin systems based on organic radicals (diradicals), along with more complex organic and organometallic systems [1], have been lately actively synthesized. They are interest of, among other things, as objects with thermally attainable triplet and singlet spin states. Such objects show promise for applications in spintronics as well as bistable memory devices and sensing materials [2].

Spin exchange interaction determines the macroscopic magnetic properties of paramagnetic substances based on mono- and diradicals. The general nature of the exchange interaction in the substance under study can be characterized by the SQUID magnetometry. In turn, the electron paramagnetic resonance (EPR) spectroscopy makes it possible to determine the g -tensor of the spin system, the amplitude of the dipole-dipole interaction, and estimate the amplitude of the spin exchange interaction.

In this work the EPR was used to study the spin exchange interaction in the crystal of N,N' -(perfluorobiphenyl-4,4'-diyl)bis(N -tert-butyl(oxy)amine diradicals). The main state of this diradical is singlet. The longitudinal and transverse spin relaxation times of the triplet state were measured by pulsed EPR spectroscopy. Knowledge of the relaxation times and the exchange interaction constant can be used in experiments to measure thermally induced spin dynamics.

This research was funded by the Russian Science Foundation, grant number 22-13-00376. We also thank Dr. E.V. Tretyakov for the samples provided.

1. Ovcharenko V.I., Kuznetsova O.V., Russ. Chem. Rev. **89**, 1261 (2020)
2. Ratera I. et.al.: Chem. Soc. Rev. **41**, 303–349 (2012)

EPR of $\text{CaMoO}_4:\text{Er}^{3+}$ crystal

**G.S. Shakurov¹, R.B. Zaripov¹, V.A. Isaev², A.V. Lebedev²,
S.A. Avanesov²**

¹Zavoisky Physical-Technical Institute, FRC Kazan Scientific Center of RAS, Kazan 420029,
Russia, shakurov@kfti.knc.ru

²Kuban State University, Krasnodar 350040, Russia, avlbv@gmail.com

Creation of an effective quantum memory on crystals activated by rare earth ions is one of the urgent problems of the present time. For practical applications, in addition to long coherence times, a necessary condition is also the possibility of transmitting information via fiber-optic communication systems. Oxide crystals doped with erbium ions satisfy these requirements most completely and have therefore been intensively studied in recent years. We studied the $\text{CaMoO}_4:\text{Er}^{3+}$ crystals using Elexsys E580 EPR spectrometer from Bruker and a broadband EPR (3–28 cm^{-1}) EPR spectrometer [1].

It is known from the literature that grown crystals contain an admixture of Mo^{5+} ions, which color the crystal blue. After annealing in air, the crystals become transparent. We have studied crystals before and after annealing. Known spectra of Er^{3+} ions were observed in transparent crystals [2]. In addition to the EPR lines caused by resonant transitions between the levels of the ground doublet, we observed transitions from the ground doublet to the first and second excited doublets. This made it possible to refine the values of the Stark splittings between doublets.

In as grown crystal, in addition to the lines of erbium ions, a dimer $\text{Er}^{3+}-\text{Mo}^{5+}$ with a characteristic hyperfine structure was observed. The ground state of the dimer was a quasi-doublet with a slight splitting in zero magnetic field. Transitions between quasi-doublet levels were recorded on both spectrometers. The excited states of the dimer (two singlet levels in the range up to 15 cm^{-1}) were determined on a broadband spectrometer. The calculation of the dimer was carried out taking into account dipole-dipole and exchange interactions using well-known analytical expressions [3].

1. Tarasov V., Shakurov G.: Appl. Magn. Reson. **2**, 571 (1991)
2. Zverev G.M., Makarenko L.V., Smirnov A.I.: Fiz. Tverdogo Tela **9**, 3651 (1967) (in russian)
3. Guillot-Noel O., Goldner. Ph., Higel P., Courier D.: J.Phys.: Condens. Matter **16**, R1 (2004)

Definition of β -Enaminone isomerism by 2D NMR and X-Ray

A. Sharipova¹, M. Volkov¹, A. Gubaidullin², O. Turanova¹, A. Turanov¹

¹Zavoisky Physical-Technical Institute, FRC Kazan Scientific Center of RAS, Kazan 420029, Russia

²Arbuzov Institute of Organic and Physical Chemistry, FRC Kazan Scientific Center of RAS
alsu_sharipova@inbox.ru

β -Enaminones are all-purpose synthetic reagents, since the characteristic pentad of atoms allows them to easily react with both electrophiles and nucleophiles. These compounds are of particular interest as biologically active molecules: they are widely used in the synthesis of antibacterial, anti-inflammatory, anti-convulsant, antiparasitic and antitumor agents. β -Enaminones molecules having a chelate structure can be used as ligand. Nonetheless, β -enaminones are much less studied than Schiff bases and β -diketones, despite their high synthetic potential.

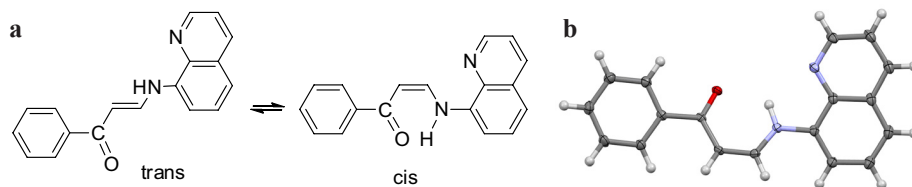


Fig. 1. a The cis-trans isomerism of the ketoamine form; b X-ray established form.

In this work, the structure and tautomeric form of the synthesized compound 1-phenyl-3-(quinolin-8-ylamino)prop-2-en-1-one has been established with help of analytical data, UV-Vis and NMR spectroscopy and by X-ray crystallography (Fig. 1b). β -Enaminone can exist in cis- trans-form (Fig. 1) and as several tautomers (Fig. 2).

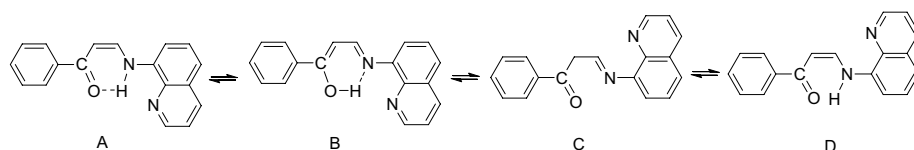


Fig. 2. Some possible tautomeric forms of the cis- isomer β -enaminones.

NMR spectroscopy and X-ray crystallography showed that the 1-phenyl-3-(quinolin-8-ylamino)prop-2-en-1-one has a cis-isomer ketoamine form (A in Fig. 2) due to the presence of a strong hydrogen bond and the formation of a quasiaromatic cycle, which increases the thermodynamic stability of the molecule both in the solid state and in acetone solution.

Photoisomerization studies by NMR, UV-visible spectroscopy and DFT of stilbene-like compounds

A. Shaidullina¹, A. Sharipova², M. Volkov², L. Savostina^{1,2},
L. Gafiyatullin², O. Turanova², A. Turanov²

¹Kazan Federal University, Kazan, Russia

²Zavoisky Physical-Technical Institute, FRC Kazan Scientific Center of RAS, Kazan 420029, Russia, alsu_sharipova@inbox.ru

Photoisomerizing stilbene-like compounds (Fig. 1) have great potential for creating new functional materials based on coordination polymers and can be used to create devices for storing, recording, and transmitting information.

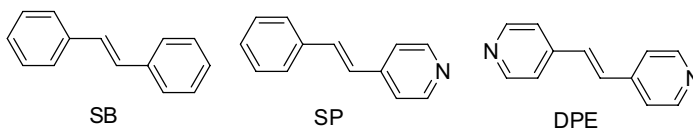


Fig. 1. Stilbene (SB), styrylpyridine (SP), 1,2-di(4-pyridyl)ethylene (DPE).

The goal of this work is research of the effect of heteroatoms in an aromatic substituent on the photoisomerization rate of stilbene-like molecules (Fig. 2).

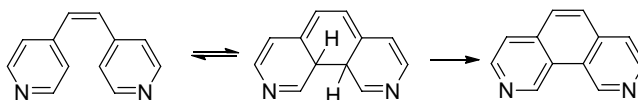


Fig. 2. The DPE photoisomerization.

The process of photoisomerization of stilbene-like compounds in solutions depends on the irradiation wavelength, solvent, etc. Using UV and NMR spectroscopy, it was shown that the kinetics of photoisomerization of the studied systems is monoexponential, the characteristic times are 378 ± 9 , 66 ± 2 , 649 ± 9 seconds for SB, SP and DPE solutions, respectively. Using the DFT method with the B3LYP functional and the def2-SVP basis set, the barriers of the DPE reaction between the transition state and the *cis*-isomer $E = 2.11$ eV and between the transition state and the *trans*-conformation $E = 2.35$ eV were determined. Photoisomerization of SP occurs much faster than SB and DPE due to the push-pull mechanism.

Influence of environment parameters on the internal mobility of pillar[5]arene according to NMR spectroscopy data

L.V. Sharipova^{1,2}, A.N. Turanov³, B.I. Khayrutdinov^{1,2}, Yu.F. Zuev¹

¹Kazan Institute of Biochemistry and Biophysics, FRC Kazan Scientific Center of RAS, Kazan 420111, Russia, lv.sharipova@yandex.ru

²Institute of Physics, Kazan Federal University, Kazan 420008, Russia

³Zavoisky Physical-Technical Institute, FRC Kazan Scientific Center of RAS, Kazan 420029, Russia

The development of modern supramolecular chemistry is aimed at creating new macrocyclic compounds for drug delivery. Pillar[n]arenes are macrocyclic compounds which can act as universal platforms for transport. They are highly symmetrical, bioavailable, highly soluble in water, have a rigid framework, planar chirality, and can be easily functionalized. These properties of pillar[n]arenes make it possible to prolong the action of the drug, prevent its premature degradation. All of these properties of pillar[n]arenes reduce the number of side effects and increases the therapeutic efficacy of the drug.

The aim of this work is to study the dynamic properties of an aqueous solution of decaammonium salt 4,8,14,18,23,26,28,31,32,35-deca(carboxymethoxy) pillar[5]arene.

In our work NMR spectroscopy have been utilized for investigation internal dynamic of pillar[5]arene depending on external conditions. Using a Carr-Purcell-Meiboom-Gill pulse sequence chemical exchange rate constants for protons of the pillar[5]arene hydroquinone fragments were determined at various temperatures and pH values of the solution. The thermodynamic parameters of pillar[5]arene hydroquinone fragment motions were found from the temperature dependence of the chemical exchange rate constant. Thus, by varying the external conditions, it is possible to manipulate the intramolecular mobility of pillar[5]arene and control the formation of complexes with various biologically significant substrates.

Peculiarities of the Q-band EPR spectra of the PbTe crystal with Mn and Cu impurities

A.V. Shestakov¹, I.I. Fazlizhanov¹, V.A. Ulanov^{1,2}

¹Zavoisky Physical-Technical Institute, FRC Kazan Scientific Center of RAS, Kazan 420029, Russia

²Kazan State Power Engineering University, Kazan 420066, Russia

The PbTe direct narrow band semiconductor belongs to the group of lead chalcogenides PbS, PbSe and PbTe with the cubic rock salt structure. It was the subject of a vast amount of theoretical and experimental work. These works were motivated not only by its technological applications, but also by their unusual physical properties. PbTe is a narrow gap semiconductor with strong ionic character. It has a positive temperature coefficient of the gap width ($dE/dT > 0$), the high static dielectric constant, and the large carrier mobility. These properties make it unique among polar compounds and make it important applications in many fields, such as infrared detectors, light-emitting devices, infrared lasers, thermoelectric materials and solar energy panels. Studies of quantum wires, dots, and wells in the bodies of PbTe semiconductors and possibilities of its applications have caused much attention in the past decades. But, a little of these studies were performed by EPR method. The reason of the latest fact is that most of the paramagnetic impurity centers form resonant levels in the conduction or valence band in the lead chalcogenides and all such centers are not observable by EPR method.

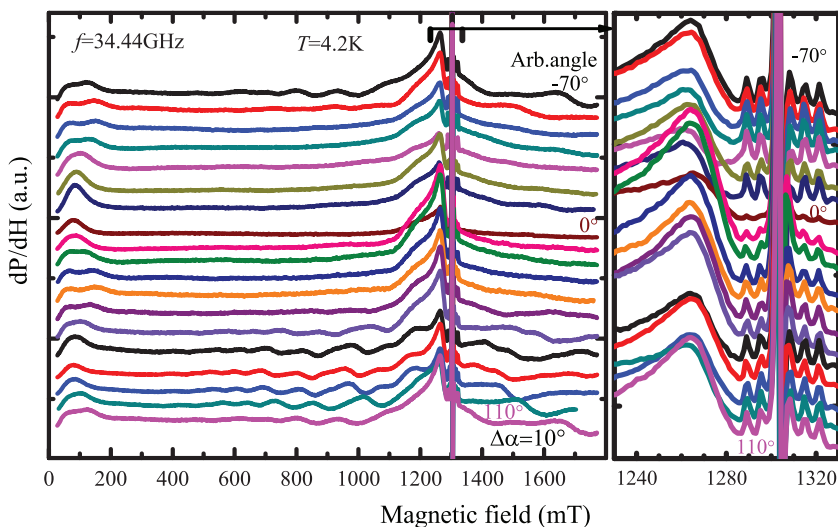


Fig. 1. A series of EPR spectra of a sample in (001) plane at various angles.

But it was found [1, 2] that the Mn^{2+} ions embedded in PbTe are well localized at the Pb sites and form local magnetic moments. Owing to the direct exchange interaction between the d-electrons and Bloch electrons of the valence and conducting bands, the latter are magnetically polarized. Through these polarized electrons, the local spins of Mn^{2+} ions interact with each other. Consequently, the manganese impurity centers can be used as paramagnetic probes to study some physical properties of PbTe semiconductors.

We report here the Q-band (34.44 GHz) EPR data on deep Mn^{2+} centers in PbTe (Mn, Cu) crystalline sample ($x_{Mn} \approx 0.0005 \div 0.001$) grown by vertical Bridgman method in quartz crucibles. This low concentration of Mn ions was chosen with the aim that the impurity ions work as a probe.

The sample was mounted in center of bottom of a cylindrical cavity resonator (with TE₀₁₂ mode) and rotated in the (100) crystallographic plane. The measurements were carried out at liquid helium temperature (4.2 K).

The EPR spectrum of this sample is very rich (see Fig. 1). We immediately note that the line at 1303 mT due to coal that was added as a reference point. Six principal Mn^{2+} hyperfine lines were observed in the EPR spectra. The field intervals between the lines were found to be isotropic under rotation in the (100) plane within the experimental error of about 0.1 mT, where $A = 165 \div 202$ MHz. The EPR broad line with $B_{res} \sim 1275$ mT was observed presumably from Cu ions. The nature of signal in the region 0–200 mT is discussed. Quantum oscillations are also observed in the ERP spectra, the period of which increases with increasing magnetic field. It is assumed that these oscillations are due to the de Haas-van Alphen effect.

All experimental facts observed in this study are discussed.

The financial support was provided by the FRC Kazan Scientific Center of RAS.

1. Ven-Chung Lee: Phys. Rev. B **34**, 5430 (1986)
2. Pifer J.H.: Phys. Rev. **157**, 272 (1967)

Advantages of using focusing short-drawn tapered fibers in vibration sensors

O.P. Shindyev¹, A.V. Shkalikov²

¹Institute of Applied Research, Academy of Sciences of the Republic of Tatarstan, Kazan 420111, Russia, integros@mail.ru

²Zavoisky Physical-Technical Institute, FRC Kazan Scientific Center of RAS, Kazan 420029, Russia, andrei_vs@rambler.ru

The reliability of equipment [1] is of the greatest importance in the electric power industry; therefore, as a rule, most of the calculations and related works [2, 3] are based on the assessment of this parameter. In recent years, more and more attention has been paid to the prevention of accidents. Thanks to the introduction of techniques that allow predicting emergency situations in the operation of equipment and preventing them, both a decrease in economic losses and an increase in the stability of electric power systems occur. Optical quartz fibers are widely used to create fiber-optic communication lines, for scientific research in various fields of physics, biomedical research, and in the creation of various diagnostic systems. In this case, fibers are used both as a means of communication and directly to create sensitive elements for various physical changes.

One of the simplest options for vibration sensors is to bring two fibers close together, one of which is partially suspended in the air, so that light passes from one fiber to another. In the case of transverse vibrations, the vibration of the fiber does not allow light to pass through. Thus, by analyzing the light intensity at the output, it is possible to control the situation in real time. In the case of using a narrowed fiber, stretch it in such a way that a microlens is formed at the tip, which allows you to increase the transmission of light from one fiber to another. Which in turn will significantly increase the signal-to-noise ratio. In Fig. 1. an example of a constricted fiber is shown.

Figure 2. An oscillogram of fluctuations in the intensity of light passing through the sensor is shown. The oscillation frequency corresponds to the vibration frequency. One of the ways to modernize such a sensor is to use an array

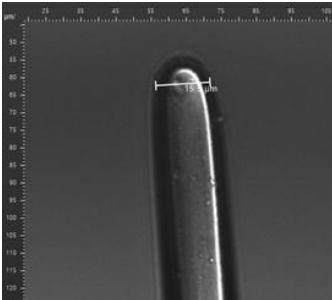


Fig. 1. Tapered fiber.

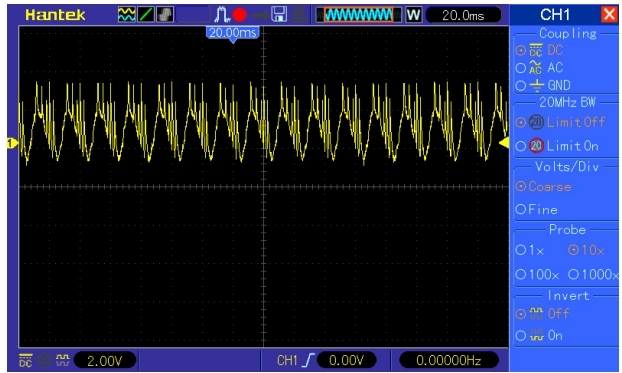


Fig. 2. Oscillogram of fluctuations in the intensity of light passing through the sensor.

of fibers at the output. This option will allow you to fix not only the maximum deviation (vibration amplitude), but also, as a result, acceleration.

In this paper, narrowed fibers obtained by high-temperature stretching and the possibility of using vibration sensors based on them to monitor the occurrence of emergency situations at the base nodes of power lines and transformer substations are investigated. Technological processes for manufacturing vibration sensors based on single-mode fiber have been studied. The characteristics of the obtained sensors are experimentally studied.

1. Apollonsky S.M., Kuklev Yu.V. Reliability and efficiency of electrical devices. St. Petersburg: Lan, 2011.
2. Ilyushin P.V., Tykvinskii A.M.: Bulletin of KSEU 11, 39 (2019)
3. Popov A.V., Idiyatullin R.G., Aukhadeev A.E.: Energy problems 5, 94 (2016)

EPR study of calcium phosphate powders

D. Shurtakova, G. Mamin, M. Gafurov

Institute of physics, Kazan Federal University, Kazan 420008, Russia, darvshurtakova@kpfu.ru

Phosphates are the most common compounds of minerals and phosphoric acid in the earth, the general chemical formula is $\text{Ca}_3(\text{PO}_4)_2$. The compounds have a crystalline structure.

Calcium phosphates are widely used in biomedicine, they are used in toothpaste and for cosmetic purposes. Hydroxyapatite (HAp) belongs to the group of apatites with the chemical formula $\text{Ca}_{10}(\text{PO}_4)_6(\text{OH})_2$. Due to the chemical similarity of HAp to the composition of bones and teeth, HAp is widely used as a coating on dental and orthopedic implants. Octacalcium phosphate (OCP) has the chemical formula $\text{Ca}_8(\text{HPO}_4)_2(\text{PO}_4)_4 \cdot 5\text{H}_2\text{O}$. OCP as a filling material enhances bone tissue regeneration, since osteoblasts located on the OCP implant initiate the deposition of new bone. Tricalcium phosphate (TCP) is also actively used in medical preparations for the restoration and remodeling of bone and dental tissue. There are varieties of β -TCP (chemical formula $(\beta\text{-Ca}_3(\text{PO}_4)_2)$) and α -TK Φ (chemical formula $(\alpha\text{-Ca}_3(\text{PO}_4)_2)$) [1].

The aim of this work is describing EPR spectra of calcium phosphates powders and comparing each other.

In this work, we investigate EPR spectra of three series of samples: nano-sized HAp, OPC and TCP. Samples of HAp were synthesized by precipitation from colloidal solutions at the Faculty of New Materials Science, Moscow State University [2]. Samples of OCP and TCP were synthesized at the Institute of Metallurgy and Materials Science (A.A. Baikova) by the wet (precipitation) technique from solutions of nitrates and ammonium hydrogen phosphate [3].

EPR spectra were obtained on an Elexsys-580/680 spectrometer in the X- and W-bands at the room temperature. EPR signals were detected in all samples after the irradiation. To describe EPR spectra we used "MatlabR2010a" (TheMathWorksInc.) with a special module "Easyspin".

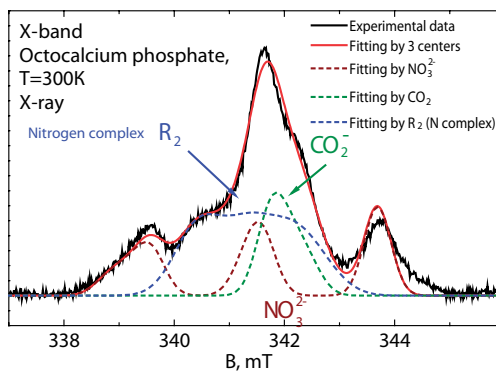
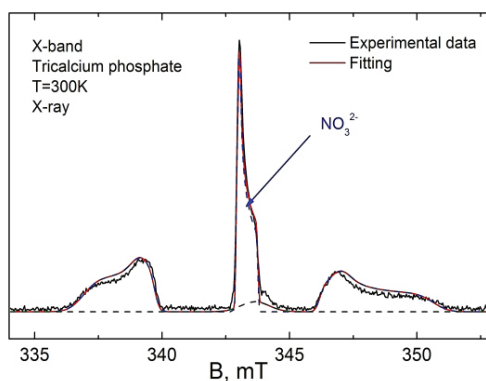
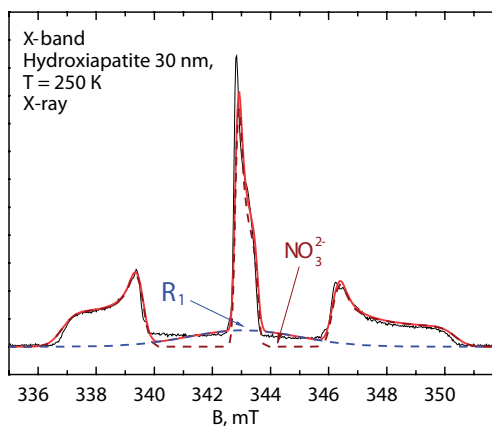
The results of the experiment and approximation are shown in Fig. 1. The figure shows that the spectra of HAp and TCP are very similar. We see 3 lines that may belong to the nitrogen center, since the nuclear spin of nitrogen is 1. Nitrogen is involved in a chemical reaction during the manufacture of samples and could get into the structure.

The spectrum of octacalcium phosphate has a more complex shape. We assumed that the octacalcium phosphate sample captured the carbon center from the air. Previously, this was observed for natural calcium phosphates.

We approximated the obtained spectra, taking into account our assumptions, simultaneously in X- and W-band.

The EPR spectrum of HAp described with parameters $g_x = g_y = 2.0084$, $g_z = 2.0047$, $A_x = A_y = 95$ MHz, $A_z = 176$ MHz.

The EPR spectrum of TCP described with parameters $g_x = 2.0032$, $g_y = 2.0024$, $g_z = 1.9985$, $A_x = 92$ MHz, $A_y = 11$ MHz, $A_z = 193$ MHz. In addition,



the distribution of parameters of hyperfine splitting of 15–20% was added to the model, which may be associated with the distribution of powders by size.

The EPR spectrum of OCP described with parameters for nitrogen complex $g_x = g_y = 2.0036$, $g_z = 2.0055$, $A_x = A_y = 56$ MHz, $A_z = 86$ MHz. However, it is not possible to describe the spectrum with only one center, so we assumed that the OCP captured the carbon center from the air, and therefore we added the carbon center to the approximation.

All spectra contain one more center of unknown nature requiring further study. Comparison of the parameters of the EPR spectra shows that the environment of the nitrogen complex for HAp and TCP is similar (parameter A are close). While for the OCF we cannot draw such a conclusion.

This work was funded by the subsidy allocated to Kazan Federal University for the state assignment in the sphere of scientific activities no. 0671-2020-0051.

1. Epple M.: Acta biomaterialia 77, 1–14 (2018)
2. Kovaleva E.S., Shabanov M.P., Putlyaev V.I.: Cent. Eur. J. Chem 7(2), 168 (2009)
3. Komlev V., Barinov S., Bozo I.: ACS Appl. Mater. Interfaces 6, 16610 (2014)

Electron spin resonance of spinon liquid with interaction

**A.I. Smirnov¹, K.Yu. Povarov², T.A. Soldatov¹, Ren-Bo Wang³,
A. Zheludev², O.A. Starykh³**

¹P. L. Kapitza Institute for Physical Problems RAS, Moscow 119334, Russia, smirnov@kapitza.ras.ru

²Laboratory for Solid State Physics, ETH Zürich, 8093 Zürich, Switzerland

³Department of Physics and Astronomy, University of Utah, Utah 84112, USA

The $S = 1/2$ Heisenberg antiferromagnetic spin chain has a quantum-disordered ground state, which may be described in terms of quantized fractionalized structures called spinons [1]. Spinons are neutral $S = 1/2$ fermions. This concept of free fermions is supported by observation of a continuum of $S = 1$ excitations (so called two-spinon continuum) and by field-dependent soft modes within continuum [1]. A fine structure of the two-spinon continuum was predicted for spin chains with a uniform Dzyaloshinsky-Moriya (DM) interaction. This interaction causes a tiny shift of the continuum, results in an energy gap $\Delta = \pi D/2$ (D is the DM parameter) and a doublet of electron spin resonance (ESR) frequencies

$$\nu_{\pm} = (g\mu_B H \pm \Delta)/2\pi\hbar . \quad (1)$$

This doublet enables one to measure precisely the width of the continuum at a certain wavevector q_{DM} [2]. Now we consider a theory and experiment on spinon doublet for a quasi 1D $S = 1/2$ antiferromagnet $K_2CuSO_4Br_2$. In a magnetic field of about a third of saturation we see a significant deviation of modes ν_{\pm} from relation (1). We used theory [3] which predicts a strong influence of the interaction between spinons on their energy. This influence results in an additional

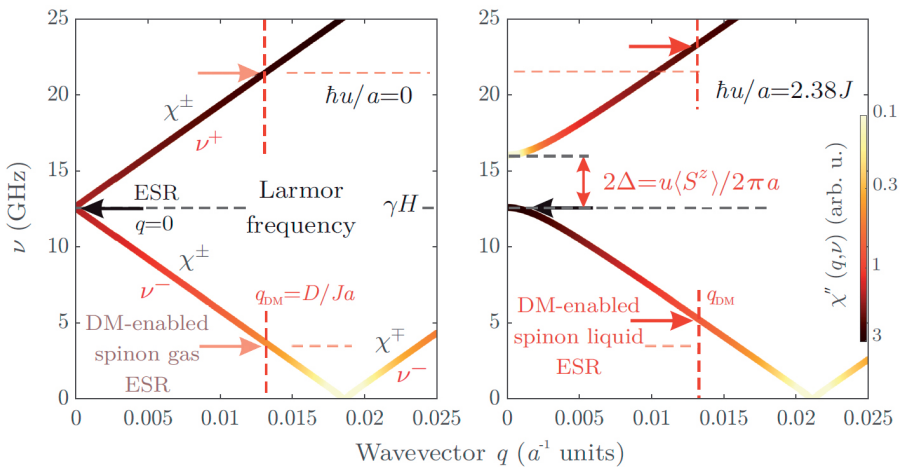


Fig. 1. Boundaries of the continuum in absence of interaction (left, $u = 0$) and with interaction (right, $u = 3.5 \cdot 10^5$ cm/s).

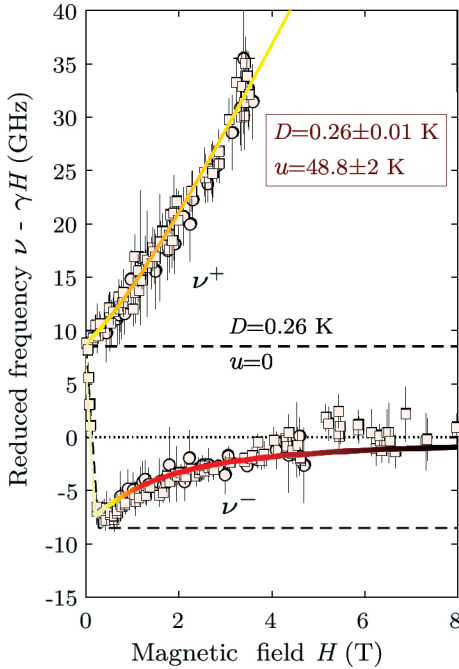


Fig. 2. ESR frequencies vs field. $T = 0.5$ K.

energy gap $\Delta_{\text{int}} = uM/\mu_B$, where u is the parameter of backscattering of spinons living near the right/left Fermi points, M is magnetization. Using the value of Δ_{int} we explain the deviation of the observed frequencies of the spinon doublet from the interaction-neglecting relation (1), with u being the fitting parameter. Fig. 1 compares boundaries of spinon continuum in the absence and presence of backscattering. Fig. 2 shows the observed distance of the doublet components from Larmor frequency $\nu_{\text{Lar}} = g\mu_B H/(2\pi\hbar)$ in a magnetic field, fitted by theory with the parameter $u = 3.5 \cdot 10^5$ cm/s (solid lines). This distance should be constant for $u = 0$ (horizontal dashed lines at ± 8.7 GHz). The fit demonstrates a quantitative correspondence of the experiment and theory.

Thus, experiment confirms a concept of interacting spinons as a basic feature of the ground state of $S = 1/2$ Heisenberg antiferromagnetic chain. The value of the spinon backscattering parameter is found experimentally. This reveals a Fermi-liquid (not a Fermi-gas) behavior of quasiparticles in a 1D antiferromagnet. There is a fundamental analogy between neutral fermions in a spin chain and electrons in a normal (nonferromagnetic) metal: the spectrum of spinons has a contribution of Fermi-interaction of spinons and, in a similar way, the Fermi-liquid interaction of electrons results in Silin spin waves [5] in a metal.

Support of RSCF Grant 22-02-00259 is acknowledged.

1. Dender D.C. et al.: Phys. Rev. Lett. **79**, 1750 (1997)
2. Smirnov A.I. et al.: Phys. Rev. B **92**, 134417 (2015)
3. Keselman A., L. Balents, O. A. Starykh, Phys. Rev. Lett. **125**, 187201 (2020)
4. Povarov Yu.K. et al.: Phys. Phys. Rev. Lett. **128**, 187202 (2022)
5. Silin V.P.: Sov. Phys. JETP **6**, 945 (1958); V.P. Silin, Sov. Phys. JETP **8**, 870 (1959)

Application of high-resolution NMR to study the influence of platinum nanoparticles on tryptophan amino-acid

M. Smirnov, G. Kupriyanova

Institute of Physics, Mathematics and Information Technology,
Immanuel Kant Baltic Federal University, Kaliningrad 236041, Russia,
smirnov.mark2015@yandex.ru

Nanoparticles based on noble metals, due to their properties, have wide applications in many places, including cancer treatment, water purification and biosensors [1]. However, the issue of the interaction of metal nanoparticles with organic compounds has not been sufficiently studied.

Nuclear magnetic resonance (NMR) spectroscopy has proven itself as an accurate method for determining the structure of chemicals. The NMR method can detect the interaction of a nanoparticle with a molecule at the atomic level [2]. In the study [3], the interaction of gold nanoparticles of different sizes with bicinchotinic acid (BCA) was studied by ^1H NMR. A decrease in the intensity of the amide group in the ^1H NMR spectrum was found with an increase in the concentration of nanoparticles.

Amino acids are organic compounds whose physicochemical behavior is explained by the simultaneous presence in the molecule of the basic amino group NH_2 and the acid carboxyl group COOH [4]. Amino acids have good prospects for creating drugs, since they perform important plastic and regulatory functions in the body. Also, aromatic amino acids, due to the presence of a system of delocalized electrons in them, can be used as fluorescent molecules (fluorophores) for coloring tissue and cell structures [5].

The aim of this study was to determine the changes that the amino acid tryptophan undergoes when platinum nanoparticles are added to a solution using high-resolution proton NMR. The objectives of our study included obtaining high-resolution ^1H NMR spectra of tryptophan, both with and without platinum nanoparticles, correlating signals in the amino acid spectrum, and identifying differences in the spectra associated with the appearance of platinum nanoparticles.

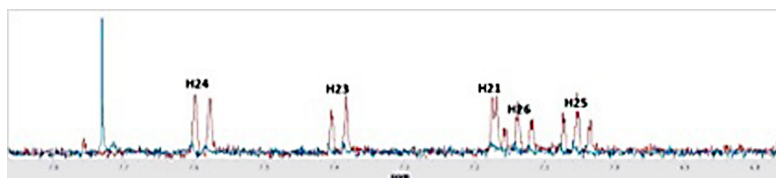


Fig. 1. Aromatic region of ^1H NMR spectrum of tryptophan. The blue color shows the sample without nanoparticles, and the red color shows the sample with the addition of platinum nanoparticles.

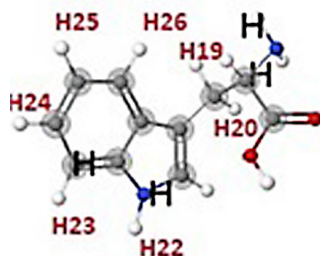


Fig. 2. Tryptophan molecule. Protons whose signals are subject to changes are marked in red.

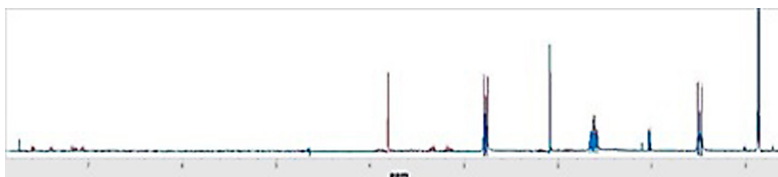


Fig. 3. ^1H NMR spectrum of tryptophan. The sample without nanoparticles is shown in blue, and with the addition of platinum nanoparticles in red.

High-resolution proton NMR spectra were obtained on a Varian 400 MHz high-resolution NMR spectrometer with a $B = 9$ T superconducting magnet. The intense water signal was suppressed using the “Water ES” pulse sequence. To stabilize the resonance conditions, 60 ml of deuterated water was added to the samples. A small amount of DSS was added to the samples to stabilize the chemical shifts.

High-resolution NMR spectra of tryptophan in aqueous solution were obtained both with and without the addition of platinum nanoparticles. Correlation of signals in the spectrum of tryptophan to individual molecular fragments was performed on the basis of the study [6].

It was found that the signals of all protons of the benzene ring (H23-H26), located at the frequency of chem. shift of 7–8 ppm, are significantly enhanced when platinum nanoparticles are added to the solution. There is also an increase in the proton signal associated with nitrogen (H22). In the aromatic region, a new signal appears at ~ 7.7 ppm. In another region of the spectrum, located at the frequency of chem. shift 0 - 4 ppm, there is an increase in two signals at a frequency of 3.0 - 3.4 ppm, which belong to the protons H19 and H20. Also at a frequency of 3.8 ppm, a new signal appears. In addition, the relative intensity of the signal changes by ~ 2 ppm towards its decrease when platinum nanoparticles are added to the solution.

1. Jose Miguel Mateo, Antonio de la Hoz, Laura Uson, Manuel Arruebo, Victor Sebastian, M. Victoria Gomez: Insights into the mechanism of the formation of noble metal NP. *Nanoscale advances*. 2020. 2, 3954–3962;
2. Yunzhi Zhang. Nuclear magnetic resonance (NMR) applications in nanoparticles: dynamic nuclear polarization and nanoparticle surface interaction: dis... Doctor of Philosophy (Chemistry). – Clemson University. 2019. – 137 pp.;
3. Y. Randika Perera, Taylor M. South, Alex C. Hughes, Ashlyn N. Parkhurst, Olivia C. Williams and etc. Using NMR Spectroscopy To Measure Protein Binding Capacity on Gold Nanoparticles. *J Chem Educ*. 2020 March 10; 97(3): 820–824.
4. Х.-Д. Якубке: Аминокислоты. Пептиды. Белки. / Х.-Д. Якубке, Х. Ешкайт. – Москва: издательство “Мир”, 1985 – 75 с.
5. Чекман И.С., Сырвая А.О., Новикова И.В., Макаров В.А., Андреева С.В., Шаповал Л.Г.: Аминокислоты – наноразмерные молекулы: клиникалабораторные исследования / Харьков, 2014. - 154 с.;
6. Wishart DS, Knox C, Guo AC, Eisner R, Young N and etc. HMDB: a knowledgebase for the human metabolome. *Nucleic Acids Res*. 2009 Jan; 37: D603-10. doi: 10.1093/nar/gkn810

Extremely low concentrations of the antimicrobial peptide chalciporin influence membrane lipid organization

**A.S. Smorygina¹, V.N. Syryamina¹, B. Biondi³, C. Peggion^{3,4},
F. Formaggio^{3,4}, S.A. Dzuba^{1,2}**

¹Voevodsky Institute of Chemical Kinetics and Combustion, RAS, Novosibirsk 630090, Russia, anna.smor.mr@gmail.com

²Department of Physics, Novosibirsk State University, Novosibirsk 630090, Russia

³Institute of Biomolecular Chemistry, Padova Unit, CNR, Padova 35131, Italy

⁴Department of Chemical Sciences, University of Padova, Padova 35131, Italy

Antimicrobial peptides (AMPs) are promising therapeutic agents against drug-resistant bacteria. Many AMPs can directly interact with bacterial membranes, disturbing their integrity and/or functionality. The advantages of AMPs are their high metabolic activity, high rate of bactericidal action, low likelihood of addiction and side effects. Here, we study at the molecular level the mechanism of action of the membrane-active peptide chalciporin A. This peptide belongs to the subclass of medium-length peptaibols (from 14- to 16-mers) and is close to the family of tylopeptins, also isolated from the fruitful body of *Sepedonium chalcipori*.

In present work, we studied influence of chalciporin on clustering of molecules spin-labeled stearic acids in model synthetic membranes. Membranes were prepared of 1-palmitoyl-2-oleoyl-sn-glycero-3-phosphocholine (POPC) lipid. The stearic acid molecules contained the spin label at the 5th, 16th or 12th position of the carbon atom in the acyl residue. To this aim, we exploited the highly informative continuous wave (CW) and pulse Electron Paramagnetic Resonance (EPR) techniques. Pulsed EPR is based on the electron spin echo (ESE) phenomenon. Two versions of ESE experiments were employed: Double Electron-Electron Resonance (DEER, also known as PELDOR) which probes molecular self-assembling, and Electron Spin Echo Envelope Modulation (ESEEM), which probes the peptide localization in the membrane.

From our in-depth EPR analysis on the medium-length peptide chalciporin A in lipid bilayers, we conclude that (i) the peptide is localized in the membrane interior at all tested P/L ratios, (ii) it is not prone to specific oligomerization at concentrations below 0.5 mol.%, (iii) but starting from ultralow concentrations (~ 0.01 mol.%) it induces the lateral rearrangement of fatty acids embedded into the bilayer.

We previously observed [1] that in the absence of chalciporin A the local concentration of 5-DSA is lower than that of 16-DSA. This behavior was attributed to alternative DSA sub-clustering in the two opposing leaflets. The findings of the present work show that in the presence of chalciporin A the local concentration of 5-DSA increases while that of 16-DSA decreases, thus tending towards the equalization of these two effective concentrations. This result may be interpreted assuming that the sub-clusters assemble around the peptides, becoming larger and mutually separated.

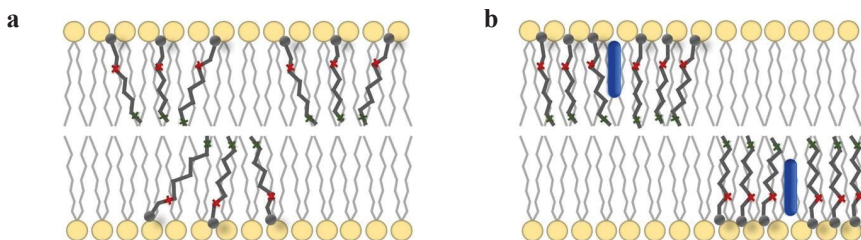


Fig. 1. Schematic presentation of clustering of stearic acids in POPC bilayer without Chalciporin A (a) and in its presence (b).

Crosses depict the spin labels in 5-DSA and in 16-DSA molecules, the peptides are depicted in blue. Without peptide, the clusters are divided into small sub-clusters, alternatively located in two opposing leaflets; the 5-DSA local concentration is effectively reduced because of mutual repulsing of the polar heads and inter-leaflet separation [1]. With peptide, the sub-clusters are assembled around the peptide, becoming larger and mutually separating; the effective local concentration for 5-DSA molecules increases because the factor of inter-leaflet separation decreases, while that for 16-DSA molecules decreases because of the sub-cluster separation. This work was supported by RSF, Grant № 21-13-00025.

1. Smorygina A.S., Golysheva E.A., Dzuba S.A.: Clustering of Stearic Acids in Model Phospholipid Membranes Revealed by Double Electron–Electron Resonance. *Langmuir* **37**(47), 13909–13916 (2021).

Study of pulse time-resolved EPR of naphthalimide-phenothiazine compact donor-acceptor dyad

A.A. Sukhanov¹, V.K. Voronkova¹, K. Ye², J. Zhao²

¹Zavoisky Physical-Technical Institute, FRC Kazan Scientific Center of RAS, Kazan 420029, Russia, vio@kfti.knc.ru

²State Key Laboratory of Fine Chemicals, School of Chemical Engineering, Dalian University of Technology, Dalian 116024, P. R. China, zhaojzh@dlut.edu.cn

Recently, thermally activated delayed fluorescence (TADF) [1] has great potential and interest for organic light emitting diodes (OLEDs) because of the potential for high efficiency without the use of heavy metals. Often, donor-acceptor systems are used to create efficient TADF materials [2]. The process of reverse intersystem crossing (rISC) is the defining process for TADF. Despite intense research interest, this rISC process is not fully understood. Recent theoretical work [3–4] predicts a model in which the energy gaps between the ³LE (local exciton triplet)-³CT (triplet charge-transfer) and ³LE-¹CT (singlet charge-transfer) states are critical activation barriers. And the relative energy order between the CT and ³LE states, along with the magnitude of each barrier, determines intersystem crossing (ISC), rISC, and hence the efficiency of TADF.

Early we studied TADF property for NI (naphthalimide)-N-PTZ (phenothiazine) sample and observed the inversion of triplet polarization pattern using continuous wave time-resolved (TR) EPR spectroscopy [5]. In this work we explained of the life-time of this inversion using pulse TR EPR. Temperature dependence of the life-time have Arrhenius behavior. We assume that the inversion of triplet polarization pattern is related to the energy gap ³LE-³CT, which we estimate from our data about 0.0146 eV.

1. Uoyama H., Goushi K., Shizu K., Nomura H., Adachi C.: *Nature* **492**, 234 (2012)
2. Nobuyasu R.S., Ren Z., Griffiths G.C., Batsanov A.S., Data P., Yan S., Monkman A.P., Bryce M.R., Dias F.B.: *Adv. Opt. Mater.* **4**, 597 (2016)
3. Gibson J., Monkman A. P., Penfold T. J.: *ChemPhysChem* **2016**, 17, 2956 (2016)
4. Etherington M., Gibson J., Higginbotham H., Penfold T.J., Monkman A.P.: *Nat. Commun.* **7**, 13680 (2016)
5. Tang G., Sukhanov A. A., Zhao J., Yang W., Wang Z., Liu Q., Voronkova V.K., Di Donato M., Escudero D., Jacquemin D.: *The Journal of Physical Chemistry C* **123**, 30171 (2019)

Change in the distance between P_{700}^+ and A_1^- radicals in the reaction centers of photosystem I upon removal of iron-sulfur clusters

A.A. Sukhanov¹, M.D. Mamedov², G.E. Milanovsky², A.Y. Semenov^{2,3}, K.M. Salikhov¹

¹Zavoisky Physical-Technical Institute, FRC Kazan Scientific Center of RAS, Kazan 420029, Russia, ansukhanov@mail.ru

²A.N. Belozersky Institute of Physical-Chemical Biology, Lomonosov Moscow State University, Moscow, Russia

³N.N. Semenov Federal Research Center for Chemical Physics, Russian Academy of Sciences, Moscow, Russia

In photosynthetic reaction centers of intact complexes of photosystem I (PS I) from cyanobacteria, electron transfer at room temperature occurs along two symmetrical branches of redox cofactors A and B in a ratio of ~3:1. Previously, this was indirectly shown using pulsed absorption spectroscopy [1] and more directly by measuring the modulation frequencies of ESEEM [2]. Distance between P_{700}^+ and A_1^- radicals was estimated as ~26 Å, which corresponds to electron transfer along the A branch. In our other work [3], the distance between P_{700}^+ and A_1^- in PS I complexes lacking the terminal 4Fe-4S F_A/F_B clusters (designated as P700- F_X core complexes) and embedded into trehalose glassy matrix was ~25 Å obtained by ESEEM method. This distance corresponds to the predominant electron transfer along the B branch.

In the present work, these distances were determined using ESEEM on PS I complexes lacking all three 4Fe-4S clusters, F_X , F_A , and F_B (designated as P₇₀₀- A_1 -core complexes). It was shown that the average distance between the centers of the $P_{700}^+A_1^-$ radical ion pair at a temperature of 150 K in an aqueous glycerol solution and in a dried trehalose matrix at a temperature of 290 K, is ~25.5 Å for P₇₀₀- A_1 -core complexes. This distance corresponds to the symmetrical electron transfer along the branches of redox cofactors A and B in a ratio of 1:1.

The study was financially supported by the RSF and the Cabinet of Ministers of the Republic of Tatarstan within the framework of the scientific project No. 22-23-20165, <https://rscf.ru/project/22-23-20165>.

1. Makita H., Hastings G.: FEBS Letters **589**, 1412 (2015)
2. Sukhanov A.A., Mamedov M.D., Möbius K., Semenov A.Y., Salikhov K.M.: Applied Magnetic Resonance **49**, 1011 (2018)
3. Sukhanov A.A., Mamedov M.D., Möbius K., Semenov A.Y., Salikhov K.M.: Applied Magnetic Resonance **51**, 909 (2020)

Creation and investigation of thin-film heterostructures based on Fe/Nb

A.A. Validov, M.I. Nasyrova, R.R. Khabibullin, I.A. Garifullin

Zavoisky Physical-Technical Institute, FRC Kazan Scientific Center of RAS, Kazan 420029, Russia, validov@kfti.knc.ru

Here we propose to create and study fundamentally new structures of superconducting spin valves. The operation of the new structures is built beyond the limits of the classical superconductor/ferromagnet proximity effect, since there will be no direct interface contact between the superconductor and ferromagnet in them.

At the first stage, we propose to create and study the structures of a superconducting spin valve based on iron (Fe) and niobium (Nb). First, niobium has wide application as a superconductor in modern superconducting spintronics due to its high superconducting transition temperature. Secondly, our group demonstrated the presence of a “dead” zone in the Fe/Nb interface. This “dead” zone at the Fe/Nb and Nb/Fe interfaces can successfully serve as insulating layers at the ferromagnet/superconductor and superconductor/ferromagnet interface in the superconducting spin valve (SSV) structures. To implement SSV of such a design, it is necessary to debug the technology for preparing Fe/Nb two-layer systems. In this work, we also fine-tuned the technology for preparing Fe/Al₂O₃/Nb three-layer structures, where aluminum oxide (Al₂O₃) is the insulating layer. As our studies show, the designs of a superconducting spin valve based on Fe/Al₂O₃/Nb are more promising for further research.

In this work, Fe/Nb-based thin-film heterostructures prepared under various conditions are studied. Here, Fe/Nb and Fe/Al₂O₃/Nb structures prepared on MgO and Al₂O₃ single-crystal substrates at various substrate temperatures during deposition were studied. According to the research results, the structures prepared at high substrate temperatures (>600 K) on MgO demonstrate the most stable and, most importantly, reproducible transport properties of the samples.

The reported study was funded by Russian Science Foundation according to the research project No. 22-22-00916.

The self-diffusion of 128-arm star-shaped polydimethylsiloxanes with a dendritic branching center

S.G. Vasil'ev¹, K.V. Panicheva^{1,2}, P.A. Tikhonov³, A.M. Muzafarov^{3,4}

¹Institute of Problems of Chemical Physics, RAS, Chernogolovka 142432, Russia

²Lomonosov Moscow State University, Moscow 119991, Russia

³Institute of Synthetic Polymeric Materials, RAS, Moscow 117393, Russia

⁴Institute of Organoelement Compounds, RAS, Moscow 119991, Russia

Multarm star-shaped polymers are members of polymeric materials with complex architecture, which commonly refer to macromolecular nanoparticles. The other representatives of this class are dendrimers, dense macromolecular brushes, hyperbranched polymers and molecular nanogels. Their distinctive features are high and, in many cases including star polymers, inhomogeneous intramolecular monomer density. In the present work we investigate the star polymers in which arms are formed by polydimethylsiloxane (PDMS) and the 6th generation carbosilane dendrimer serves a branching center [1]. The ability to compensate the inherent mismatch in density by the star interpenetration and shape adjustment allow forming nanofluids, which are homogeneous up to submicron size in a wide temperature range [2]. The dynamics of such objects in solutions and melts lie in the borderline between the polymers and colloids. Investigation of the translational dynamics by PFG NMR presented in this study represent new interesting peculiarities.

The measurements were performed using stimulated spin echo experiment on a Bruker Avance III 400 spectrometer on ¹H nuclei. Four samples of 128 arm stars with different arm lengths were investigated.

The graph shown on the left side of Fig. 1 demonstrate the diffusion decays for samples with different arm lengths in diluted solutions of toluene (about 1%

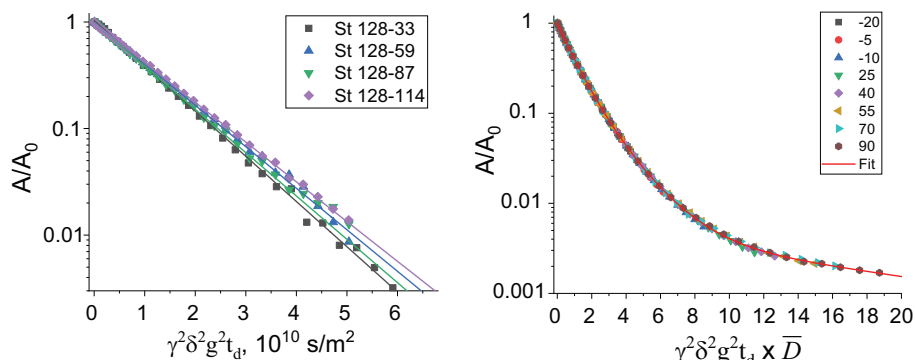


Fig. 1. The diffusion decays for 128-arm star-shaped PDMS: diluted solutions in toluene for samples with different arm lengths (left) and neat stars with the arm length of 59 units at different temperatures (right).

of polymer). The shapes of the decays are exponential confirming the narrow molecular weight distributions of the investigated polymers. The hydrodynamic radii calculated using Stokes-Einstein formula give the values in the range of 4–4.6 nm. For the samples in the absence of the solvent the diffusion decays are clearly deviate from a single exponential decay as shown in the right side of Fig. 1. Intuitively the appearance of such polydispersity of the diffusing species can be explained by the formation of some aggregates or regions with different mobility. Such features are often observed near the glass transition. The dynamics is expected to be time dependent but the experiments with different diffusion times didn't show the changes of the diffusion decays. The investigated temperature region is far above the glass transition (which is below -120 °C for all samples). No any signs of the heterogeneity was observed in experiments.

It was found that the shape of the diffusion decays does not depend on temperature for the melts of 128-arm star-shaped PDMS. This is shown in Fig. 1 (right) for one of the samples. The data on the right side of Fig. 1 shown with x axis multiplied by the average self-diffusion coefficient determined at each temperature from the initial slope of the decay. The conservation of the shape of diffusion decays were also observed for other samples. The changes of the average self-diffusion coefficient can be well described by the Arrhenius dependence. The obtained data indicate that the features of the diffusion decay shapes can be attributed to the manifestation of the rotational motion of the star-shaped PDMS.

Acknowledgements. This work has been supported by the grants the Russian Science Foundation (project No 22-43-04439)

1. Tikhonov P.A., Vasilenko N.G., Gallyamov M.O., Cherkaev G.V., Vasil'ev V.G., Demchenko N.V., Buzin M.I., Vasil'ev S.G., Muzafarov A.M.: *Molecules* **26**(11), 3280 (2021)
2. Malkin A.Ya., Polyakova M.Yu., Subbotin A.V., Meshkov I.B., Bystrova A.V., Kulichikhin V.G., Muzafarov A.M.: *J. Mol. Liq.* **286**, 110852 (2019)

Study of a spin-variable Fe(III) complex by ^1H NMR spectroscopy

M. Volkov¹, E. Batueva², O. Turanova¹, A. Turanov¹

¹Zavoisky Physical-Technical Institute, FRC Kazan Scientific Center of RAS, Kazan 420029, Russia, mihael-volkov@yandex.ru

²Institute of Physics, Kazan Federal University, Kazan, Russia

In addition to magnetometry and EPR spectroscopy, NMR spectroscopy is also used in order to study the magnetic properties of Fe (III) complexes in solutions. Initially, the Evans method was used to determine the magnetic susceptibilities of solutions of paramagnetic complexes [1]. Then the methods of spherocylindrical [2] and oblong-shaped [3] glass container appeared. All these methods are based on the effect of changing the chemical shifts of the nuclei caused by the non-standard shape of the glass container, in which the studied liquid is placed.

However, no less interesting is an attempt to study solutions of paramagnetic complexes by recording their NMR spectra and subsequent analysis of the width of those NMR signals that correspond to the nuclear spins of the complex molecules. As nuclear spins suitable for such a study, an isotope ^1H of the hydrogen nucleus can be used only, because the isotopes of the nuclei of carbon ^{13}C , nitrogen ^{15}N and oxygen ^{17}O (possessing a non-zero nuclear spin) have a very low natural abundance and, therefore, such experiments require too much time.

In this work a Fe(III) complex $[\text{Fe}(\text{bzacen})(\text{Im})_2]\text{BPh}_4$ (see Fig. 1) was chosen as the studied complex. It is known that it exhibits spin-crossover properties in powders [4]. This complex was dissolved in deuterated acetone and its ^1H NMR spectra were recorded by a Bruker Avance 400 NMR spectrometer. In order to assign ^1H NMR signals to nuclear spins of protons of the complex molecule, all components of this complex were also studied, namely, the bzacen ligand, imidazole, and sodium tetraphenylborate (containing the tetraphenylborate ion). ^1H NMR spectra of solutions of these substances in deuterated acetone were recorded separately by the Bruker Avance 400 NMR spectrometer, and the procedure of assignment ^1H NMR signals to nuclear spins of protons belong-

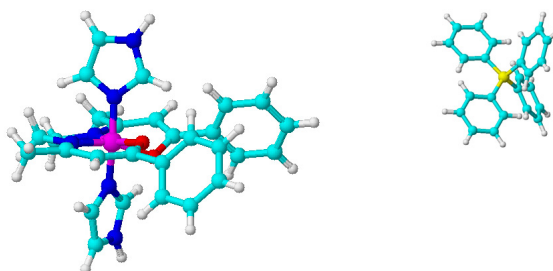


Fig. 1. 3D view of the molecule of the studied complex $[\text{Fe}(\text{bzacen})(\text{Im})_2]\text{BPh}_4$.

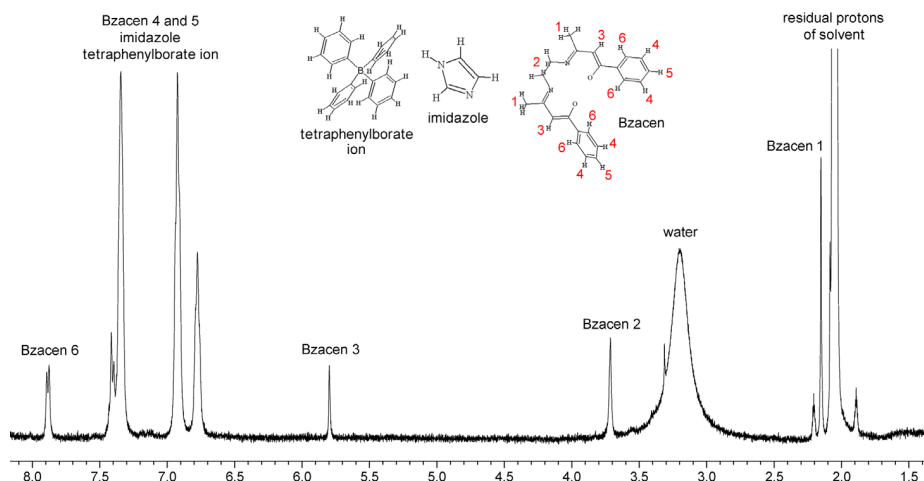


Fig. 2. ^1H NMR spectrum of a solution of the complex $[\text{Fe}(\text{bzacen})(\text{Im})_2]\text{BPh}_4$ in deuterated acetone.

ing to these molecules was also carried out for them. In order to facilitate the assignment procedure, the ^1H NMR spectra of each of these compounds were preliminarily calculated by the ACD Labs software.

Fig. 2 demonstrates the result of assignment ^1H NMR signals to nuclear spins of protons in the molecules of the complex. The set of lines in the range of chemical shifts from 6.7 to 7.5 ppm represents the overlap of the proton signals of the bzacen ligand, imidazole, and tetraphenylborate ion. At the same time the signals at 2.15 ppm, 3.72 ppm, 5.8 ppm and 7.88 ppm correspond individual chemical groups of the bzacen ligand. Because the signals at 2.15 ppm, 3.72 ppm and 5.8 ppm are single lines, the temperature dependences of the width of these lines were studied.

1. Evans D.F.: *J. Chem. Soc.* 2003 (1959)
2. Hatada K., Terawaki Y., Okuda H.: *Bull. Chem. Soc. Jpn.* **42**, 1781 (1969)
3. Kovesdi I.: *J. Magn. Res.* **43**, 1 (1981)
4. Nishida Y., Oshio S., Kida S.: *Bull. Chem. Soc. Japan* **50**, 119 (1977)

NMR structure of antimicrobial peptide megin-1

P. Skvortsova¹, M. Volkov², Yu. Zuev¹, E. Ermakova¹

¹Kazan Institute of Biochemistry and Biophysics, FRC Kazan Scientific Center of RAS,
Kazan 420111, Russia, kibmail@kibb.knc.ru

²Zavoisky Physical-Technical Institute, FRC Kazan Scientific Center of RAS, Kazan 420029,
Russia, mihael-volkov@yandex.ru

Here we investigated the structure of a new antimicrobial peptide named megin-1 extracted from skin venoms of spadefoot toad *Megophrys minor*. Megin-1 consists of 18 amino acid residues (FLKGCWTKWYSLKPKCPF) with two cysteine residues and can exist in an oxidized form with a disulfide bond (M1) or in a reduced form with a broken disulfide bond (M1R).

The three-dimensional structure of the two megin-1 forms was determined by solution NMR spectroscopy (Fig. 1). M1R takes an elongated shape in solution, which is probably stabilized by four positively charged lysine residues. M1 assumes a loop-like shape by forming a disulfide bond between 5 and 16 cysteine residues.

The three-dimensional structure of megin-1R was determined at pH 2.4. Increasing pH of the solution to 3.4 causes a change in the peptide structure. One can see in Fig. 2 that the NMR spectrum is changed – the intensity of some signals decreases and new signals appear with chemical shifts corresponding to the cyclic megin-1. It can be assumed that disulfide bonds are formed in the peptide.

The linear form of megin-1 passes into a cyclic form in an aqueous solution at pH = 3.4. The Gibbs free energy of 24.2 kcal/mol and the change of entropy of 10 kcal/mol at 293 K characterize the oxidation of protein cysteine thiolates.

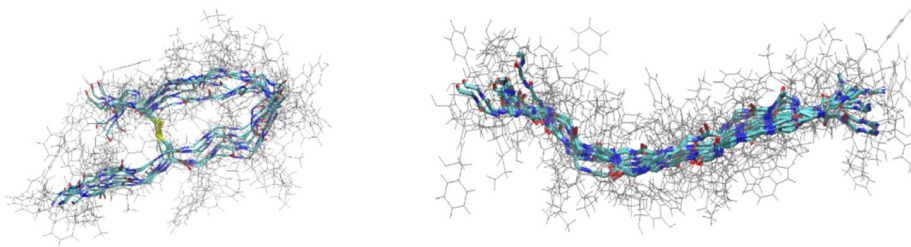


Fig. 1. Three-dimensional NMR structure of megin-1 (left – M1, right – M1R). Superposition of six lowest-energy structures. The backbone is shown in color, whereas side chains are shown in gray lines. Cysteine residues are shown as yellow bonds.

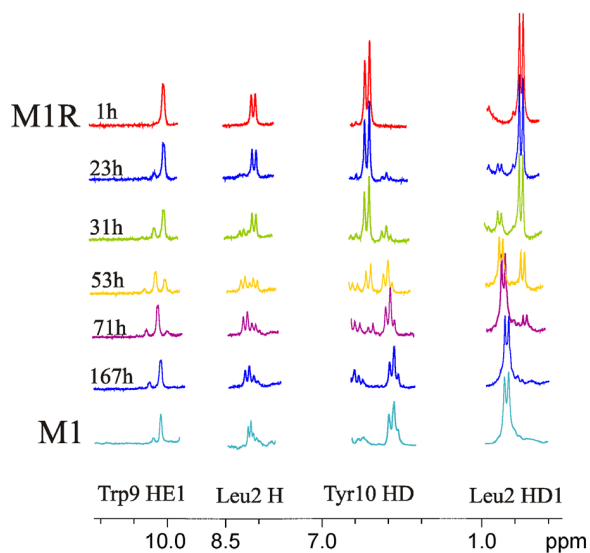


Fig. 2. Time evolution of the megin-1R NMR spectrum in a water solution at $\text{pH} = 3.4$ and $T = 293 \text{ K}$.

This work was performed by the financial support from the government assignment for Federal Research Center (FRC) Kazan Scientific Center of Russian Academy of Sciences (RAS).

The NMR measurements have been carried out using the equipment of Distributed Spectral-Analytical Center of Shared Facilities for Study of Structure, Composition and Properties of Substances and Materials of FRC Kazan Scientific Center of RAS.

Unusually slow intramolecular triplet-triplet energy transfer in naphthalenediimide-anthracene compact donor-acceptor dyads. TR EPR study

A.A. Sukhanov¹, V.K. Voronkova², Xi Chen², M. Taddei³, J. Zhao²,
M.Di Donato³

¹Zavoisky Physical-Technical Institute, FRC Kazan Scientific Center of RAS, Kazan 420029, Russia, vio@kfti.knc.ru

²State Key Laboratory of Fine Chemicals, School of Chemical Engineering, Dalian University of Technology, Dalian 116024, P. R. China. zhaozh@dut.edu.cn

³LENS (European Laboratory for Non-Linear Spectroscopy), 50019 Sesto Fiorentino, Italy

Photoinduced charge separation/recombination processes, intersystem crossing (ISC) and intramolecular triplet-triplet energy transfer (TTET) have attracted much attention due to their significance in the study of fundamental photochemistry.

Here we present the discussion of these processes on example of three new compact electron donor-acceptor dyads, with naphthalenediimide (NDI) as the electron acceptor and anthracene (An) as the electron donor. The distance and mutual orientation of the donor and acceptor are varied to study the relationship between the molecular structure and ISC efficiency including the spin orbit charge transfer intersystem crossing (SOCT-ISC) efficiency. In 9-An-NDI, the anthryl moiety is directly connected at the imide position of the NDI chromophore, this linkage is beneficial to attain an orthogonal geometry, which is believed to be helpful for achieving efficient SOCT-ISC. For 9-An-Ph-NDI and 2-An-Ph-NDI, one intervening phenyl moiety was used, increasing the distance among the two units. The different distance, orientation and electronic coupling between the electron donor an acceptor may lead to different photophysical properties for these dyads.

Using time-resolved EPR (TR EPR) method the photoinduced states, mechanisms of their formation, the time dependence electron spin polarization (ESP) phase patterns were studied. The results indicate that the triplet production mechanism is SOCT-ISC for all the three dyads. However, the TR EPR spectra of three dyads differ. Spectrum analysis shows that only the ³An state is observed for 9-An-NDI, while for the other two dyads, both ³NDI and ³An states were observed, with their relative population changing with increasing delay time. We propose that the mechanism populating the state is not an ordinary SOC-ISC, that the ³An state is formed by intramolecular TTET from the ³NDI state. This is supported by the time-dependent evolution of the TREPR spectra of 9-An-Ph-NDI: as the delay time increases, the spectral ratio ³An/³NDI increases.

For 9-An-NDI, although only ³An state is observed in TR EPR and ns-TA spectra, the involvement of the intermediate ³NDI state cannot be completely excluded. Possibly the ultrafast intramolecular TTET ³NDI↔³An makes the detection of the ³NDI state impossible. The obtained results show strong effect of distance, orientation and electronic coupling between the electron donor an acceptor on the photophysical properties of dyads.

EPR study of ATP-sensitive potassium channels and nitric oxide role in preconditioning effect to brain stroke

**Kh. Gainutdinov^{1,2}, G. Yafarova², S. Gavrilova³, O. Deryagin³,
V. Andrianov^{1,2}, V. Iyudin¹, S. Buravkov³, M. Akhmetshina³, A. Erdiakov³,
V. Koshelev³**

¹Zavoisky Physical-Technical Institute, FRC Kazan Scientific Center of RAS, Kazan 420029, Russia, kh_gainutdinov@mail.ru

²Institute of Fundamental Medicine and Biology, Kazan Federal University, Kazan 420008, Russia, gusadila@mail.ru

³Facility of Fundamental Medicine, Lomonosov Moscow State University, Moscow 119192, Russia, sgavrilova@mail.ru

Brain resistance to blood supply deficiency can be increased under the influence of short episodes of ischemia/reperfusion or hypoxia, short periods of hypothermia and other moderate stress effects which are capable of activating endogenous protective mechanisms and increasing resistance to subsequent severe ischemia [1–3]. This phenomenon is called “preconditioning”. Nitric oxide (NO) and K_{ATP}^+ channels play an important role in the mechanisms of ischemic damage of cells. Moderate activation of NO during preconditioning could provide a neuroprotective effects, activating antioxidant enzymes, triggering anti-apoptotic mechanisms and increasing the level of cerebral blood flow [4]. Activation of K_{ATP}^+ -channels is considered to be a main component of response in preconditioning models [2, 5, 6]. The role of NO in the development of ischemic cell damage is equally important [7, 8]. The present study focuses on the relationship between K_{ATP}^+ channels and NO in brain ischemia.

Ischemic preconditioning (IP) of the brain performed by alternately closing the right and left common carotid arteries (OSMA) for 5 minutes with 5 minutes reperfusion during 1 hour. Subsequently study of early (3 hours) and delayed (24 hour) phase of the protective effect of IP development was carried. Measurement of NO content in brain tissue and venous blood were performed by the method of electron paramagnetic resonance (EPR). We used a spin capture method based on the reaction of a radical (in this case NO) with a spin trap [9]. As a result of the reaction, an adduct with a characteristic EPR spectrum is formed, when the Fe^{2+} with diethyldithiocarbamate (DETC) forms a stable triple complex $(DETC)_2-Fe^{2+}-NO$ [9, 10]. The method allows direct measurements, and is highly sensitive due to the use of spin traps. The components of the spin trap NO (DETC-Na, $FeSO_4$, sodium citrate) was injected 30 minutes before the extraction of studied tissue. The measurements of the spectra of the complex $(DETC)_2-Fe^{2+}-NO$ were performed on the spectrometer EMX/plus with a temperature module ER 4112HV in the X band (9.50 GHz). The amplitude of the EPR spectra was always normalized to the weight of the sample (details of the EPR signal measurement technique described earlier [11]).

The amount of the complex $(DETC)_2-Fe^{2+}-NO$ in cortical brain structures of the control group of rats with OSMA was two times less than in intact animals

at all time points. The average level of NO in the cortex of intact animals made up 1.16 nm/g after 5 hours of OSMA in the area of ischemia was observed a minimum concentration of 0.3 nm/g, increasing as the distance from the damage area (of 0.48 nm/g) to 0.68 nm/g in the contralateral hemisphere and 0.83 nm/g in the cerebellum. The average level of NO in 9, 24 and 72 h after OSMA was 0.62 nm/g and 0.65 nm/g and 0.75 nm/g respectively. In the group of animals treated with a blocker of K_{ATP}^+ channels glibenclamide, on the third day after the operation was observed by the increase of NO level by 65% compared to. the introduction of the activator of K_{ATP}^+ channels, diazoxide a day before OSMA has led to a decrease of NO level at all time points on 25–41%. Thus, the relationship between K_{ATP}^+ channels and NO in rats with ischemic preconditioning.

This work was part of Kazan Federal University Strategic Academic Leadership Program (PRIORITY-2030) and funded by subsidy allocated to Kazan Federal University for the state assignment № 0671-2020-0059 in the sphere of scientific activities. Electron spin resonance measurements were performed with the financial support from the government assignment for FRC Kazan Scientific Center of RAS.

1. Shmonin A.A., Baisa A.E. et al.: *Neuroscience and Behavioral Physiology* **42**(6), 643–650 (2012)
2. Samoilenkova N.S., Gavrilova S.A., Koshelev V.B.: *Regionarnoe krovoobrashchenie i mikrotsirkulyatsiya*; **1**(25), 82–92 (2008)
3. Ding ZM, Wu B. et al.: *Int. J. Mol. Sci.* **13**(5), 6089–6101 (2012)
4. Jung K.H., Chu K. et al.: *Stroke* **37**, no. 11, 2744–2750 (2006)
5. Sasaki N., Sato T. et al.: **101**, no. 4, 439–445 (2000)
6. Дерягин О.Г., Гаврилова С.А. и др. *Журн. неврол. психиатр.* **116**(8), 17–23 (2016)
7. Bolanos J.P., Almeida A.: *Biochim. Biophys. Acta.* **1411**, 415–436 (1999)
8. J.R. Steinert, T. Chernova, I.D. Forsythe. *Neuroscientist* **16**(4), 435–452 (2010)
9. Vanin A.F., Huisman A. et al.: *Methods in Enzymology* **359**, 27–42 (2003)
10. V.D. Mikoyan, L.N. Kubrina, et al.: *Biochim. Biophys. Acta* **1336**, 225–234 (1997)
11. Gainutdinov Kh.L., Gavrilova S.A. et al.: *Appl. Magn. Reson.* **40**, no. 3, 267–278 (2011)

pH-Sensitive spin probes for determination of water acidity in the inter-plane space of graphite oxide

T.S. Yankova¹, N.A. Chumakova^{1,2}

¹Chemistry Department, Lomonosov Moscow State University, Moscow 119991, Russia, yankovats@my.msu.ru

²Semenov Institute of Chemical Physics, Moscow 119991, Russia

Nowadays graphene oxide (GO) attracts researcher's attention as a promising drug delivery carrier. GO is a layered material comprising graphene-like unoxidized domains and regions of oxygen-functionalized graphene. GO-based drug delivery systems are commonly used as water dispersions. Since many drug molecules are pH-labile, one of the most important characteristics of such system is pH value of water inside the inter-plane space of GO.

In this work acidity of water intercalated into GO was measured for the first time. Two pH-sensitive nitroxides (MTI, DPI) were used for this purpose (see Fig. 1). EPR spectrum of MTI in GO containing intercalated water is shown in Fig. 2. The distance $2a_N$ reflects pH value of water confined between the oxidized graphene layers. pH value of water intercalated into GO synthesized according to Brodie method was found to be 2.25 ± 0.05 .

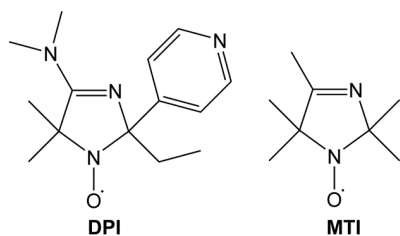


Fig. 1. pH-sensitive spin probes used.

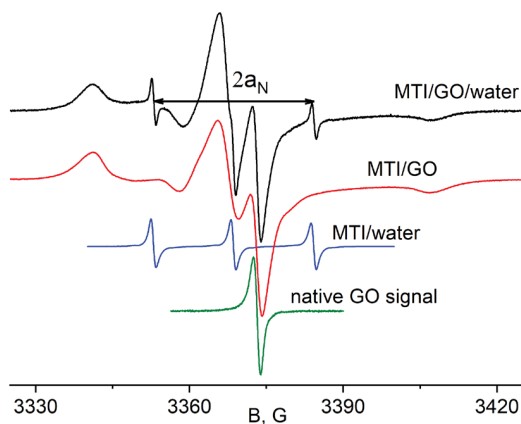


Fig. 2. X-band EPR spectrum of MTI/GO/water sample and its components.

Investigation of gallium iron oxide by the ESR method

I.V. Yatsyk¹, R.M. Eremina¹, E.M. Moshkina²

¹Zavoisky Physical-Technical Institute, FRC Kazan Scientific Center of RAS, Kazan 420029, Russia, I.Yatsyk@gmail.com

²Kirensky Institute of Physics, Federal Research Center KSC SB RAS, Akademgorodok 50, Krasnoyarsk 660036, Russia

The multiferroic materials, which exhibit coexistence and coupling of magnetic and electric orders, have emerged as promising candidates for basic understanding of the coupling between magnetic and electronic properties and uses of the

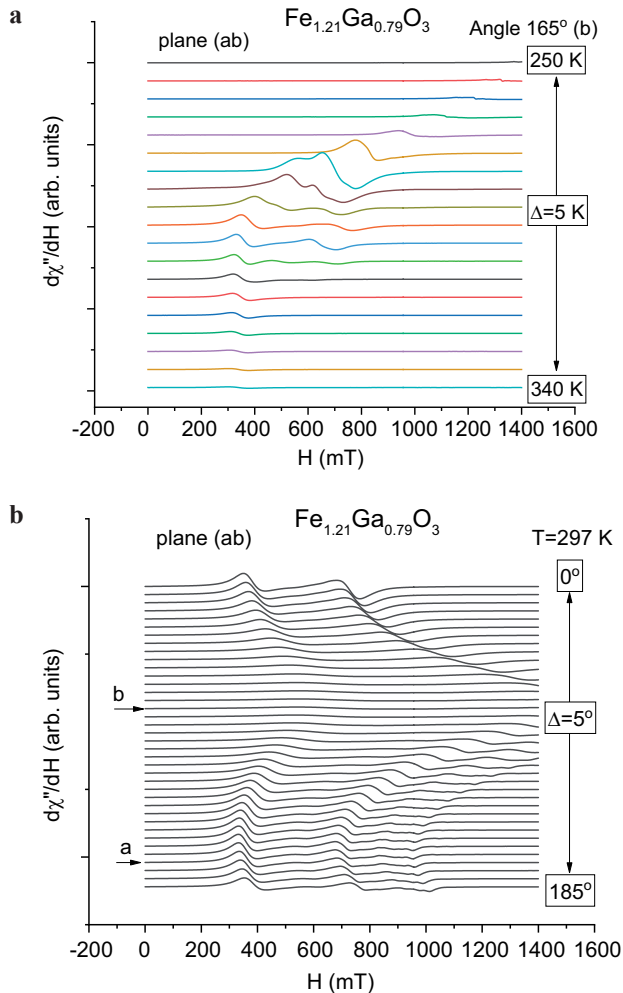


Fig. 1. Temperature (a) and angular (b) evolution of the ESR line in (ab) plane.

materials in magnetoelectric devices, such as memory, logic devices, sensors, and voltage-driven magnetic tunnel junctions [1–6]. The integration of naturally existing or artificially designed multiferroic materials into devices opens up a new field to achieve the energy-saving and miniaturization of the devices [7]. Some transition metal oxides (BiFeO_3 , TbMnO_3 , BiMnO_3 , HoMnO_3 , DyFeO_3 , and GaFeO_3) have shown multiferroic properties [1–7] and majority of these oxides showed magnetic order at low temperatures.

The aim of this work is to study by ESR, magnetometry methods magnetic properties of $\text{Fe}_{1.21}\text{Ga}_{0.79}\text{O}_3$. Temperature and angular evolution of the ESR line in (*ab*) plane is shown in Fig. 1. At 70° , there is a sharp increase in the ESR linewidth and resonant field up to 700 mT. We believe that this is the ferromagnetic lines.

I.V.Y. and R.M.E. acknowledge the financial support from the government assignment for FRC Kazan Scientific Center of RAS.

1. Lone A.G., Bhowmik R.N.: *Journal of Alloys and Compounds* **905**, 164164 (2022)
2. Fiebig M., Lottermoser T., Meier D., Trassin M., *Nat. Rev. Mater.* **1**, 16046 (2016)
3. Lu C., Wu M., Lin L., Liu J.M.: *Natl. Sci. Rev.* **6**, 4 (2019)
4. Spaldin N.A.: *Proc. R. Soc. A* **476**, 20190542 (2020)
5. Catalan G., Scott J.F.: *Adv. Mater.* **21**, 2463–2485 (2009)
6. Wang Y.J., Li J.F., Viehland D.: *Mater. Today* **17**, 269–275(2014)
7. Pyatakov A.P., Zvezdin A.K.: *Phys. Usp.* **55**, 557–581 (2012)

Impact of the lithium deficiency to the electrochemical performance of $\text{Li}_3\text{V}_2(\text{PO}_4)_3/\text{Li}_3\text{PO}_4$ composites

T.P. Gavrilova¹, I.V. Yatsyk¹, J.A. Deeva², T.I. Chupakhina²,
N.M. Suleimanov¹, S.M. Khantimerov¹

¹Zavoisky Physical-Technical Institute, FRC Kazan Scientific Center of RAS, Kazan 420029, Russia,

²Institute of Solid State Chemistry of RAS (UB), Ekaterinburg 620990, Russia

Compounds based on lithium-vanadium phosphate $\text{Li}_3\text{V}_2(\text{PO}_4)_3$ can be used as a cathode material in metal-ion batteries due to the stability of their crystal structure with respect to the change in the valence state of transition ion caused by the processes of intercalation/deintercalation of an alkaline element during the charge/discharge process of the electrochemical cell. One of the interesting problems is the study of a pure $\text{Li}_3\text{V}_2(\text{PO}_4)_3$ sample with a lithium deficiency, assuming that its initial structure will be more predisposed to the Li intercalation/deintercalation process and more resistant to mechanical stress and degrade less as it was expected in the case of the nanostructured cathode materials with the high energy density, high rate capability, and excellent cycling stability due to their huge surface area, short distance for mass and charge transport, and freedom for volume change.

To the present moment, we have developed a synthesis method for composites containing a Li_3PO_4 as an additional phase that makes this system promising in terms of improving the electrochemical properties. Moreover, it was found that the phase with a deficiency of lithium $\text{Li}_{3-x}\text{V}_2(\text{PO}_4)_3$ is stable formed in

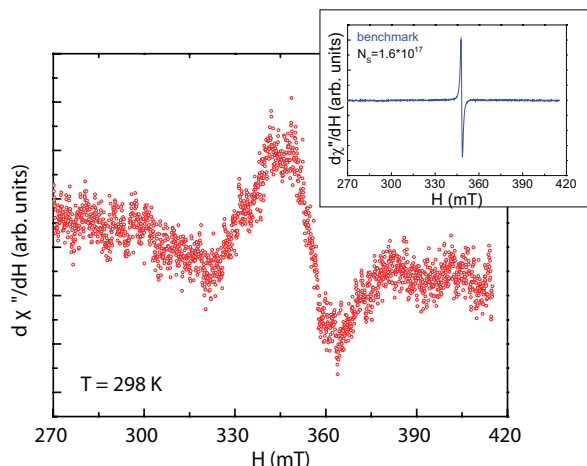


Fig. 1. Electron resonance spectrum of the $\text{Li}_3\text{V}_2(\text{PO}_4)_3$ (86 wt%)/ Li_3PO_4 (14 wt.%) composite at room temperature at the X-band frequency. Inset shows the electron spin resonance spectrum of the benchmark containing $N_s = 1.6 \cdot 10^{17}$ spins.

the composition of $\text{Li}_3\text{V}_2(\text{PO}_4)_3/\text{Li}_3\text{PO}_4$ solid solutions. The magnetic properties $\text{Li}_3\text{V}_2(\text{PO}_4)_3/\text{Li}_3\text{PO}_4$ were investigated using the electron spin resonance (ESR) method; one of the experimentally observed ESR spectra is presented in Fig. 1. When discussing the nature of the ESR signal, it is necessary to note that V^{3+} ($3d^2$, $S = 1$) has an even number of electrons in the respective electronic shells and singlet ground-state levels may result so that no ESR is observable. Thus, as it was suggested in our previous works, the observed ESR spectra is most probably due to a small amount of V^{4+} ions ($3d^1$, $S = 1/2$). To estimate the number of V^{4+} ions, the integral intensity of the $\text{Li}_3\text{V}_2(\text{PO}_4)_3/\text{Li}_3\text{PO}_4$ spectrum was compared with the same parameters for the benchmark (inset Fig. 1). The change in the valence state of vanadium ions from V^{3+} to V^{4+} can be associated with the lithium non-stoichiometry in the investigated compound; that is, to maintain the electrochemical neutrality of the unit cell the change in valence of one vanadium ion from 3+ to 4+ corresponds to the deintercalation of one lithium ion. Taking into account the vanadium to lithium ratio in the chemical formula, it is possible to estimate the degree of lithium nonstoichiometry in the investigated samples. We observed that the increase in Li_3PO_4 amount in LVPO/LPO composites leads to the decrease in the Li stoichiometry, which can affect (improve) the electrochemical properties.

The further investigations of the electrochemical properties showed that the specific capacity is 10% higher for the sample with a higher lithium non-stoichiometry (with a higher content of the Li_3PO_4 salt). The obtained results also showed that the $\text{Li}_3\text{V}_2(\text{PO}_4)_3/\text{Li}_3\text{PO}_4$ composites demonstrate lower initial specific charge-discharge capacity compared to $\text{Li}_3\text{V}_2(\text{PO}_4)_3/\text{C}$, however, at the same time, they retained their specific capacity during multiple cycling (up to 200 cycles), whereas for the $\text{Li}_3\text{V}_2(\text{PO}_4)_3/\text{C}$ sample, the specific capacity value decreased by tens of percent even after 25 cycles.

The reported research was funded by Russian Science Foundation (grant No 19-79-10216), <https://rscf.ru/project/19-79-10216/>.

Study of nitrogen monoxide sorption into robust radical-containing materials by EPR spectroscopy

**A. Yazikova^{1,2}, A. Poryvaev², D. Polyukhov², A. Efremov^{1,2},
M. Fedin^{1,2}**

¹Novosibirsk State University, Novosibirsk 630090, Russia, a.yazikova@tomo.nsc.ru

²International Tomography Center SB RAS, Novosibirsk 630090, Russia

Ecology problems such as air pollution come to the fore nowadays. One of the most widespread toxic waste gases is NO_x mixture. NO participates in chain reactions of photochemical smog formation and being released in the atmosphere it can react with oxygen converting to NO₂ which contribute acid rain formation. NO_x gases participates in formation of tropospheric ozone which is biologically toxic. The prime anthropogenic source of NO_x emission is fuel combustion. Adsorption of NO_x from the flue gas is a good method in order to reduce negative affection to environment. Accordingly, this field is attracted interest of the scientific community and industry.

Organosilica materials have established themselves as perspective sorbents that find applications in many areas. The materials are perspective for specific sorption application due to the ease of morphology tailoring and surface functionalization. In particular, the introduction of paramagnetic sites in material is promising way for development sorbent that capture paramagnetic gases effectively.

Electron paramagnetic resonance is a spectroscopic technique for studying systems having unpaired electrons. Thus EPR is suitable approach for monitoring radical centers behavior during paramagnetic gas sorption and desorption.

In this work we studied NO sorption in Blatter radical-containing silica robust materials: xerogels and SBA-15. We demonstrated that Blatter radical-containing materials are able to interact with NO forming diamagnetic product. We studied desorption by heating up to different temperatures and monitoring numeric change of radical centers by EPR. Quantitative EPR analysis of radical content during repetitive sorption/desorption revealed gradual decreasing of sorption capacity. Selective capturing of nitric oxide from flue gas model mixture by radical containing materials was approved by EPR spectroscopy.

Acknowledgements: This work was funded by RFBR (No 20-53-12005) and the Deutsche Forschungsgemeinschaft (DFG, German Research Foundation) – Projektnummer 429839772 in a DFG-RFBR collaborative project.

Nuclear gamma resonance studies of natural iron-rich borates vonsenite and hulsite

A.L. Zinnatullin¹, Y.P. Biryukov², F.G. Vagizov¹

¹Kazan Federal University, Kazan 420008, Russia, ALLZinnatullin@kpfu.ru

²Institute of Silicate Chemistry of the Russian Academy of Sciences, Saint Petersburg 199034, Russia

In recent years, iron borates have received a lot of attention due to the development of unique magnetic structures and cascades of magnetic phase transitions. Such properties make them very interesting and promising both from fundamental and practical sides. Also, in mixed valence iron borates, a number of interesting phenomena, including oxidation, changes in crystal structure expansion, etc., occur with the temperature increase [1, 2]. These observations require detailed investigations of the materials using both bulk and microscopical methods.

Mössbauer spectroscopy is the commonly used method for the study of iron-bearing materials. This method allows to investigate valence and magnetic states of the resonant atoms and their local environment. Various transformations in materials may be explored using temperature dependent Mössbauer studies.

We provided ⁵⁷Fe Mössbauer effect studies in a wide temperature range of two natural iron-rich oxoborates dimorphous in part of the end-member formula $\text{Fe}^{2+}_2\text{Fe}^{3+}(\text{BO}_3)_2\text{O}_2$, namely orthorhombic vonsenite and monoclinic hulsite. These minerals belong to the ludwigite (*Pbam*) and pinakiolite (*P2/m*) groups, respectively. The minerals were collected from the Titovskoe boron skarn deposit, Sakha Republic, Russia.

Room temperature Mössbauer spectrum of vonsenite was processed within four doublets corresponding to the four crystallographic sites in the structure. With a temperature decrease, charge ordering (≈ 200 K) and two magnetic phase transitions (≈ 114 K and ≈ 70 K) occur. Mössbauer spectrum of hulsite collected at 398 K was fitted by five doublets corresponding to the nonequivalent iron sites in the structure. Two magnetic phase transitions at ≈ 383 K and ≈ 125 K were found. Manifestation of two magnetic phase transitions in both minerals related to various temperatures of magnetic ordering at the iron sites. Paramagnetic and magnetically ordered iron ions coexist in these minerals in a wide temperature range.

This work was supported by the Russian Science Foundation, project no. 22-77-00038.

1. Biryukov Y.P. et al.: Acta Cryst. B **77**, 1021 (2021)
2. Biryukov Y.P. et al.: Acta Cryst. B **76**, 543 (2020)

SPONSOR

ОФИЦИАЛЬНЫЙ АВТОРИЗОВАННЫЙ ПРЕДСТАВИТЕЛЬ

Спектрометры электронного парамагнитного резонанса



X и W-диапазона с магнитными полями от 0,5 до 6 Т

ZHONGTAI

YOUNG IN
Chromass



Флэш хроматографы

для очистки продуктов органического и биотехнологического синтеза



a santai science company
SANTAI
TECHNOLOGIES
quality since 2004



Элемент

- поставка оборудования
- пуско-наладочные работы
- обучение
- сервисное обслуживание

Вспомогательное и общелaborаторное оборудование

системы очистки воды, генераторы газов, центрифуги, роторные испарители, гомогенизаторы, магнитные мешалки и многое другое



Расходные материалы для лаборатории

аналитические колонки, стеклянные и кварцевые кюветы, лампы с полым катодом, D2-лампы и многое другое

www.element-msc.ru

Москва
тел/факс: (495) 514-00-47
msc@element-msc.ru

Екатеринбург
тел/факс: (343) 278-34-64 (65-69)
ekb@element-msc.ru

Новосибирск
тел/факс: (383) 21-12-726
nsk@element-msc.ru

AUTHOR INDEX

Afanasiev, M.M.	69
Agrachev, M.	12
Akhatov, A.	107
Akhmedzhanov, R.A.	126
Akhmetov, M.M.	131
Akhmetshina, M.	220
Akimov, A.V.	103, 128
Alexandrov, A.	158
Alexandrova, N.	44
Alimov, D.	43
Alkahtani, M.H.	122
Andrianov, V.V.	32, 133, 220
Ashuiev, A.	12
Astvatsaturov, D.A.	72
Avanesov, S.A.	193
Avilova, I.	21
Babunts, R.A.	84
Bagryanskaya, E.	91, 170
Bakirov, M.M.	32, 102, 135, 155, 136
Baranov, P.G.	4, 84
Batueva, E.	215
Batulin, R.G.	60
Bayazitov, A.	112, 138
Bayer, M.	69
Bazan, L.V.	32, 133, 145
Bekmacheva, E.	107
Belotelov, V.I.	47
Berezhnoi, A.D.	129
Biondi, B.	208
Biryukov, Y.P.	228
Blokhin, D.	176
Bochkin, G.A.	118
Bogachev, Yu.	172, 181
Bogodvid, T.Kh.	133
Bolshedvorski, S.V.	103
Borodulina, A.V.	139

Bowman, M.K.	8, 16, 91
Bunkov, Yu.M.	47
Buravkov, S.	220
Cakal, A.F.	104
Cao, H.	136
Chazov, A.I.	92
Chen, Xi	219
Chernyak, A.	21, 79
Cherosov, M.A.	60, 182
Chibirev, A.O.	140
Chumakova, N.A.	37, 66, 72, 97, 153, 222
Chupakhina, T.I.	65, 147, 225
Clavijo, J.E.	123
Cojocaru, I.S.	103
Colak, B.	104
Dai, J.	13
Davydov, M.	116
Davydov, R.	113, 116
Davydov, V.	113, 116
Deeva, J.A.	147, 225
Demishev, S.V.	9
Deryagin, O.	220
Doğan, E.	104
Donato, M.Di	219
Drouhin, H.-J.	84
Drovosekov, A.B.	73
Dudnikova, V.	96
Dugin, M.	91
Dvinskikh, S.V.	13
Dzuba, S.A.	31, 208
Edinach, E.V.	84
Efremov, A.	141, 184, 227
Endutkin, A.	170
Erdiakov, A.	220
Eremina, R.M.	65, 162, 169, 182, 223
Eremin, M.V.	60
Ermakova, E.	217
Fadeeva, I.V.	188
Fakhrutdinov, A.	112, 138
Falin, M.L.	142
Farrakhov, B.F.	143
Fattakhova, M.	107
Fattakhov, Ya.V.	112, 138, 143, 158, 173, 175
Fazlizhanov, I.I.	197

-
- Fedin, M.V. 27, 141, 184, 192, 227
Fedorova, V. 107
Fedunov, R.G. 54
Fel'dman, E.B. 118
Fischer, J. 12
Formaggio, F. 208
Forysenkova, A.A. 188
Frolova, E. 145
Gabbasov, B. 50, 60, 99
Gafarova, A.R. 146
Gafiyatullin, L. 195
Gafurov, M.R. 180, 188, 201
Gainutdinov, Kh.L. 32, 133, 220
Garifullin, I.A. 152, 212
Garif'yanov, N.N. 140
Gavrilova, S. 220
Gavrilova, T.P. 147, 182, 225
Gerasimov, K.I. 124
Geru, I.I. 17
Glebov, E.M. 54
Goldberg, A. 116
Golovchanskiy, I. 50
Golysheva, E.A. 31
Gorbunov, A. 181
Gordeev, A.S. 178
Goryunov, Yu. 148
Gracheva, I. 77, 82, 98
Großer, A. 157
Gubaidullin, A. 194
Gumarov, A. 50
Gumarov, G.G. 131, 146
Gurin, A.S. 84
Gushchin, L.A. 126
Haijun, Y. 87
Hara, S. 11
Hemmer, P. 121
Herpich, J. 56
Hoffman, B.M. 5
Isaev, N. 91
Isaev, V.A. 193
Islamov, T. 158
Ivanov, A.I. 124
Ivanov, M. 43, 91
Iyudin, V. 133, 220

Jastrabik, L.	99
Jeschke, G.	12
Kadikova, A.H.	150
Kalachev, A.A.	129
Kalevich, V.K.	69
Kamashev, A.A.	152
Kandrashkin, Yu.E.	23, 24, 25, 136
Kaplin, A.V.	97, 153
Kapralov, P.O.	47
Khabibullin, R.R.	212
Khabipov, R.	107
Khaidukov, N.M.	142
Khairutdinov, I.T.	25, 102, 135, 155
Khantimerov, S.M.	147, 225
Khayrutdinov, B.I.	196
Khisameeva, R.	75, 157
Khrykina, O.N.	153
Khusnutdinov, R.	104
Kiiamov, A.	50, 60
Kirstein, E.	69
Kiryukhin, D.P.	118
Kiryutin, A.S.	160
Klochkov, V.	176
Klose, D.	12
Knyazev, G.A.	47
Kochetkov, I.	113
Kokorin, A.	36, 37, 42, 45
Kolesova, A.	158
Kondratenko, A.	44
Konov, K.B.	162
Konstantinova, E.A.	34, 40
Konygin, G.N.	131, 146
Korobov, M.	97, 153
Koshelev, V.	220
Koshman, V.	159
Kozinenko, V.P.	160
Kozlov, Yu.N.	37
Kozyrev, N.V.	69
Krasnozhon, V.	107
Kreines, N.M.	73
Krumkacheva, O.A.	27
Krylov, M.F.	123
Kuibida, L.V.	54
Kuklinov, M.L.	92

-
- Kukushkin, I.V. 75, 157
Kulchitchky, V.A. 133
Kupriyanova, G. 89, 166, 167, 205
Kupriyanov, P. 104
Kushch, P.P. 118
Kusova, A.M. 161
Kusrayev, Yu.G. 69
Kuzmichev, A.N. 47
Kytina, E.V. 34, 40
Lambert, Ch. 56
Latypov, V.A. 142
Lebedev, A.V. 193
Leontyev, A.V. 122, 123, 140, 152
Likerov, R.F. 162
Lobkov, V.S. 122, 123
Lobova, N. 44
Lomanovich, K. 91
Lopatina, S.A. 75
Lukzen, N.N. 56
Lundin, A.A. 19
Maeda, K. 53
Majhi, D. 13
Malevannaya, E.I. 124
Mamedov, M.D. 211
Mamin, G. 77, 82, 98, 188, 201
Mamin, R.F. 140, 152
Marikutsa, A.V. 40
Maryasov, A.G. 8, 16
Matanin, A.R. 124
Matveev, M. 97, 164
Melnikov, A. 91
Melnikova, D. 158, 178
Melnikov, A.R. 139
Mershiev, I. 89, 166, 167
Mikolajick, T. 157
Milanovsky, G.E. 211
Mims, D. 56
Mirochnik, A.G. 190
Mirsalimova, K.R. 161
Mityushkin, E.O. 122, 123
Moiseeva, E. 167
Moiseev, E.S. 124
Moiseev, S.A. 124
Morgun, L. 59

Moshkina, E.M.	169, 182, 223
Moskalenko, I.	42, 45
Mozzhukhin, G.V.	104
Muftakhutdinov, A.R.	169
Murzakhanov, F.	77, 82, 98, 188
Muzafarov, A.M.	213
Nasonov, D.	170
Nasyrova, M.I.	212
Nateprov, A.	148
Nesterov, P.	36, 42, 45
Nikiforov, V.G.	122, 123
Nikitina, A.	172, 181
Nikolaev, G.A.	75
Nikolaev, S.N.	73
Nikul'shin, P.V.	54
Nizov, N.A.	126
Nizov, V.A.	126
Odivanov, V.	112, 138, 158, 173, 175
Ohmichi, E.	11
Ohta, H.	11
Okubo, S.	11
Opra, D.P.	67
Osetrina, D.	176
Ovcherenko, S.	170
Ovchinnikov, I.	145
Panicheva, K.V.	213
Parfenova, D.A.	178
Pavlov, D.V.	179
Peggion, C.	208
Petrova, A.A.	180
Petrov, A.S.	92
Petrov, D.N.	123
Petrov, P.E.	47
Pichkovskiy, I.S.	51
Pobedimova, E.	181
Polishchuk, V.R.	108
Polovyanenko, D.	91
Polozov, V.I.	124
Polyakov, N.	159
Polyukhov, D.	27, 141, 184, 227
Popov, D.S.	153
Popov, D.V.	182
Poryvaev, A.	27, 141, 184, 227

Povarov, K. Yu.	63, 203
Pudalov, V.	59
Pudovkin, M.S.	185
Pylaeva, S.	43
Rafalskiy, V.	167
Rakhmatullin, R.M.	185
Rameev, B.	104
Rebrikova, A.	97, 153
Rodionov, A.A.	99, 180, 185
Rodionov, I.A.	124
Romanov, N.G.	95
Rubinas, O.R.	103
Ryabushkin, D.S.	186
Rybin, D.S.	131, 146
Rylkov, V.V.	73
Sadovnikova, M.	77, 82, 188
Saenko, N.S.	190
Safarov, V.I.	84
Sakhin, V.	59
Sakurai, T.	11
Salewski, M.	69
Salikhov, K.M.	7, 96, 102, 135, 211
Samoilov, A.A.	124
Samsonenko, A.A.	192
Sannikov, K.	98
Saritsky, D.A.	67
Sato, K.	15
Savchuk, T.P.	34
Savostina, L.	195
Schmid, S.P.	12
Schmult, S.	157
Selyutina, O.	159
Semenov, A.Y.	211
Shagalov, V.	112, 138
Shaginyan, V.R.	58
Shaidullina, A.	195
Shakurov, G.S.	106, 193
Sharipova, A.	145, 194, 195
Sharipova, L.V.	196
Shayakhmetov, N.G.	32
Shchepetilnikov, A.V.	75, 157
Shelepova, E.	159
Shernyukov, A.	170
Shestakov, A.V.	197

Shilovskikh, V.	42
Shindyev, O.P.	199
Shiomi, D.	15
Shishkina, M.	172, 181
Shishov, A.S.	190
Shkalikov, A.V.	199
Shmelev, A.G.	122, 123
Shubin, A.A.	37
Shurtakova, D.	201
Shustov, V.A.	162, 182
Sidorov, I.	158
Sitnikov, A.V.	73
Skirda, V.	158, 178
Skorb, E.	36, 42
Skvortsova, P.	217
Slesarenko, N.	79
Smirnov, A.I.	63, 203
Smirnov, M.	205
Smirnov, N.S.	124
Smolyaninov, A.N.	103
Smorygina, A.S.	208
Sobgayda, D.A.	126
Soldatov, T.A.	63, 203
Solovyev, V.V.	157
Soltamov, V.	98
Sorokin, V.N.	103
Soshenko, V.V.	103
Starykh, O.A.	63, 203
Stass, D.V.	54
Steiner, U.E.	56
Subbotin, K.	96
Subramanian, S.	2
Sugisaki, K.	15
Sukhanov, A.A.	32, 28, 96, 136, 210, 211, 219
Sukharzhevsky, S.	172
Suleimanov, N.M.	147, 225
Syryamina, V.N.	208
Taddei, M.	219
Tagirov, L.	50
Takahashi, H.	11
Takui, T.	15
Tarasov, V.	96
Teitel'baum, G.	59
Tikhonov, P.A.	213

- Timralieva, A. 36, 42, 45
Titova, Yu.Yu. 179
Tokalchik, Y.P. 133
Toyota, K. 15
Trepakov, V. 99
Troshin, P. 21
Turanov, A. 161, 194, 195, 196, 215
Turanova, O. 145, 194, 195, 215
Ulanov, V.A. 106, 197
Vagizov, F.G. 228
Validov, A.A. 212
Vanin, A.F. 6
Vasil'ev, S.G. 118, 213
Vasin, K.V. 60
Veber, S.L. 91, 139, 192
Vetoshko, P.M. 47
Volkov, M. 155, 194, 195, 215, 217
Volkov, V. 21, 79
Voronkova, V.K. 28, 136, 210, 219
Wang, Ren-Bo 63, 203
Wenyu, L. 87
Wurmehl, S. 89
Yafarova, G.G. 32, 133, 220
Yakovlev, D.R. 69
Yamane, T. 15
Yanilkin, I. 50
Yankova, T.S. 222
Yatsyk, I.V. 65, 106, 147, 162, 182, 223, 225
Yazikova, A. 184, 227
Ye, K. 210
Yingying, F. 87
Yong, L. 87
Yulan, T. 87
Yurkovskaya, A.V. 160
Yusupov, R. 50, 60, 77, 99
Zamaro, A.S. 133
Zaripov, R.B. 23, 24, 25, 32, 102, 106, 131, 135, 146, 155, 162, 193
Zelensky, I.V. 126
Zhao, J. 28, 136, 210, 219
Zhao, X. 28
Zharikov, E. 96
Zharkov, D. 122, 123, 170
Zheleznov, V.V. 67
Zheludev, A. 63, 203

Zhifu, S.	87
Zhukov, E.A.	69
Ziatdinov, A.M.	67, 108, 190
Zikiy, E.V.	124
Zinnatullin, A.L.	60, 228
Zirui, Q.	87
Zobov, V.E.	19, 51
Zubkov, V.	172
Zuev, Yu.F.	161, 196, 217
Zverev, D.	99

© Казанский физико-технический институт им. Е. К. Завойского –
обособленное структурное подразделение Федерального государственного
бюджетного учреждения науки “Федеральный исследовательский центр
“Казанский научный центр Российской академии наук”, 2022

Ответственный редактор: В. К. Воронкова; редакторы С. М. Ахмин, Л. В. Мосина; технический редактор
О. Б. Яндуганова. Издательство ФИЦ КазНЦ РАН,
420029, Казань, Сибирский тракт, 10/7, лицензия № 0325 от 07.12.2000.

